The Dissertation Committee for Nicholas David Perez Certifies that this is the approved version of the following dissertation:

Cenozoic deformation history of the Andean plateau in southern Peru: Stratigraphic, structural, and geochronologic constraints

Committee:

Brian K. Horton, Supervisor

Sean Gulick

Nadine McQuarrie

Ron Steel

Daniel F. Stockli

Cenozoic deformation history of the Andean plateau in southern Peru: Stratigraphic, structural, and geochronologic constraints

by

Nicholas David Perez, B.S. Geo. Sci.

Dissertation

Presented to the Faculty of the Graduate School of

The University of Texas at Austin

in Partial Fulfillment

of the Requirements

for the Degree of

Doctor of Philosophy

The University of Texas at Austin

August 2015

Acknowledgements

This work would not have been possible without help, love, and support from many people. My advisor Brian Horton has provided immense guidance throughout my undergraduate and graduate career. Members of his research group graciously contributed considerable time, constructive feedback, and experience which helped me tremendously. This includes vintage members Veronica Anderson, Katie Bales, Meredith Bush, Amanda Calle, Elizabeth Cassel, Alejandra Eljuri, Justin Fitch, Kelly Hansard, Renas Koshnow, Sebastian Ramirez, Joel Saylor, Ben Siks and new arrivals Tomas Capaldi, Lily Jackson, Sarah George, and Chelsea Mackaman-Lofland. Fellow graduate students helped in myriad ways, especially Paul Betka, Nate Eichelberger, Michelle Gilmore, Mauricio Ibanez, Richard Lease, Mike Prior, Josue Pujols, Bobby Reece, and Travis Wicks. Thank you.

Throughout graduate school, friends have provided inspiration, encouragement, or a necessary distraction from time to time. Thank you Josh Verduzco, Cait Taylor, Alan Andrews, Gavin Mynhardt, Jason Chandrapal, Zach Buie, Rudy Madrid, Timmy Chang Whitney, Andrew Nicholson, David Conwell, Jah Fong-Ngern, Sarah and Brian Periman, Luke and Laura Fidler, Jess Hudock, Guy Fitz, Erin Beimford, Rachel Peace, Jesslene Ames, Nabiel Eldam, Travis Kloss, Bryant Kopriva, Mike Hester, Mike Vigliotti and many others. I'm not sure I'd have retained my sanity as well without you, whether you were aware or not.

I have been lucky to have great teachers and mentors throughout my education. Thank you to Sheryl Jones, Vicki Hebert, David Jones, Susan Curtis, Phyllis Woods, Diane Gorzycki, Mike Mellinger, and Otis Murphy, who helped shape my pre-geology

years. In geology, I learned greatly from Esti Ukar, Jamie Levine, Miriam Barquero-Molina, Chris Bell, Bill Carlson, Mark Helper, Randy Marrett, Antonio Teixell, Sharon Mosher, Ron Steel, Sean Gulick, Danny Stockli, Nathan Bangs, Charlie Kerans, Nadine McQuarrie, Todd Ehlers, and Konstanze Stübner.

This work was completed in Peru. The experience of working there positively impacted my life and worldview. Thank you to Franco Bedoya and family for your hospitality and logistical help. Thank you Vicente Paloma of Tinajani Canyon, Ayaviri, Puno Department and family for your hospitality and safekeeping. Thank you to the people of Ayaviri and southern Peru. Many thanks to Victor Carlotto for his guidance and work on the geology of Peru.

My family has always been an incredible support throughout my various endeavors. Much of my success in life is directly linked to that love. Thank you Mom, Dad, Eli, grandparents, aunts, uncles, cousins, second-cousins, second-double cousins et cetera from the extended Perez, Goodwin, Pils, Ott, Peters, Williams mega-family extraordinaire. Thank you to my new family Wendy and Paul, and Robert and Connie.

Finally and most importantly, I would like to thank my wife Nataleigh. It's been a great adventure so far, and we are just getting started.

Cenozoic deformation history of the Central Andes of southern Peru: Stratigraphic, structural, and geochronologic constraints

Nicholas David Perez, Ph.D.

The University of Texas at Austin, 2015

Supervisor: Brian K. Horton

Cenozoic shortening in the central Andes of southern Peru was accommodated by thin- and thick-skinned deformation that governed hinterland/foreland basin dynamics, the timing and location of exhumation, and development of modern high topography. A new line-length balanced cross section estimates 130 km of shortening (38%) across the Eastern Cordillera and Subandean Zone. I propose the location of a pre-Andean extensional basin in the Eastern Cordillera, and a kinematic model that links selectively inverted basement-involved normal faults to shallow detachments that accommodate thin-skinned deformation across the orogen. New U-Pb zircon geochronologic data from synrift deposits establishes Triassic age deposition, and suggests compartmentalized rift basins were filled with local Eastern Cordillera sediment sources.

Eocene exhumation in the Eastern Cordillera represents reactivation of Triassic normal faults and the onset of Andean deformation. deformation was transferred westward from the Eastern Cordillera to the Altiplano by the thin-skinned Central Andean Backthrust Belt and induced flexural subsidence in the Ayaviri hinterland basin beginning at ~30 Ma. Facies analyses, sediment provenance, geochronology, and structural mapping define multiple phases of basin reorganization that are temporally correlative with motion along basin margin thrust faults. Major middle Miocene

reorganization of the Ayaviri basin is linked to ~17 Ma out-of-sequence thrust fault motion in the Western Cordillera. Oligocene-Miocene hinterland basin evolution in the northern Altiplano was driven by thrust tectonics.

U-Pb detrital zircon geochronologic results from Cretaceous through Cenozoic clastic deposits in hinterland and foreland basins record distinct provenance differences since the Cretaceous. This is the detrital record of either an inherited structural high in the Eastern Cordillera that predated Eocene shortening and created two depocenters with distinct provenance, or lateral provenance variations across a large retroarc foreland basin. Existing K/Ar, $^{40}Ar/^{39}Ar$, and new zircon (U-Th)/He thermochronologic data suggest Eocene-Oligocene exhumation in the Eastern Cordillera was synchronous ~400 km along strike. New apatite (U-Th)/He thermochronometric data from the Eastern Cordillera demonstrate a change to localized, diachronous exhumation and uplift events in the Miocene-Pliocene. Apatite (U-Th)/He thermochronologic results demonstrates onset of deformation in the Subandean Zone by ~15 Ma, after shortening and exhumation in the Eastern and Western Cordillera ceased.

Table of Contents

List of Tables

List of Figures

Chapter 1: Oligocene-Miocene deformational and depositional history of the Andean hinterland basin in the northern Altiplano plateau, southern Peru

ABSTRACT

Cenozoic basin fill of the northern Altiplano plateau records the tectonic development of the flanking Western Cordillera magmatic arc and Eastern Cordillera fold-thrust belt. The Ayaviri hinterland basin of southern Peru contains a ~2300 m thick succession of fluvial sandstones and overbank siltstones (Late Oligocene Puno Group, early Miocene Lower Tinajani Formation) capped by ~400 m of alluvial fan conglomerates (middle Miocene Upper Tinajani Formation). New U-Pb zircon chronostratigraphic constraints from ~30 to 15 Ma yield sediment accumulation rates of 110-660 m/Myr. Newly dated growth strata highlight the genetic role played by thrust displacement in basin evolution. A several-phase accumulation history derived from chronostratigraphic, provenance and structural data reveals Oligocene basin filling by fluvial sand and mud that changes provenance from Western Cordillera Mesozoic-Cenozoic volcanic rocks to Paleozoic-Mesozoic Eastern Cordillera sedimentary rocks driven by deformation along the southwest directed, northeastern basin margin Ayaviri thrust at 28-26 Ma. Continued early Miocene fluvial deposition was sourced solely from the Eastern Cordillera. An abrupt middle Miocene shift to coarse alluvial fan deposition sourced from the Western Cordillera was driven by out-of-sequence deformation along the northeast-directed, southwestern basin margin Pasani thrust at 18-16 Ma. This northern Altiplano out-of-sequence deformation was coincident with increased Eastern and Western Cordillera exhumation and thrusting and may be symptomatic of changes in

critical wedge dynamics. The overall record of basin sedimentation and syndepositional fold-thrust deformation emphasizes the role of regional shortening in governing crustal thickening and basin evolution in the central Andes during the Oligocene to Miocene.

2. INTRODUCTION

The mechanisms responsible for the evolution of long-lived sedimentary basins in hinterland settings of convergent orogenic systems remain poorly constrained. Debate has centered on the establishment of internal drainage, partitioning, and coalescence of basin depocenters, modes of syndepositional deformation, and processes responsible for basin subsidence [*Jordan and Alonso,* 1987; *Allmendinger et al.,* 1997; *Tapponnier et al.,* 2001; *Sobel et al.,* 2003; *Carroll et al.,* 2010; *Horton,* 2012]. For example, hinterland basins of the Altiplano-Puna plateau have been variably interpreted as the product of thrust-related flexural subsidence, sediment ponding within internally drained topographic lows, or subsidence driven by strike-slip deformation [e.g., *Sempere et al.,* 1990; *Baby et al.,* 1990; *Vandervoort et al.,* 1995; *Rochat et al.,* 1999; *Horton et al.,* 2002; *Elger et al.,* 2005; *Rousse et al.,* 2005; *Carlotto,* 2013]. Successfully reconstructing the spatial and temporal history of these basins in the context of convergent margin dynamics remains a challenge, yet provides critical evidence for the history and style of deformation controlling the orogenic evolution of elevated hinterland regions.

In the central Andes (Figure 1), the Altiplano plateau preserves a series of internally drained hinterland basins in Bolivia and southern Peru containing up to ~12 km of synorogenic Cenozoic sediment [*Horton et al.,* 2001, 2002; *Carlotto,* 2013]. These

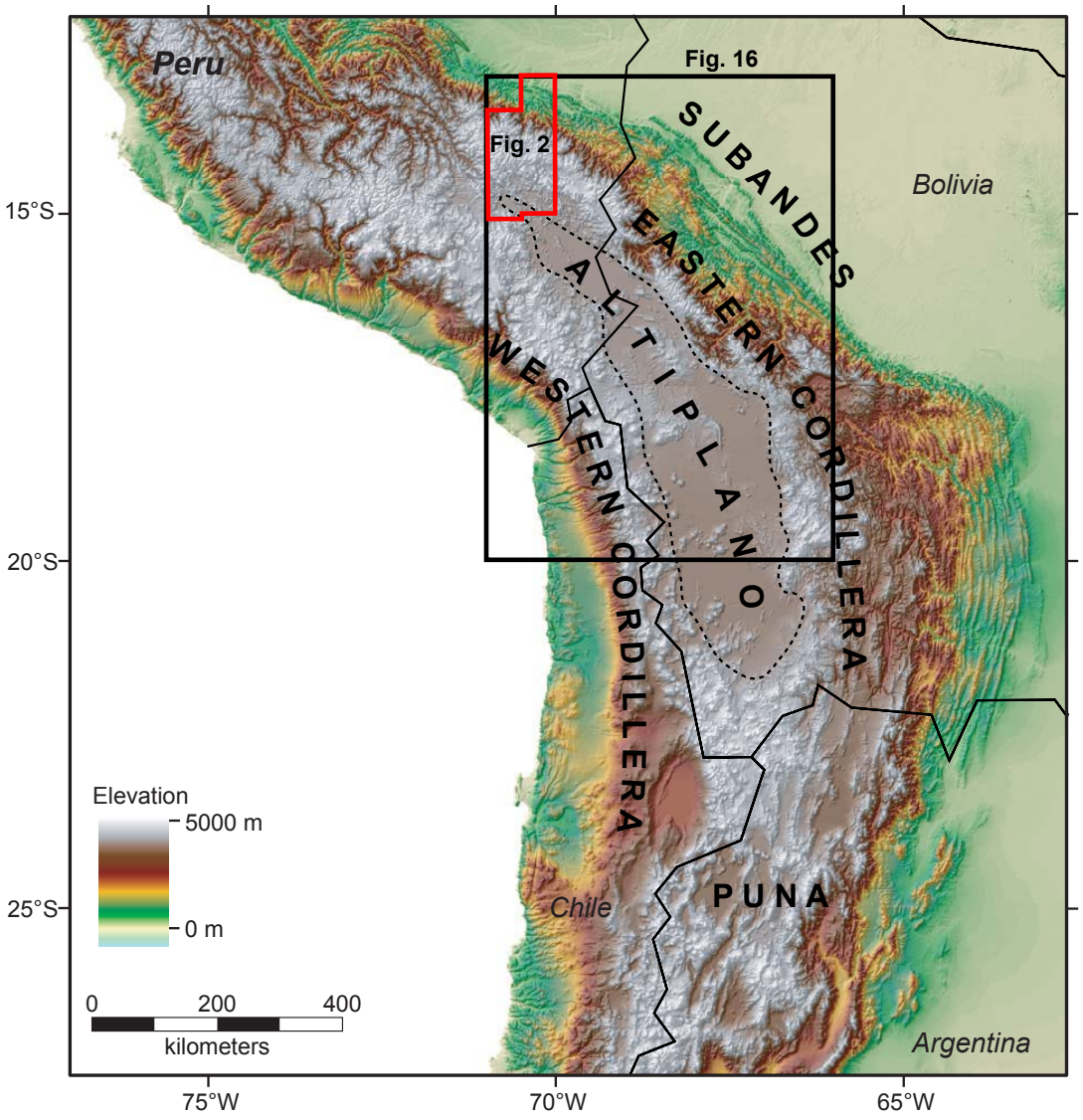

nonmarine hinterland basins are a key recorder of the tectonic processes that controlled Altiplano development throughout the Cenozoic. Although unconformable relationships

Figure 1.1. Topographic map of the central Andes showing the southern Peruvian study area (thick red outline, Figure 2; thick black outline, Figure 16), situated at the northern tip of Altiplano. Study area encompasses Altiplano, Eastern Cordillera and Subandes

within the stratigraphic record have long been used to propose multiple separate pulses of deformation with intervening periods of quiescence [e.g., *Steinmann,* 1929; *Mégard et al.,* 1984; *Ellison et al.,* 1989; *Noblet et al.,* 1996], most syntheses of available depositional records demonstrate continuous, long-lived subsidence and sedimentation in the Cenozoic basins of the central Andean hinterland [*Jordan and Alonso,* 1987; *Allmendinger et al.,* 1997; *Horton,* 2012; *Carlotto,* 2013].

Hinterland basins have also been used to define the history of surface uplift in the Altiplano. Significant debate persists over the apparently heterogeneous and localized surface uplift events that postdate most Andean shortening. Rapid uplift events have been proposed for the Altiplano of Bolivia [~10-6 Ma; *Garzione et al.,* 2006], Eastern Cordillera of Bolivia [after 12-9 Ma, *Barke and Lamb,* 2006; 24-15 Ma, *Leier et al.,* 2013] and Western Cordillera of Peru [~19-16 Ma; *Saylor and Horton,* 2014] based on paleoaltimetric and canyon incision proxies. Many studies have called on foundering or delamination of continental lithosphere as a potential mechanism to explain rapid high-magnitude surface uplift events throughout the central Andes [*Kay and Kay,* 1993; *Garzione et al.,* 2006; *DeCelles et al.,* 2009] although some regions retain subcrustal lithosphere [*Beck and Zandt,* 2002]. Improved records of upper crustal shortening are needed in localities with accompanying paleoaltimetric studies to evaluate the links between the timing and magnitude of deformation and the onset of surface uplift.

Key questions remain regarding the timing and style of deformation across the Central Andes despite long-lived depositional records. It remains unclear whether the central (Bolivian) and northern (Peruvian) Altiplano structural systems are linked by a shared history of upper-crustal deformation, including proposed major phases of thrust and strike-slip faulting. Existing timing constraints from the Eastern Cordillera in Bolivia

and southern Peru suggest widespread Eocene cooling associated with advance of the deformation front [*Farrar et al.,* 1988; *Barnes et al.,* 2006; *Gillis et al.,* 2006; *Murray et al.,* 2010; *Leier et al.,* 2010; *Mosolf et al.,* 2011]. In Peru, the potential kinematic links between major structural features such as the Cordillera de Carabaya, central Andean backthrust belt, and Altiplano bounding structures (Pasani and Ayaviri faults) remain poorly constrained [*Sempere et al.,* 1990; *Sandeman et al.,* 1995; *Carlotto,* 2013]. Likewise, the potential broader links between deformation, deposition, and variations in slab processes are not well resolved. Using depositional and deformational records, some have argued for long-term Andean shortening that advanced systematically toward the Amazonian craton [*Noblet et al.,* 1996; *DeCelles and Horton,* 2003; *McQuarrie et al.,* 2005], in contrast with previous studies arguing for short discrete phases of deformation with long intervening quiescent periods [e.g., *Sebrier et al.,* 1988; *Sempere et al.,* 1990]. Others have suggested that shortening was spatially distributed for protracted periods of time, progressed irregularly or out-of-sequence, potentially due to an inherited crustal framework [*Oncken et al.,* 2006; *Hongn et al.,* 2007; *Mortimer et al.,* 2007; *Strecker et al.,* 2009]. Still others have attributed major shortening events to punctuated shifts in the dynamics of the subducting slab [*Jordan et al.,* 1983; *Sandeman et al.,* 1995; *James and Sacks,* 1999]. Regardless, shortening plays a key role in the construction of the Altiplano [*Isacks,* 1988]. Comparing the shortening history of Peru and Bolivia will help assess whether deformation in the central Andes was part of a widespread organized structural system or accommodated by a collection of independent disconnected zones.

This study provides an improved record of northern Altiplano deposition from the Ayaviri basin and precise age constraints on the timing and nature of Cenozoic upper-crustal deformation in the Andean hinterland. We use new sedimentological, structural and geochronologic datasets to define the history of sediment accumulation, timing and

style of basin-controlling structures, and sedimentary response to changes in Andean tectonics in southern Peru. Finally, we highlight important similarities in structure and basin style spanning southern Peru and Bolivia, suggesting potential regional links between the deformation and subsidence history across the Altiplano.

3. GEOLOGIC BACKGROUND

The central Andean (Altiplano-Puna) plateau (Figure 1) spans the elevated hinterland regions of southern Peru, Bolivia and northern Argentina at an average elevation of ~3.7 km [*Isacks,* 1988; *Allmendinger et al.,* 1997]. This high topography is the result of long-lived crustal shortening along the convergent margin of western South America [*Coira et al.,* 1982] and crustal thickening may rely on magmatic addition [*Kay and Coira*, 2009] removal of lower lithosphere [*Beck and Zandt,* 2002] or crustal flow [*Husson and Sempere*, 2003]. The central Andes have experienced the greatest shortening within the orogenic belt, with over 300 km of margin-perpendicular shortening [*Kley and Monaldi,* 1998; *McQuarrie,* 2002]. Cenozoic hinterland basins preserved within the Altiplano contain the sedimentary record of Andean orogenesis. The position of these hinterland basins, situated between the volcanic arc (Western Cordillera) and retroarc fold-thrust belt (Eastern Cordillera/Subandes), highlights their role as a major repository of the erosional products of Andean volcanism and shortening (Figure 2).

The geologic history of southern Peru is highlighted by the main tectonic features defining the central Andes at 13–15°S (Figure 2). The Western Cordillera has been the locus of significant, generally continuous volcanic activity since the Late Cretaceous. The

position of the magmatic arc has migrated across the western margin throughout the Cenozoic, at times overlapping the northernmost Altiplano [*Mamani et al*., 2010]. The

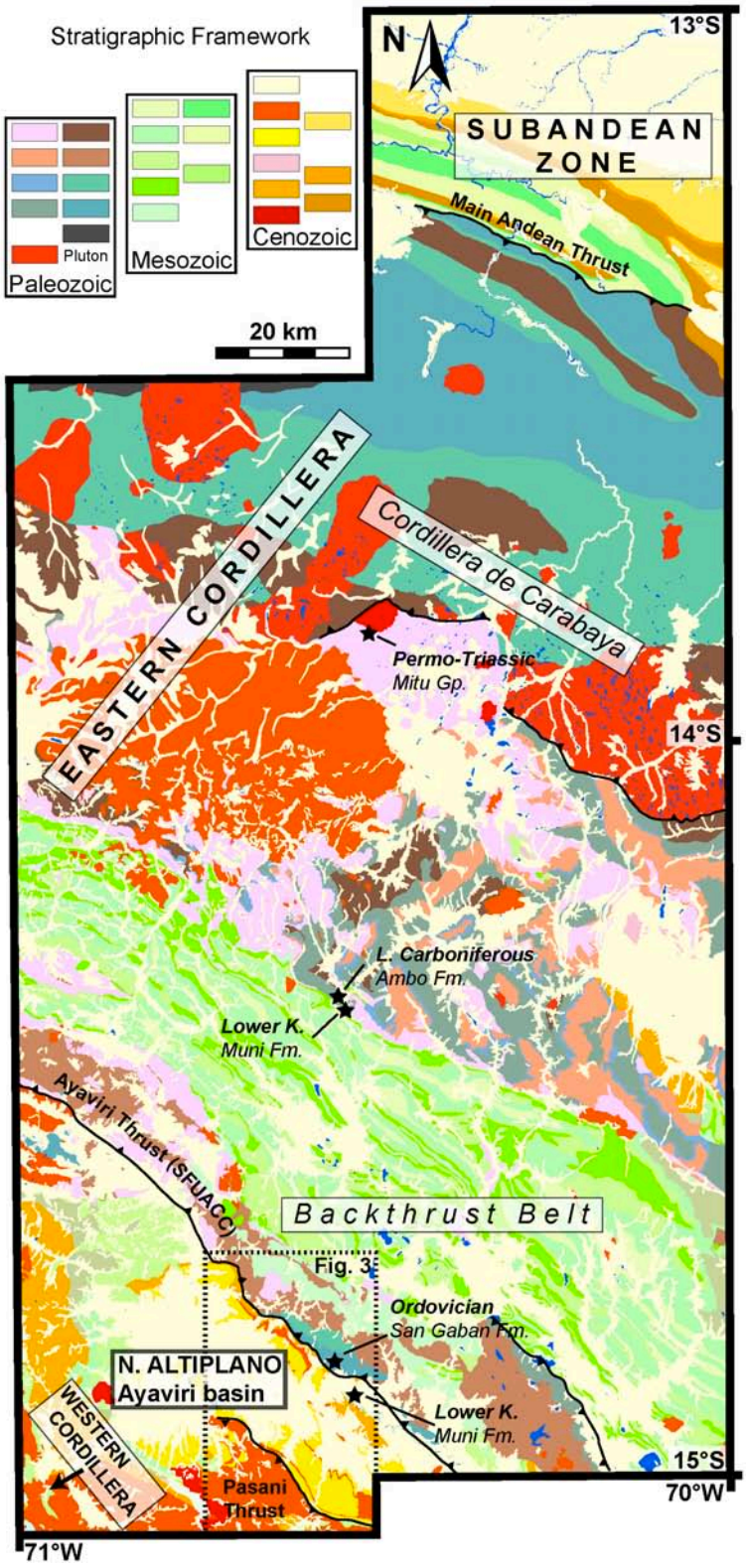
Stratigraphic Framework
Pluton
Paleozoic
Mesozoic
Cenozoic
20 km
N
13°S
SUBANDEAN ZONE
Main Andean Thrust
EASTERN CORDILLERA
Cordillera de Carabaya
Permo-Triassic
Mitu Gp.
14°S
L. Carboniferous
Ambo Fm.
Lower K.
Muni Fm.
Ayaviri Thrust (SFUACC)
Backthrust Belt
Fig. 3
Ordovician
San Gaban Fm.
N. ALTIPLANO
Ayaviri basin
Lower K.
Muni Fm.
WESTERN CORDILLERA
Pasani Thrust
15°S
70°W
71°W

Figure 1.2. Regional geologic map (after INGEMMET, this study) across the Western Cordillera, Altiplano, Eastern Cordillera (including the Cordillera de Carabaya and Backthrust belt), and Subandean Zone showing major thrust faults, and Ayaviri study area (blue box; Figure 3). Black stars with corresponding labels (listing depositional age, stratigraphic unit) denote locations of five U-Pb detrital zircon samples from Mesozoic and Paleozoic units used to characterize potential sediment sources for Cenozoic basin fill (Figure 9).

Eastern Cordillera of southern Peru contains the central Andean backthrust belt defined by generally southwest-verging fold-thrust structures dominated by Cretaceous marine sandstones and limestones [*Sempere et al.,* 1990]. To the northeast of the backthrust belt is the Cordillera de Carabaya and Cordillera Real in Bolivia, northwest-striking ranges composed largely of Triassic and mid to late Cenozoic igneous rocks [*McBride et al.,* 1983; *Farrar et al.,* 1988; *Kontak et al.,* 1990; *Sandeman et al.,* 1995]. Between the backthrust belt and the Cordillera de Carabaya is a region of non-coaxially deformed, middle to upper Paleozoic strata with fold and fault orientations that deviate from the regional tectonic strike of Andean structures. These orientations have been attributed to probable late Paleozoic deformation [*Mégard et al.,* 1971; *Laubacher,* 1978; *Clark et al.,* 1990] prior to Andean shortening and are overlapped by a series of Miocene-Pliocene ash flow tuffs (the Macusani volcanic rocks) notable for their magmatic andalusite, muscovite and high Al_2O_3 [*Laubacher,* 1978; *Pichavant et al.,* 1988; *Sandeman et al.,* 1995]. The southern Peruvian forearc, Western Cordillera, and Eastern Cordillera have experienced significant counterclockwise vertical axis rotations that accommodated oroclinal bending, suggesting that strike-slip faulting, in addition to shortening, may have played a key role in Central Andean tectonics [*Rousse et al.,* 2002; *Gilder et al.,* 2003; *Rousse et al.,* 2003; *Roperch et al.,* 2006].

Despite the unique position and large areal distribution of the Andean hinterland basins, the complete Cenozoic history and structures controlling many of these basins remain unclear. Previous studies of hinterland basins in Bolivia [*Horton et al.,* 2001, 2002; *Hampton and Horton,* 2007; *Leier et al.,* 2010; *Murray et al.,* 2010; *Horton,* 2012] conclude that upper-crustal shortening largely dictated basin genesis and the establishment of a plateau morphology in the central Altiplano. These studies posit that an early foreland basin was partitioned into a hinterland basin and subsequent Subandean

foreland basin during large-scale eastward advance of deformation [e.g., *Roeder and Chamberlain,* 1995; *DeCelles and Horton,* 2003; *McQuarrie et al.,* 2005; *Siks and Horton,* 2011]. In contrast, studies of Altiplano basins in southern Peru suggest that Cenozoic basin evolution was localized and largely controlled by strike-slip faulting [*Carlotto,* 2013].

The Ayaviri hinterland basin in southern Peru occupies the narrow, northern tip of the Altiplano, where the flanking Eastern and Western Cordillera are in close proximity (Figures 2 and 3). In contrast to the north-south tectonic strike defining most of the Andean orogenic belt, the southern Peruvian segment is defined by a northwest-southeast strike, paralleling the continental margin. The northwest-striking structures bounding the Ayaviri basin also approximate the structural boundaries between the Altiplano and flanking Eastern Cordillera and Western Cordillera. The northeastern and southwestern basin margins are defined by the Ayaviri and Pasani faults, respectively. To the southwest of the Ayaviri basin, Cenozoic volcanic deposits limit exposures of the underlying Mesozoic and Paleozoic succession to local isolated windows. To the northeast, Cenozoic volcanic rocks are limited, with Eastern Cordillera exposures dominated by Paleozoic and Mesozoic metasedimentary and sedimentary units.

The Ayaviri basin consists of >5–10 km of Cenozoic nonmarine clastic fill that unconformably overlie a mixed marine and nonmarine section of deformed Cretaceous strata. A western zone near the towns of Macari and Llalli preserves 3–6 km of mostly Paleogene deposits, whereas ~2700 m of the latest Oligocene to Miocene deposits are preserved near the town of Ayaviri and in Tinajani Canyon [*LaTorre et al.,* 2004; *Rodriguez et al.,* 1999]. Complex spatial and temporal variations in the Cenozoic stratigraphic framework of southern Peru led *Carlotto* [2013] to refer to the Oligo-Miocene deposits studied here as the Tinajani basin, in contrast to *Rousse et al.* [2005]

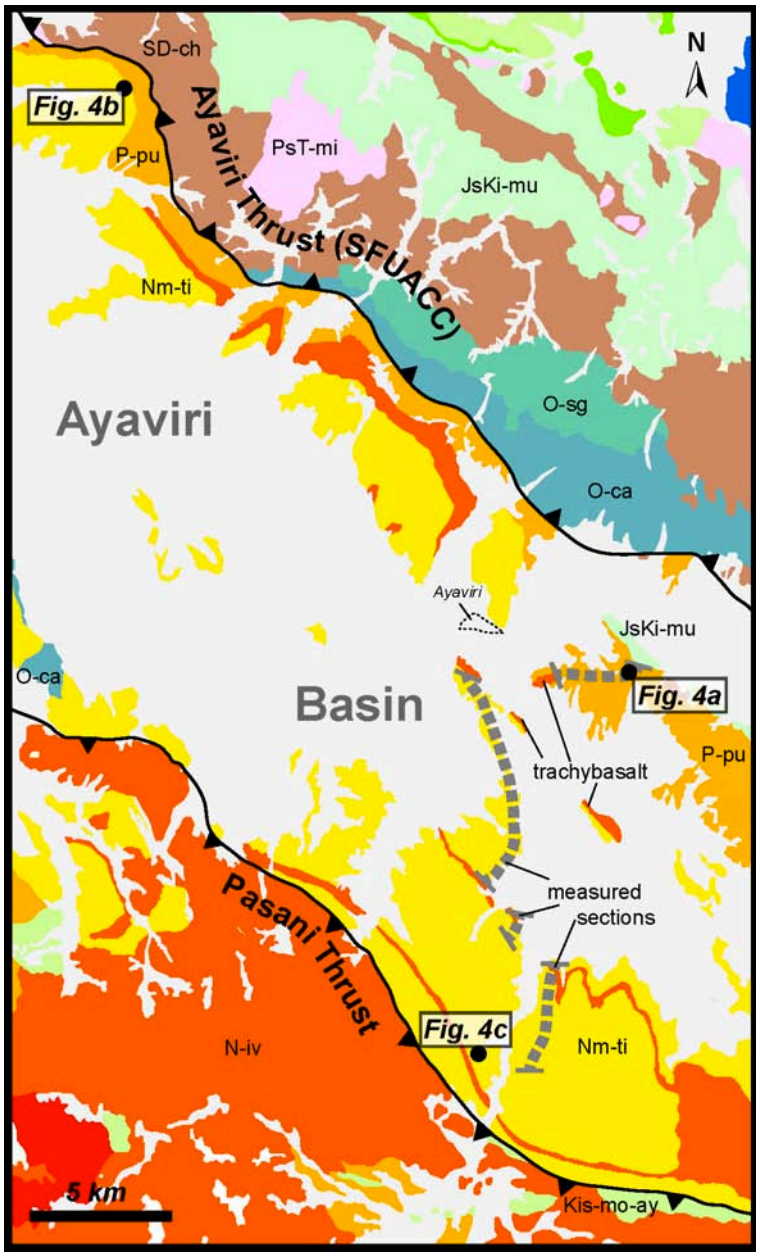

Figure 1.3. Simplified geologic map of the Ayaviri basin (after INGEMMET, this study) showing the principal stratigraphic units (same key as Figure 1.2), the basin-bounding Ayaviri and Pasani thrusts, locations of growth strata outcrops and accompanying photos (Figure 4), and locations of measured sections (thick dashed gray lines with horizontal end caps).

who retain the Ayaviri basin designation. Beneath the Cretaceous-Cenozoic cover is a panel of Paleozoic and Permo-Triassic rocks that are proposed to have been deposited and deformed during multiple pre-Andean events [*Newell,* 1949; *Mégard,* 1971; *Laubacher,* 1978; *Martinez,* 1980; *Laubacher and Mégard,* 1985; *Sempere et al.,* 2002; *Jimenez,* 2009].

The Oligo-Miocene fill of the Ayaviri basin consists of ~2700 m of Puno Group and Tinajani Formation that are dominated by sandstones, siltstones and conglomerates with minor lacustrine carbonates. Previous Oligocene to middle Miocene age constraints for the succession were based on dates from two volcanic horizons. The lower volcanic interval has been referred to as the Monterino or Cerro Ocuro volcanic rocks dated between ~29 and 25 Ma [*Bonhomme et al.,* 1985; *Fornari et al.,* 2002]. Upsection, interbedded ignimbrites commonly referred to as the Ocuviri tuffs were dated between 17.5 ± 0.6 and 17.3 ± 0.1 Ma [*Flores and Rodriguez,* 1999; *Rodriguez et al.,* 1999; *Ibarra et al.,* 2004; *Rousse et al.,* 2005; *Carlotto,* 2013]. Previous attempts to improve the Ayaviri basin chronostratigraphy using magnetostratigraphic techniques were hampered by significant post-deformational and recent magnetization [*Rousse et al.,* 2005].

4. BASIN-MARGIN STRUCTURES

Previous and new mapping efforts for the Ayaviri basin and basin-margin structures provide constraints on major structural elements associated with basin evolution [*Flores and Rodriguez,* 1999; *Rodriguez et al.,* 1999; *Ibarra et al.,* 2004; *Carlotto,* 2005; R*ousse et al.,* 2005; *Carlotto,* 2013]. The northeastern basin margin is defined by the northeast-dipping Ayaviri fault, which is part of a larger system of faults

known as both the Urcos-Ayaviri-Copacabana-Coniri Fault System (SFUACC acronym in Spanish) [*Sempere et al.,* 1990] or the Cusco Vilcanota Fault System [*Carlier et al.,* 2005] and can be traced ~350 km from southern Peru to Bolivia. It forms the structural boundary between the Altiplano and the Eastern Cordillera backthrust belt. The fault juxtaposes Middle Ordovician strata against Oligocene Puno Group. Bedding orientations from the ~5-6 km thick panel of Ordovician through Devonian strata in the northeast fault block dip approximately 40-45° to the northeast, suggesting that the fault dips similarly to the northeast for several tens of kilometers along strike. Along strike, variable Paleozoic units in the northeastern hanging-wall block are juxtaposed against the Oligocene Puno Group in the footwall of the Ayaviri fault. The largest stratigraphic separation of approximately 7 km is observed north of the town of Ayaviri. Along strike to the northwest, the stratigraphic separation decreases to approximately 3 km, where the Permian Mitu Group is juxtaposed against the Oligocene Puno Group. The southwestern basin margin is defined by the southwest-dipping Pasani fault that places the Cretaceous Ayavacas Formation on the middle Miocene Upper Tinajani Formation. The northwestern trace of the Pasani fault strikes northwest-southeast, but the fault changes along strike to a west-northwest/east-southeast orientation. Much of the southwestern hangingwall block of the Pasani fault is covered by Neogene volcanic and hypabyssal intrusive rocks. However, local exposures of Oligocene Puno Group below the volcanic cover demonstrate an anticline trending parallel to the trace of the Pasani fault in the hangingwall. Local exposures of Cretaceous Ayavacas Formation beneath the Neogene volcanic cover suggests that fault separation is approximately 4-5 km.

Both faults are associated with significant footwall growth synclines that parallel the fault trace for tens of kilometers. The Ayaviri fault exhibits a flat on ramp cutoff relationship, with northeast-dipping Paleozoic rocks thrust onto a footwall syncline

composed of southwest-dipping, and locally overturned northeast-dipping, strata of the Oligocene Puno Group. The folded Puno strata are consistently observed in the footwall of the Ayaviri fault for more than 45 km along strike. Fault cutoff relationships show a systematic decrease from 7 to 3 km of stratigraphic separation from southeast to northwest along strike of the Ayaviri fault, from Middle Ordovician strata to Permian strata thrust onto Oligocene strata, suggesting decreasing thrust displacement along strike and/or the presence of a lateral ramp at depth. Hanging-wall cutoffs for the Ayaviri fault have been eroded. The Pasani fault exhibits a ramp on ramp cutoff relationship with 4-5 km of stratigraphic separation and a hanging-wall anticline preserved in Oligocene Puno Group strata exposed beneath a Neogene volcanic cover. The footwall syncline and growth relationships persist for more than 30 km along strike on the Pasani fault.

On the southwestern side of the Ayaviri fault (northeast basin margin), coarse sandstones and siltstones of the Oligocene Puno Group have fanning stratal dip values that are characteristic of growth strata [*Shaw et al.,* 2004] (Figure 4). Individual beds of the stratigraphically lower pre-growth strata have the steepest dips ranging between 54 degrees overturned to the northeast and 71 degrees upright to the southwest. Each bed has laterally consistent dips along strike. In contrast, overlying beds within the growth strata panel have dips that range between 60 and 8 degrees upright to the southwest. Along the northeastern side of the Pasani fault (southwest basin margin), cobble conglomerates of the middle Miocene Upper Tinajani Formation preserve similar fanning dips. Individual beds within the pre-growth strata panel have laterally consistent dips that may vary between 70 and 40 degrees upright to the northeast. Individual beds within the growth strata panel preserve dips that progressively vary between approximately 55 degrees upright to the northeast and 5 degrees upright to the southwest. Individual beds within both the Ayaviri and Pasani fault growth strata panels preserve progressive variation in

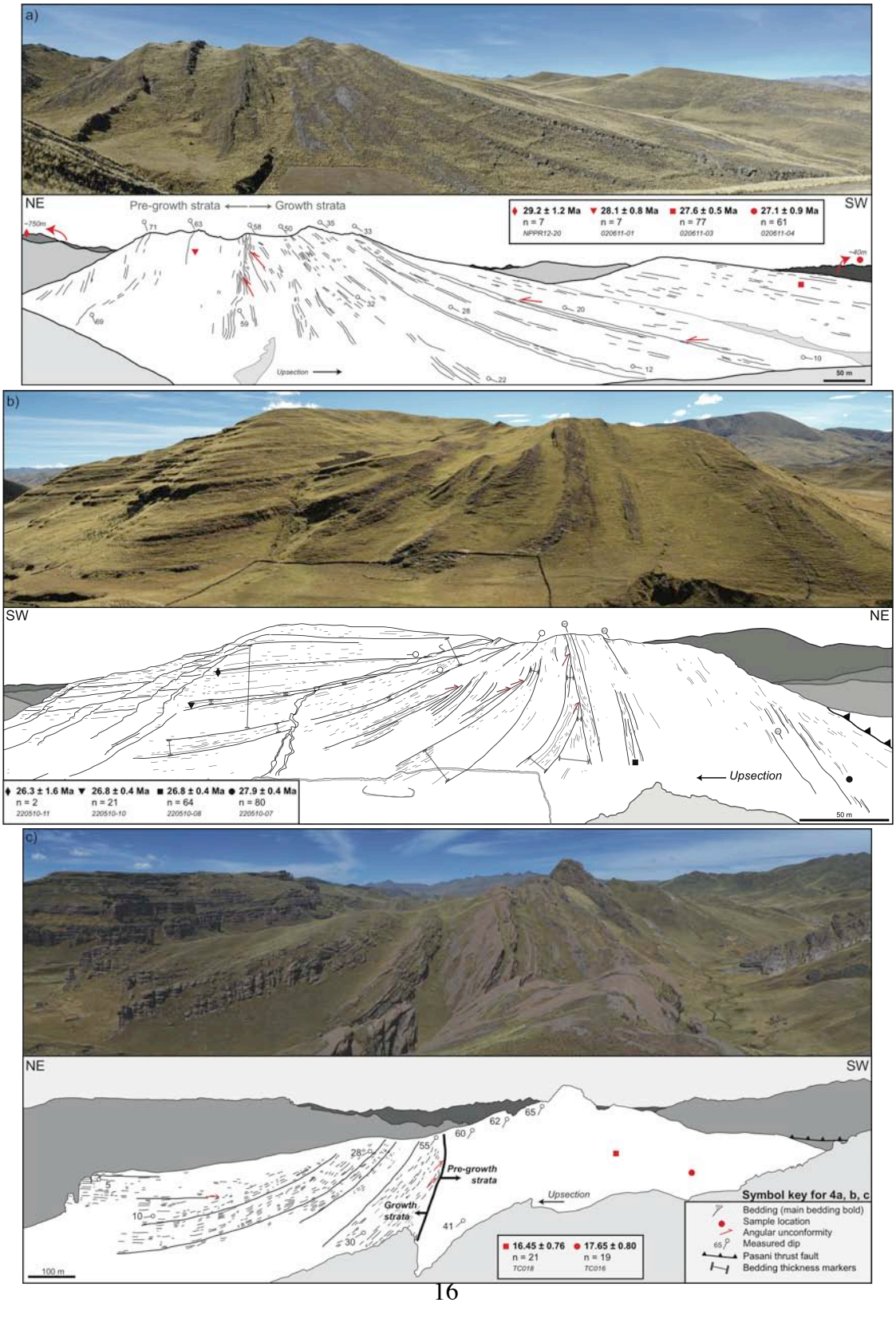
a)
NE
Pre-growth strata
Growth strata
SW
29.2 ± 1.2 Ma
n = 7
NPPR12-20
28.1 ± 0.8 Ma
n = 7
020611-01
27.6 ± 0.5 Ma
n = 77
020611-03
27.1 ± 0.9 Ma
n = 61
020611-04
~750m
~40m
Upsection
50 m
b)
SW
NE
Upsection
26.3 ± 1.6 Ma
n = 2
220510-11
26.8 ± 0.4 Ma
n = 21
220510-10
26.8 ± 0.4 Ma
n = 64
220510-08
27.9 ± 0.4 Ma
n = 80
220510-07
50 m
c)
NE
SW
Pre-growth strata
Growth strata
Upsection
16.45 ± 0.76
n = 21
TC018
17.65 ± 0.80
n = 19
TC016
100 m
Symbol key for 4a, b, c
Bedding (main bedding bold)
Sample location
Angular unconformity
Measured dip
Pasani thrust fault
Bedding thickness markers

Figure 1.4. Three examples of growth strata preserved along the Ayaviri fault (a, b) and Pasani fault (c). Ages from U-Pb zircon analyses of tuff or youngest detrital zircon population. Red symbols are tuff samples, black symbols are detrital zircon sandstone samples.

dip over a lateral distance of a few hundred meters. Both sets of growth strata display up-section decreases in bedding dip and increased bedding flatness. The range of stratal dip variation is comparable to growth strata observed in the Pyrenees [*Riba,* 1976; *Anadón,* 1986; *Ford et al.,* 1997].

Distinctive panels of recessive facies bounded by resistant sandstone beds within the growth strata along the Ayaviri fault can be traced laterally and consistently show thicknesses that increase away from the faults (Figure 4). Increases of the thickness of individual resistant sandstone beds are less apparent. The updip terminations of these recessive intervals may be truncated by an unconformity between the overlying and underlying resistant sandstone bed, but are more often not observed due to erosion. Lateral thickness variations within the growth strata along the Pasani fault are difficult to observe within a single bed, but are observed within intervals of cliff forming conglomerates and the intervening recessive units.

Multiple internal angular unconformities are associated with the footwall growth strata preserved along the Ayaviri and Pasani faults (Figure 4). Both growth strata locations along the Ayaviri fault (Figure 3) preserve one principal unconformity and multiple minor unconformities [*Ford et al.,* 1997; *Aschoff and Schmitt*, 2008]. The principal unconformity separates two stratigraphic units characterized by different geometries. The stratigraphically lower interval below the principal unconformity preserves dominantly tabular beds that have laterally consistent near vertical dips and show no obvious internal angular unconformities. These are interpreted as pre-growth strata. The stratigraphically higher interval above the principal unconformity preserves beds that contain internal minor unconformities and represent growth strata. Angular variation across the principal unconformity varies between approximately 15° and 30°. The minor unconformities within the upper interval are dominantly low angle (< 5°)

offlap relationships. Growth strata along the Pasani fault does not preserve a principal unconformity, and internal angular unconformities are rarely observed, potentially because of the coarse cobble conglomerates and thick bedding. The minor unconformities that are observed are less than approximately 10°.

The bedding geometries and angular unconformities within growth strata have been used to infer relative rates of uplift and sediment accumulation during active uplift and deformation of a structure as well as the style of fault or fold deformation. The prevalence of offlap geometries and a major unconformity with moderate angular discordance observed in growth strata along the Ayaviri fault is consistent with models suggesting that the relative rate of uplift in the hanging wall of the Ayaviri fault was greater than the sediment accumulation rate during the late Oligocene [*Anadón,* 1986; *Burbank and Verges,* 1994]. In contrast to the Ayaviri fault, the paucity of internal unconformities but prominent up-section decrease in bedding dip preserved in the growth strata along the Pasani fault may indicate that sediment accumulation rate outpaced local uplift of the hangingwall during the middle Miocene [*Aschoff and Schmitt,* 2008]. The lack of discrete dip domains within the growth strata panels along the Ayaviri and Pasani faults and the clear progressive dip variation along strike within individual beds suggests progressive limb rotation, rather than kink-band migration, was the dominant folding mechanism [*Suppe et al.,* 1992; *Zapata and Allmendinger,* 1996]. The geometries preserved in the growth strata along both faults are similar to models of fault propagation and trishear deformation [*Erslev,* 1991; *Ford et al.,* 1997].

5. DEPOSITIONAL SYSTEMS

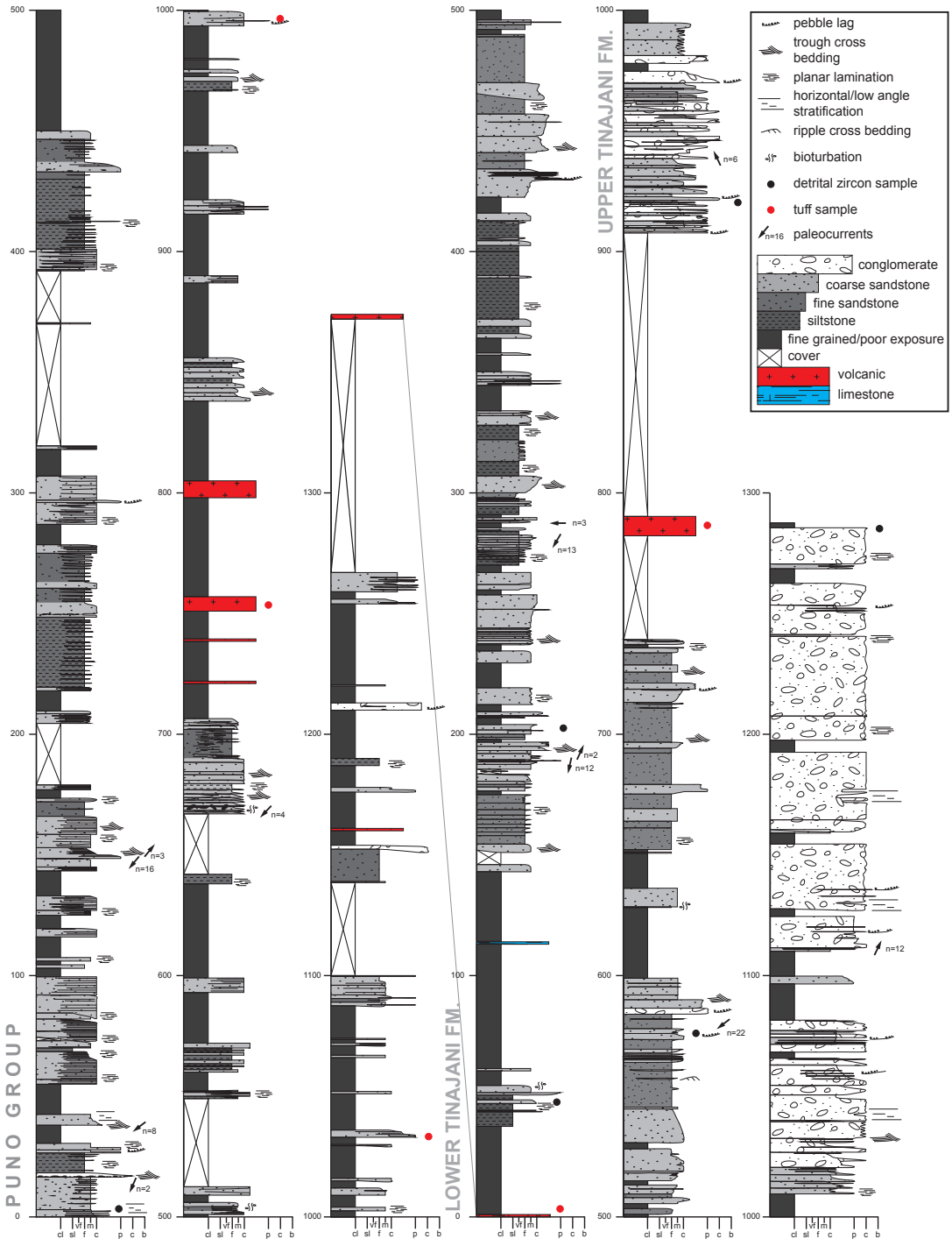
PUNO GROUP
LOWER TINAJANI FM.
UPPER TINAJANI FM.
pebble lag
trough cross bedding
planar lamination
horizontal/low angle stratification
ripple cross bedding
bioturbation
detrital zircon sample
tuff sample
paleocurrents
conglomerate
coarse sandstone
fine sandstone
siltstone
fine grained/poor exposure
cover
volcanic
limestone
cl sl f c p c b
vf m

Figure 1.5. Composite measured section showing lithofacies and sedimentary structures of the Ayaviri basin. The lower interval (section 1, Puno Group) disconformably overlies the Cretaceous Muni Formation east of Ayaviri. The upper interval (section 2, Lower and Upper Tinajani Formations) is conformable with underlying Puno Group, correlated by the trachybasalt flow.

The ~2700 m thick Oligocene-Miocene Puno Group and Lower/Upper Tinajani Formations [*Carlotto,* 2013] preserved in the Ayaviri basin (Figure 5) [*Flores and Rodriguez,* 1999; *Rousse et al.,* 2005] can be summarized as follows. The lower ~2300 m (Puno Group and Lower Tinajani Formation) is interpreted as deposits of a sand-dominated braided and meandering fluvial system, characterized by high width to thickness ratios. The upper ~400 m (Upper Tinajani Formation) is characterized by an abrupt change to thick pebble-boulder conglomerates representing sheetflood, debris flow and streamflow deposition on an alluvial fan. Below are summaries of the key lithofacies, lithofacies assemblages, and interpreted depositional environments (Figure 6 a-j; Table 1). Despite changes in provenance and depositional environments, many of the deposits exhibit sheetlike geometries characteristic of other Altiplano basins [*Hampton and Horton,* 2007].

5.1. Lower section: Fluvial channel and floodplain deposits

The lower ~2300 m is composed of numerous ~1-10 m thick upward-fining intervals. Sandstones are typically tabular and laterally widespread (tens to hundreds of meters), with minor lenticular sandstones. Fine-grained intervals are poorly exposed, with limited carbonates and paleosol horizons. This lower section is interpreted to be deposited in a sand-dominated braided fluvial system transitioning upsection to isolated anastomosing channels with localized carbonate-producing lakes developed in overbank settings. The lower section also preserves growth strata (~750-1050 m level) associated with motion along the southwest-directed Ayaviri backthrust (Figure 4a, b).

Table 1.

Facies Association	Lithofacies	Description	Interpretation
F1: Thinly interbedded mudstone, fine sandstone	Fl	Structureless, planar laminated, ripple-cross laminated, minor bioturbation and soft sediment deformation; contains C1, S3	Fluvial overbank floodplain deposition
S1: Tabular medium, coarse sandstone	Sh, Sl, Sm, Sp, St	Structureless, subhorizontal, low-angle stratified sheetlike sandstone; lack scour; fine upwards; isolated, dispersed pebbles; 0.5-2 m thick	Sandy braided river plain
S2: Lenticular medium, coarse sandstone	Sp, St, Ss, Gt	Associated with S1 facies; planar, trough-cross stratified sandstones; minor scouring; occasional basal pebble lag; lenticular profile; <1m thick	Sandy channel fill with pebble lags in braided river
S3: Lenticular fine-medium sandstone	Sp	Lenticular, planar-cross stratified sandstone; encased in F1.	Anastomosing river
S4: Cross-stratified coarse sandstone, pebble conglomerate	St, Gt, Sp, Gp	Well organized trough-cross stratified coarse sandstone; pebble lag common; sharp base, top; 1-2 m scouring; lateral interfingering with G3	Coarse channel fill on alluvial fan
G1: Cross-stratified pebble conglomerates	Gp	>1m tall planar-cross strata, lenticular profile contained within facies S1	Pebbly main channel fill in braided river
G2: Poorly bedded conglomerates	Gms, Gm	Disorganized; thickly bedded > 5m; elevated coarse clasts at bed tops; diffuse or sharp bedding contacts; basal reserves grading; mostly no grain size trends; sometimes multiple upward coarsening, fining 5–10 cm cycles;	Surging debris flow on alluvial fan

Table 1 (continued).

G3: Sheetlike conglomerates and sandstones	Gm, Gh, Sh	Structureless, planar laminated, horizontally stratified thick sandstone, conglomerate couplet sheets; may fine or coarsen up; rare clast imbrication	Sheetflood on alluvial fan
C1: Thin carbonate, pedogenically altered sandstone	C, P, Fr	Bioturbated red marl grading upsection to structureless white micritic limtestone; sharp based carbonates interbedded with siltstones containing carbonated nodules	Ponded lacustrine and subaerially exposed floodplain

5.1.1. Tabular sandstones (S1):

Tabular medium- to coarse-grained sandstones are common throughout the lower section. The subhorizontal to low-angle (<10°) stratified beds are 0.5-2 m thick, persist laterally for hundreds of meters and gradually taper and pinch out. These sheet sandstones often appear structureless but may contain planar or trough-cross laminations. Isolated and dispersed pebbles suggest dominantly sand with minor gravel bedload. Most sandstone packages lack significant basal scour and often fine upwards. We interpret these laterally persistent, often structureless sandstones as longitudinal bars. Miall [1977] suggested that sediment transport in structureless braided fluvial bars occurred in planar sheets possibly at high flow regime. Overall these tabular, sheetlike sandstones with high width to depth ratios are interpreted as braided fluvial deposits [Smith, 1974; Miall, 1977; Rust, 1978].

5.1.2. Lenticular sandstones (S2):

Lenticular medium- to coarse-grained sandstones are less common, but associated with the laterally persistent tabular sandstones described above. They are ~0.5-1 m thick, well-bedded, with planar to trough-cross stratification, lenticular profiles, and scoured

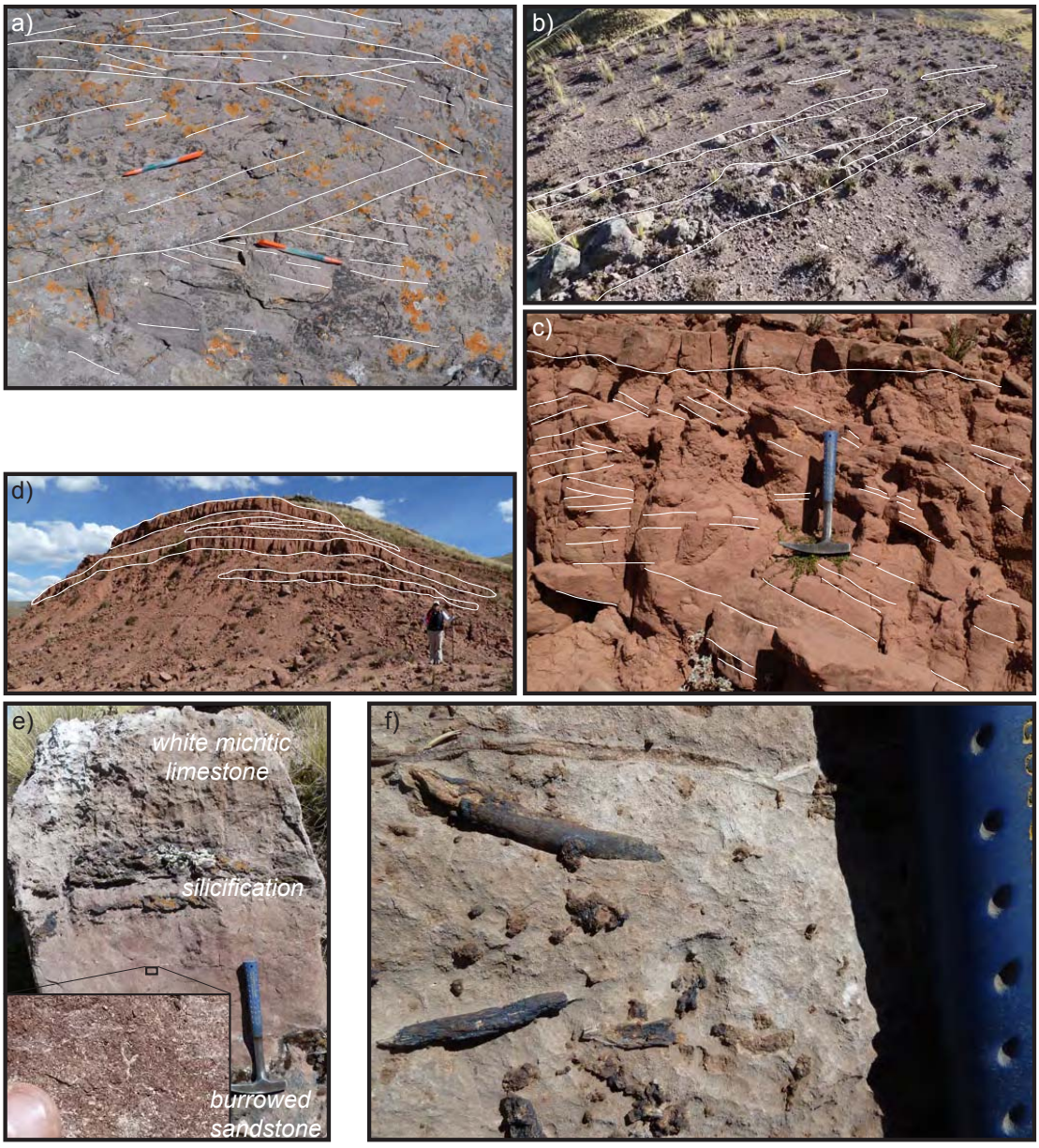
a)
b)
c)
d)
e)
white micritic limestone
silicification
burrowed sandstone
f)

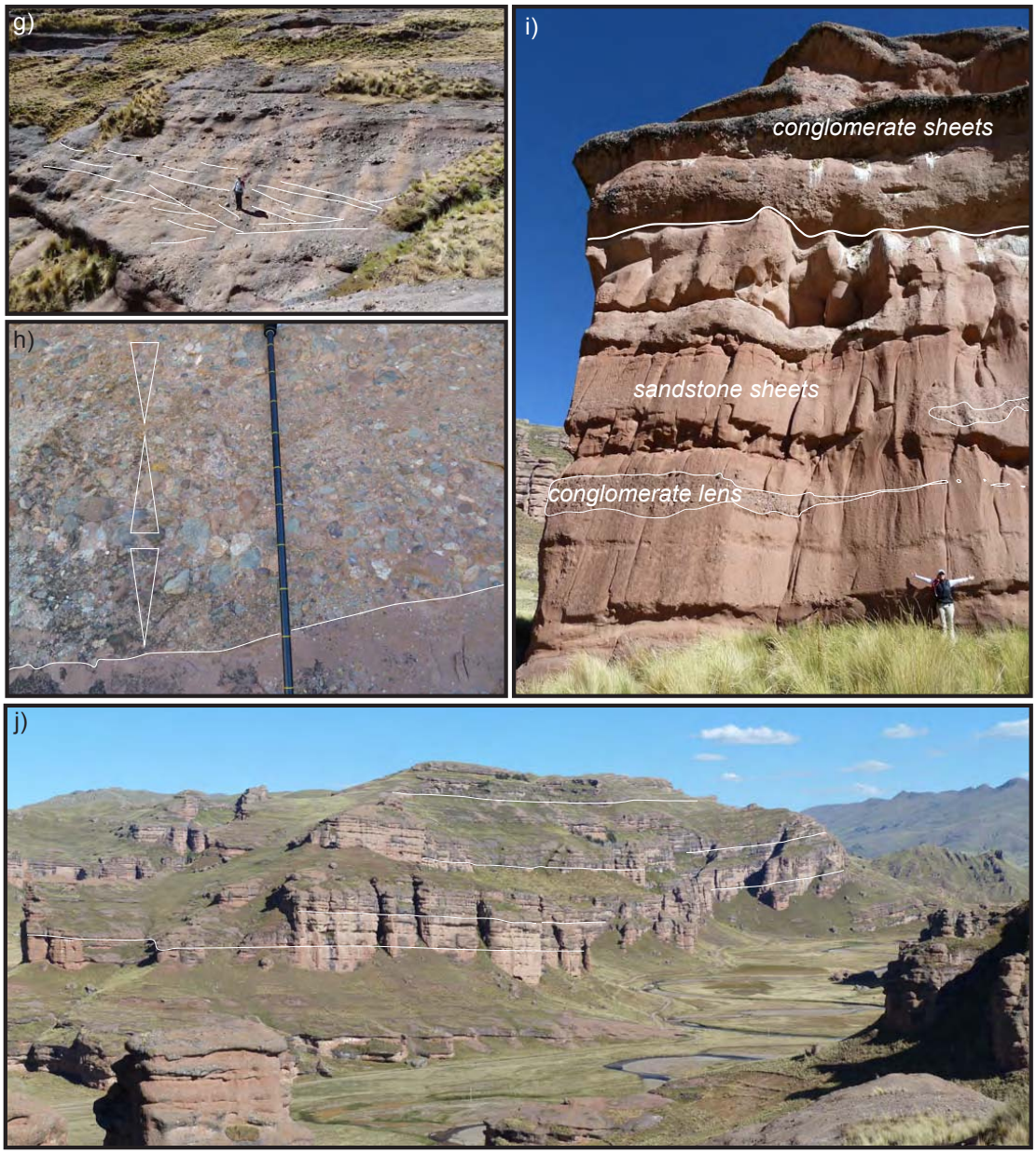
g)
h)
i)
conglomerate sheets
sandstone sheets
conglomerate lens
j)

Figure 1.6. Photos of lithofacies and stratigraphic units from the lower ~2300 m sandstone-dominated section (Puno Group-Lower Tinajani Formation, photos a-f) and upper ~400 m conglomeratic section (Upper Tinajani Formation, photos g-j) of the Ayaviri basin. a) Cross-stratified, medium- to coarse-grained lenticular sandstones interpreted as braided channel fill. Pens for scale. b) Interbedded medium sandstones (white outline) and siltstones representing overbank deposits. Hammer for scale. c) Planar cross-stratified fine- to medium-grained sandstones filling d) anastomosing sandstone channels encased in fine siltstone. e) Lacustrine deposits with gradational contact between red-brown burrowed sandstone below and white micritic limestone, separated by discontinuous chert. f) Fossils preserved in limestone. g) Cross-bedded coarse sandstone and pebble-boulder conglomerate interpreted as deposits in an alluvial fan setting. Person for scale. h) Clast-supported pebble-boulder conglomerates from surging debris flow deposits. Note sharp non-erosional base (white line) and multiple fining- and coarsening-upwards cycles (denoted by white triangles). Jacob staff divisions are 10 cm. i) Laterally continuous pebble-boulder conglomerate and coarse sandstone beds interpreted as sheetflood deposits on an alluvial fan. Person for scale. j) Laterally continuous conglomerate and sandstone sheets of the Upper Tinajani Formation exposed in Tinajani Canyon. For scale, river elevation ~3950 m, ridgetop elevation ~ 4210 m.

bases with occasional basal pebble lags. The lack of lateral accretion surfaces and presence of lenticular geometries are consistent with channel fill in a braided fluvial system (Figure 6a) [*Miall,* 1977].

5.1.3. Interbedded mud- and sandstones (F1):

Thinly interbedded mudstones and sandstones are common, occurring in ~0.5-10 m packages that are often poorly exposed and likely constitute most of the measured covered intervals. Where well exposed, the silt- and mudstones show mm- to cm-scale planar and ripple-cross laminations with mud drapes, minor bioturbation, and minor small-scale soft-sediment deformation. Interbedded are thin (<0.2m), lenticular, structureless, planar and ripple laminated sandstones. Within the slope-forming mudstone intervals are 10 to 100 cm beds of massive carbonate mudstone and possible pedogenic horizons defined by small calcrete nodule development, color mottling and faint thin vertical features interpreted as possible root traces. Collectively, these intervals are interpreted as overbank deposits in broad fluvial floodplains with associated short-term lacustrine environments [Miall, 1977; Miall, 1978].

5.1.4. Carbonates (C1):

Thin carbonate and pedogenically altered sandstones are laterally restricted to less than a few hundred meters and commonly thinner than 1 m. They are preserved in association with overbank deposits. Carbonates lack lamination. Those with sharp bases are tabular in shape and found above fine sandstone and siltstones. Other carbonates may have diffuse bases, gradationally transitioning vertically over ~1 m thickness from structureless red-brown marly sandstone to pure carbonate (Figure 6e). Carbonates and associated sandstones may preserve thin, faint, lightly colored traces interpreted as bioturbation (Figure 6e inset). The change from underlying burrowed red-brown

sandstone below to white micritic limestone above may have a discontinuous, bedding parallel thin nodular chert layer. *Platt* [1989] interpreted similar deposits as ponded lacustrine environments in a distal floodplain. Silicification is interpreted as evidence for evaporative conditions. Carbonates are generally fossil poor macroscopically, but preserve rare twigs (Figure 6f). Some structureless fine sandstones and siltstones within overbank deposits preserve mottled textures and vertically elongated carbonate nodules [*Leeder,* 1975; *Nijman and Puigdefabregas,* 1978]. These are interpreted as rhysoliths, and the lack of bedding is interpreted as a result of bioturbation. These zones themselves are interpreted as pedogenically altered, suggesting incipient soil formation and subaerial exposure. We interpret these beds as lacustrine deposits and pedogenic zones that developed in fluvial overbank and floodplain environments that experienced subaerial exposure and periodic inundation [*Miall,* 1978; *Platt,* 1989].

5.1.5. Isolated lenticular sandstones (S3):

Lenticular medium-grained sandstones are distinguished from the aforementioned lenticular sandstone facies by their isolated occurrence within siltstone-dominated intervals rather than an association with sheetlike sandstone bodies and the presence of numerous 10-30 cm thick cross stratification. These lenticular sandstones are typically observed near the top of the Lower Tinajani Formation. The macroform of these sandstones encased in fine-grained intervals at first suggests isolated meandering channel bodies. However, the numerous inclined surfaces are different from the epsilon shaped cross stratification typical of meandering streams [*Puigdefabregas and Van Vilet,* 1978]. These isolated channel bodies appear to have filled by dune migration, where the channels remained stationary until they were completely filled. We interpret these

stationary channels lacking the hallmarks of meandering rivers as anastomosing rivers [*Hampton and Horton,* 2007] (Figure 6 c, d).

5.1.6. Lenticular pebble conglomerates (G1):

Cross-stratified pebble conglomerates are confined to the Puno Group at the base of the section. Pebbles are well rounded and commonly well organized along >1m tall planar cross strata. They are lenticular in profile and interbedded or contained within the coarse-grained tabular sandstones facies (S1). Large scale cross stratification suggests the passage of coarse gravel bars. We interpret these deposits as main channel body fill within a braided fluvial network [*Miall,* 1977; *Miall,* 1978].

5.2. Upper section: Alluvial fan deposits

The ~400 m Upper Tinajani Formation, exposed in Tinajani Canyon, contains substantially coarser material, including thick-bedded (1-5 m) cobble to boulder conglomerates interpreted as alluvial fan deposits. This upper interval preserves growth strata (~2300-2500 m level) associated with motion along the northeast-directed Pasani fault.

5.2.1. Sheetlike sandstones (S4):

Cross-bedded coarse-grained sandstones and pebble conglomerates are well organized, with cross beds defined by pebble-cobble lags. Packages are well stratified with generally sharp bases and tops. Cross beds can be > 1 meter tall. Packages generally exhibit > 1 m of scouring into underlying strata. Laterally these deposits interfinger with planar laminated or structureless thickly bedded sandstones and conglomerates with sheetlike geometries. These deposits are interpreted as incised channels filled with pebble

lags on an alluvial fan (Figure 6g) [*Puigdefabregas and Van Vilet,* 1978; *Blair and McPherson,* 1994].

5.2.2. Disorganized conglomerates (G2):

Disorganized, poorly bedded pebble-boulder conglomerates occur throughout the upper succession. Beds up to ~5 m thick may be either clast or matrix supported, with the largest clasts sometimes protruding above the upper bed surfaces. Clasts are often poorly sorted, except along sharp basal contacts with limited or no scour that express thin zones of reverse grading and localized shear [*Nemec and Steel,* 1984]. Diffuse bedding contacts are common. Some individual packages contain multiple upward coarsening and fining cycles, suggesting amalgamation of multiple depositional events. Most show no grain size trend, but some may fine or coarsen upwards. This facies is interpreted as debris flow deposits on a alluvial fan, with surging debris flows recording brief alternating periods of waning and intensified flow evidenced by multiple upward fining and coarsening variations in a single package (Figure 6h) [*Nemec and Steel,* 1984; *Blair and McPherson,* 1994; *Hartley et al*., 2005]

5.2.3. Sheetlike conglomerates (G3):

Sheetlike pebble-boulder conglomerates and coarse-grained sandstones occur throughout the upper succession and are distinguished by their large lateral extent over 1000 m. They are up to ~5 m thick, and are better organized than the aforementioned debris flow deposits and contain rare clast imbrication. Upper and lower bed contacts are commonly irregular and scoured with common internal horizontal stratification, although faint and poorly developed. The beds exhibit limited internal sorting and either fine or coarsen upwards. Conglomeratic lenses within the larger sandstone sheets tend to display better developed cross-bedding than surrounding beds [*Wells,* 1984]. These are similar to

the gravel-sandstone couplets of *Blair and McPherson* [1994] and *Hartley et al.,* [2005] interpreted as sheetflood deposits typical of alluvial fan environments (Figure 6i, j). These better organized conglomerates can be found in close association with the disorganized conglomerate (G2) facies, suggesting coexisting or alternating events of stream and debris flow processes.

6. SEDIMENT PROVENANCE

6.1. Conglomerate clast compositions and paleocurrents

Conglomerate clasts were counted at 19 stratigraphic levels throughout the upper ~1700 m of section (Figure 7). At lower levels, only two horizons in the Lower Tinajani Formation contained sufficiently large clasts to identify clast lithologies. Both clast counts are dominated by sandstone, chert, siltstone, and quartzite lithologies, with only one volcanic clast observed. These lithologies are commonly observed in the Paleozoic succession exposed in the hanging wall of the Ayaviri thrust and other Paleozoic and Mesozoic units exposed in the Eastern Cordillera. Other isolated clasts or conglomeratic pebble lags observed throughout the section matched these clast count stations, but lacked sufficient clasts ($n < 100$) for a station. Paleocurrent measurements, although limited, show that the lower ~2.3 km of section (Puno Group and Lower Tinajani Formation) had generally southwest-directed paleoflow.

At higher levels, 17 clast counts for the conglomeratic Upper Tinajani Formation (Figure 7) reveal a mix of extrusive, intrusive, limestone and sedimentary rock clasts, in marked contrast to clast compositions of lower stratigraphic levels. Although no significant upsection trends are observed within the Upper Tinajani Formation clast

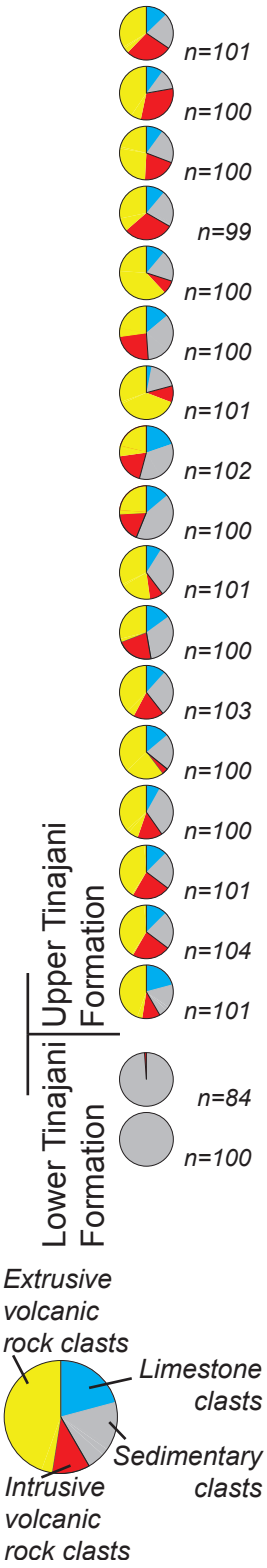
n=101
n=100
n=100
n=99
n=100
n=100
n=101
n=102
n=100
n=101
n=100
n=103
n=100
n=100
n=101
n=104
n=101
n=84
n=100
Upper Tinajani Formation
Lower Tinajani Formation
Extrusive volcanic rock clasts
Limestone clasts
Sedimentary clasts
Intrusive volcanic rock clasts

Figure 1.7. Clast count stations results. Note change in clast composition between the Lower and Upper Tinajani Formation.

compositions, the igneous clasts are common throughout the Western Cordillera and a local source of carbonate is present in mapped Cretaceous rocks in the proximal hanging wall of the Pasani thrust. The Upper Tinajani Formation had very limited paleoflow indicators, but data suggest transport directed towards the north-northeast. Therefore, we interpret the Upper Tinajani Formation shift in clast composition as evidence for a shift from Eastern Cordillera provenance to a dominant sediment source in the Western Cordillera.

The clast count and paleocurrent data suggest that the lower ~2.3 km of section was sourced from the Eastern Cordillera, and transported generally towards the southwest. In contrast, the ~400 m Upper Tinajani Formation conglomerates and paleocurrents suggest sediment was sourced from the immediate Pasani fault hanging wall and Western Cordillera and transported generally towards the north.

6.2. Sandstone petrographic compositions

Fourteen petrographic thin section samples were analyzed using the Gazzi-Dickinson point-counting method to characterize the framework grain assemblage variability throughout the succession [*Dickinson and Suczek,* 1979]. Thin sections were stained for potassium and calcium feldspars. At least 300 sand grains (>0.0625 mm) per sample were counted.

Figure 8 shows the point-count results for all 14 samples from the succession. Results are summarized in table 3 and in three ternary diagrams: Q-F-L, (total quartz, feldspar and lithic grains; Figure 8a); Qm-P-K, (monocrystalline quartz, calcium plagioclase, potassium feldspar; Figure 8b); Qp-Lv-Ls, (polycrystalline quartz, volcanic lithics, sedimentary lithics; Figure 8c) [all diagrams after

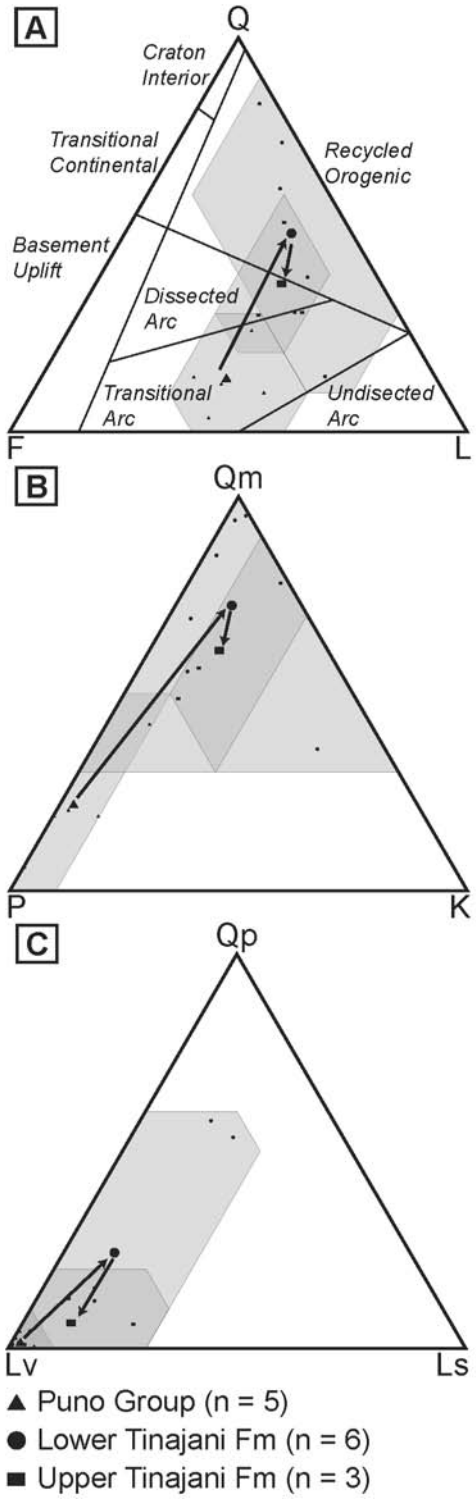
A
Q
Craton Interior
Transitional Continental
Recycled Orogenic
Basement Uplift
Dissected Arc
Transitional Arc
Undisected Arc
F
L
B
Qm
P
K
C
Qp
Lv
Ls
▲ Puno Group (n = 5)
● Lower Tinajani Fm (n = 6)
■ Upper Tinajani Fm (n = 3)

Figure 1.8. Point count results from 14 thin sections from the Ayaviri basin. Provenance results reveal an upsection trend from transitional arc to recycled orogenic to dissected arc sources for the Puno Group, Lower Tinajani Formation and Upper Tinajani Formation, respectively.

Table 3.

		Q F L %			Qm F Lt %			Qm P K %			Qp Lv Ls %		
Sample	**Unit**	Q	F	L	Qm	F	Lt	Qm	P	K	Qp	Lv	Ls
220510-03	Puno Group	12.3	47.6	40.1	12.3	47.6	40.1	20.5	77.0	2.5	0.0	94.4	5.6
220510-07	Puno Group	13.9	52.8	33.3	12.5	53.6	33.8	19.0	81.0	0.0	4.3	95.7	0.0
220510-08	Puno Group	3.6	54.6	41.7	3.6	54.6	41.7	6.3	93.8	0.0	0.0	100.0	0.0
220510-10	Puno Group	10.1	38.8	51.1	9.2	39.1	51.6	19.0	70.7	10.2	1.9	98.1	0.0
220510-11	Puno Group	25.7	34.2	40.1	25.2	34.4	40.4	42.2	48.3	9.4	1.7	96.7	1.7
240510-05	Lower Tinajani Formation	14.1	23.9	62.0	13.6	24.1	62.3	36.1	14.8	49.2	1.0	96.0	3.0
TC034	Lower Tinajani Formation	39.2	15.2	45.6	35.9	16.0	48.1	69.1	25.9	4.9	12.1	75.2	12.8
240510-08	Lower Tinajani Formation	83.2	3.7	13.1	80.7	4.2	15.1	95.0	0.9	4.1	53.5	23.9	22.5
TC038	Lower Tinajani Formation	30.4	22.4	47.2	28.8	22.9	48.3	55.8	33.3	10.9	4.4	93.1	2.5
240510-10	Lower Tinajani Formation	73.3	3.7	23.0	68.5	4.4	27.1	94.0	3.8	2.2	57.7	26.9	15.4
TC045	Lower Tinajani Formation	61.7	10.0	28.3	59.9	10.5	29.6	85.1	12.3	2.6	15.3	73.5	11.2
240510-13	Upper Tinajani Formation	52.9	13.5	33.6	50.6	14.2	35.2	78.1	1.8	20.1	12.6	80.6	6.8
TC072	Upper Tinajani Formation	29.5	30.7	39.8	29.3	30.8	39.9	48.7	38.9	12.4	0.8	99.2	0.0
TC076	Upper Tinajani Formation	30.2	20.8	49.0	28.0	21.5	50.5	56.5	30.4	13.0	6.1	69.6	24.3

Dickinson and Suczek, 1979). Photomicrographs of the various observed lithic fragments are presented after the conclusions (Figure 18). Results are shown for both individual samples and the average composition of each the Puno Group, Lower Tinajani Formation and Upper Tinajani Formation. The average Puno Group composition ($Q_{13}F_{46}L_{41}$) is dominated by generally equal contributions of feldspars and lithic fragments, with subordinate quartz contributions, consistent with erosion of a transitional arc source. The average Lower Tinajani Formation composition ($Q_{50}F_{13}L_{37}$) is consistent with a recycled orogenic source. It is typified by decreased contributions from feldspars. Quartz and lithic fragment content varies considerably throughout this formation, with compositions spanning recycled orogenic and arc sources. The average composition of the Upper Tinajani Formation ($Q_{37}F_{22}L_{41}$) has a lithic fragment contribution similar to the Puno Group, yet has higher quartz contributions and lower feldspar contributions than the Puno Group. Sandstone compositions from the Upper Tinajani Formation suggest erosion of a dissected arc.

7. U-PB GEOCHRONOLOGY

7.1. Methods.

Zircon U-Pb results are presented for 23 samples to constrain both maximum depositional ages and sediment provenance, including 10 Cenozoic sandstones and 8 volcanic tuffs from the Ayaviri basin and five Paleozoic-Mesozoic sandstones from the adjacent Eastern Cordillera. After crushing, water table, heavy liquid and magnetic separation of zircon grains from the sandstones and tuffs, U-Pb geochronologic laser-ablation-multicollector inductively coupled plasma-mass-spectrometry (LA-MC-ICPMS)

analyses were conducted at the University of Arizona LaserChron center [*Gehrels,* 2000, *Gehrels et al*., 2008].

Approximately 120 individual zircon grains ranging between 30-100 μm were randomly analyzed from each sandstone sample. Parts of grains with cracks or inclusions were not ablated. Sri Lankan zircon crystals with a known age of 564 ± 4 Ma (2σ error) were used as standards every fifth measurement to correct for intra- and interelement fractionation. Resulting uncertainties were commonly 1-2% (2σ error) for both $^{206}Pb/^{238}U$ and $^{206}Pb/^{207}Pb$ ages. Additional details regarding methods for conducting analyses are presented by *Gehrels et al*., [2008]. Reported ages represent $^{206}Pb/^{238}U$ ages for zircon grains younger than 1000 Ma and $^{206}Pb/^{207}Pb$ ages for zircon grains older than 1000 Ma. Grain analyses with >30% discordance, >5% reverse discordance or >10% uncertainty were discarded from further evaluation and interpretation.

7.2. U-Pb detrital zircon provenance

7.2.1. Potential zircon sources:

To characterize the potential detrital contributions from the Eastern Cordillera, we conducted LA-MC-ICPMS analyses of detrital zircon grains from five new sandstone samples representing Ordovician, Carboniferous, Permo-Triassic, and Cretaceous units (Figure 9). Although several key U-Pb age populations allow discrimination of potential zircon sources, other populations are non-diagnostic, as they are shared by multiple samples (e.g., ~1000 Ma Sunsas/Grenville), suggesting long-lived zircon grains and protracted sediment recycling throughout the Phanerozoic. Key age populations are highlighted: Cratonic (1500-2500 Ma), Sunsas/Grenville (900-1200 Ma), Pampean-Braziliano (500-700 Ma), Famatinian (400-500 Ma), Permo-Triassic (200-300 Ma) and

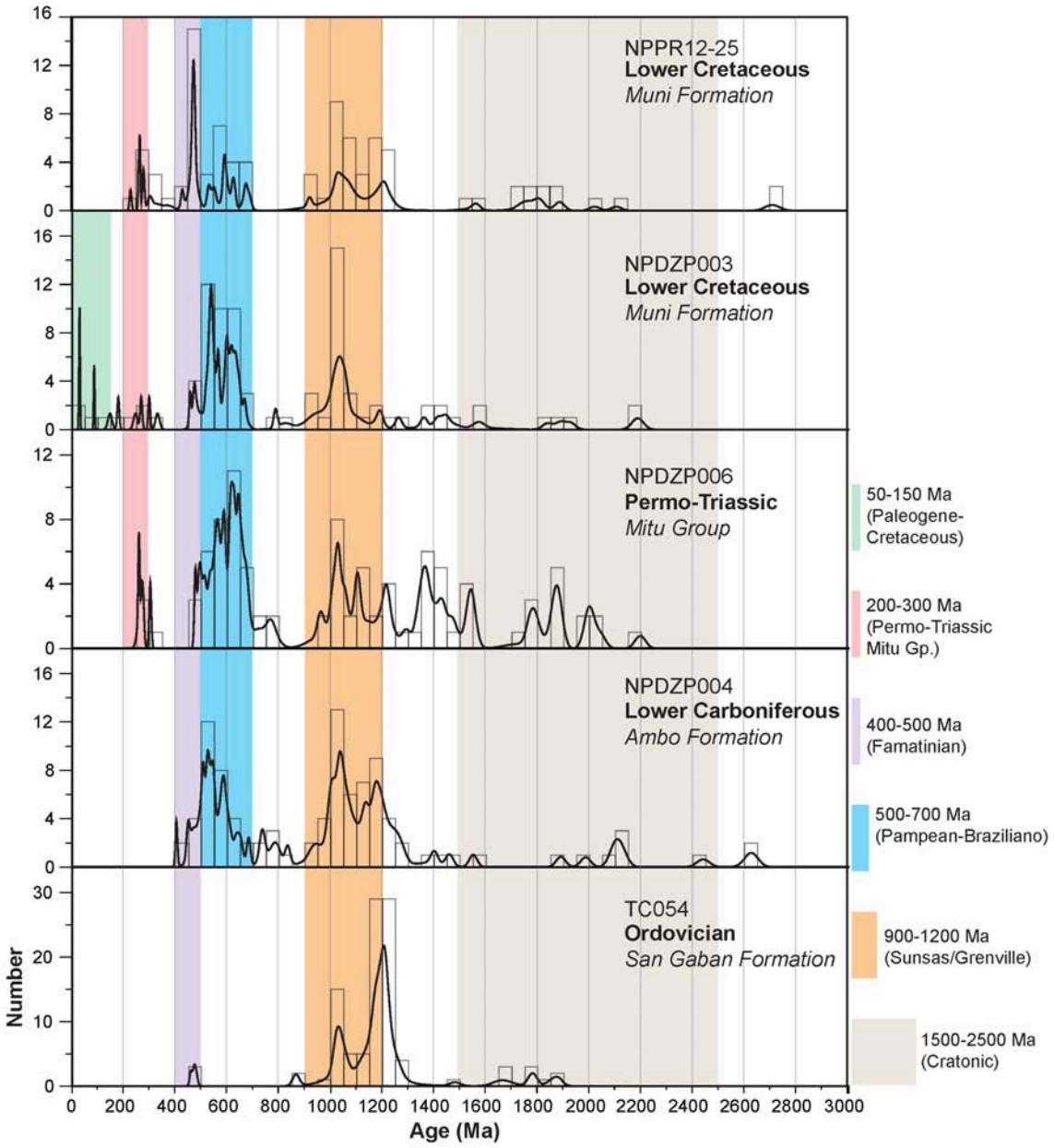
NPPR12-25
Lower Cretaceous
Muni Formation
NPDZP003
Lower Cretaceous
Muni Formation
NPDZP006
Permo-Triassic
Mitu Group
NPDZP004
Lower Carboniferous
Ambo Formation
TC054
Ordovician
San Gaban Formation
Number
Age (Ma)
50-150 Ma (Paleogene-Cretaceous)
200-300 Ma (Permo-Triassic Mitu Gp.)
400-500 Ma (Famatinian)
500-700 Ma (Pampean-Braziliano)
900-1200 Ma (Sunsas/Grenville)
1500-2500 Ma (Cratonic)

Figure 1.9. U-Pb age histograms (black bars) and probability density functions (red curves) depicting detrital zircon geochronologic results for five pre-Cenozoic sandstone samples from the Eastern Cordillera of southern Peru. Sample locations from Figure 2. Samples presented in stratigraphic order (oldest at base), with each histogram bin spanning 50 Myr and variable vertical axes based on number of zircon grains. Used to compare age spectra with Cenozoic Ayaviri basin detrital zircon samples shown in Figure 10. The presence of similar age populations in multiple samples suggests significant recycling. Note the paucity of Cretaceous zircons in the two Cretaceous samples.

Eocene-Cretaceous (50-150 Ma). Cratonic, Sunsas/Grenville and Famatinian age populations are found in all samples. Famatinian zircons are found in all samples except the Ordovician San Gaban Formation (TC054). Permo-Triassic zircons are found in the Permo-Triassic and both Cretaceous samples (NPDZP006, NPDZP003, NPPR12-25). Cretaceous zircon populations are relatively rare in the source samples from the Eastern Cordillera, with n=3 Cretaceous zircons for Cretaceous sample NPDZP003 and none for Cretaceous sample NPPR12-25.

7.2.2. Cenozoic basin-fill samples:

U-Pb results are presented for ten Cenozoic sandstone samples from the Ayaviri basin (Figure 10). See Figure 17 for these samples displayed as kernel density estimation plots [*Vermeesch,* 2012]. The five lowest samples include NPPR12-20 from the base of the measured section (Figure 5), and four overlying samples (220510-07, 220510-08, 220510-10 and 220510-11) collected ~26 km along strike north of Ayaviri in growth strata along the Ayaviri backthrust (Figure 4). Stratigraphically above the trachybasalt flow at Cerro Ocuro (1372 m level in measured section, Figure 5; sample TC052 in Figure 11) are the upper five samples (240510-05, 240510-08, 240510-10, 240510-13, and TC076).

All of the Cenozoic sandstone samples contain contributions from Phanerozoic and Proterozoic zircon populations. Because samples 220510-07 and 220510-08 are dominated by Cenozoic zircons ($n > 70$) and have limited ($n \leq 30$) pre-Cenozoic zircons, the associated provenance interpretations are made with caution, as the statistical probability of representing all older zircon age populations in these two samples is relatively low [*Vermeesch,* 2004]. Several Precambrian to lower Paleozoic populations are present in nearly all basin-fill samples, including: older cratonic ages (>1.2 Ga);

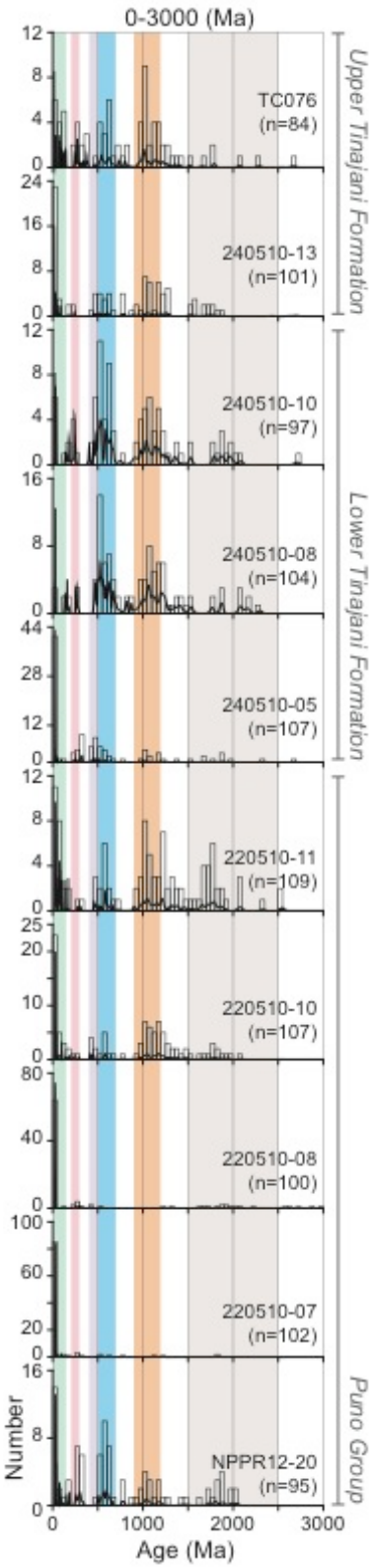
0-3000 (Ma)
TC076
(n=84)
240510-13
(n=101)
240510-10
(n=97)
240510-08
(n=104)
240510-05
(n=107)
220510-11
(n=109)
220510-10
(n=107)
220510-08
(n=100)
220510-07
(n=102)
NPPR12-20
(n=95)
Upper Tinajani Formation
Lower Tinajani Formation
Puno Group
Number
Age (Ma)
0
1000
2000
3000

Figure 1.10. U-Pb age histograms (black bars) and probability density functions (black curves) depicting detrital zircon geochronologic results for 10 sandstone samples from Oligocene-Miocene fill of the Ayaviri basin. Samples presented in stratigraphic order (oldest at base), with each histogram bin spanning 50 Myr and variable vertical axes based on number of zircon grains. Color bars highlight the presence of age populations considered to be significant ($n \geq 3$ per histogram bin). Same color bar key as figure 9.

Sunsas/Grenville ages (1-1.2 Ga); and Braziliano (~700 Ma) through Pampean ages (~500 Ma). Other populations, however, show significant variability among basin-fill samples, including: Famatinian (400-500 Ma), Eocene-Cretaceous (50-150 Ma), and Cenozoic (50-15 Ma) populations. Upsection variations in detrital zircon age spectra provide insight into changes in sediment provenance associated with shifts in relative topography, drainage patterns, and/or basin architecture, and are summarized below.

7.2.3. Cretaceous zircons:

Six of the 10 basin-fill samples from the Puno Group and Upper Tinajani Formations have significant ($n \geq 3$) Cretaceous age populations (Figure 10). Such populations are relatively rare in the source samples from the Eastern Cordillera (Figure 9), with n=3 Cretaceous zircons among both Cretaceous samples. Although limited Cretaceous intrusive units are found in the Eastern Cordillera, the most significant sources of Cretaceous zircons are volcanic-arc rocks of the Western Cordillera [e.g., Chocolate and Toquepala arcs, *Mamani et al.,* 2010]. We interpret the presence of Cretaceous zircons in the Puno Group and Upper Tinajani Formation as evidence for delivery of sediment either from the Western Cordillera, or reworked from Cenozoic deposits that have been eroded from the Eastern Cordillera.

7.2.4. Famatinian zircons:

Famatinian (~400-500 Ma) zircon populations are absent from the lowest two samples but are significant ($n > 3$) in the next 7 samples, and absent from the uppermost sample. *Bahlburg et al.,* [2011] show that most Ordovician volcanic and sedimentary rocks in Peru are found in the Eastern Cordillera. Isolated Ordovician intrusions in the Arequipa Massif [*Loewy et al.,* 2004], or in the Marañon Massif [*Ramos,* 2009]. We interpret the appearance and persistence of this age population throughout deposition of

the Puno Group, Lower Tinajani Formation and basal Upper Tinajani Formation as evidence for likely delivery of sediment from the Paleozoic rocks found in the Eastern Cordillera which contain a presence of Famatinian zircons, or less likely from isolated Ordovician intrusions in the Arequipa Massif, or from Ordovician intrusions found in the Marañon Massif hundreds of kilometers to the northwest.

7.3. U-Pb depositional age constraints

Continuous arc magmatism during the Cenozoic in southern Peru [*Mamani et al.*, 2010] suggests the potential for a steady supply of syndepositional volcanic zircons throughout the basin accumulation history. Accordingly, young zircon U-Pb ages are expected to be present in not only sampled tuffs but also in the detrital component of sampled sandstones. The U-Pb results (Figure 11) provide critical new geochronological constraints for the measured sections, including delineation of young detrital zircon age populations and volcanic tuff zircon populations. The following text highlights the important horizons for establishing the chronostratigraphic framework for the Ayaviri basin.

At the base of the measured section, ~30 m above the contact with the underlying Cretaceous Muni Formation, a sandstone sample (NPPR12-20) from the Puno Group yields a youngest zircon U-Pb age population of 29.6 ± 1.2 Ma (n = 15). At the ~750-1050 meter levels are the three lowest samples of interbedded volcanic horizons found in the Puno Group within the Ayaviri backthrust growth strata east of Ayaviri (Figure 4a; Figure 3 location). These three volcanic ages are 28.06 ± 0.82 Ma, 27.56 ± 0.50 Ma and 27.06 ± 0.88 Ma (samples 020611-01, 020611-03, 020611-04 respectively). Four sandstone samples (220510-07, 220510-08, 220510-10, 220510-11) from the equivalent

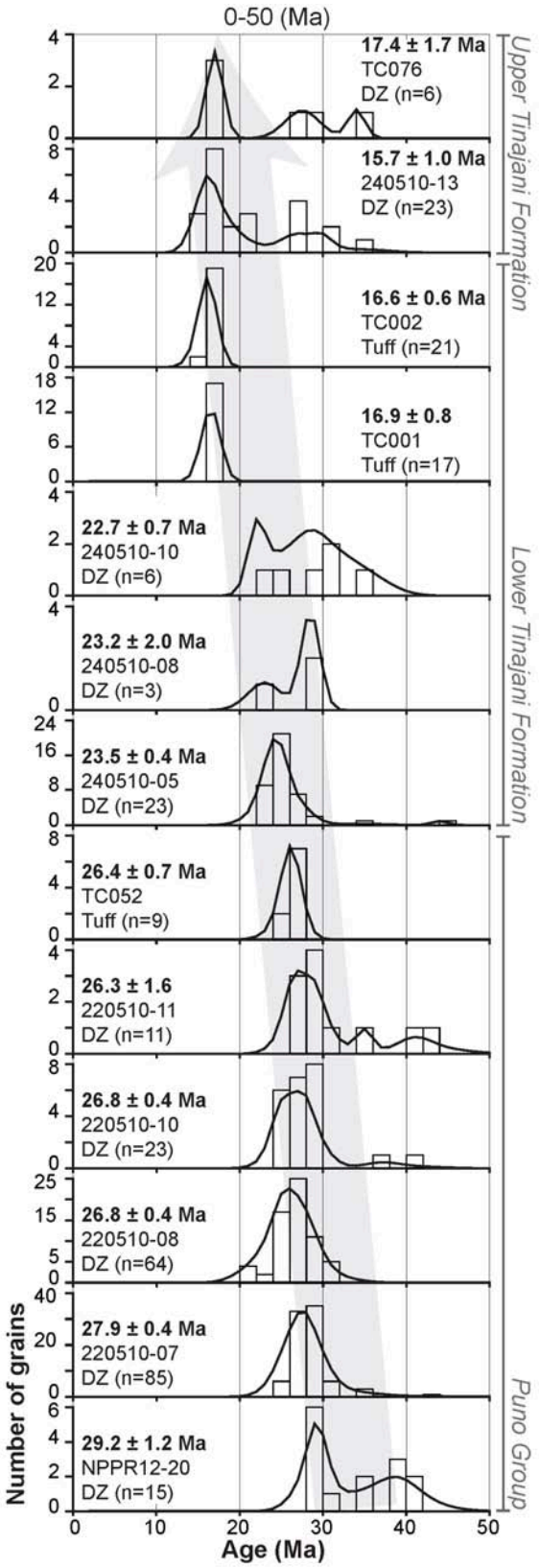
0-50 (Ma)
17.4 ± 1.7 Ma
TC076
DZ (n=6)
15.7 ± 1.0 Ma
240510-13
DZ (n=23)
16.6 ± 0.6 Ma
TC002
Tuff (n=21)
16.9 ± 0.8
TC001
Tuff (n=17)
22.7 ± 0.7 Ma
240510-10
DZ (n=6)
23.2 ± 2.0 Ma
240510-08
DZ (n=3)
23.5 ± 0.4 Ma
240510-05
DZ (n=23)
26.4 ± 0.7 Ma
TC052
Tuff (n=9)
26.3 ± 1.6
220510-11
DZ (n=11)
26.8 ± 0.4 Ma
220510-10
DZ (n=23)
26.8 ± 0.4 Ma
220510-08
DZ (n=64)
27.9 ± 0.4 Ma
220510-07
DZ (n=85)
29.2 ± 1.2 Ma
NPPR12-20
DZ (n=15)
Upper Tinajani Formation
Lower Tinajani Formation
Puno Group
Number of grains
Age (Ma)

Figure 1.11. U-Pb age histograms (black bars) and probability density functions (black curves) depicting geochronologic results (0-50 Ma) for all 10 detrital zircon ("DZ") sandstone samples and three interbedded volcanic ("Tuff") horizons from Oligocene-Miocene fill of the Ayaviri basin. Samples are depicted in stratigraphic order (oldest at base), with each histogram bin spanning 2 Myr. Sample labels provide the weighted mean age calculated for the youngest population of zircon grains, with the number (n) of analyzed grains ≥ 3. Four samples are from growth strata north of Ayaviri (Figure 4b; 220510-07, -08, -10, -11); all other samples are from the measured section south of Ayaviri (Figure 5). Systematically decreasing ages upsection (highlighted by wide gray arrow) suggest that the youngest detrital zircon peaks may represent true depositional ages.

growth strata succession exposed along strike north of Ayaviri, where volcanic horizons are absent (Figure 4b, Figure 3 location) demonstrate an upsection decrease in the youngest detrital age populations and agree with geochronologic constraints stratigraphically below, above and along strike. At the 1372 meter level, a trachybasalt flow at Cerro Ocuro south of Ayaviri, variably dated between 28.3 ± 1.0 and 26.9 ± 1.0 by *Bonhomme et al.,* [1985], yields a U-Pb zircon age of 26.37 ± 0.68 Ma (n = 9, sample TC052).

Upsection, the next three U-Pb detrital zircon samples (240510-05, 240510-08, 240510-10) of the Lower Tinajani Formation show decreasing ages (23.51 ± 0.35; 23.2 ± 2.0; 22.73 ± 0.72 Ma) for the youngest detrital zircon populations, in agreement with dated volcanic horizons below and within this interval. Zircon ages for tuff samples TC001 (16.92 ± 0.75 Ma, n = 17) and TC002 (16.56 ± 0.63 Ma, n = 21) provide constraints on the age of the uppermost levels of the Lower Tinajani Formation at meter level ~2150.

The two stratigraphically highest sandstone samples from the uppermost exposures of the Upper Tinajani Formation yield youngest grain population ages yield ages of 15.71 ± 0.97 and 17.4 ± 1.7 Ma (samples 240510-13 and TC076, respectively). The stratigraphically highest sample, TC076, is the only detrital zircon sample that does not continue the upsection trend of decreasing age of the youngest detrital zircon population. Excluding this highest sample, all of the other 14 analyzed samples yield volcanic zircon ages and young detrital zircon populations that become progressively younger upsection, suggesting that syn- or nearly syndepositional zircons are present in the youngest detrital zircon populations for each sample. This allows the use of both volcanic and youngest detrital zircon populations to constrain a maximum depositional age that approaches the true depositional age.

8. DISCUSSION

The similarities in physiographic expression between the northern and central Altiplano segments suggest a shared tectonic setting, yet debate persists regarding the style and timing of deformation and the subsidence mechanisms acting in these hinterland regions. Previous workers have suggested that the northern Altiplano was dominated by strike-slip tectonics and associated transtensional basin formation [*Carlotto,* 2013]. In the Central Altiplano, shortening and thrust tectonics have been emphasized for the Cenozoic deformation and subsidence histories [*Leier et al.,* 2010]. This study focuses on the Cenozoic deformation and depositional history from the northern Altiplano. We present basin and tectonic reconstructions based on new provenance, stratigraphic, geochronologic and structural datasets from the northern Altiplano of southern Peru (Figure 13, 14). Patterns of provenance, subsidence and timing of deformation suggest that the northern Altiplano, like the central Altiplano, was dominated by thrust tectonics during the late Oligocene to middle Miocene and attendant flexural subsidence in hinterland basins. We conclude that the northern and central segments of the Altiplano have a shared Cenozoic tectonic history controlled by along-strike similarities in structural geometries and kinematics (Figure 16), bolstering stratigraphic records that suggest a comparable geologic history for these hinterland regions that experienced later partitioning by out-of-sequence thrust deformation.

8.1. Basin Reconstruction

The late Oligocene Puno Group represents deposition in a sand-dominated braided fluvial system sourced from the flanking Eastern Cordillera along the northeast basin margin and from volcanic cover in the Western Cordillera. U-Pb detrital zircon

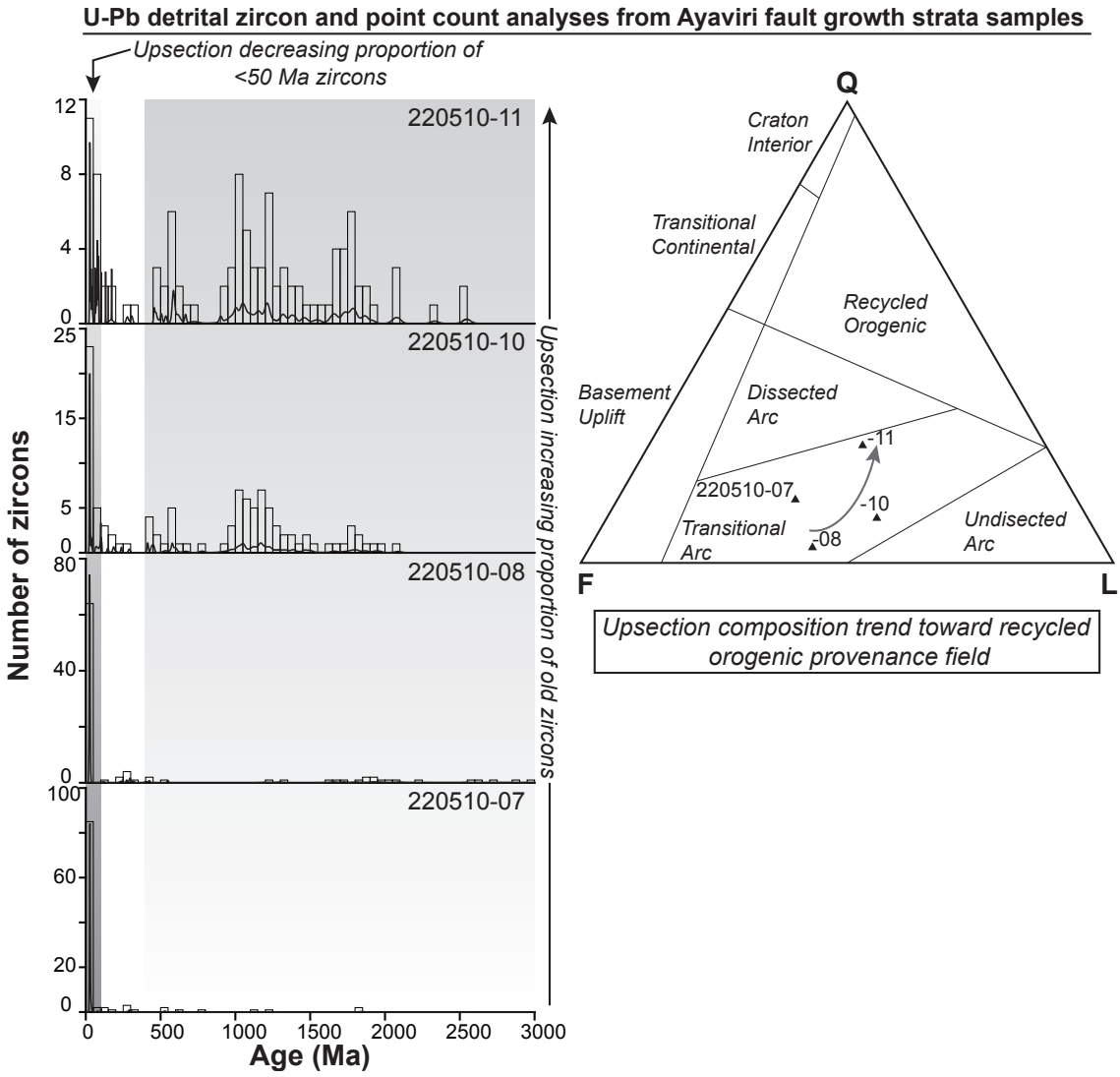

Figure 1.12. U-Pb detrital zircon and thin section point count analyses from four Puno Group samples taken from the Ayaviri fault growth strata outcrop located north of Ayaviri (see Figure 4b). Detrital zircon results show an upsection increase in the proportion of > 50 Ma zircons, and a decrease in the number of <50 Ma zircons across the horizon preserving initial growth strata deposits. Corresponding thin section point analyses show an upsection trend from arc related towards recycled orogenic provenance.

samples dominated by young zircons and sandstone petrographic point counts yield sandstone compositions consistent with erosion of a volcanic-rich source. Paleocurrents, isolated pebble clasts and Paleozoic-Proterozoic zircons support derivation of sediment consistent with exhumation of Paleozoic to Mesozoic strata found in the Eastern Cordillera. Independently, these contrasting results might be interpreted as coeval provenance from both the Western Cordillera volcanic arc and Eastern Cordillera fold-thrust belt. However, this would suggest opposing paleocurrents and complex pathways that incorporated sediment from both the Eastern and Western Cordillera, which have not been observed in the Ayaviri basin. Four key U-Pb detrital zircon samples taken from the growth strata panel preserved along the Ayaviri fault reveal the role of thrust tectonics in driving hinterland basin evolution and provenance variability (Figure 12). Sandstone compositions of these four samples suggest a transitional arc source, yet systematically trend upsection towards recycled orogenic and dissected arc sources. Accompanying detrital zircon samples reveal an upsection gradual decrease in zircons <50 Ma and an abrupt increase in Paleozoic-Proterozoic zircons across the horizon preserving initial growth strata. Young zircon populations and interbedded tuffs demonstrate deposition between 28 and 26 Ma. We suggest that these four samples from growth strata along the Ayaviri fault record a ~2 Myr provenance record where the principal sediment source changed from a Western Cordillera to Eastern Cordillera provenance due to major thrust deformation in the Eastern Cordillera and along the Ayaviri fault. The early phase of basin sedimentation appears to be governed by exhumation of the Eastern Cordillera driven by shortening along the Ayaviri fault. The Eastern Cordillera became the dominant sediment source for the northern Altiplano during the late Oligocene. Tectonic loading of the actively shortening Eastern Cordillera and thrust motion along the Ayaviri fault drove flexural subsidence during Puno Group deposition.

The early to middle Miocene Lower Tinajani Formation represents continued deposition in a fluvial system, yet is generally finer grained than the Puno Group and an environment with increased anastomosing river character. U-Pb detrital zircon, sandstone petrographic point counts, paleocurrents and conglomerate clast counts suggest continued unroofing of the Eastern Cordillera. The Lower Tinajani Formation records basin fill with the highest subsidence rates from this succession, suggesting increased flexural subsidence induced by further thrust loading. We interpret deposition of the Lower Tinajani Formation was driven by flexural subsidence that resulted from continued thrust loading in the Eastern Cordillera.

The middle Miocene Upper Tinajani Formation represents a shift in basin architecture driven by reverse motion along the Pasani fault. The coarse sandstones to boulder conglomerates of the Upper Tinajani Formation were deposited in an alluvial fan environment preserved as growth strata adjacent to the actively deforming Pasani fault. U-Pb detrital zircon, conglomerate clast counts, sandstone petrographic point counts and paleocurrents show sediment transport was sourced in the Pasani fault hanging wall situated to the southwest of the basin. We interpret this final phase of basin subsidence as a period of reorganization in the sediment delivery pathway and provenance driven by thrust motion along the Pasani fault between 18 and 16 Ma. The Puno Group and Lower Tinajani Formation were dominated by deposition of fluvial sandstones sourced from the Eastern Cordillera fold-thrust belt and Ayaviri fault, whereas the Upper Tinajani Formation represents deposition in a coarse alluvial fan setting sourced from the Western Cordillera and Pasani fault hangingwall.

A simplified stratigraphic column is presented in figure 13, and a simplified cross section spanning the northern Altiplano is presented in figure 14. In summary, shortening along the Ayaviri fault from 28 to 26 Ma resulted in an Eastern Cordillera provenance

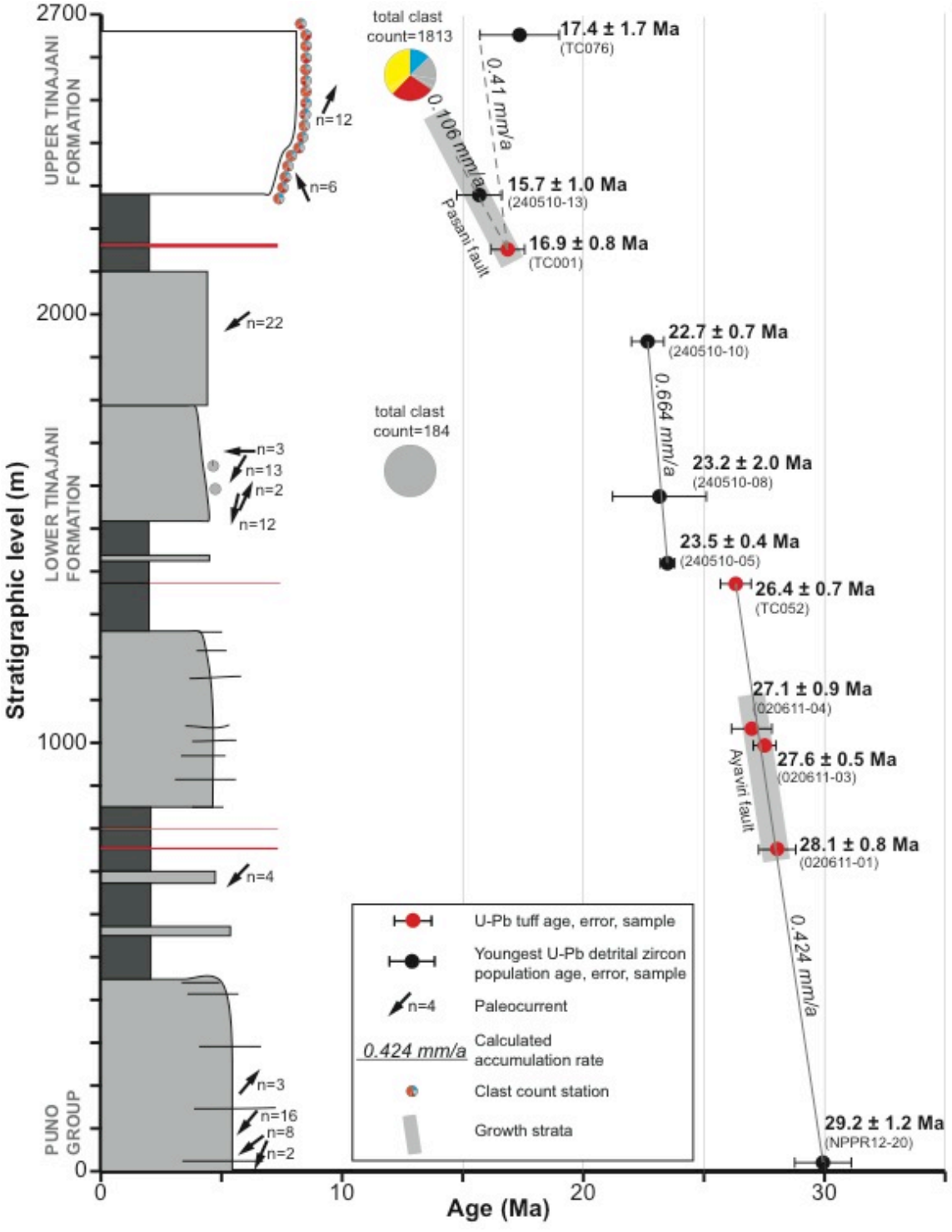
Stratigraphic level (m)
2700
2000
1000
0
UPPER TINAJANI FORMATION
LOWER TINAJANI FORMATION
PUNO GROUP
n=12
n=6
n=22
n=3
n=13
n=2
n=12
n=4
n=3
n=16
n=8
n=2
total clast count=1813
total clast count=184
17.4 ± 1.7 Ma
(TC076)
0.41 mm/a
0.106 mm/a
15.7 ± 1.0 Ma
(240510-13)
Pasani fault
16.9 ± 0.8 Ma
(TC001)
22.7 ± 0.7 Ma
(240510-10)
0.664 mm/a
23.2 ± 2.0 Ma
(240510-08)
23.5 ± 0.4 Ma
(240510-05)
26.4 ± 0.7 Ma
(TC052)
27.1 ± 0.9 Ma
(020611-04)
27.6 ± 0.5 Ma
(020611-03)
Ayaviri fault
28.1 ± 0.8 Ma
(020611-01)
0.424 mm/a
29.2 ± 1.2 Ma
(NPPR12-20)
U-Pb tuff age, error, sample
Youngest U-Pb detrital zircon population age, error, sample
n=4
Paleocurrent
0.424 mm/a
Calculated accumulation rate
Clast count station
Growth strata
0
10
20
30
Age (Ma)

Figure 1.13. Generalized stratigraphic column with accumulation rates showing new isotopic age control from U-Pb zircon geochronology of sandstones (black circles) and interbedded tuffs (red circles). Small pie diagrams show clast count results by station. Large pie diagrams show average composition for multiple clast count stations. Each station is n ≈ 100 clasts. Gray bars highlight timing of growth strata and fault motion. Arrows show paleocurrent directions. Major shifts in paleocurrents and clast composition correspond with abrupt coarsening at the ~2300 m level associated with Pasani fault growth strata.

and southwest directed sediment transport during accumulation of the Puno Group and Lower Tinajani Formation. Thrusting along the Ayaviri fault also initiated rapid sedimentation. A second pulse of shortening along the Pasani fault (southwest basin margin) between 18 and 16 Ma initiated a change to Western Cordillera provenance, alluvial fan deposition, north directed sediment transport, and a second phase of rapid sedimentation.

8.2. Thrust tectonics and northern Altiplano evolution

Previous workers have interpreted the Ayaviri and Pasani faults as strike-slip features that experienced either dextral or sinistral offset based on the map-view rhombohedral shape of the present-day extent of the Ayaviri basin, and on the association of fault traces with alkalinic and shoshonitic volcanic suites [*Carlier et al.,* 1996; *Mamani and Ibarra,* 2000; *Carlier et al.,* 2005; *Rousse et al.,* 2005; *Carlotto,* 2013]. On the basis of the thin-skinned thrust fault relationships, syndepositional folding, moderate fault dip, stratigraphic separation, ramp-flat cutoff variation and systematic fault offset variation along strike, we suggest that the ~28-16 Ma history of these faults has accommodated significant reverse motion rather than strike-slip deformation. If significant strike slip deformation did occur, it must have taken place before or after the record of thrust deformation preserved along the Ayaviri and Pasani faults, in agreement with many timing estimates for vertical axis rotations in southern Peru [*Rousse et al.,* 2002; *Gilder et al.,* 2003; *Rousse et al.,* 2003; *Roperch et al.,* 2006].

Structural, chronostratigraphic, and provenance datasets define depositional phases for the Oligo-Miocene Ayaviri basin in the northernmost Altiplano that are temporally correlated with punctuated thrust motion along basin margin faults.

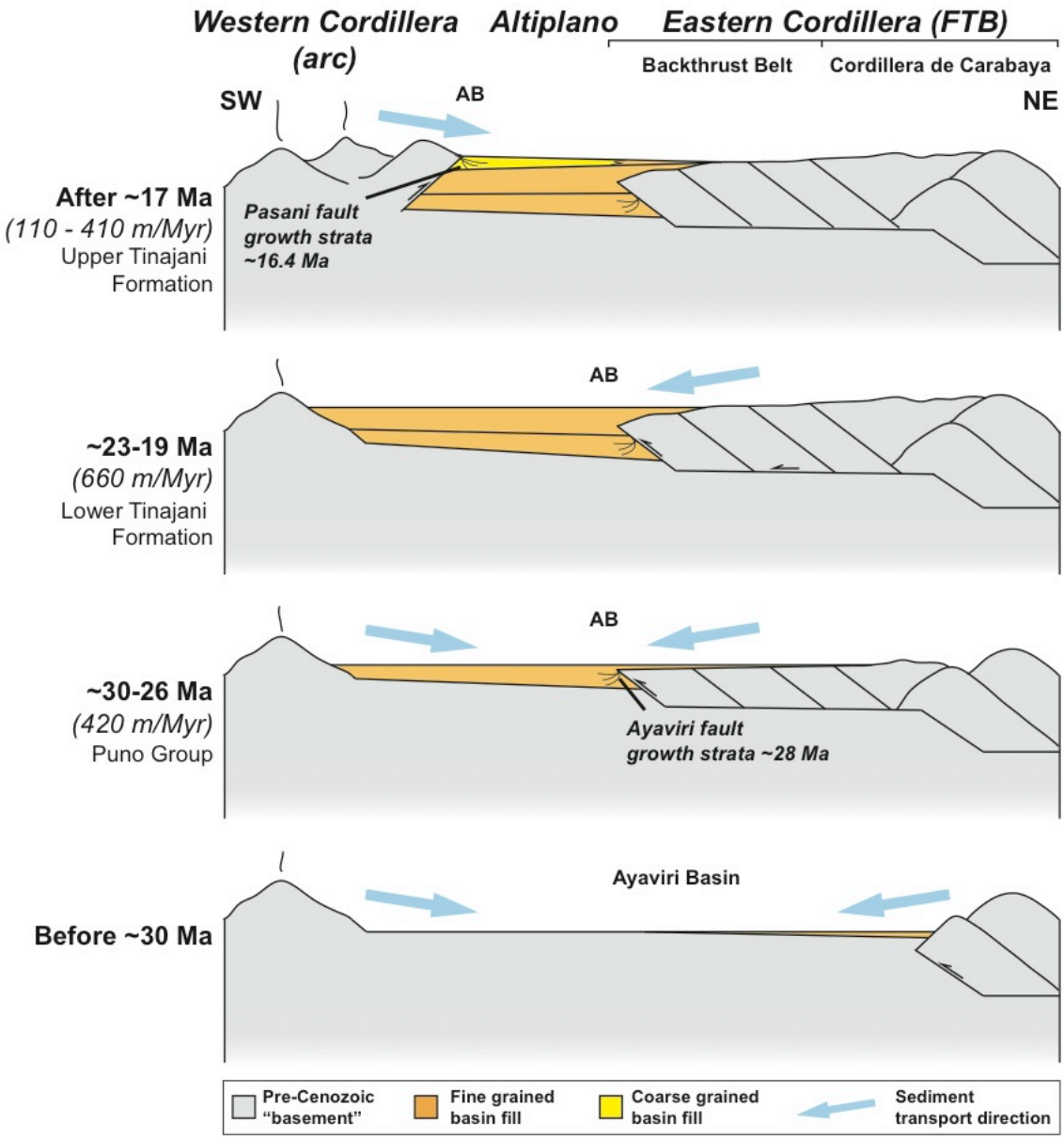
Western Cordillera (arc)
Altiplano
Eastern Cordillera (FTB)
Backthrust Belt
Cordillera de Carabaya
SW
NE
AB
After ~17 Ma
(110 - 410 m/Myr)
Upper Tinajani Formation
Pasani fault growth strata ~16.4 Ma
AB
~23-19 Ma
(660 m/Myr)
Lower Tinajani Formation
AB
~30-26 Ma
(420 m/Myr)
Puno Group
Ayaviri fault growth strata ~28 Ma
Ayaviri Basin
Before ~30 Ma
Pre-Cenozoic "basement"
Fine grained basin fill
Coarse grained basin fill
Sediment transport direction

Figure 1.14. Schematic cross section spanning Western Cordillera, Altiplano and Eastern Cordillera. 'AB' represents Ayaviri Basin section location, mm/yr shows subsidence rates for time interval. Before ~30 Ma, no Cenozoic preserved in this study area, although other locations have isolated Eocene-Oligocene deposits. ~30-26 Ma: shortening in the backthrust belt reaches the Ayaviri fault, creates growth strata, switches to Eastern Cordillera provenance, and initiates high subsidence rate. ~23-19 Ma: continued Eastern Cordillera provenance in sand dominated fluvial setting, continued high subsidence driven by Eastern Cordillera shortening. After ~17 Ma: Pasani fault motion created growth strata, change to Western Cordillera provenance, switch to coarse alluvial fan deposits.

Provenance records from the first phase record a major reversal during Puno Group deposition from a dominantly western (magmatic arc) to eastern (sedimentary) source area between 28 and 26 Ma, coincident with thrust activation along the Eastern Cordillera-Altiplano boundary, the Ayaviri fault. Lower Tinajani Formation preserves continued Eastern Cordillera provenance and finer grained deposits. The last phase was also coincident with thrust motion, but along the opposing basin margin to the west, the Pasani fault. Motion along the out-of-sequence Pasani fault was coeval with a shift to Western Cordillera provenance, paleocurrent reversal and depositional environment change between 18 and 16 Ma. The intervening time between these phases preserves limited paleosol development, lacustrine carbonate deposits, and lower sediment accumulation rates. The continuous subsidence history, record of shortening and reorganization associated with thrust faulting preserved in the Ayaviri basin demonstrates that flexural loading from thrust deformation along the flanks of the northernmost Altiplano was the principal driver in hinterland basin initiation and evolution between ~28 and 16 Ma (Figure 14).

The sediment accumulation style and rates of the northern Altiplano suggest it behaved as a flexural basin controlled by shortening along the basin margins. Both rapid subsidence phases record sediment accumulation rates between ~410 and 660 m/Myr, comparable to the highest rates observed in other Altiplano basins (Figure 15) [*Allmendinger et al.,* 1997; *Horton et al.,* 2001, 2002], yet preserved basin deposits are thinner than the thickest accumulations observed elsewhere in the Altiplano. Late Oligocene and middle Miocene phases of high sediment accumulation and provenance changes are coeval with Eastern Cordillera fold-thrust deformation and active Ayaviri thrust fault motion, or Pasani thrust motion, respectively. This suggests that thrust motion along basin margin faults, as evidenced by footwall syncline growth strata successions

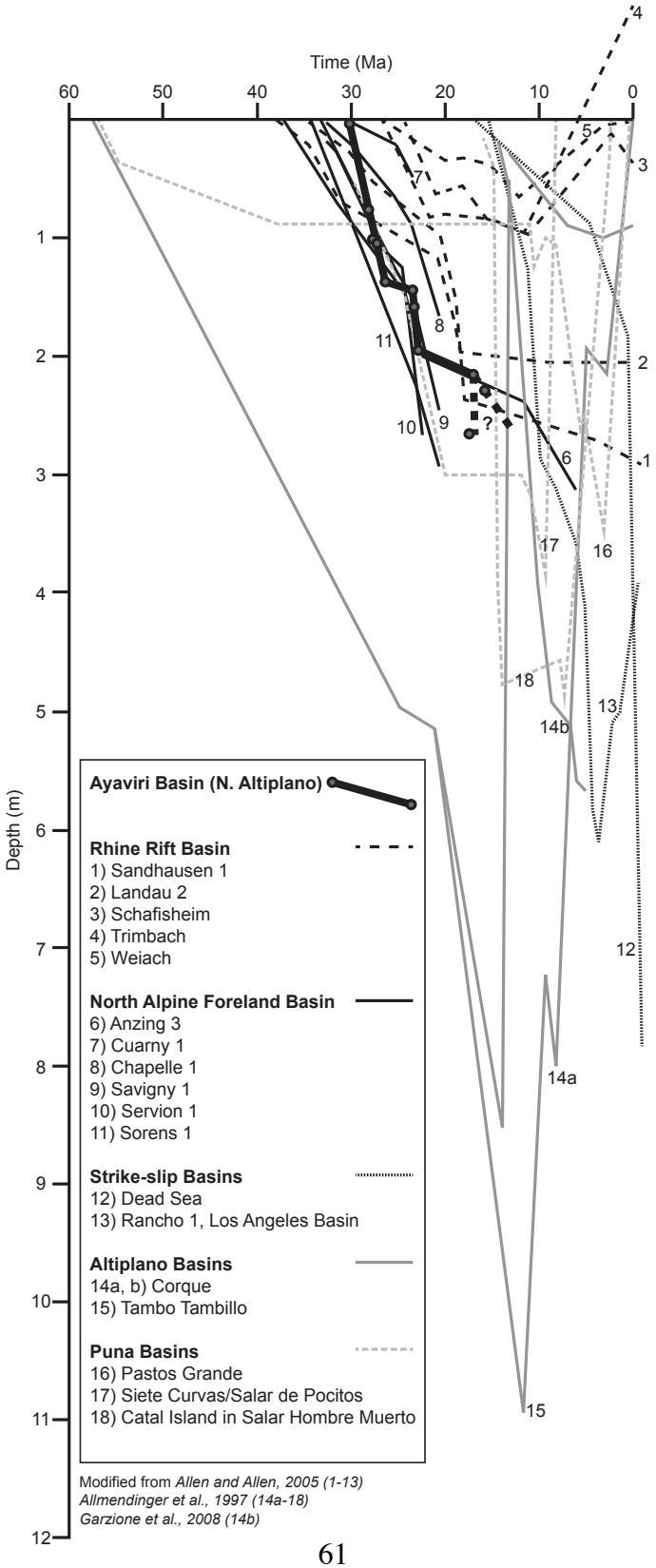

Modified from *Allen and Allen, 2005 (1-13)*
Allmendinger et al., 1997 (14a-18)
Garzione et al., 2008 (14b)

Figure 1.15. Comparison of the sediment accumulation history of the Ayaviri basin (thick black line) relative to foreland (thin black line), rift (dashed lines) and strike sip (dotted lines) basins [after *Allen and Allen*, 2005]. Also plotted are other Altiplano and Puna Plateau basins [after *Allmendinger et al*., 1997]. New age control for the Ayaviri basin from U-Pb zircon ages for detrital and volcanic samples (Figure 13 for summary). The Ayaviri basin sediment accumulation rates are similar to other major Altiplano basins.

preserved along both fault traces, generated loads that were the drivers of flexural subsidence in the northern Altiplano between ~28 and 16 Ma. This interpretation is consistent with basins in the central Altiplano that also demonstrate flexural subsidence controlled by basin margin shortening.

The continuity of major structural features spanning the southern Peruvian and Bolivian Andean segments provides additional support to the interpretation of a shared geologic history in the northern and central Altiplano and the role of regional shortening in controlling central Andean tectonics. Middle to late Eocene timing constraints for initial cooling in the Eastern Cordillera are consistent along strike and have been attributed to shortening [*Farrar et al*., 1989; *Gillis et al*., 2006]. The backthrust belt and fold-thrust belt that spans the northern and central Altiplano of southern Peru and Bolivia kinematically link deformation in the Eastern Cordillera to the Altiplano. The boundary between the Eastern Cordillera backthrust belt and the Ayaviri basin is the Ayaviri fault, part of the SFUACC. Our newly dated footwall growth strata require thrust motion along the Ayaviri fault between 28 and 26 Ma. *Sempere et al*., [1990] demonstrate deformation along the SFUACC in Bolivia at ~28-25 Ma approximately 350 km along strike suggesting deformation along this structure developed coevally throughout southern Peru and Bolivia. The along-strike continuity, synchronous activation, geometric and kinematic similarities between the major structural features in the Peruvian and Bolivian segments of the Eastern Cordillera and Altiplano suggest a deformation history driven by regionally continuous shortening systems throughout the northern and central Altiplano (Figure 16).

New geochronologic constraints on upper crustal shortening from the northern Altiplano reveal the out-of-sequence timing of thrust deformation along the Pasani fault between 18 to 16 Ma, approximately 10 Myr younger than motion along the Ayaviri

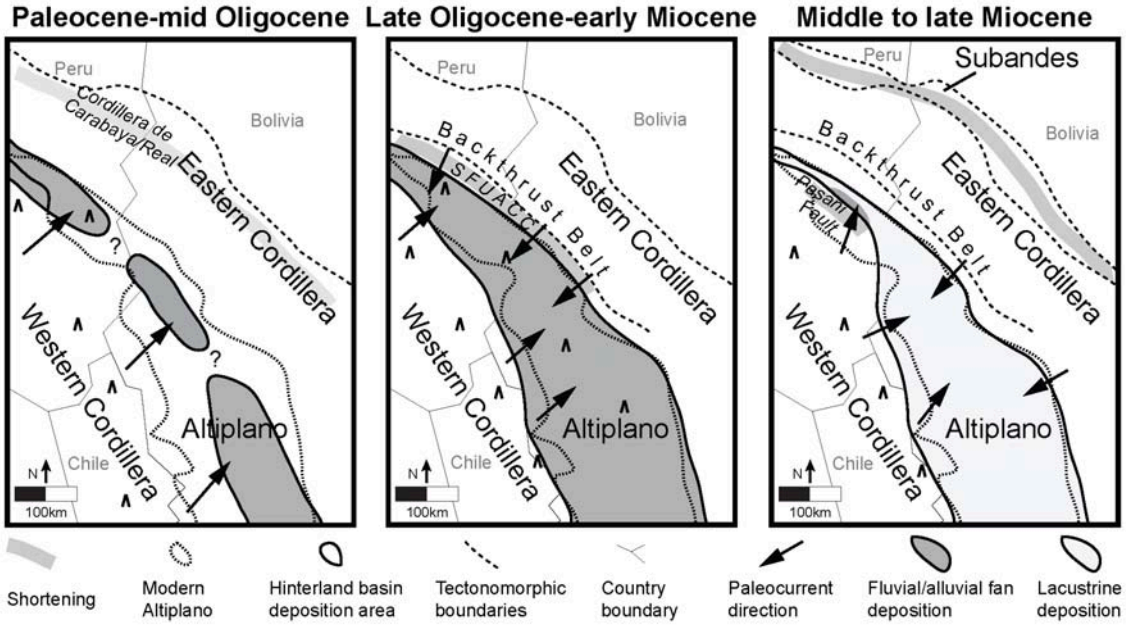

Figure 1.16. Proposed Altiplano scale integrated basin and deformation history. See Figure 1 for map outline. Thin gray strips represent areas of active shortening. Note tectonomorphic zones. Eocene characterized by onset of widescale deposition in the Bolivian Altiplano, yet isolated or poorly preserved deposition in Peru, sourced from the Eastern Cordillera, coincident with initial widespread cooling along the Cordillera de Carabaya/Cordillera Real of Peru/Bolivia. By Oligocene, deformation propagated to the Eastern Cordillera/Altiplano boundary (SFUACC) via the Backthrust belt. Peru basins were still dominated by Eastern Cordillera sediment; Bolivian basins began receiving Western Cordillera sediment sources. In the Miocene, coeval shortening occurs in both the hinterland (out-of-sequence Pasani fault) and Subandes. Altiplano basins received sediment from a dominantly Western Cordillera source.

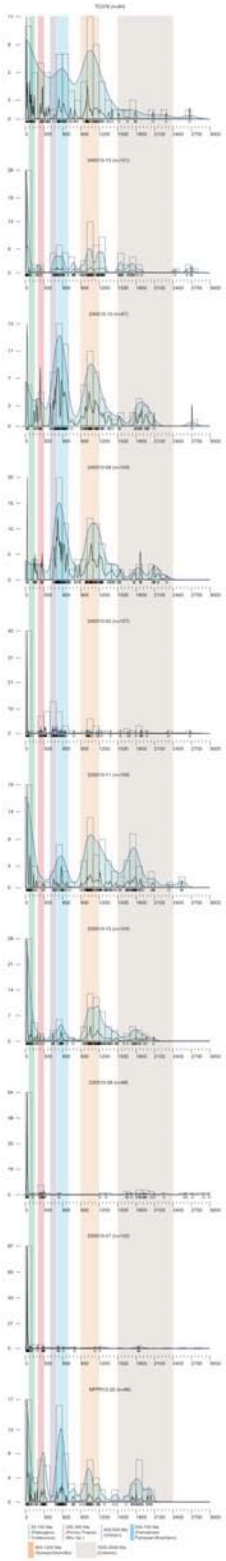

Figure 1.17. U-Pb detrital zircon results presented as kernel density estimation plots [*Vermeesch*, 2012]. Color bars from figures 9, 10.

fault. Its potential link to geodynamic events requires further investigation. The timing of Pasani fault motion may be symptomatic of a regional phase of distributed shortening [*Oncken et al., 2006*]. Other examples of out-of-sequence thrust deformation in the Altiplano have been linked to changes in arc/slab dynamics [*Lamb,* 2011], changes in critical wedge dynamics [*McQuarrie,* 2002] and in the Puna plateau as a result of inherited crustal structures [*Strecker et al.,* 2009]. This out-of-sequence deformation in the Altiplano of Peru precedes estimates for the timing of rapid surface uplift in the Altiplano of Bolivia [~10-6 Ma; *Garzione et al.,* 2006], Eastern Cordillera of Bolivia [after 12-9 Ma, *Barke and Lamb,* 2006], western escarpment of the Western Cordillera of Peru [~11-8 Ma; *Schildgen et al.,* 2009a, b], shortening in the Subandes [~15 Ma, *Gillis et al.,* 2006], arrival of conglomerates sourced from proximal sources with high relief in the Western Cordillera of Peru [~15-10 Ma; *Decou et al.,* 2011] and is generally coeval with the proposed timing of uplift from the Western Cordillera of Peru [~19-16 Ma; *Saylor and Horton,* 2014] and other segments of the Eastern Cordillera of Bolivia [~24-15 Ma; *Leier et al.,* 2013]. The potential geodynamic drivers for out-of-sequence upper crustal shortening in the northern Altiplano require further investigation.

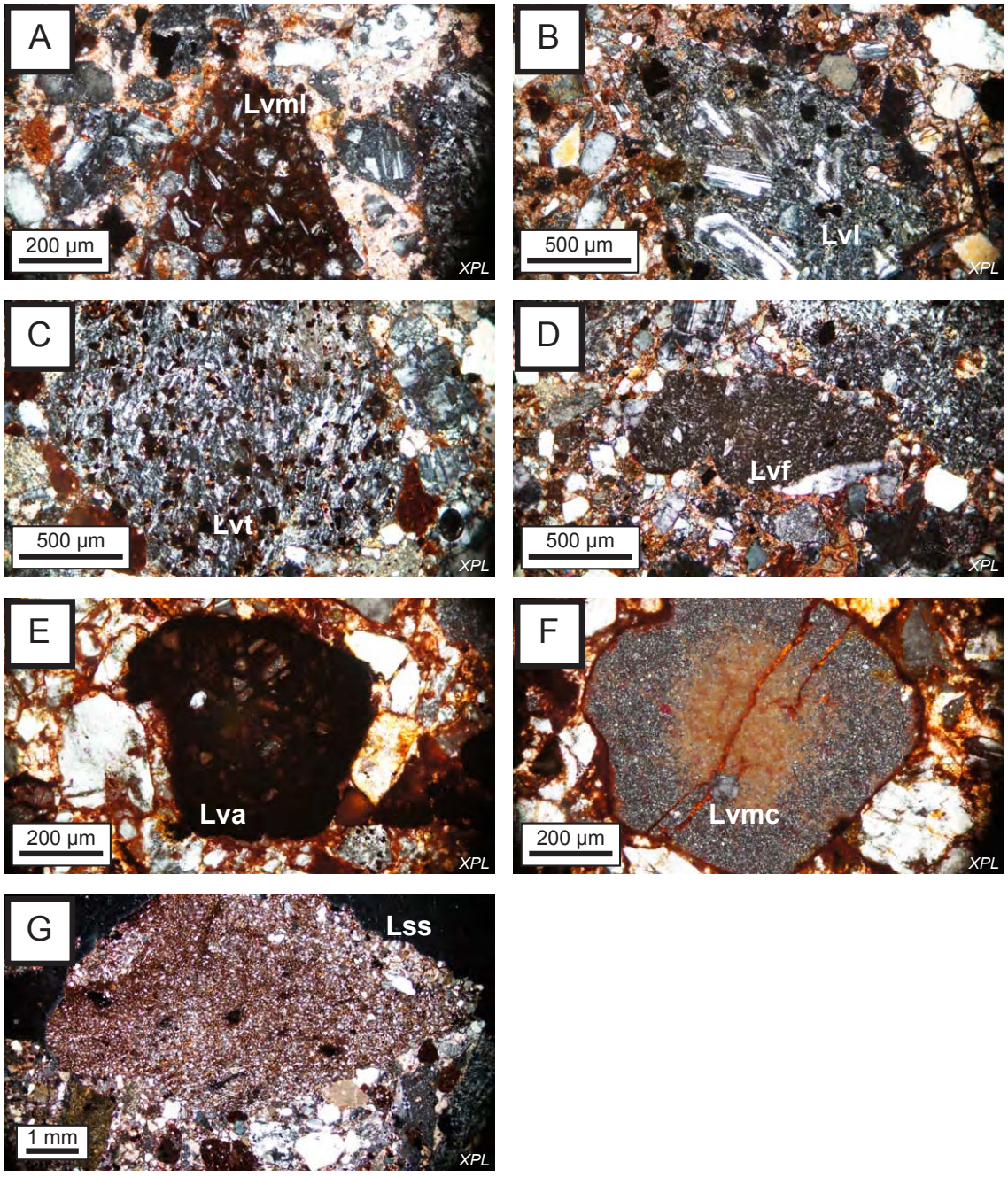
A
Lvml
200 µm
XPL
B
500 µm
Lvl
XPL
C
500 µm
Lvt
XPL
D
Lvf
500 µm
XPL
E
Lva
200 µm
XPL
F
Lvmc
200 µm
XPL
G
Lss
1 mm
XPL

Figure 1.18. Thin section photomicrographs demonstrating the range of lithic fragments observed throughout the Ayaviri basin fill. (A) Microlitic volcanic lithic fragment. (B) Lathwork volcanic lithic fragment. (C) Trachyte volcanic lithic fragment. (D) Felsitic volcanic lithic fragment. (E) Altered volcanic lithic fragment. (F) Microcrystalline volcanic lithic fragment, altering to opaque material in the center. (G) Sandstone/siltstone lithic fragment. All images taken in cross-polarized light.

9. CONCLUSIONS

1) New zircon U-Pb ages for tuff and sandstone samples constrain the depositional age of the ~2700 m Cenozoic nonmarine northern Altiplano Ayaviri hinterland basin between 29.6 ± 1.2 Ma and 15.71 ± 0.97 Ma. The Ayaviri basin is characterized by a lower ~2300 m section (Puno Group and Lower Tinajani Formation) interpreted as a sand-dominated fluvial environment, and an upper ~400 m section (Upper Tinajani Formation) characterized by thick pebble-boulder alluvial fan conglomerates.

2) Footwall growth strata along Ayaviri and Pasani faults constrain the syndepositional timing of thrust activity along opposing basin margins at 28.1 ± 0.8 to 26.3 ± 1.6 Ma and 17.7 ± 0.8 to 16.5 ± 0.8 Ma, respectively. Ramp-flat relationships, systematic along strike changes in stratigraphic offset, fault dip and growth strata geometries suggest both faults are thrusts. Deformation in the northern Altiplano was dominated by thrust tectonics between 28-16 Ma.

3) Basin margin thrust faults controlled sediment provenance and accumulation patterns in the northern Altiplano. New provenance datasets (U-Pb detrital zircon, paleocurrents, sandstone point counts, clast counts) record a shift from Western Cordillera to Eastern Cordillera source in the Late Oligocene coincident with Ayaviri thrust fault motion. Middle Miocene thrust motion along the Pasani fault resulted in a shift from Eastern to Western Cordillera provenance. Both phases of thrust activity were accompanied by pulses of rapid sediment accumulation at rates comparable to other

Altiplano depocenters. Thrust tectonics played a major role in controlling the depositional and provenance patterns the northern Altiplano between 28-16 Ma.

4) The pattern of flexural subsidence and upper crustal shortening observed in the northern Altiplano is consistent with shortening tectonics proposed for the central Altiplano. The along strike continuity and coeval motion/cooling of major structural features spanning southern Peru and Bolivia suggest a shared geologic setting. The Cenozoic deformation history was driven by regionally continuous shortening systems throughout the northern and central Altiplano.

5) Geochronologic results demonstrate that thrust motion along the Pasani fault is out-of-sequence and may be symptomatic of distributed deformation, potentially linked to subcritical wedge dynamics, arc/slab dynamics or surface uplift.

Chapter 2: The role of upper crustal and basement-involved deformation on subsidence and exhumation in orogen interiors: an example from the Ayaviri basin, southern Peru

ABSTRACT

Coupled zircon U-Pb geochronology of sandstones and feldspar $^{40}Ar/^{39}Ar$ of volcanic horizons within growth strata of the Altiplano of southern Peru demonstrate two phases of motion on key structures in the Central Andean hinterland at 28-26 Ma along the Ayaviri thrust and 17-16 Ma along the Pasani thrust. New feldspar $^{40}Ar/^{39}Ar$ geochronology replicate zircon U-Pb crystallization ages from volcanic horizons in growth strata along the Western Cordillera-Altiplano boundary Pasani thrust and confirm 17-16 Ma fault motion. The ages of young populations from interbedded detrital zircon U-Pb geochronology samples agree with interbedded volcanic horizon ages and decrease upsection. The chronostratigraphic framework established by these methods reveals amplified sediment accumulation coeval with fault motion. These results highlight the potential of detrital geochronology to provide absolute age control in proximal, nonmarine, synorogenic facies from volcanic-rich source regions that otherwise lack absolute age control. Apatite (U-Th)/He low-temperature thermochronology reveals partially reset ages across the Ayaviri fault attributed to an unappreciated phase of basin margin burial postdating thrust motion.

We interpret pulses of Oligocene and Miocene rapid sediment accumulation coeval with thrust fault motion as evidence for flexural subsidence in the Ayaviri basin. Oligocene motion along the Ayaviri fault, a segment of the ca. 400 km long basement-involved Eastern Cordillera-Altiplano boundary, is consistent with other Oligocene to

early Miocene growth strata along the same structure suggesting regionally synchronous activation of basement-involved deformation during Cenozoic central Andean construction. Flexural subsidence induced by out-of-sequence Pasani thrust fault motion may have generated sediments that buried the Ayaviri fault. Exhumation after ~15 Ma reveals an important shift from a net depositional to erosional hinterland setting, potentially linked to recently proposed rapid ~19-16 Ma surface uplift.

2. INTRODUCTION

Coarse-grained synorogenic deposits are often used to delineate key structural relationships along basin margins, and to trace temporal evolution of deformation in basin fill potentially linked with deformation (DeCelles et al., 1991). Despite their role in defining geometric and kinematic relationships in orogenic belts, these coarse deposits are commonly devoid of biostratigraphic or volcanic horizons necessary for absolute age control. This paradox can undermine the utility of coarse-grained clastic deposits that are essential for regional kinematic reconstructions, hinterland and foreland basin provenance, and stratigraphic correlation (DeCelles et al., 1991; Khadivi et al., 2010, Lawton and Bradford, 2011). Although the upsurge in detrital zircon U-Pb geochronology has provided important constraints on maximum depositional age and provenance (Fildani et al., 2003; Barth et al., 2004; DeCelles et al., 2007; Jennings et al., 2013), a lack of syndepositional volcanic material precludes precise age control of proximal facies. The timing of transition to proximal basin deposition, potentially marked by these coarse grained deposits, has implications for tectonic reconstructions and the onset of orogenesis (Beck et al., 1995; Fildani et al., 2003).

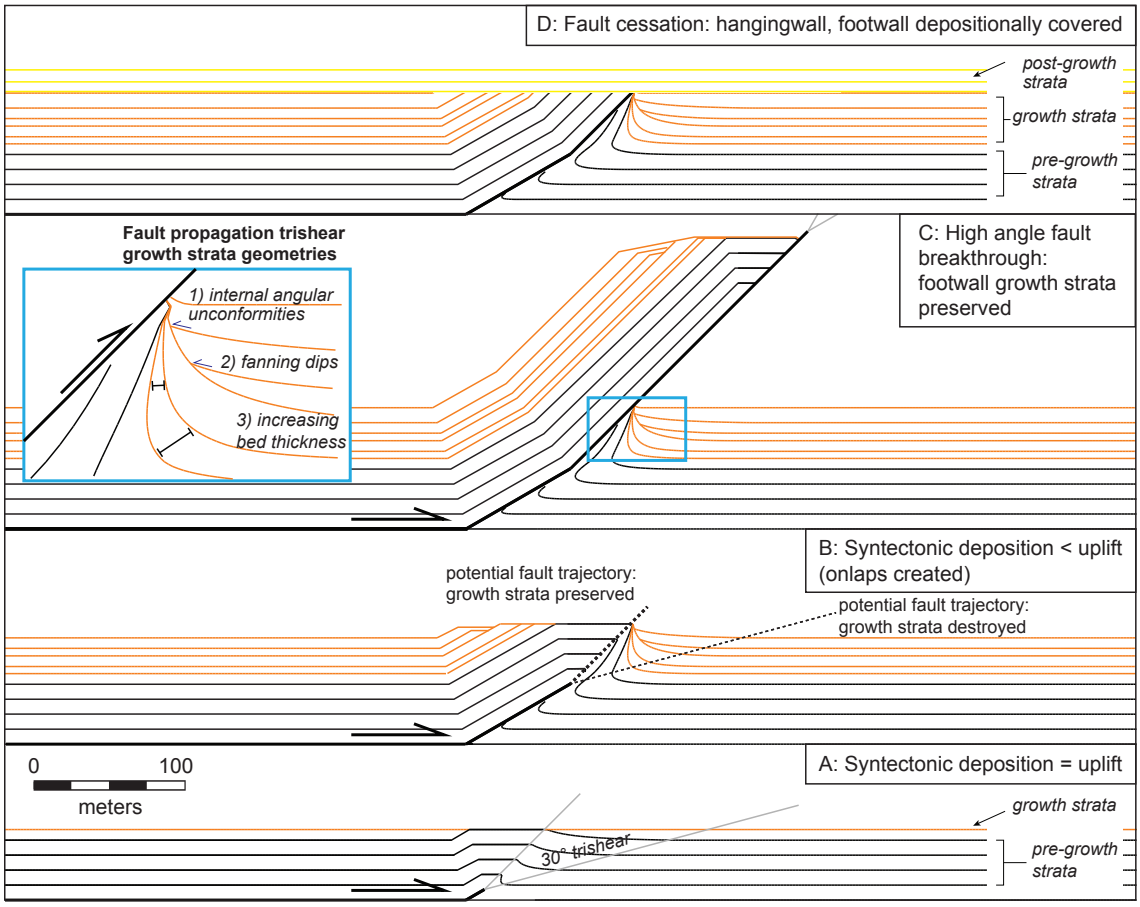

Figure 2.1. Schematic reconstruction of growth strata produced during deformation of a fault propagation-trishear thrust fault. Black lines represent strata deposited before thrust fault motion (pre-growth strata). Orange strata represent syntectonic deposition (growth strata). A) Initial time step shows 30° ramp angle, 30° trishear angle. The relative rate of deposition is equal to the uplift rate of the growing fold. Growth strata deposits just fill created accommodation space. B). Continued thrust deformation with similar ramp and trishear angle as A. The relative rate of fold uplift is greater than the growth strata deposition rate which creates onlap stratigraphic relationships. Note two potential future trajectories of the thrust ramp. A low angle fault ramp will cut through growth strata, prevent preservation. A high angle fault ramp will cut above growth strata, allowing for potential preservation. C) High angle (45°) fault break through preserves growth strata. Inset: note key growth stratal geometries.

In the central Andes, multiple coarse proximal basin fill deposits preserved along the boundary between the Eastern Cordillera and Altiplano display growth strata geometries (Riba, 1976; Sempere et al., 1990; DeCelles and Horton, 2003; Gillis et al., 2006; Leier et al., 2010; Murray et al., 2010; Perez and Horton, 2014). The depositional ages for several of these coarse growth strata successions remains poorly defined. Likewise, the phase of structure development recorded by growth strata remains debated. Locating and refining the temporal and spatial distribution of growth strata has implications for unraveling deformation patterns along and across strike. In Bolivia workers have addressed potential links between timing and location of shortening and surface uplift (Oncken et al., 2006) although uncertainty remains regarding the fidelity of deformation and uplift temporal constraints. The lack of along strike constraints on deformation timing inhibits expansion of such regional syntheses.

Long-lived accumulation in hinterland basin regions records multiple episodes of active basin margin deformation and subsidence (Murray et al., 2006; Gillis et al., 2006; Leier et al., 2010; Perez and Horton, 2014; Schoenbohm and Carrapa, 2015). Whereas growth strata constrain the onset of basin margin deformation, preserved "overlap assemblages" constrain the end of deformation and subsequent burial of the once active basin margin. Erosion and evacuation of these previously filled depocenters can remove this record, which may lead to uncertainties regarding total basin accumulation, fault motion timing, and the flexural load required to achieve true subsidence magnitudes (Hilley and Strecker, 2005; Davila and Lithgow-Bertollini, 2013). Recent studies defining the thermochronologic cooling record of basin sediments have revealed previously underappreciated burial and exhumational histories after the main phase of basin subsidence (Levina et al., 2014). Quantifying the magnitude of burial and timing of

exhumation has implications for modes of basin subsidence, regional tectonic reconstructions and mechanisms driving erosion.

Here we present new data that address the timing of fault activation and cessation constrained by growth strata geochronology, basin chronostratigraphy, apatite (U-Th)/He and overlap assemblages. Paired detrital zircon U-Pb geochronology and feldspar $^{40}Ar/^{39}Ar$ geochronology from interbedded tuffs confirms the depositional age of growth strata and timing of fault motion. Agreement between the maximum depositional age constrained from detrital zircon U-Pb geochronology and volcanic horizons demonstrates that a high fidelity chronological record may be obtained from coarse-grained facies. We show that ~28-26 Ma growth strata found at two locations in the Ayaviri fault footwall are consistent with coeval growth strata observed at other localities along the ca. 400 km Altiplano/Eastern Cordillera structural margin. These growth strata attest to synchronous motion along the length of the basement-involved backthrust. Overlap assemblages suggest cessation of fault motion by ~24 Ma, suggesting rapid fault slip. New apatite (U-Th)/He thermochronologic cooling records across the Ayaviri thrust reveal previously unappreciated burial after fault motion. Subsequent exhumation may have occurred after a phase of rapid surface uplift or movement over a basement ramp. Our study highlights the complex evolution of hinterland basins during active shortening, subsidence, uplift, and unroofing.

3. GEOLOGIC FRAMEWORK, NORTHERN ALTIPLANO

The northernmost Altiplano in southern Peru is occupied by the Ayaviri basin, an internally drained hinterland basin preserving Cenozoic non-marine deposits (Figure 2)

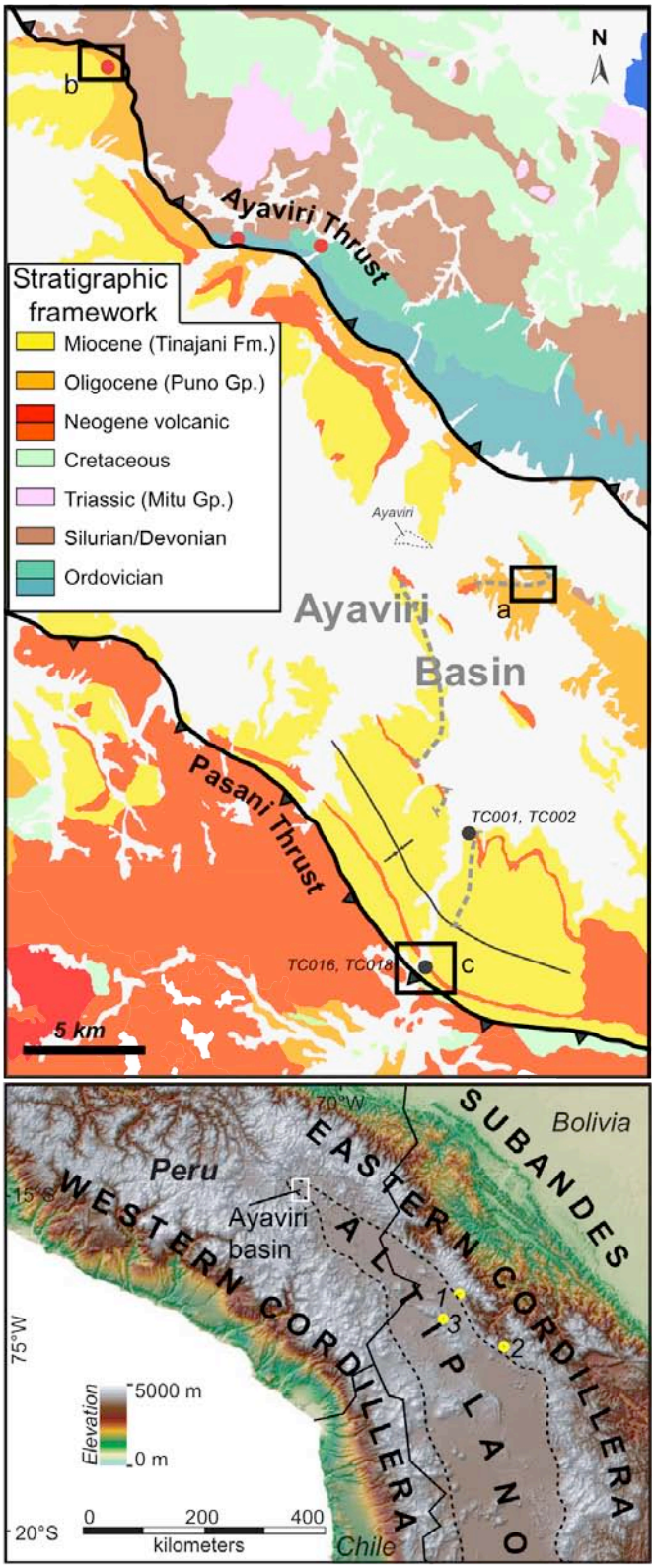
N
b
Ayaviri Thrust
Stratigraphic framework
Miocene (Tinajani Fm.)
Oligocene (Puno Gp.)
Neogene volcanic
Cretaceous
Triassic (Mitu Gp.)
Silurian/Devonian
Ordovician
Ayaviri
a
Ayaviri Basin
Pasani Thrust
TC001, TC002
TC016, TC018
c
5 km
70°W
Bolivia
SUBANDES
EASTERN CORDILLERA
Peru
15°S
Ayaviri basin
WESTERN CORDILLERA
ALTIPLANO
1
3
2
75°W
Elevation
5000 m
0 m
0
200
400
kilometers
20°S
Chile

Figure 2.2. Top: Geologic map of the Ayaviri basin study area. Note two major basin margin faults, location of measured section. Black rectangles (a, b, c) outline growth strata outcrops and maps shown in figures 4 and 5, respectively. Red circles show apatite (U-Th)/He sample locations. Black dots show locations of tuffs analyzed by U-Pb zircon and $^{40}Ar/^{39}Ar$ feldspar geochronology. Bottom: DEM map of the northern central Andes. White rectangle outlines Ayaviri basin study area (figure 2). Yellow dots 1, 2, and 3 represent growth strata localities described in Murray et al., (2010), Leier et al., (2010), and Sempere et al., (1990), respectively.

(Perez and Horton, 2014; Horton et al., 2014). It is situated in the transition zone between the Western Cordillera (modern magmatic arc, Mesozoic back-arc basin and early Andean fold thrust belt), and the Eastern Cordillera (Cenozoic fold-thrust belt). The Ayaviri basin preserves 4+ km of Cenozoic basin fill recording the transition from a flexurally controlled foreland basin to a hinterland basin (Perez and Horton, 2014; Horton et al., 2015). The northeast basin margin is the northwest-trending Ayaviri fault, a segment of a larger ~400 km long fault system which defines the Altiplano and Eastern Cordillera boundary. The fault juxtaposes Ordovician to Devonian strata in the hangingwall on Oligocene basin fill in the footwall. This fault is a major southwest-directed thrust fault within the central Andean backthrust belt (CABB), a main feature of the Eastern Cordillera. The CABB spans >1000 km from southern central Peru to southern Bolivia (Sempere et al., 1990; McQuarrie and DeCelles, 2001). The southwest Ayaviri basin margin is the Pasani fault, a northwest-trending, northeast verging thrust fault that juxtaposes Neogene volcanics and Cretaceous carbonates on mid-Miocene alluvial fan deposits (Rodriguez, 1999; Rouse et al., 2005; Perez and Horton, 2014).

A ~4 km thick Paleogene San Jeronimo Group succession in the western Ayaviri basin preserves non-marine fluvial and alluvial fan sandstones and conglomerates, recording rapid subsidence in a retroarc foreland basin (Horton et al., 2014). The eastern Ayaviri basin preserves a ~1375 m thick accumulation of Oligocene Puno Group deposits (Figure 2). Previous workers have treated the San Jeronimo and Puno Groups as geographically distinct yet temporally correlative units (Carlotto, 2013). Oligocene growth strata preserved along the Ayaviri backthrust footwall define the timing of Altiplano margin structural development, and transition to a hinterland basin setting. South of the village of Ayaviri near Tinajani Canyon, ~1300 m of Miocene Tinajani Fm. deposits are preserved in a broad asymmetric northwest trending syncline. Although these

are the youngest rocks preserved locally, other hinterland basins in southern Peru preserve younger deposits (Carlotto, 2013; Saylor and Horton, 2014), suggesting additional basin fill may have been removed from the Ayaviri basin. Near the uppermost exposures of the section, interbedded coarse sandstones and cobble conglomerates preserve growth strata along the Pasani fault. Growth stratal successions along the Ayaviri fault and Pasani fault preserve interbedded volcanic tuff horizons, affording the opportunity to accurately date the timing of fault motion.

3.1. Fault geometry

The surface trace and position of growth strata along the Ayaviri fault suggests it behaves as a thin skinned thrust at shallow depths. Growth strata are observed at reentrants along the Ayaviri fault where Silurian/Devonian strata are exposed in the hanging wall. Between these growth strata localities, the Ayaviri fault exhibits a curved salient geometry with Ordovician strata exposed in the hangingwall. In contrast to the lateral changes in hanging wall cutoff, the footwall cutoff is consistently in Oligocene Puno Group rocks. We suggest that these systematic variations in hangingwall cutoff may be attributed to fault displacement that is greatest in the middle of the fault and decreases laterally, or due to lateral hangingwall ramps. This ramp-flat geometry is typical of thin-skinned deformation observed in the CABB.

Despite these thin-skinned characteristics, stratigraphic separation across the Altiplano-Eastern Cordillera boundary consistently juxtaposes lower Paleozoic rocks on mid-Cenozoic basin fill. The along strike continuity and separation observed across this boundary suggests the fault may represent a significant step in the basement. Carlier et al., (2005) noted that the Ayaviri fault (their “Cusco Vilcanota Fault System”) separates

two regions with distinctive magmatic lineaments and isotopic variability among potassic to ultra-potassic volcanic rocks. They suggested that this fault system represents an inherited lithospheric scale feature separating two mantle blocks. This fault system spans >400 km from Cusco to northern Bolivia. This major structure also aligns with the proposed eastern boundary of the Arequipa-Antofalla terrane (Jaillard et al., 2000; Loewy et al., 2004; Chew et al., 2007; Ramos, 2008a; Ramos, 2009). Future geophysical investigations may provide insights into the deep crustal structure associated with this structure. These surface observations must be rectified with a balanced cross section, as the basement expression of these potential inherited structures has likely been translated laterally due to subsequent thin-skinned thrust fault deformation.

3.2. Growth strata

Growth strata are syndeformational deposits that accumulate on the flanks of actively deforming faults and folds (Figure 1). Field observations, seismic examples, and numerical models often reveal three key stratal geometries of growth strata. These may be evident in plan and section view: fanning or upsection flattening of stratal dips, increasing bed thickness away from the structure, and internal angular unconformities. Outcrop examples of growth strata are observed in fold-thrust belts worldwide (Riba, 1976; Sempere et al., 1990; DeCelles et al., 1991; Burbank and Verges, 1994; Zapata and Allmendinger, 1996; Horton et al., 2002; Homke et al., 2004; Murray et al., 2006; Aschoff and Schmitt, 2008; Leier et al., 2010; Perez and Horton, 2014; Schoenbohm and Carrapa, 2015;). Identification of growth strata from field relationships alone remains challenging and depends on sufficient exposures and access. Defining pre-growth strata is key to locating the stratigraphic level associated with initial motion along the controlling

structure. Pre-growth strata lack the geometric and stratal relationships characteristic of syndeformational deposits. Beds are parallel, lack rapid lateral thickness variation, have uniform dipping panels, and tend to be finer grained.

In the Ayaviri basin of the northern Altiplano in southern Peru, we have documented two basin margin thrust faults with preserved footwall growth strata (Rodriguez, 1999; Rousse et al., 2005; Perez and Horton, 2014). The Ayaviri fault defines the NE basin margin and preserves two exceptional outcrop exposures of growth strata separated along strike by ca. 30 km (Figure 2). Pre-growth strata and growth strata are developed in fluvial sandstones, siltstones and minor conglomerates of the Oligocene Puno Group. Pre-growth strata have parallel, tabular bedding and range from upright 60-70° SW to overturned 70° NE. A detrital zircon sample from pre-growth strata in the Ayaviri fault footwall demonstrates that Oligocene Puno Group deposition had initiated at 29.2 ± 1.2 Ma prior to motion along the Ayaviri fault.

Ayaviri fault slip and continued Puno Group deposition during the Oligocene created growth strata. Zircon U-Pb geochronologic data from detrital and volcanic zircon samples are consistent within error, and reveal ~28-26 Ma fault motion (Perez and Horton, 2014). Initial growth strata deposits are identified in plan and section view by onlap geometries onto underlying pre-growth deposits with angular discordance >10° (Figure 3, 5) ("traditional type"; Aschoff and Schmitt, 2008). Above this stratigraphic level, growth strata geometries are observed in the two localities (Figure 2, 3), and have not been identified elsewhere along strike. The map trace of the Ayaviri fault is sinuous (Figure 2). The two growth strata locations are situated at reentrants along the Ayaviri fault to the NW and SE, respectively, of Ordovician strata that are exposed in a salient of the Ayaviri fault.

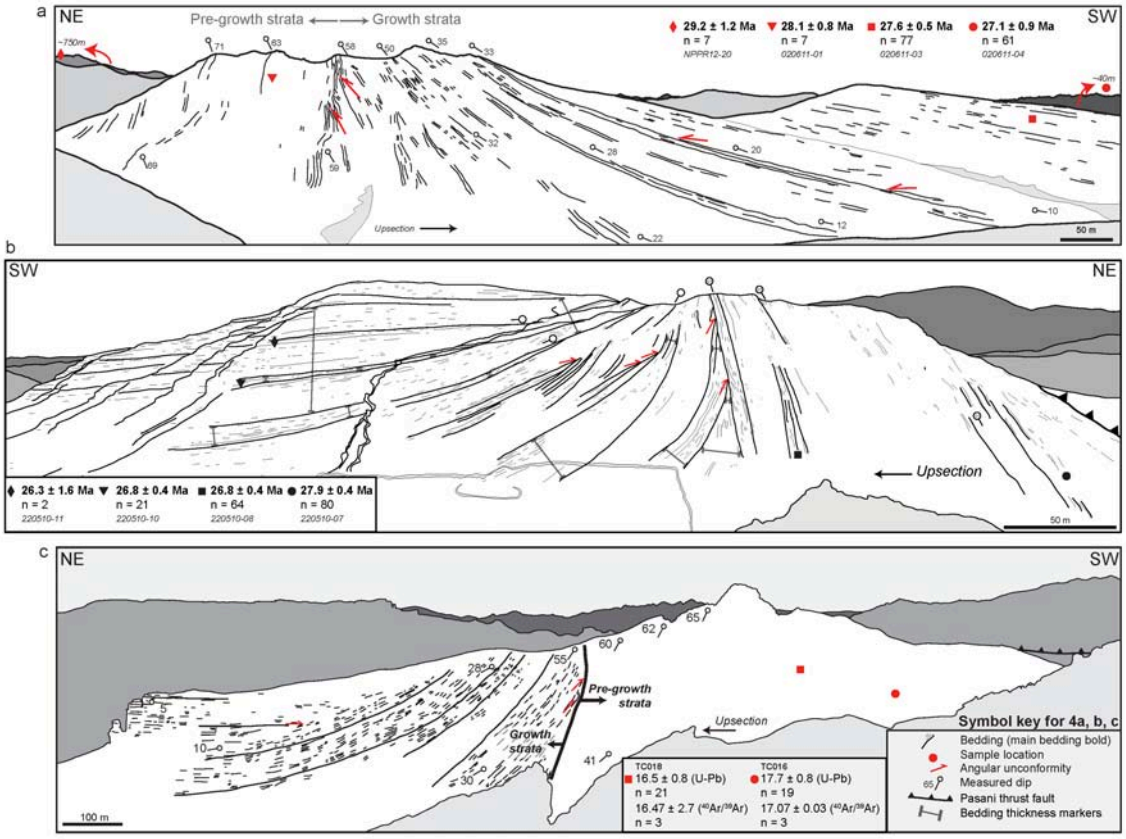

Figure 2.3. Outcrop examples of growth strata from figure 2. A) and B) Growth strata preserved in the Ayaviri fault footwall. C) Growth strata preserved in the Pasani fault footwall (modified from Perez and Horton, 2014).

Ayaviri fault motion ceased by ~26-24 Ma. The youngest deposits that preserve demonstrable growth strata geometries (Figure 3, 5) are dated at 26.3 ± 1.6 Ma with zircon U-Pb geochronology. These uppermost Puno Group deposits are generally restricted to the footwall of the Ayaviri fault, except for isolated deposits ~30 km SE of the town of Ayaviri. Here, poorly exposed Paleogene Puno Group rocks are sometimes covered by upper Paleogene-lower Neogene Tacaza Group rocks. Existing chronostratigraphic constraints for the Tacaza Group suggest it is no younger than ~24 Ma (Carlotto, 2013). Both units were deposited unconformably on underlying Cretaceous and Paleozoic strata. The Tacaza Group is interpreted as the overlap assemblage, sealing deformation along the Ayaviri fault. If existing geochronologic constraints are upheld, Ayaviri fault motion ceased by ~24 Ma, if not earlier. Neogene deposits depositionally overlapped the fault and are preserved in the Ayaviri fault footwall (Ayaviri basin).

Along the SW basin margin, the Pasani thrust juxtaposes Cretaceous sedimentary and Neogene volcanic rocks against middle Miocene non-marine conglomerate, sandstone and siltstone alluvial fan deposits of the Tinajani Formation. Growth strata preserved in the Pasani fault footwall are exposed throughout Tinajani Canyon (Figure 2, 3). Pre-growth strata dip 60-70˚ NE. Growth strata systematically decrease from dip <60 to ~10˚ NE upright, and record onlap geometries, fanning bed dips, and increasing bedding thickness away from the Pasani fault (Figure 3, 5). Zircon U-Pb geochronologic results from tuffs at the base of the growth strata suggest ~16-18 Ma fault motion (Perez and Horton, 2014). The map view trace of the Pasani fault displays a conspicuous bend, changing trend from ~330˚ to 290˚ and creating a reentrant map geometry. As with the Ayaviri fault, growth strata along the Pasani fault are observed in the Tinajani Canyon locale occupying the reentrant.

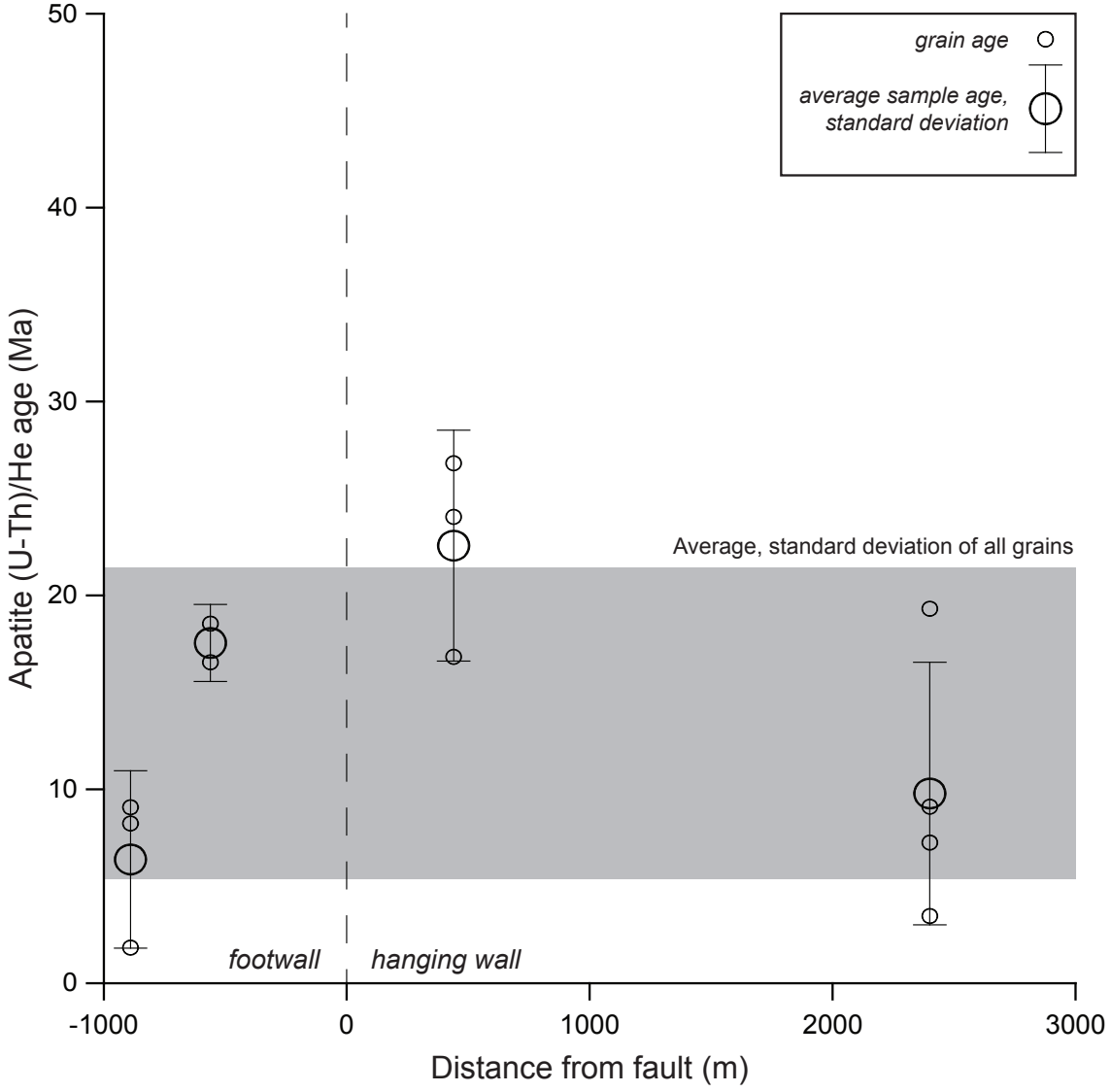

Figure 2.4. Results from apatite (U-Th)/He thermochronology from the Ayaviri fault hangingwall and footwall. Distance from fault trace measured perpendicular to map contact shown on x axis. Positive distance indicates hangingwall position. Negative distance indicates footwall position. Small circles show individual grain ages. Large circles and brackets show mean and standard deviation for grains in each sample. The composite mean age and standard deviation for all ages is marked by gray shading. Ages show no pattern across strike, and all ages are younger than ~28-26 Ma Ayaviri fault motion.

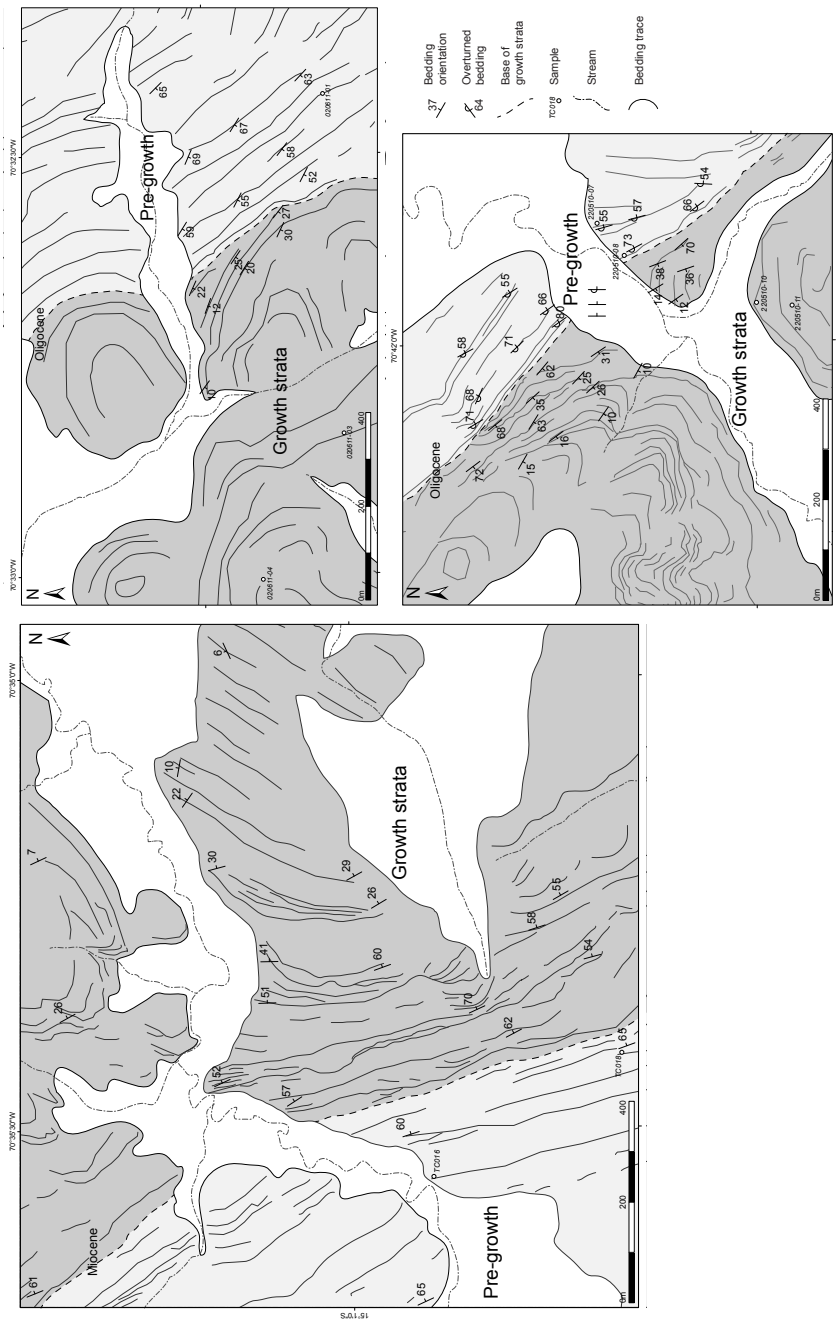

Figure 2.5. Map view of growth strata locations from figure 2. A) and B) Growth strata preserved along the Ayaviri fault. C) Growth strata preserved along the Pasani fault.

4. ^{40}AR/^{39}AR AND U-PB GEOCHRONOLOGY

4.1. Background and Methods

U-Pb in zircon and ^{40}Ar/^{39}Ar in feldspars are common geochronometers of silicic volcanic rocks (Bowring and Schmitz, 2001 RIMG). Uncertainties regarding eruption pace, magma residence time and ^{40}K decay constant have been implicated in discrepancies observed between ages obtained from the two techniques (Renne et al., 1994; Schmitz and Bowring, 2001; Min et al., 2001). Establishing an accurate and precise chronostratigraphy has implications for basin histories, fault motion, and tectonic reconstructions. Where basins preserve syndeformational growth strata, these uncertainties in stratigraphic age may impact interpretations of fault timing.

Zircons were separated from whole-rock samples using standard mechanical, density and magnetic techniques (Gehrels, 2000; Gehrels, 2011). High purity zircon separates were mounted in epoxy and imaged with low-resolution cathodoluminescence to identify internal zonation. Samples were analyzed using laser ablation inductively coupled plasma mass spectrometry at the Arizona LaserChron center. A total of 80 zircons from these four samples were analyzed.

Feldspar grains were separated and purified from whole-rock samples using magnetic, HF acid etching, and visual separation techniques. Samples were irradiated for 16 hours in the central thimble of the USGS TRIGA reactor using Taylor Creek Sanidine (TCR-2) as an irradiation flux monitor. A total of 40 single-crystal laser-fusion analyses were performed at the U.S. Geological Survey in Menlo Park, CA using a 30W CO_2 laser and analyzed on an MAP 216 spectrometer. The standard (TCR-2) age used during analysis was 27.87 Ma, however all results reported here were recalculated using $R_{FCT-2}^{TCR-2} = 1.006552 \pm 0.000585$ to make them equivalent to a 28.02 Ma Fish Canyon

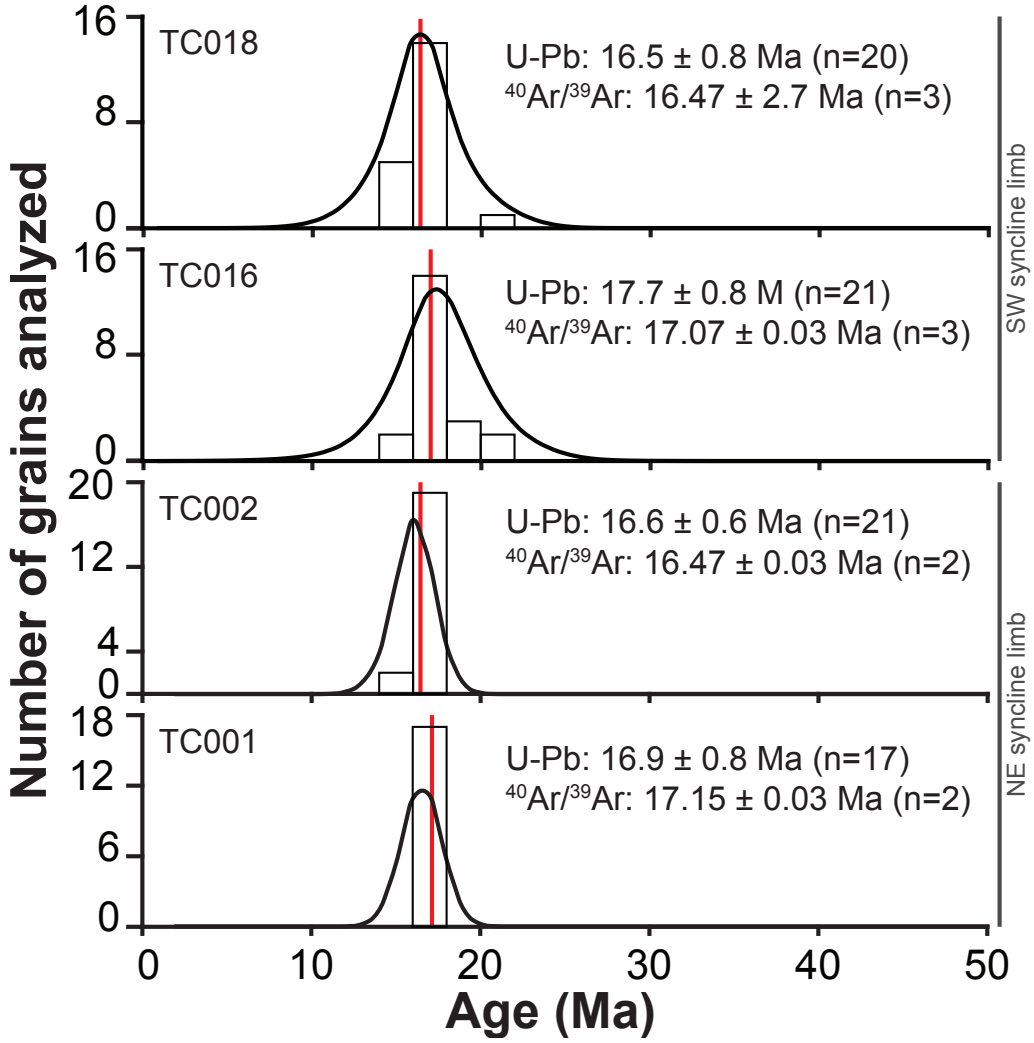

Figure 2.6. Comparison between U-Pb zircon and $^{40}Ar/^{39}Ar$ feldspar geochronology results. Histograms and black probability distribution functions plot U-Pb data. Weighted mean and error reported for zircon ages. Vertical red line shows age only of $^{40}Ar/^{39}Ar$ feldspar ages. Average age and error reported for feldspar ages.

sanidine age. The $^{40}Ar/^{39}Ar$ age determinations are reported with 2σ analytical uncertainties (Figure 6).

4.2. Timing of deposition

Here we compare new ages obtained from $^{40}Ar/^{39}Ar$ in feldspar with previously reported U-Pb zircon ages (Perez and Horton, 2014) from four well preserved welded ignimbrite samples interbedded in middle Miocene growth strata along the Pasani fault. The comparison yields ages from both techniques that are in agreement within error, reaffirming that zircon U-Pb geochronology is an adequate tool for establishing true eruption and depositional ages. After demonstrating the fidelity of U-Pb zircon geochronology in these deposits, we can more confidently interpret previously reported zircon U-Pb ages from weathered tuffs interbedded in Oligocene growth strata along the Ayaviri backthrust (Perez and Horton, 2014) where $^{40}Ar/^{39}Ar$ geochronology in feldspars was not possible.

Two tuffs were analyzed from the NE and SW limbs of a syncline in the footwall of the Pasani thrust (samples TC001, TC002 and TC016, TC018, respectively) (Figure 2, 6). Samples from the southwest limb are interbedded in growth strata deposited during Pasani thrust motion. The beds in the NE limb dip 10-15˚ SW and do not preserve growth strata geometries. Map relationships and lithologic similarities suggest that the two tuffs are correlative across the syncline, but exposures are inconclusive.

Results from zircon U-Pb and $^{40}Ar/^{39}Ar$ in feldspar are shown in figure 6. Ages from both techniques are consistent within analytical uncertainty. This confirms the age of growth strata and Pasani thrust fault motion at ca. 16-18 Ma (Perez and Horton, 2014).

This also highlights that zircon U-Pb geochronology is an appropriate tool to establish the timing of eruption within similar precision of $^{40}Ar/^{39}Ar$ in feldspar.

Below these 4 volcanic tuffs are a series of 8 detrital zircon U-Pb samples (Perez and Horton, 2014). The youngest population age from each detrital zircon sample decreases upsection, but all are older than the 4 volcanic tuffs dated by both zircon U-Pb and feldspar $^{40}Ar/^{39}Ar$ geochronology. These detrital zircon samples are also in agreement with ages obtained from other interbedded volcanic horizons dated only with zircon U-Pb. Only one detrital zircon U-Pb sample is not in agreement. The upper most sample has a youngest age population that is 17.4 ± 1.7 Ma, older than the detrital zircon sample stratigraphically below it, and approximately the same age as the older two Pasani growth strata tuffs. In sum, a succession of ages from 9 detrital zircon samples and 8 volcanic tuff samples are in agreement. Only one detrital zircon sample at the top of the section displays an anomalously old age. Despite this single sample, we show that high fidelity ages may be obtained from non-marine basin fill deposits.

5. THERMOCHRONOLOGY

5.1. Background and methods

Apatite (U-Th)/He low temperature thermochronology measures the accumulation of ^{4}He produced from the decay of radioactive parent isotopes ^{238}U, ^{235}U, ^{232}Th, and ^{147}Sm. The rate of diffusion of daughter product ^{4}He through a mineral lattice is determined by temperature, He diffusivity specific to that mineral, and radiation damage. For apatite, He diffuses out of the grain at temperatures higher than ~80-85° C (Stockli et al., 2003; Reiners et al., 2005). Apatite becomes a closed (non-diffusing) system at temperatures as

low as ~45-50° C (Stockli et al., 2003; Flowers et al., 2009). Between these temperatures, the grain transitions from an open to closed system where He retention increases through the partial retention zone (PRZ). At typical geothermal gradients, PRZ temperatures represents depths < 3 km, making apatite (U-Th)/He thermochronology an ideal tool to constrain cooling in the upper crust. Determining the age of cooling has been applied in orogenic settings to define the spatial pattern of exhumation (Batt et al., 2001, Barnes et al., 2006), incision along topographic boundaries (Lease and Ehlers, 2013) or to determine the timing of range exhumation (Carrapa et al., 2005).

Four samples (two from hangingwall and footwall each) were analyzed from the Ayaviri fault (Figure 2). Samples were prepared using mechanical, density and magnetic separation. Clear apatite grains without inclusions, impurities or cracks were selected using a binocular microscope. However, all samples are detrital, and in some instances it was not possible to select apatites using our criteria. The grain dimensions were measured for the calculation of the alpha-correction factor after Farley et al. (1996). Single grains were packed in Nb-tubes for U-Th/He analysis. In general we analyzed 3-5 aliquots per sample. Helium was measured in the Patterson Helium-extraction line at the University of Tübingen, which is equipped with a 960 nm diode laser. Apatite grains were heated for 5 min at 11 A and zircon grains for 10 min at 20 A. Each grain was re-heated and analyzed to make sure that the grain was degassed entirely in the first step. The re-extracts generally showed <1% of the first signal. Concentrations of U, Th and Sm were determined by isotope dilution using the Thermo Fisher iCAP ICP-MS at University Tübingen equipped with an all-PFA sample introduction system. Apatite samples together with the Nb-tubes were spiked with a calibrated mixed spike of ^{233}U + ^{230}Th + ^{149}Sm and dissolved over night in 2 ml 5% HNO3 + 0.1% HF at 65 °C. The grain mass of

each sample was estimated from measured 43Ca concentrations assuming 39.4 wt-% Ca in apatite.

The analytical error of the mass spectrometer measurements are generally very low and do not exceed 2%. In contrast, the reproducibility of the sample age constitutes a much larger error. We therefore report the mean U-Th/He age and the standard deviation of the measured aliquots as the sample error. For single grain ages we apply a 5% 2-sigma error based on the reproducibility of standard measurements in the lab.

5.2. Exhumational cooling

We investigated the burial and exhumation history of the Ayaviri basin margin along the Ayaviri fault using low-temperature apatite (U-Th)/He thermochronology. Four new samples are presented here, two each from Ordovician quartzites in the hangingwall and Oligocene sandstones in the footwall, collected within 3 km of the Ayaviri fault trace. All four samples were collected between 4000 and 4100 meters elevation. Based on > 6 km of structural relief exposed in the Ayaviri fault hangingwall, we expect the two hangingwall samples resided below the apatite PRZ before onset of Ayaviri fault motion. The Oligocene depositional age of the two footwall samples is confirmed by U-Pb zircon geochronology from volcanic and detrital horizons.

Single grain apatite (U-Th)/He ages from all four samples show considerable spread, but all are younger than ~28-26 Ma fault motion constrained by growth strata. The hangingwall samples reveal mean ages of 22.6 ± 6.0 Ma and 9.8 ± 6.8 Ma. The footwall samples have weighted mean ages of 6.4 ± 4.6 Ma and 17.5 ± 2.0 Ma. The average cooling age of all grains is 13.4 ± 8.0 Ma (Figure 4). If apatite (U-Th)/He ages from the Ayaviri fault hangingwall were driven by Ayaviri fault motion, we would expect

these ages to be consistent with ~28-26 Ma growth strata ages. Despite the considerable spread among individual grain ages, nearly all are consistently younger than the timing of fault motion. Detrital apatites from the two footwall samples were sourced from rocks older than the late Oligocene depositional age. As such, apatite (U-Th)/He cooling ages from footwall samples should be older than fault motion if those samples were never reset after deposition. Although we find a range of grain cooling ages from footwall samples, all grains are younger than Ayaviri fault motion, similar to observations from the hangingwall samples. In sum, 11 of 12 apatite grains analyzed across the Ayaviri fault yield ages younger than ~28-26 Ma fault motion. The remaining grain has an age of 26.82 Ma, which is approximately the same as the youngest growth strata preserved in the Ayaviri fault footwall.

The paucity of Cenozoic deposits preserved east of the Ayaviri fault hinders estimates of the original spatial coverage of the northern Altiplano basin. Our new apatite (U-Th)/He results show a spread of ages that are younger than well-defined ~28-26 Ma Ayaviri fault motion. We interpret this as evidence for burial of both Ayaviri fault blocks to the apatite PRZ after fault motion ceased by ~24 Ma. Our preliminary investigation of flexural subsidence magnitudes demonstrates that >2 km of basin fill may have been deposited above the Ayaviri fault (Figure 8). Assuming a geothermal gradient of 25-30° C/km, this is consistent with thermochronologic data showing burial of the Ayaviri fault to the apatite PRZ. Residence in the PRZ causes helium diffusion from apatite that varies with the radiation and volume of the crystal (Flowers et al., 2009). Because burial of apatite to the PRZ does not fully reset grains, the individual apatite grain cooling ages may vary and the timing of exhumation is difficult to constrain.

6. BASIN SUBSIDENCE

In flexurally controlled basins, there is a genetic link between tectonic loading and subsidence (Jordan, 1981; Flemings and Jordan, 1989). Temporal correlations between the timing of thrust faulting and the onset of rapid sediment accumulation in the Ayaviri basin suggest subsidence was the flexural response to tectonic loads. Although existing constraints prevent detailed models of flexural subsidence from thrust loading, we investigate basic 2D basin models to test the role of flexural subsidence on observed stratigraphic thickness preserved in the Ayaviri basin. For all models, Young's modulus (100 Gpa), Poisson's ratio (0.25) and mantle density (3300 g/cm^3) were constant. Using trial and error, we established that an effective elastic thickness value of 10 km recreated basin thickness and width observations. Although this value is similar to modern estimates from Tassara et al., (2007), the value is unrealistically low for a flexurally controlled basin. We created a simple two-step subsidence model using Flex2D (Cardozo, 2015). Step one involved two rectangular blocks that represented tectonic loads: the Ayaviri fault hanging wall block (15 km wide, 8.5 km thick, ϱ_{load}=2650 g/cm^3), and the CABB (35 km wide, 3 km tall, ϱ_{load}=2650 g/cm^3). This 8.5 km thickness matches the thickness of the Ordovician through Cretaceous stratigraphy in the Ayaviri fault hangingwall. Widths were measured from modern map exposure widths of these blocks, and heights were chosen from conservative estimates of stratigraphic separation. Resulting subsidence values next to this load are ~2270 m, consistent with total sediment preserved during the first pulse of subsidence (~2100 m).

The second step involved one block (30 km wide, 3 km high ϱ=2650 g/cm^3) representing the Pasani fault hangingwall that was thrust onto the Ayaviri basin fill at ~17 Ma. Maximum subsidence is ~960 m, which is sufficient to accumulate the ~600 m of

strata observed within and above Pasani fault growth strata. In the Ayaviri basin, the Pasani fault is situated ~15 km SW of the Ayaviri fault trace. In our model, the subsidence magnitude 15 km away from the Pasani block is ~650 m, suggesting thrust loading from the Pasani fault would have induced flexural subsidence of the Ayaviri fault hangingwall and footwall blocks (Figure 8).

The maximum subsidence achieved after the two-step model is ~2900 m. This simple example demonstrates that the ~2700 m of sediment preserved in the Ayaviri basin is consistent with the flexural subsidence response induced by thrust loading on opposing basin margins. It also demonstrates that Pasani fault loading would have caused some subsidence across the Ayaviri fault and potentially buried it with sediment. The stratigraphic thickness preserved above the top of the Ayaviri growth strata level is ~1600 m. Our flexural subsidence investigation suggests an additional ~650 m of sediment may have been deposited on the Ayaviri fault. The Ayaviri fault may have been buried with > 2 km of basin fill after ~28-26 fault motion.

7. DISCUSSION

7.1. Kinematics of basement involved growth structure

The preservation of growth strata near reentrants may also be attributed to variations in fault breakthrough angle, where high breakthrough angles result in reentrants and preservation of growth strata in the footwall. Lower breakthrough angles result in destruction of footwall growth strata (Figure 1).

Sempere et al., (1990) noted growth strata in late Oligocene deposits in Bolivia along the Coniri Fault, part of a fault system that includes the Ayaviri fault in southern

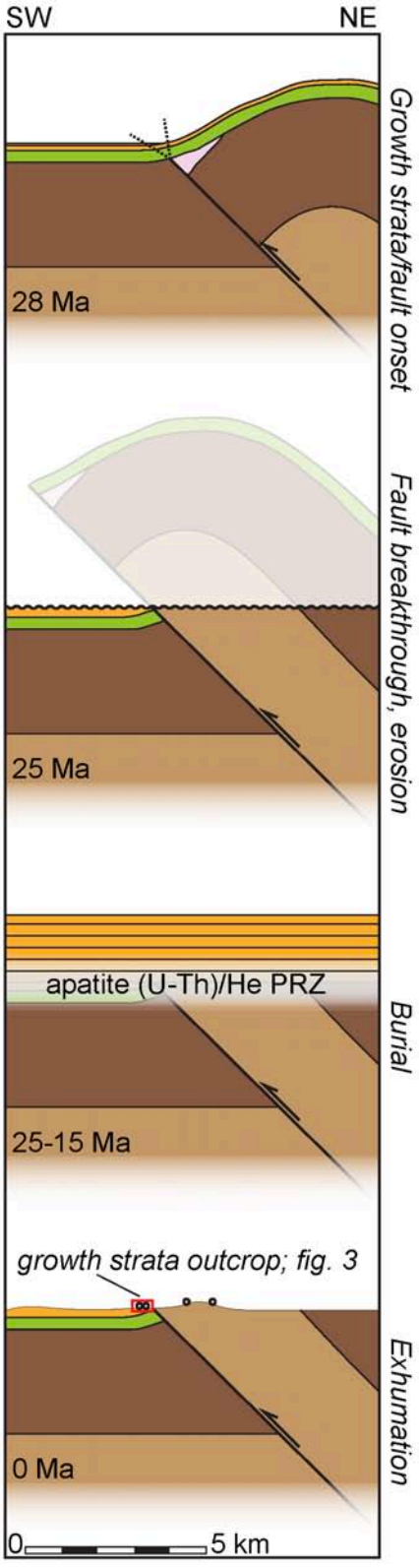
SW
NE
Growth strata/fault onset
28 Ma
Fault breakthrough, erosion
25 Ma
apatite (U-Th)/He PRZ
Burial
25-15 Ma
growth strata outcrop; fig. 3
Exhumation
0 Ma
0
5 km

Figure 2.7. Proposed schematic reconstruction for the Eastern Cordillera/Altiplano structural boundary from 28-0 Ma. Note fault motion occurred for no more than ~4 Myr between ~28-24 Ma. Burial of the Ayaviri fault trace induced by Pasani fault loading and continued subsidence driven by Eastern Cordillera load. Red box in lower diagram outlines position of growth strata observed in outcrops along the Ayaviri fault.

Peru. Farther north, Carlotto (2013) noted growth strata in late Oligocene San Jeronimo Group strata preserved along the same fault system preserved > 400 km along strike south of Cusco. The fault system has previously been referred to as the SFUACC (Spanish acronym for Urcos-Ayaviri-Copacabana-Coniri fault system). Here we will refer to this as the Ayaviri fault system (AFS). The three growth strata localities that occur along the AFS mark the westernmost edge of the backthrust belt and define the boundary between the Eastern Cordillera and Altiplano. Despite lack of precise chronostratigraphic control at those locations, our zircon U-Pb chronostratigraphic constraints from the Ayaviri basin demonstrate ~28-26 Ma fault motion, suggesting synchronous motion along the entire AFS.

Near the Ayaviri region, we estimate minimum ~8.5 km of displacement based on observations of > 6 km stratigraphic separation, a ~45° NE dipping fault plane, and cross section reconstruction. A hangingwall flat exposed at the surface suggests the hangingwall anticline has been eroded and total displacement is greater than stratigraphic separation. Growth strata and overlap assemblages demonstrate fault motion occurred over 4 Myr between ~28 and 24 Ma, and potentially between ~28-26 Ma. Using a conservative estimate of 8.5 km total displacement spanning 4 Myr, a slip rate of 2.1 km/Myr (2.1 mm/a) is found. Total shortening rates in the central Andes (21° S) were ~7-9 mm/a (Oncken et al., 2006), however shortening rates may have differed at 14.9° S latitude. Using these shortening estimates, slip along the Ayaviri fault would have accommodated ~23-30% total shortening during late Oligocene-early Miocene. These results demonstrate that the Ayaviri fault played a key role in development of the Eastern Cordillera, accommodating strain during Andean convergence, and that improved chronostratigraphic constraints from zircon U-Pb provide insights into tectonic and basin evolution studies.

Various temporal and spatial patterns of basement thrust activation suggest important links to along strike orogen history (Kley et al., 1999). In the central Andes of Bolivia, Kley et al., (1996) argued for basement thrust sheets activated with in-sequence advance of the deformation front. Giambiagi et al., (2008) suggest simultaneous deformation of basement and thin-skinned fold-thrust belt, whereas Laramide and Sierras Pampeanas basement uplifts initiated after significant thin-skinned deformation (DeCelles, 2004; Jordan and Allmendinger, 1986). Our constraints on Ayaviri fault motion provide new insights on thin-skinned thrust activity. If structural and stratigraphic relationships across and along strike of the Ayaviri fault system support our suggestion that this fault was initially a basement controlled structure, our new timing constraints will inform the pattern of basement-involved deformation in the northern central Andes. Here, the timing and location of basement involved deformation in the Eastern Cordillera remains poorly constrained. Cooling ages from Triassic synrift plutons situated east of the Ayaviri fault in the Eastern Cordillera of Peru and Bolivia reveal Eocene exhumation attributed to shortening, although controlling structures have not been identified. Mesozoic basement involved normal faults, which governed pre-Andean structure and stratigraphy, were inverted during Eocene Marañon fold-thrust belt deformation in central Peru (Mégard, 1984; Scherrenberg et al., 2012). The early history of the Eastern Cordillera in southern Peru may have also been governed by motion along inherited basement structures. Synchronous Oligocene motion along the entire Ayaviri fault system attests to a potentially long-lived history of basement and thin-skinned deformation interactions during Eastern Cordillera construction.

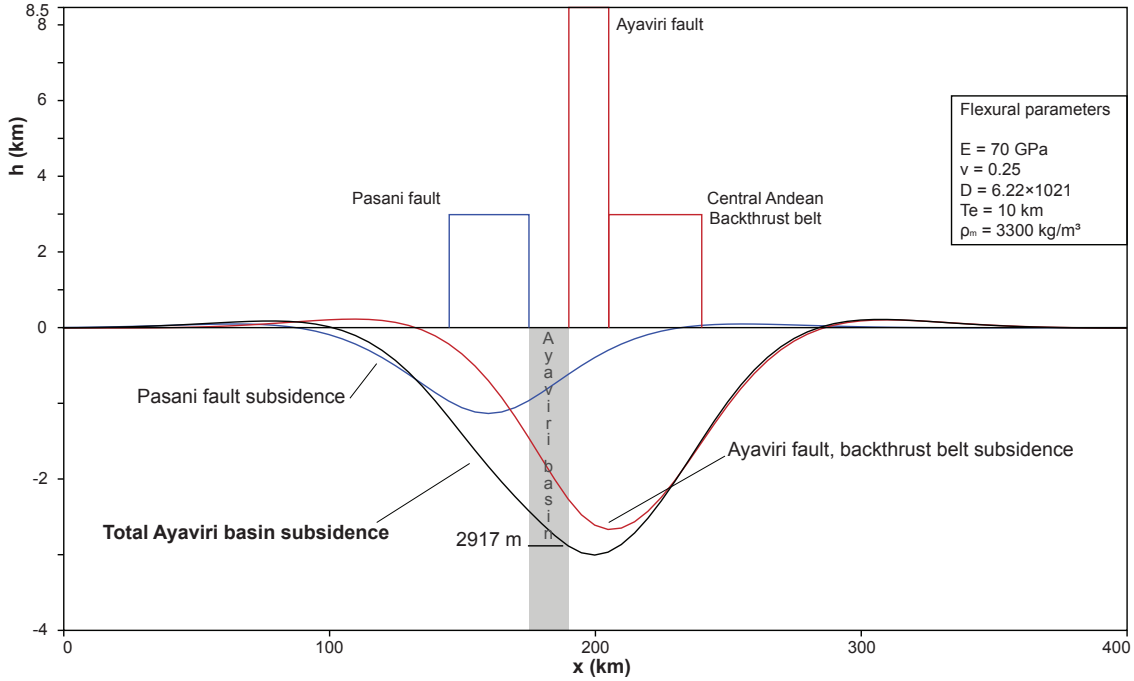

Figure 2.8. 2D flexural model of the Ayaviri basin. Red blocks represent Eastern Cordillera blocks. Blue block represent Pasani fault hangingwall. Red curve shows subsidence profile induced by loading from the Ayaviri fault and the CABB. Blue curve shows loading induced from only the Pasani fault. Black curve is the cumulative subsidence in the Ayaviri basin. Note that Pasani fault motion induces subsidence across the Ayaviri fault. Gray vertical shading marks modern width and position of the Ayaviri basin.

7.2. Basin subsidence, burial and exhumation

The Cenozoic Ayaviri basin history is characterized by continuous non-marine deposition with pulses of rapid sediment accumulation from ~30-15 Ma. Pulses of sediment accumulation were coeval with fault motion, suggesting thrust loading drove flexural subsidence in the northern Altiplano. The first pulse of rapid sediment accumulation spanned ~30-22 Ma and records ~28-26 Ma growth strata along the Ayaviri fault. This defines the structural development of the Altiplano-Eastern Cordillera boundary, and marks further partitioning of the hinterland basin setting. A total of ~2300 m of undecompacted sediment is preserved from this first pulse. Approximately ~1000 m of sediment was deposited above the top of the Ayaviri fault growth strata succession during the first pulse. The second pulse of rapid sediment accumulation began with motion along the Pasani thrust at ~17-16 Ma. A total of ~400 m of undecompacted sediment is preserved above the Pasani fault growth strata. The top of the second pulse is not preserved, but persisted until at least ~15 Ma.

Drivers of hinterland basin subsidence and excavation are linked to tectonic, climatic and erosional processes (Hilley and Strecker, 2005). In some instances, tectonic loads have been insufficient to drive total observed subsidence magnitudes, which has led some to propose dynamic subsidence (Royden and Karner, 1984; Gurnis, 1992; DeCelles, 2004; Flament et al., 2013) and delamination (Göğüş and Pysklywec, 2008) as other important mechanisms that may induce basin subsidence. In the Ayaviri basin, northern Altiplano, we have demonstrated that continuous ~30-15 basin subsidence was likely a flexural response to loading by basin margin thrust fault deformation (Jordan, 1981; Heller et al., 1986; Flemings and Jordan, 1989). Although delamination has been

proposed for other segments of the central Andes to explain Miocene rapid surface uplift (Garzione et al., 2006), we do not suggest it is necessary to explain observed subsidence magnitudes in the northern Altiplano.

Although apatite (U-Th)/He ages do not constrain the timing of cooling, the continuous record of subsidence suggests that exhumation of the Ayaviri fault did not occur until after ~15 Ma. Saylor and Horton (2014) document a rapid surface uplift event in southern Peru from ~19-16 Ma. Although the driver of the transition from deposition to erosion in the Ayaviri basin remains unclear, we suggest exhumation of the Ayaviri fault may be linked to initial uplift of the northern Altiplano.

8. CONCLUSIONS

1) Ages obtained for four tuffs from zircon U-Pb and feldspar $^{40}Ar/^{39}Ar$ geochronology are in agreement. Young populations from detrital zircon U-Pb geochronologic results yield high fidelity chronostratigraphic constraints in agreement with both zircon U-Pb and feldspar $^{40}Ar/^{39}Ar$ geochronology of interbedded volcanic horizons. Detrital zircon geochronology may provide age control for basins along volcanic rich margins even if few volcanic horizons are observed.

2) Growth strata preserved along the basement involved Ayaviri thrust demonstrates late Oligocene age of fault motion. This is in agreement with other late Oligocene growth strata preserved ~400 km along strike of the Ayaviri fault system, suggesting synchronous motion of the Eastern Cordillera-Altiplano boundary.

3) Pulses of rapid basin subsidence were coeval with thrust motion constrained by growth strata, suggesting flexural subsidence in the northern Altiplano. Preliminary 2D models demonstrate that tectonic loads along the basin margins recreate the magnitude of observed stratigraphic thickness in the Ayaviri basin, supporting flexural subsidence as the mode of basin sediment accumulation.

4) Apatite (U-Th)/He thermochronologic data demonstrate that hangingwall and footwall Ayaviri fault blocks were buried to the apatite PRZ after Ayaviri fault motion ended by ~24 Ma. and exhumed.

5) Continuous basin subsidence from 30-15 Ma suggests exhumation of the Ayaviri fault from apatite PRZ could not have initiated until < 15 Ma. A proposed 19-16 Ma surface uplift may explain the transition from subsiding to eroding hinterland basin.

Chapter 3: Structural inheritance and selective reactivation in the northern Altiplano: Andean deformation guided by Triassic extensional structures

ABSTRACT

Structural, stratigraphic, and geochronologic constraints from the Eastern Cordillera, within the central Andean plateau of southern Peru (14-15°S), demonstrate the existence and location of major pre-Andean normal faults that controlled the provenance and initial accumulation of synrift clastic fill composing the Triassic Mitu Group. The timing of initial deposition of the Mitu Group is here constrained to ~242-233 Ma on the basis of detrital and volcanic zircon U-Pb geochronology. Regionally distinct variations in provenance for the Mitu Group, as provided by U-Pb age populations, demonstrate erosion of multiple diagnostic sources from diverse rift-flank uplifts preserved in localized synrift accumulations. Stratigraphic correlations along strike suggest synchronous initiation of extensional basins containing the Mitu Group, in contrast with previous interpretations of southward rift propagation. Field and map observations identify three new pre-Andean normal faults. Subcrop and stratigraphic thickness relationships across the Ayaviri backthrust along the Altiplano-Eastern Cordillera boundary may be features inherited from a pre-Andean normal fault active during Triassic Mitu Group deposition. The orientation of a different non-reactivated normal fault in the Eastern Cordillera suggests selective inversion of individual structures was dependent on fault dip and strike. Motion along the NE dipping San Anton normal fault accommodated up to 7 km of throw and hangingwall deposition of a >2.5 km succession of synrift Mitu Group. A ~4 km thick succession of Carboniferous to Permian strata is selectively preserved only in the subsided hangingwall of this fault, below the synrift

Mitu Group, consistent with large scale erosional removal in the uplifted footwall. The reactivation history of the San Anton normal fault, which guided Cenozoic shortening in the central Andean backthrust belt and contributed to structural compartmentalization of the Eastern Cordillera, may highlight the underappreciated role of pre-Andean structural inheritance in the history of Cenozoic shortening and plateau uplift in the central Andes.

2. INTRODUCTION

The effect of inherited crustal architecture on the style, magnitude and distribution of Andean shortening remains poorly constrained. Many examples worldwide demonstrate that pre-orogenic structural and stratigraphic features define important initial conditions on the evolution of major mountain belts including the Himalayan and Alpine-Appenine systems and North and South American Cordilleras, among others (Argand, 1916; Jackson, 1980; Allmendinger et al., 1983; Allègre et al., 1984; Gillcrist et al., 1987; Colletta et al., 1990; Grier et al., 1991; Allmendinger and Gubbels, 1996; Yin and Harrison, 2000; McQuarrie 2002; DeCelles, 2004; Butler et al., 2006; Mescua and Giambiagi, 2012). At regional scales, pre-orogenic crustal architecture and lithospheric strength may control shortening and regulate uplift of high topography (Barragan et al., 2005; Mouthereau et al., 2013). At local scales, selective reactivation of individual inherited structures potentially dictates the structural style, degree of basement involvement, and geometries of basin evolution (Bayona et al., 2008; Giambiagi et al 2011). Shortening along continental margins with inherited rift systems may result in complex deformational and depositional styles that challenge reconstruction efforts. In the Andes, multiple Proterozoic to Mesozoic deformation events have been proposed

along the western margin of South America. Locating these antecedent structures and, in particular, the distribution of normal faults and associated rift basins, remains a challenge in intensely shortened regions such as the central Andes.

In the Andes, Mesozoic intracontinental rifts and extensional back-arc basins have been identified in the northern (Colleta et al., 1990; Mora et al., 2006), central (Manceda and Figueroa, 1995; Sempere et al., 2002), and southern (Dalziel, 1981) segments of the orogenic belt. The age, location and structural grain of these pre-Andean features vary along strike, potentially influencing subsequent Cenozoic deformation. Inherited crustal and stratigraphic architectures played a key role in developing thick- and thin-skinned deformation, in delimiting the along-strike segmentation of structural style, and in driving variable subsidence in accompanying foreland basins (Kley et al., 1999; Bayona et al., 2008; Giambiagi et al 2012). In the northern Andes of Colombia, the main phase of pre-Andean extension began in the Late Jurassic-Early Cretaceous and was accommodated by multiple rapidly subsiding half-graben basins (Casero et al., 1997). Selective inversion of pre-existing, basement-involved normal faults strongly influenced the development of Cenozoic fold-thrust structures and modern topography in the Eastern Cordillera fold-thrust belt (Mora et al., 2006). In Argentina, basement-involved Cretaceous rifting occurred at variable orientations relative to later N-S Andean structural trends (Cominguez and Ramos, 1995). Cenozoic inversion of favorably oriented normal faults contributed to thick-skinned deformation in the Eastern Cordillera of northwest Argentina (Monaldi et al., 2008). Inversion of late Paleozoic-early Mesozoic half-graben basins within the Neuquén region of Argentina controlled the formation of the Malargüe fold-thrust belt (Manceda and Figueroa, 1995; Giambiagi et al., 2012). These examples demonstrate that the variable timing, orientation, style, and potential basement involvement of pre-existing normal faults may help govern the style, rate, and magnitude

of deformation and basin evolution in certain segments of the Andes. Despite many documented cases of pre-Andean deformation along the orogen, few examples of reactivated structures exist in the central Andean segment. This raises the question whether structural inheritance is key throughout the Andes or remains an important characteristic along only certain segments.

The reactivation of pre-existing normal faults throughout the Andes often involves thick-skinned deformation (Kley, 1996; Mora et al., 2006; Mescua and Giambiagi, 2012), may contribute to along strike changes in orogen width and total shortening (Kley et al., 1999), and may control transfer of deformation to thin-skinned domains (Giambiagi et al., 2009). Basement structures may also have the effect of compartmentalizing structural domains (Rosas et al., 2007). The geometry and kinematics of shortening are often guided by the location, orientation, and potential reactivation of pre-existing structures (Sibson, 1985; Sibson, 1990; Seeber and Sorlien, 2000; Di Domenica et al., 2014). In northern Peru, Hermoza et al., (2005) demonstrate that Eocene-Pliocene subsidence and shortening in the Huallaga basin was influenced by graben inversion. In Colombia and central Peru, the development of passive roof duplexes and hinterland-verging thrusts have been linked to the location and subsurface orientation of normal faults in the Subandean foreland (Mora et al., 2014). In elevated segments of the Andean fold-thrust belt, however, identifying the geometries and kinematics associated with inversion remains challenging without the aid of subsurface datasets.

The Eastern Cordillera of southern Peru forms the high-elevation, NW-trending range separating the northern Altiplano hinterland basin from the Subandean fold-thrust belt and foreland basin. Sempere et al. (2002) proposed a pre-Andean rift along the modern Eastern Cordillera that initiated in central Peru during the Late Permian and

propagated to southern Bolivia by the Middle Jurassic. Although the proposed rift location generally coincides with the preserved synrift Permo-Triassic Mitu Group, the location, orientation, and polarity of major bounding normal faults have not been adequately defined. The geodynamic setting for deposition of the Mitu Group remains debated. Early interpretations attributed the Mitu Group to erosion of a western coastal orogen (Newell, 1953), whereas more recent interpretations have suggested deposition in diverse extensional settings, including a back-arc extensional province (Noble et al., 1978; Reitsma, 2012), continental rift (Dalmayrac et al., 1980), or extension related to orogenic collapse (Dewey, 1988; Rosas et al., 2007; Ramos et al., 2009; McGroder et al., 2015). Although some extensional structures linked with Mitu Group accumulation have been located from geophysical imaging of the Subandean zone in central and northern Peru (Hermoza et al., 2005; Rosas et al., 2007), and hypothesized for southern Peru (McGroder et al., 2015), the exact location of exposed pre-Andean normal faults in southern Peru has not been established.

Recent changes to the Mesozoic chronostratigraphic framework for central and southern Peru highlight key remaining questions in the timing and style of extension (Carlotto et al., 2010). Originally attributed to Permian deposition (Newell, 1953), subsequent studies of the Mitu Group have suggested depositional ages of Late Permian to Early Triassic (Sempere et al., 2002), or exclusively Triassic age (Reitsma, 2012). Although the widespread occurrence of the Mitu Group rocks along the Eastern Cordillera throughout Peru suggests a potentially continuous series of interconnected extensional basins, rapid lateral variations in thickness, facies, and depositional environments suggest the potential for localized subsidence in discrete graben basins (Newell, 1953; Reitsma, 2012). These unresolved questions regarding the potential connection, distribution, and age of Mitu Group basins have hindered reconstruction of

Permian-Triassic basin geometries and regional subsidence patterns. The chronostratigraphic framework, spatio-temporal provenance history, and overall distribution of synrift facies of the Mitu Group are poorly constrained, yet are critical to establishing the pre-Andean structural and stratigraphic architecture.

Here we demonstrate the location of major pre-Andean normal faults within the central Andean plateau using regional subcrop, map, thickness, and facies relationships of the Permian-Triassic Mitu Group. Key cross-cutting structural relationships define several structural domains that delimit these pre-Andean structures in southern Peru, suggesting that potentially basement-involved deformation guided structural compartmentalization. We further refine the chronostratigraphy and provenance of the Mitu Group and assess the timing of basin initiation and coalescence along strike. Finally, we show how selective reactivation of a major normal fault transferred deformation from deeper basement levels to shallow cover strata, influencing the structural development of the Eastern Cordillera.

3. GEOLOGIC FRAMEWORK

The Andes of southern Peru define a NW-trending orogen comprised of the subduction trench, onshore forearc slope, Western Cordillera magmatic arc, Altiplano plateau, Eastern Cordillera fold-thrust belt, and Subandean zone deformation front and modern foreland basin (Figure 1). The Eastern Cordillera preserves two major features that are expressed for hundreds of km along strike in Peru and Bolivia. The first is the NW-trending Cordillera de Carabaya (and Cordillera Real of Bolivia), defined by Triassic plutonic rocks intruded into Ordovician-Devonian metasediments that support a high-elevation (>5-6 km) geomorphologic boundary (drainage divide) between the 4-km-

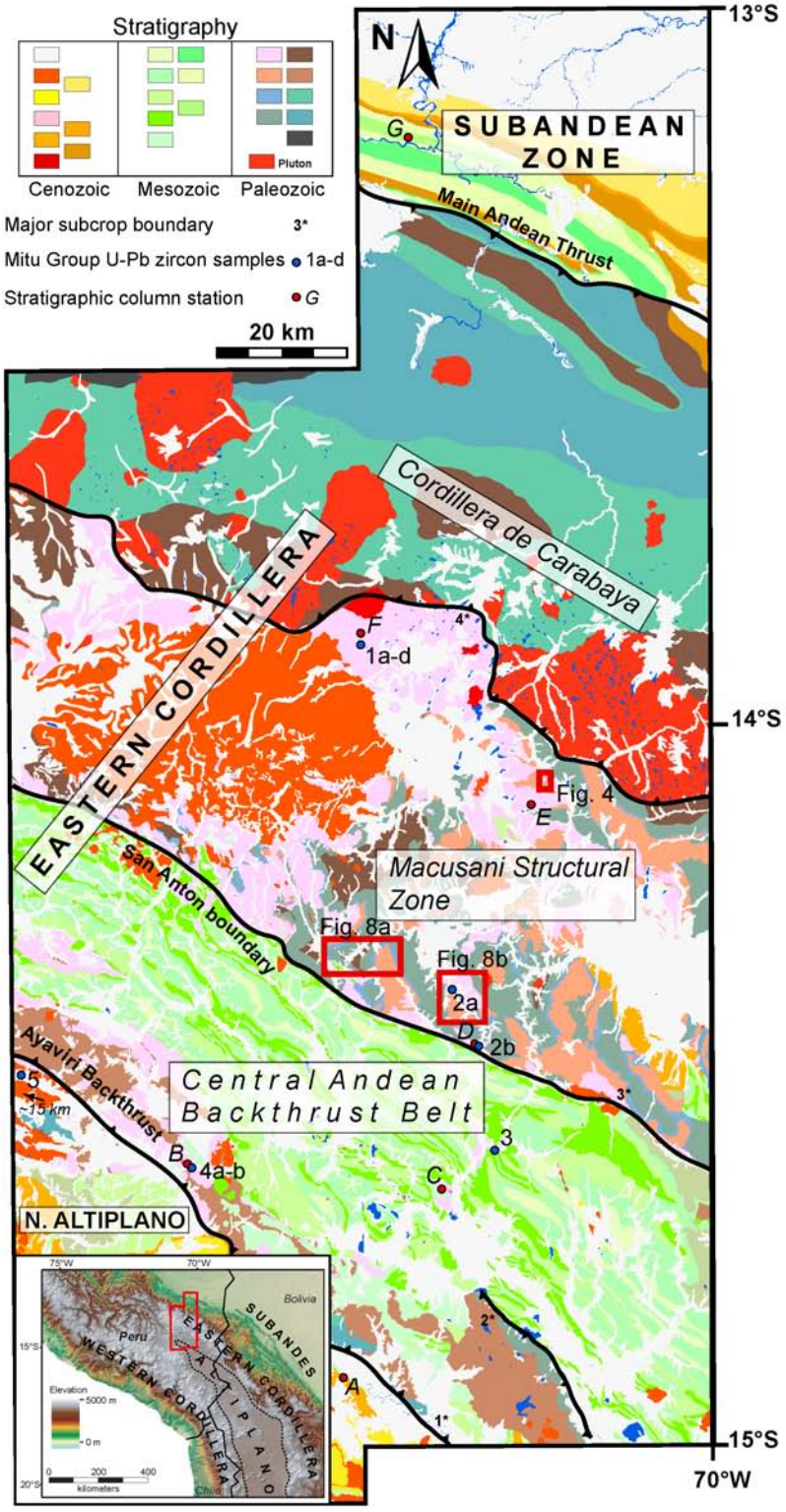
Stratigraphy
Cenozoic
Mesozoic
Paleozoic
Pluton
Major subcrop boundary 3*
Mitu Group U-Pb zircon samples 1a-d
Stratigraphic column station G
20 km
N
13°S
SUBANDEAN ZONE
G
Main Andean Thrust
Cordillera de Carabaya
EASTERN CORDILLERA
F
1a-d
4*
14°S
Fig. 4
E
San Anton boundary
Macusani Structural Zone
Fig. 8a
Fig. 8b
2a
D
2b
Ayaviri Backthrust
5
~15 km
Central Andean Backthrust Belt
3*
3
B
4a-b
C
N. ALTIPLANO
2*
A
1*
15°S
70°W
75°W
70°W
15°S
20°S
Bolivia
Peru
Chile
SUBANDES
EASTERN CORDILLERA
ALTIPLANO
WESTERN CORDILLERA
Elevation
5000 m
0 m
0
200
400
kilometers

Figure 3.1. Geologic map after INGEMMET (1999).

high Altiplano and <1-km-high Subandean zone. The second is the NW-trending central Andean backthrust belt (CABB; Figure 1), defined by dominantly SW-verging, NW fold-thrust structures involving Cretaceous marine sandstones, shales and limestones. The CABB continues in Bolivia (including the Huarina fold-thrust belt), where it exposes dominantly Paleozoic structural levels (McQuarrie and DeCelles, 2001). The structural boundary between the Altiplano and Eastern Cordillera in Peru is the Ayaviri fault, part of a larger Ayaviri fault system (AFS), one of the major backthrust structures within the CABB that was previously referred to by the Spanish acronym SFUACC (Sempere et al., 1990; Ibarra et al., 2004; Perez and Horton, 2014). Between the Cordillera de Carabaya and the CABB is the Macusani Structural Zone, also known as the Precordillera de Carabaya (Kontak et al., 1990; Sandeman et al., 1997) or "the domain of Tardihercynian folds" (English translation from French; Laubacher, 1978) where exposures are dominated by Carboniferous, Permian and Triassic Mitu Group rocks. Faults and folds within the Macusani Structural Zone are not parallel with typical Andean trends, but preserve NS, NE-SW and NNW-SSE orientations.

The tectonic setting of the western Peruvian margin during late Paleozoic-early Mesozoic time remains debated. In Argentina, Carboniferous–Permian rocks folded during the Permian San Rafael orogeny are unconformably overlain by intercalated biomodal volcanics and non-marine siliciclastics of the Triassic synrift Choiyoi Group. This has been interpreted as Triassic collapse of the late Paleozoic orogeny (Dewey, 1988; Mpodozis and Kay, 1992; Ramos, 2009; McGroder et al., 2015). In southern Peru, similar relationships between the Mitu Group and underlying folded Carboniferous to Permian rocks suggest orogenic collapse may have been widespread after Permian orogenesis (Mpodozis and Kay, 1992; Rosas et al., 2007). Other workers, however, have suggested Triassic extension occurred within an intracontinental rift system (e.g.,

Dalmayrac et al., 1980; Kontak et al., 1990; Sempere et al., 2002). Alternatively, Noble et al. (1978) and Reitsma (2012) proposed that this Triassic extension occurred in a back-arc setting, where Triassic plutons emplaced in the Cordillera de Carabaya represent magmatism inboard of a volcanic arc that was largely destroyed by later subduction erosion.

Various subcrop relationships are preserved in the Ordovician to Cretaceous stratigraphic succession exposed in the Eastern Cordillera of southern Peru and provide insights into the pre-Andean structural and stratigraphic framework. The following is a summary of the major patterns, although local variations are common. A thick (up to 10 km) succession of Ordovician to Devonian slates, phyllites and metasedimentary rocks is exposed in the Altiplano, Eastern Cordillera and Subandean zone (Laubacher and Mégard, 1985). No Cambrian or older rocks are observed in the study area. A major unconformity attributed to the Eohercynian orogeny (early Carboniferous) separates the Ordovician through Devonian strata from overlying rocks, which may be Carboniferous, Permian, Triassic, or Cretaceous units (Steinmann and Hoek, 1912; Newell, 1949; Newell et al., 1953; Ahlfeld and Branisa, 1960; Rivas, 1971; Isaacson, 1975; Suarez Soruco, 1976, 1992, 2000; Castaños and Rodrigo, 1978; Dalmayrac, 1978; Laubacher, 1978; Marocco, 1978; Martinez, 1980; Dalmayrac et al., 1980; Sempere et al., 2004). Up to 4 km (Barros and Carneiro, 1991) of Carboniferous shales and quartzites to Permian limestones with 3-5 km wavelength folds are locally preserved beneath an angular unconformity. Cross cutting relationships suggest that these folds formed during latest Permian to earliest Triassic deformation, attributed to the Tardihercynian orogeny (Audebaud and Laubacher, 1969; Laubacher, 1978; Soler and Bonhomme, 1987) also known as the Juruá orogeny (Barros and Carneiro, 1991; Tankard, 2001; Rosas et al., 2007). Where the Carboniferous to Permian units are preserved, the Mitu Group is

preserved above this angular unconformity (Newell, 1953). In other localities, the Mitu Group may overlie Silurian to Devonian rocks. Late Jurassic to Cretaceous marine sandstones, shales and limestones often overlie the Mitu Group with disconformable or angular unconformable contacts, but may also overlie Silurian-Devonian or Carboniferous units where the Mitu Group is not preserved. The Jurassic Pucará Group is not observed in southern Peru, but is present in central and northern Peru overlying the Mitu Group (Rosas et al., 2007).

The Mitu Group of Peru has been defined as the intercalated non-marine red sandstones, shales, conglomerates, volcaniclastics, agglomerates and alkali volcanic rocks capping Permian Copacabana Formation carbonates and underlying Jurassic to Cretaceous marine siliciclastic and limestone rocks (Newell et al., 1953; Laubacher, 1978; Kontak et al., 1990). In southern Peru, Mitu Group deposits are preserved between the Ayaviri backthrust and the Cordillera de Carabaya. The thickest and highest-quality exposures of the Mitu Group are preserved in the Macusani Structural Zone, where rapid lateral thickness and facies changes are observed (Figure 2). Previous workers have linked deposition of the bimodal calc-alkaline volcanic and non-marine siliciclastic Mitu Group deposits in Peru with the intrusion of monzogranitoids along the Eastern Cordillera, and suggested synrift deposition occurred in multiple half-grabens with associated magmatism (Mégard, 1978; Laubacher, 1978; Dalmayrac et al., 1980; Kontak et al., 1990; Sempere et al., 2002; Mišković et al., 2009). Chronostratigraphy of the Mitu Group remains poorly defined, but has been commonly attributed to Permian through Triassic deposition on the basis of regional stratigraphic relationships and correlations (Newell, 1953; Dalmayrac et al., 1980; Kontak et al., 1990; Sempere et al., 2002). Recent workers have refined chronostratigraphic constraints for Altiplano exposures of the Mitu

Figure 3.2. Facies variation within the Triassic Mitu Group from Macusani Structural Zone outcrops. A) Cross stratified coarse sandstone. B) Agglomerate. C) Breccia with volcaniclastic matrix. D) Poorly sorted matrix supported quartzite pebble conglomerate. E) Poorly sorted clast supported limestone cobble conglomerate. F) Bedding surface of planar and ripple cross laminated siltstone.

Group near Cusco and Sicuani, suggesting solely Triassic deposition (Reitsma et al., 2010; Reitsma, 2012).

The observation that deep structural levels are exposed at high elevations within the Eastern Cordillera coinciding with exposures of potential synrift Mitu Group rocks has led authors to suggest the Triassic rift basin was inverted during Cenozoic Andean shortening (Mégard, 1984; Barros and Carneiro, 1991; Rosas et al., 2007; Scherrenberg et al., 2012). Despite this assumption, the locations of major rift structures along the Eastern Cordillera have not been defined. Reconstructing the Mitu basin and identifying the main rift bounding normal faults is necessary to define the upper crustal structural and stratigraphic architecture inherited at the onset of Andean orogenesis.

4. DEPOSITIONAL AGE AND PROVENANCE OF THE SYNRIFT MITU GROUP

4.1. U-Pb zircon geochronology methods

Five medium to coarse-grained sandstones from various levels of the Mitu Group were collected in the Eastern Cordillera of southern Peru for zircon U-Pb geochronology in order to assess depositional (stratigraphic) ages and sediment provenance (Figure 3). Samples were collected from three localities (1, 2, and 5; Figure 1). Sample locations displayed variable facies including medium to coarse-grained sandstone, pebble to cobble conglomerate, volcaniclastic, thin extrusive basalt deposits and volcanic agglomerate. We interpret the general coarse Mitu Group deposits as evidence for proximal and localized, as opposed to far traveled, sediment sources.

Samples 1b and 1c were collected near the base and top, respectively, of Mitu Group exposures near locality 1 (Figure 1). Samples 2 a and b were collected near the

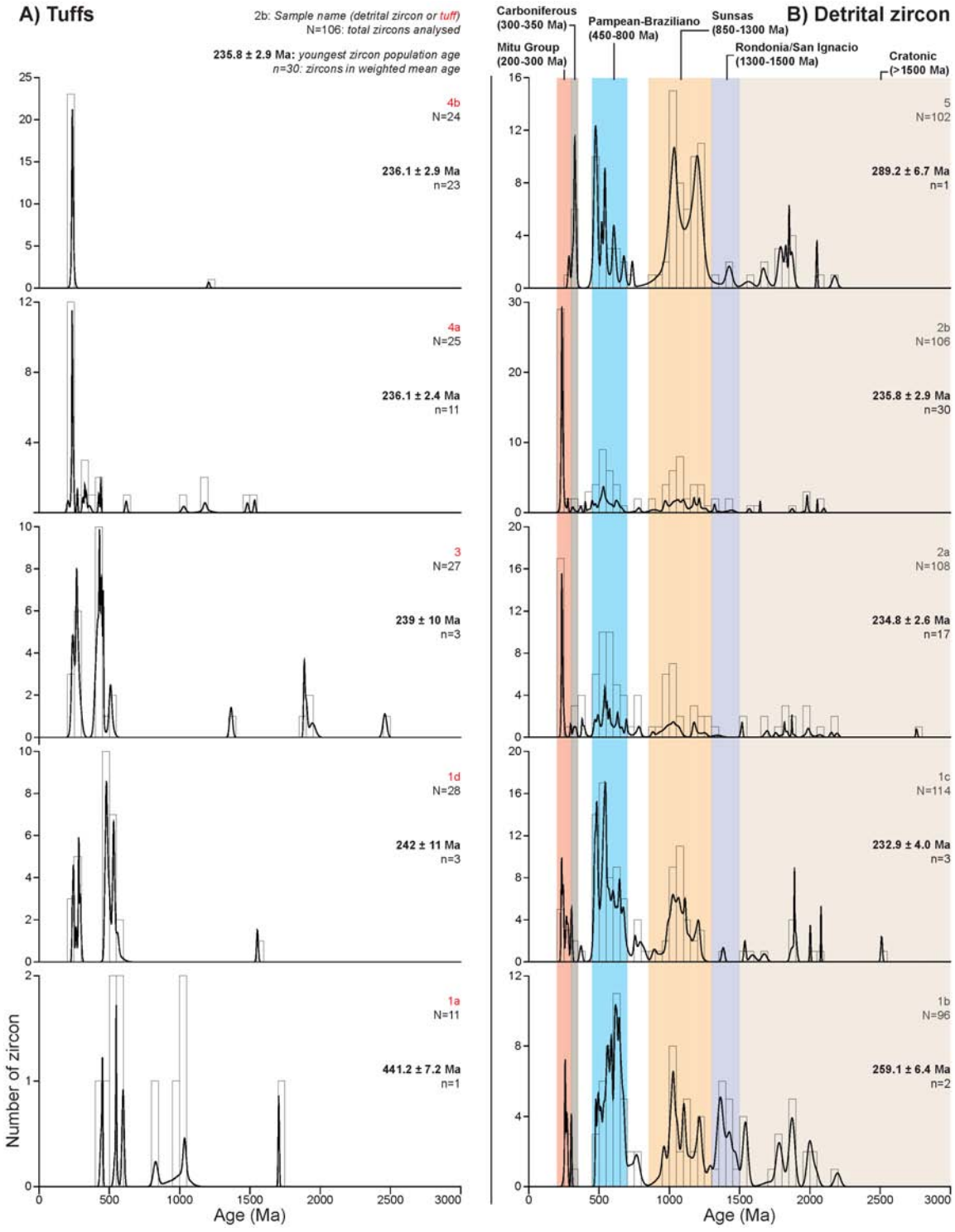
A) Tuffs
2b: Sample name (detrital zircon or tuff)
N=106: total zircons analysed
235.8 ± 2.9 Ma: youngest zircon population age
n=30: zircons in weighted mean age
4b
N=24
236.1 ± 2.9 Ma
n=23
4a
N=25
236.1 ± 2.4 Ma
n=11
3
N=27
239 ± 10 Ma
n=3
1d
N=28
242 ± 11 Ma
n=3
1a
N=11
441.2 ± 7.2 Ma
n=1
Number of zircon
Age (Ma)
B) Detrital zircon
Carboniferous (300-350 Ma)
Mitu Group (200-300 Ma)
Pampean-Braziliano (450-800 Ma)
Sunsas (850-1300 Ma)
Rondonia/San Ignacio (1300-1500 Ma)
Cratonic (>1500 Ma)
5
N=102
289.2 ± 6.7 Ma
n=1
2b
N=106
235.8 ± 2.9 Ma
n=30
2a
N=108
234.8 ± 2.6 Ma
n=17
1c
N=114
232.9 ± 4.0 Ma
n=3
1b
N=96
259.1 ± 6.4 Ma
n=2
Age (Ma)

Figure 3.3. U-Pb zircon geochronology from Mitu Group samples. X axis for all plots from 0-3000 Ma. Y axis for all plots is number of zircons. A) Samples from tuffs interbedded in Mitu Group deposits. B) Detrital zircon samples. Age populations highlighted by colored rectangles.

base and top, respectively, of Mitu Group exposures near locality *2*. Sample 5 was collected from a thin exposure of Mitu Group at locality 5. Samples were prepared using standard crushing, density and magnetic separation techniques (Gehrels, 2000; Gehrels et al., 2008). High purity zircon separates were mounted into epoxy pucks, polished to reveal zircon interiors, and analyzed by laser ablation-multicollector-inductively coupled plasma-mass spectrometry at the Arizona LaserChron Center at the University of Arizona following standard procedures (Gehrels et al., 2008). Approximately 120 zircons of varying size, shape and quality were randomly analyzed from each sample. Zircons with obvious inclusions were avoided.

Results from LA-MC-ICP-MS analyses are plotted as normalized relative age probability plots with age distribution histograms of 50 Myr bins (Figure 3). Populations of zircon ages are depicted as peaks in the probability plot and reflect contribution from source regions with variable zircon ages. Differences among zircon populations between samples have been interpreted as variable contributions from distinct sediment source areas.

4.2. U-Pb detrital zircon results

We identify six populations of detrital zircon ages from the samples. Following is a discussion of populations from oldest to youngest.

Detrital zircon grains exhibiting ages between 1500 and 3000 Ma are observed in all five samples. These Mesoproterozoic zircons have multiple potential original source regions, including South American cratonic blocks, the Arequipa terrane in the Western Cordillera (Loewy et al., 2004; Ramos, 2009; Bahlburg et al., 2011), or recycled from Paleozoic strata of the Eastern and Western Cordillera (Reimann et al., 2010; Bahlburg et

al., 2011; Perez and Horton, 2014). The detrital zircon signature of detritus sourced directly from cratonic blocks would likely reflect dominantly Mesoproterozoic populations and lack Paleozoic age zircons. The minor presence of Mesoproterozoic zircons and higher population of Paleozoic populations observed in all five detrital samples from the Mitu Group is similar to detrital populations observed in Eastern and Western Cordillera units. We suggest this population represents recycled detritus from either the Western or Eastern Cordillera, rather than far traveled first cycle zircons shed directly from the craton.

A 1300-1500 Ma age population (n=13) is observed in sample 1b (lowest detrital sample at locality 1), but is much reduced ($n \leq 4$) in all other samples. This age signature has two likely sources. The first is the Rondonia/San Ignacio cratonic block of Bolivia (Teixeira et al., 1989; Cordani and Teixeira, 2007; Bettencourt et al., 2010). The other potential source is from isolated orthogneiss exposures in central to northern Peru (Chew et al., 2008). This population is relatively rare in Paleozoic sedimentary and intrusive rocks from the Western and Eastern Cordillera of southern Peru (Mišković et al., 2009; Reimann et al., 2010; Bahlburg et al., 2011; Perez and Horton, 2014). If the high proportion of 1300-1500 Ma zircon age population in sample 1b was sourced from orthogneiss rocks situated N or NW of our study, along strike sediment transport from north to south would likely result in this population being observed in correlative stratigraphy along strike. However, this population is not observed in Mitu samples near Cusco (Reitsma, 2012) situated between the northern Peru source and our southern Peru study area, suggesting north to south sediment transport is unlikely. Alternatively, we suggest that this zircon age population was delivered by west directed sediment transport from the Rondonia/San Ignacio block in Bolivia towards the Eastern Cordillera of Peru.

A broad 850-1300 Ma population is observed in all five samples of the Mitu Group. This zircon age population has multiple potential sources, including first cycle zircons shed directly from the Sunsas orogen situated towards the east along the Brazilian craton-Andean interface (Bahlburg et al., 2011), or the Arequipa terrane in the Western Cordillera (Loewy et al., 2004). Alternatively, this age population may represent recycled zircons from Paleozoic strata throughout Peru. The omnipresence of this age population from eastern and western sources presents a challenge to determine a unique sediment source.

A 450-800 Ma age population is present in all five samples. This population is common in Paleozoic strata in the Eastern and Western Cordilleras throughout Peru. Zircon ages alone are insufficient to determine from where this population was sourced.

Carboniferous zircons (300-350 Ma) are present in all five samples. In samples 1b, 1c, 2a, and 2b, this population is insignificant ($n \leq 2$). In sample 5, this population is more prominent (n=6). Potential sources for this population are limited to Carboniferous plutons and Ambo Group rocks from the Eastern Cordillera near Cusco (Mišković and Schaltegger, 2009; Reitsma, 2012). This population was not observed in Ambo Group rocks in this study area situated SE of Cusco (n=0, Perez and Horton, 2014). We interpret this population as evidence for along strike SE directed sediment transport potentially sourced from the Cusco region.

A population of 200-300 Ma zircons is present in all five samples, and is a large proportion of samples 2a and 2b (>10%). Sample 5, the westernmost sample, has the fewest (n=1) zircons from this age population. Late Paleozoic to early Mesozoic zircons are observed in Mitu Group rocks are likely first cycle volcanic zircons. Potential sources are limited to synrift volcanic or plutonic rocks in the Eastern Cordillera, probably situated close to the modern Cordillera de Carabaya plutons.

4.3. Interpretation

The five samples from the base, middle and top of Mitu Group exposures at three locations span ~100 km across the Eastern Cordillera, and hence constrain both temporal and spatial provenance variation of the Mitu Group in southern Peru. We note three key provenance variations in this study that we interpret as evidence for multiple non-integrated rift basins that had different sediment sources. Temporal provenance changes suggest sediment provenance evolved during rift development.

The only significant 1300-1500 Ma zircon population is observed in the stratigraphically lowest detrital zircon sample (1b; n=13) from the easternmost locality, and likely reflects west directed sediment transport from the Rondonia/San Ignacio cratonic block in Bolivia. Upsection at the same locality, the Rondonia/San Ignacio population nearly disappears (sample 1c; n=1). Locality 1 also exhibits an upsection increase in Triassic zircon proportion, potentially reflecting increased silica-rich volcanic production through time (Panca et al., 2011). The lack of the 1300-1500 Ma population in all other study areas suggests west directed sediment transport that carried Rondonia/San Ignacio cratonic zircons from Bolivia was prevented from reaching the other localities. The upsection disappearance of this population at locality 1 suggests either a reorganization of the sediment routing pathway, or development of a rift shoulder situated between the Rondonia/San Ignacio craton and the Eastern Cordillera that effectively blocked cratonic detritus from reaching the study area.

The second provenance variation is the presence of Carboniferous zircons at the westernmost locality (sample 5; n=6) and paucity of this population in all other localities ($n \leq 2$). We suggest that axial sediment transport from the Cusco region south towards the

study area delivered Carboniferous zircons to locality 5. The lack of significant Carboniferous zircon populations at other localities may reflect source dilution, or could support evidence for multiple, non-integrated rift basins separated by rift flanks that prevented mixing of sediment sources.

The third provenance variation is the lack of a syndepositional zircon age population at locality 5, but strong presence in localities 1 and 2. The absence of this population may be attributed dilution of the distant Eastern Cordillera source of synrift volcanic products. Alternatively, the lack of synrift zircons at locality 5 further supports the presence of boundaries between individual rift basins that prevented wide spread sediment transport across the study area.

Although the structural and sediment dispersal framework of the Triassic rift remains unsatisfactorily constrained, spatial and temporal changes in Mitu Group provenance suggest rift basins were not integrated into a large continuous basin. This finding is supported by rapid lateral facies variations (Figure 2).

4.4. U-Pb depositional age constraints

Zircon U-Pb ages of interbedded volcanic horizons and the youngest populations from detrital zircon samples provide chronostratigraphic constraints for Mitu Group deposition in the study area (Figure 3). Geochronologic results from tuffs constrain the true depositional age, whereas the youngest population of detrital zircons in a sample constrains the maximum depositional age. The true depositional age of these detrital samples may be younger. Locality 1 represents the thickest preserved Mitu Group succession (>2 km) in the study area. Sample 1a is the stratigraphically lowest. The sample is an extrusive basaltic-andesite interbedded in coarse-grained Mitu Group clastic

and volcaniclastic deposits. The sample yielded few zircons. The youngest single zircon is 441.2 ± 7.2 Ma, which is older than the stratigraphically constrained late Permian to Triassic age for the base of the Mitu Group. Sample 1b is ~1000 m upsection and is a detrital zircon sample with maximum depositional age of 259.1 ± 6.4 Ma (n=2). The true depositional age could be younger. Samples 1c and 1d (detrital zircon and reworked tuff, respectively) are a farther ~1000 m upsection and dated as 232.9 ± 4.0 Ma and 242 ± 11 Ma, respectively. The detrital zircon sample 1c is ~3 m above 1d, but has a younger, more precise age than the underlying reworked tuff. Overall we interpret locality 1 as Late Permian to early Late Triassic deposition of the Mitu Group.

Detrital zircon samples at locality 2 constrain the depositional age for the base and top of the Mitu Group (2a and 2b, respectively) and were collected within 7 km NE of the major San Anton map subcrop boundary (Figure 1). Here, the preserved Mitu Group succession is <1.5 km thick. Basal sample 2a was collected ~20 m above the angular unconformity separating Permian Copacabana limestones below from Mitu Group conglomerates and coarse sandstones above. The maximum depositional age is 234.8 ± 2.6 Ma (n=17). Sample 2b was collected <150 m below the depositional contact with the overlying Cretaceous Muni Formation. The maximum depositional age of 2b is 235.8 ± 2.9 Ma (n=30). Within error, both samples from locality 2 have the same age, and are slightly older than the youngest depositional age at locality 1. If these new geochronologic constraints accurately approximate true depositional age, the 1.5 km thick Mitu Group deposits in this locality may have accumulated rapidly. Alternatively, the ~235 Ma zircon age population observed in both samples may have derived from a significant main pulse of synrift volcanism at the onset of Mitu rift subsidence. Subsequent volcanism, if it occurred, was not a major contributor of sediment to locality 2. Instead, the entire succession of Mitu Group deposits at locality 2 may have derived

from ~235 Ma volcanic and pluton sources, which would result in uniform detrital zircon maximum depositional ages throughout the succession. In general, locality 2 preserves early Late Triassic depositional ages for the Mitu Group.

Sample 3 was collected at from a localized exposure within the CABB of Mitu Group below an angular unconformity with overlying Cretaceous Muni Formation. The sample is from a fine-grained purple andesitic tuff that has been deformed by penetrative cleavage development and small amplitude folds that do not affect the overlying Cretaceous rocks. The sample yielded few zircons, and many were inherited older zircons. A population of three youngest zircons yielded an age of 239 ± 10 Ma, consistent with Middle to Late Triassic deposition of the Mitu Group in the CABB.

Two samples from locality 4 were collected near the base and top of a 300-400 m thick succession of intercalated medium-grained tuffs and volcaniclastic deposits. The base of the Mitu Group is defined by an angular unconformity with the Silurian/Devonian Chagrapi Formation below. The top of the Mitu Group is defined by an angular unconformity with the Cretaceous Muni Formation above. Samples 4a and 4b have ages of 236.1 ± 2.4 Ma and 236.1 ± 2.9 Ma, respectively. Locality 4 preserves Middle to Late Triassic Mitu Group deposition and volcanism.

Locality 5 has one detrital zircon sample and is the westernmost locality. The youngest detrital zircon grain has an age of 289.2 ± 6.7 Ma. This date is older than the Leonardian age suggested for the top of the underlying Copacabana Formation, based on biostratigraphic constraints (Carlotto, 2010). Hence, the true depositional age of the Mitu Group is younger than the single detrital zircon grain age, but remains poorly constrained at this location.

The zircon U-Pb geochronologic constraints for the Mitu Group exposed in the Eastern Cordillera of southern Peru broadly support Late Permian to early Late Triassic

ages suggested previously (Newell et al., 1953; Laubacher, 1978; Kontak et al., 1990). However, we suggest that the youngest age populations provided by samples 1a, 1b, and 5 do not reflect the true depositional ages of the corresponding samples. The young populations for sandstone samples 1b and 5 are composed of very few (n=2 and 1, respectively) ages. Sample 1a is from an extrusive basaltic-andesite within the Mitu Group, yet contains multiple zircons older than 440 Ma, suggesting entrainment of inherited zircons from the surrounding Paleozoic host rock. A lack of eruptive zircons may be attributable to the relatively mafic geochemistry of these igneous materials. In contrast, other detrital zircon samples, tuffs and volcaniclastic samples have significant ($n \geq 3$) populations of potentially syndepositional zircons. These samples (1c, 1d, 2a, 2b, 3, 4a, 4b) have ages between 242 ± 11 Ma and 232.9 ± 4.0 Ma, suggesting a Triassic age for deposition of the Mitu Group in southern Peru. Reitsma (2012) demonstrated onset of Mitu Group deposition between 241.5 ± 6.0 Ma and 234.3 ± 0.3 for areas up to ~700 km NW from this study area. Our new depositional age constraints are consistent with those workers.

We interpret these results in two potential scenarios. The first is that synrift Mitu Group deposition may have initiated in the late Permian but lacked the acidic volcanism necessary for zircon crystallization. We suggest this is unlikely, as the upper Copacabana Formation is well constrained as Late Permian in age. Additionally, ages of intrusions that cross cut folded Permian Copacabana Formation have been dated as ~245-233 Ma (Soler and Bonhomme, 1987). The Mitu Group is often deposited on folded Permian Copacabana Formation strata and therefore postdates both the folding and Early Triassic intrusions. In the second preferred scenario, we interpret zircon U-Pb constraints from the Abancay and Cusco regions (Reitsma, 2012) and this study as evidence for nearly uniform Middle to Late

Triassic initiation of Mitu Group deposition ~700 km along strike. This consistency suggests that the onset of rifting was also synchronous along strike.

5. PRE-ANDEAN NORMAL FAULTS

5.1. Outcrop example

Few outcrop examples of pre-Andean normal faults have been identified in the Eastern Cordillera of the central Andes. Here we present a previously undocumented normal fault situated at ~4800 m elevation ~20 km east of the town of Macusani in southern Peru (Figure 4). The fault is exposed along the west side of a glacially carved ~500 m deep valley. It strikes ~290° and is exposed for <2 km along strike. Cross-cutting relationships demonstrate that the ~40°SW dipping normal fault post-dated harmonic folding of the Permian Copacabana Formation limestones and older rocks. Deposits of volcaniclastic and conglomerate Mitu Group in the hangingwall show slight thickening towards the fault, which may represent deposition during normal fault motion and hangingwall subsidence. No overlap assemblage is preserved that seals, and therefore post-dates, normal fault motion.

Mitu Group rocks preserved in the normal fault hanging wall dip ~20° N. Assuming that the Mitu Group beds were deposited subhorizontally, the original normal fault dip ~60° SW. We observed no evidence for folding of the Mitu Group at this outcrop, suggesting minimal post depositional deformation, except for regional tilting of the normal fault and associated fault blocks. We attribute tilting of Mitu Group deposits and the normal fault to subsequent deformation related to Andean orogenesis.

Figure 3.4. Outcrop example of Triassic normal fault. Location from Figure 1. Schematic location in Figure 5 and 6.

This outcrop example of a pre-Andean normal fault of probable Triassic age does not appear to have been reactivated as a thrust fault. Typical normal fault inversion geometries such as footwall shortcuts or hangingwall anticlines are not observed. The NW-SE strike of the normal fault trend is subparallel to Andean structures. As such, we suggest that the key factor inhibiting reactivation was high fault plane dip, rather than strike orientation. This interpretation is consistent with other workers who suggest normal fault inversion is most likely for faults dipping < ~45° (Sibson 1985, 1990).

Although the fault is not reactivated, surrounding geologic relationships suggest that it is linked to a larger normal fault that controlled Cenozoic deformation. The outcrop scale normal fault (Figure 4) is synthetic to a proposed larger SW dipping normal fault that accumulated thick Mitu Group deposits and preserved ~4 km of Carboniferous to Permian strata in its hangingwall. An NE dipping SW verging Andean thrust fault juxtaposes Carboniferous strata and Triassic plutonic rocks on Permian Copacabana Formation and Triassic Mitu Group rocks. The pattern of Andean thrust fault interacting with an inherited Triassic normal fault (Figure 5) is similar to proposed Alpine fold-thrust structures (Welbon and Butler, 1992; Butler et al., 2006).

5.2. Subcrop relationships and lateral thickness variations

Depositional, unconformable and fault relationships were evaluated across the Eastern Cordillera for the Carboniferous (Ambo Group and Tarma Formation), Permian (Copacabana Formation), Triassic (Mitu Group), and Cretaceous units based on existing geologic maps (INGEMMET, 1999), our own observations, and previous studies (Audebaud and Laubacher, 1973; Mégard, 1978; Dalmayrac et al., 1980). We agree with previous workers on the presence of three major unconformities. Well-constrained

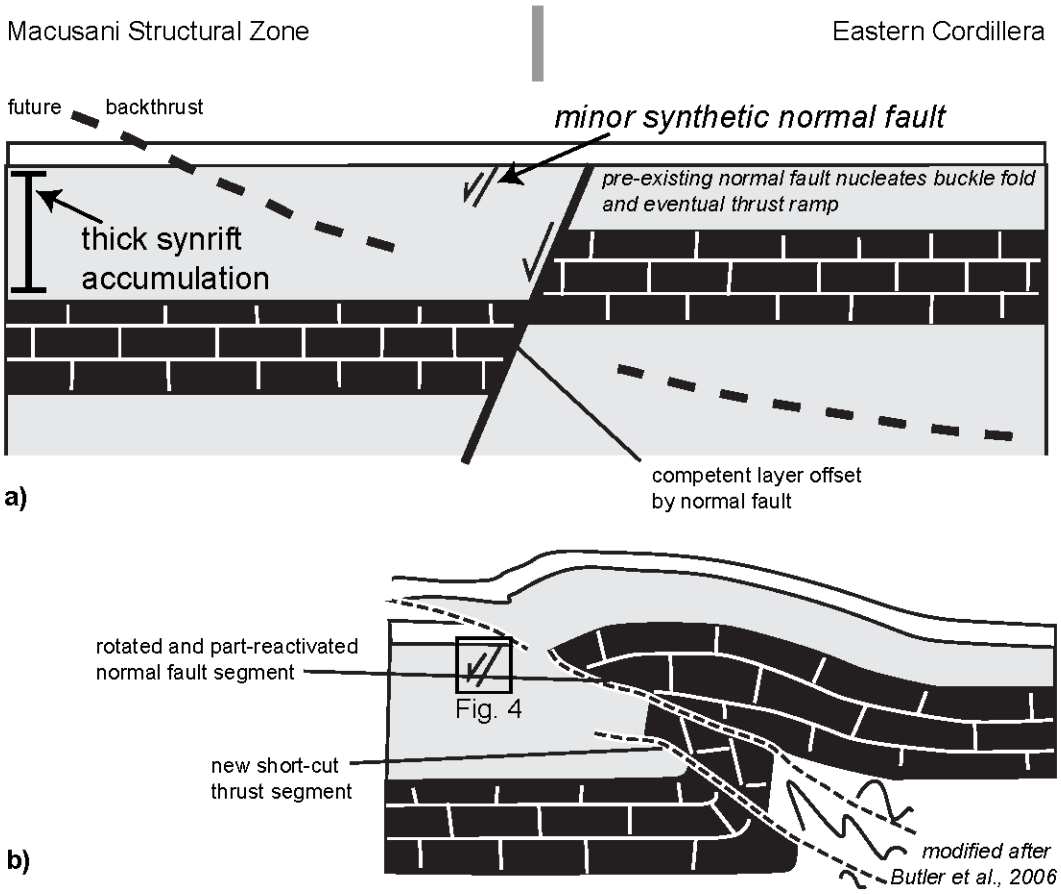

Figure 3.5. Schematic illustration of how normal faults may nucleate new thrust faults that dip opposite direction. Note schematic of location of normal fault from Figure 4. Modified after Butler et al., (2006).

sections at seven key stations A-G (Figure 1, Figure 6a) illustrate lateral changes in thickness, subcrop relationships and these unconformities across the Eastern Cordillera.

A cross-sectional synthesis of these subcrop and thickness variations (Figure 6a) reveals relationships that necessitate pre-Andean structures (Figure 6b). The dip direction of normal faults 1* - 3* are correlated with the modern thrust faults that mark the subcrop and thickness boundaries. We suggest these may be inverted normal faults. Fault 4* is inferred based on stratigraphic and subcrop relationships; it is the conjugate to fault 3*. One of the most significant subcrop and thickness changes is observed between stations C and D across the major San Anton map boundary (3*, Figure 1). At station C we demonstrate that >2 km of Cretaceous rocks are deposited disconformably on <300 m of Mitu Group rocks, which lay unconformably on Devonian and older strata. Carboniferous to Permian strata are absent. In contrast, station D situated 10-20 km NE preserves ~4 km of folded Carboniferous to Permian rocks beneath up to 700 m of Mitu Group rocks. At the surface, there is no fault relationship at the San Anton boundary. However, we suggest that this boundary was achieved by a NE dipping normal fault at depth.

We present two possible scenarios to explain the above observations across the San Anton boundary (Figure 7). Both scenarios use a conservative thickness estimate of 3500 m for Carboniferous to Mitu Group, although true thicknesses are often greater. Scenario 1 recreates the subcrop and thickness relationships with a tapered stratigraphic wedge and does not require a pre-Andean structure. We investigate two cases for typical stratigraphic wedges, which dip less than 10°, and often <3°. With these dips a wedge ~20-66 km wide is required to create a 3500 m thick Carboniferous to Mitu Group succession. To laterally juxtapose this thick package within ~10 km of the <300 m thick Mitu Group would require ~19-61 km of shortening. We consider this scenario unlikely, as published total shortening estimates for this segment of the Andes is 123 km (Gotberg

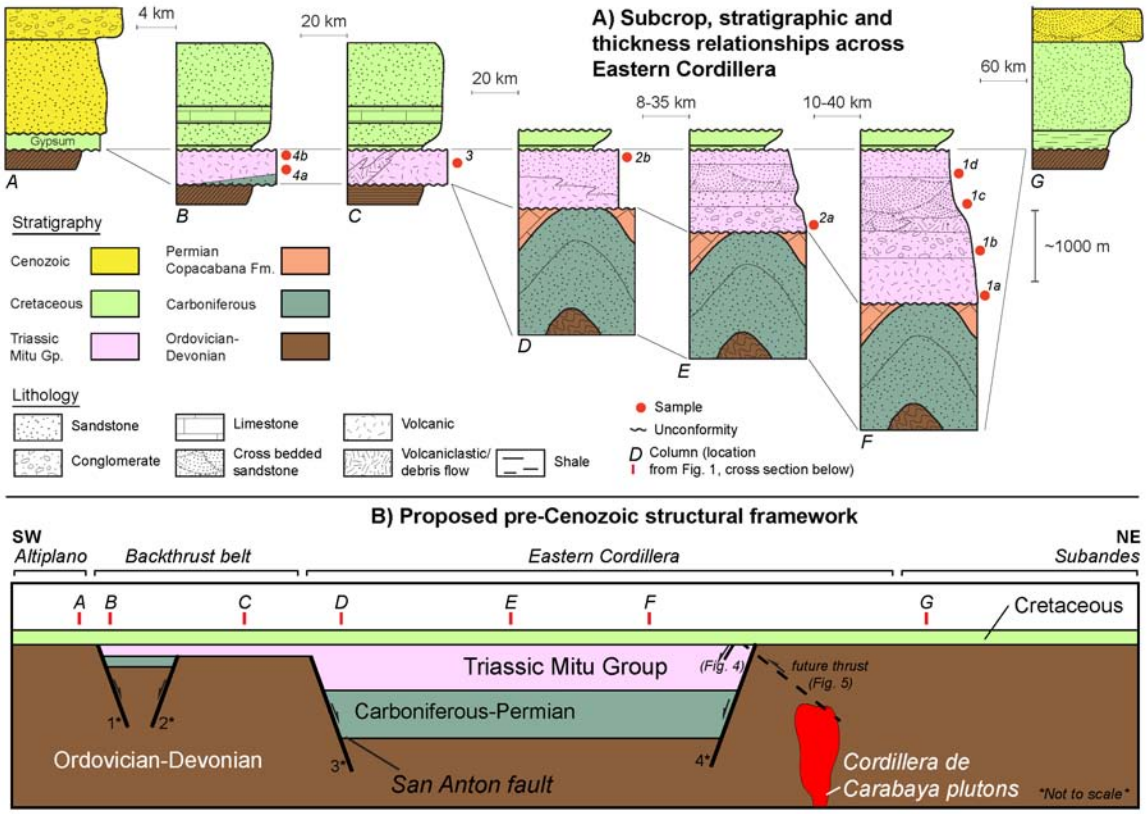

Figure 3.6. A) Subcrop and thickness variations across the Eastern Cordillera. Station location from Figure 1. Subcrop, thickness relationships from field and map data. Distance between stations measured perpendicular to Andean strike. B) Schematic proposed pre-Cenozoic structural framework. Subcrop and thickness variations recreated with normal faults 1*-4*. Fault numbers from Figure 1.

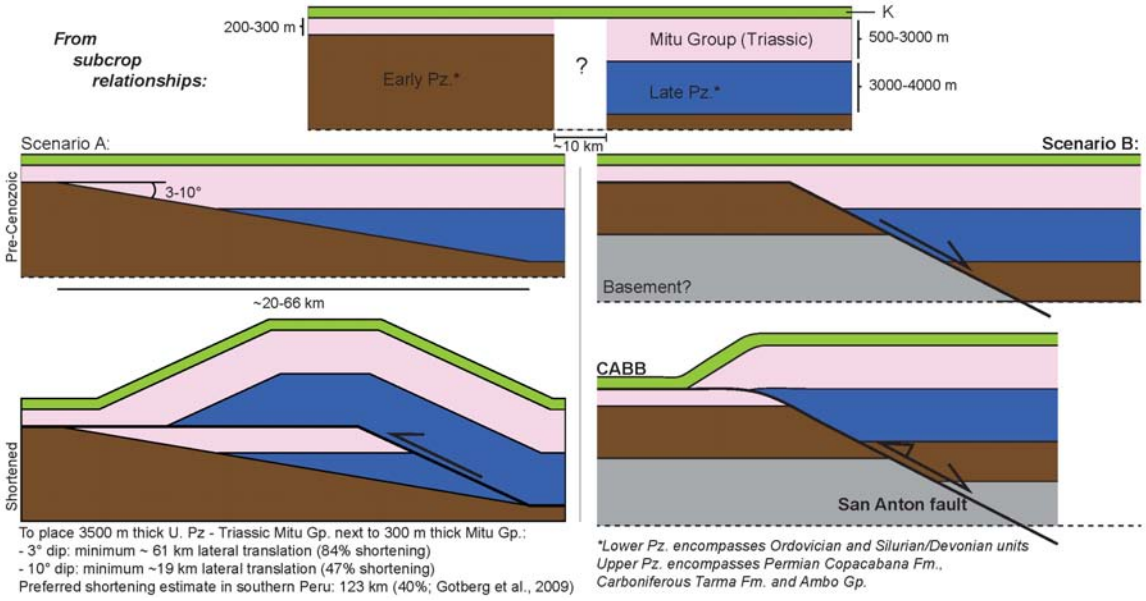

Figure 3.7. Two potential scenarios to explain subcrop and thickness changes between stations C and D (Figure 1, 6).

et al., 2010). The shortening required in scenario 1 (~19-61) km suggests up to ~49% of total shortening was accommodated along a single structure. We consider this unlikely.

Scenario 2 recreates the subcrop and thickness variations with a NE dipping normal fault that preserves Carboniferous to Permian strata and deposition of thick Mitu Group strata in the hangingwall. In this setting, a steeply dipping normal fault would require low total extension to accumulate minimum 3500 m of Carboniferous to Mitu Group strata. In the footwall, Carboniferous to Permian strata was not preserved. We suggest these units were eroded from the footwall. Observations of the Mitu Group immediately to the NE of the San Anton boundary at sample localities 2a, b and station D demonstrate a mix of coarse volcaniclastics interbedded with pebble to cobble conglomerates composed primarily of Permian limestone clasts (Figure 2e). Absence of Permian Copacabana Formation limestones in the proposed footwall and the presence of Copacabana limestone clasts in Mitu Group deposits in the proposed hangingwall is consistent with a normal fault at this position. These fault proximal facies, subcrop relationships and thickness variations observed across the San Anton boundary suggest it is the result of a pre-Andean normal fault. The thickness of strata preserved in the hangingwall (up to 7 km) suggests the San Anton boundary represents a major normal fault that controlled the Mitu Rift.

5.3. Pre-Andean deformation preserved by structural compartmentalization

Multiple phases of shortening and a phase of extension have been proposed in the central Andes of southern Peru (Mégard et al., 1971; Laubacher, 1978; Mégard, 1978; Dalmayrac et al., 1980; Laubacher and Mégard, 1985; Jimenez et al., 2009). Identifying the pre-Andean San Anton normal fault is key because Paleozoic rocks preserved in the

hanging wall (Macusani Structural Zone) record multiple pre-Andean deformational events. These pre-Andean deformational events have variable trends, including non-coaxial orientations that are oblique to typical Andean trends. Outside of the Macusani Structural Zone, Andean structures trend NW-SE. In the CABB and Eastern Cordillera, Cretaceous and older strata are deformed by NW trending, SW verging faults and folds. In the Macusani Structural Zone, post-Triassic, potentially Andean age thrust faults have variable orientations that are not parallel to Andean trends, and often reutilized pre-Andean structural fabrics.

The earliest phase (Eohercynian deformation) is evident as NW trending, shallowing plunging fold axes in Silurian-Devonian shales and older units (Figure 8a). Cross cutting relationships suggest deformation occurred during late Devonian to early Carboniferous (Dalmayrac et al., 1980; Laubacher and Mégard, 1985). Folding is generally harmonic, with moderately dipping limbs and ~1 km wavelength. Silurian-Devonian units that preserve this deformation are observed in localized erosional windows beneath an angular unconformity attributed to the Eohercynian phase.

Above this unconformity are Carboniferous to Permian shales, quartzites and carbonates folded in broad synclines and anticlines at ~3-5 km wavelengths with 6-7 km long axial traces (Figure 8a, b). These folds are upright, with moderately dipping limbs, and rounded hinges and do not affect overlying Mitu Group rocks. Cross cutting relationships suggest late Permian age deformation (Mégard et al., 1971, Laubacher, 1978; Marocco, 1978) attributed to the Juruá orogeny. Similar cross cutting relationships have been referred to as the San Rafael orogenesis in Argentina (Kleiman and Japas, 2009; Ramos, 2009). Fold axes trend NNW-SSE, NE-SW and N-S. Folds are < 20 km long and often terminate into other non-parallel folds. Some folds change orientation along strike, either from NNW-SSE to ENE-WSW or from NE-SW to NNW-SSE.

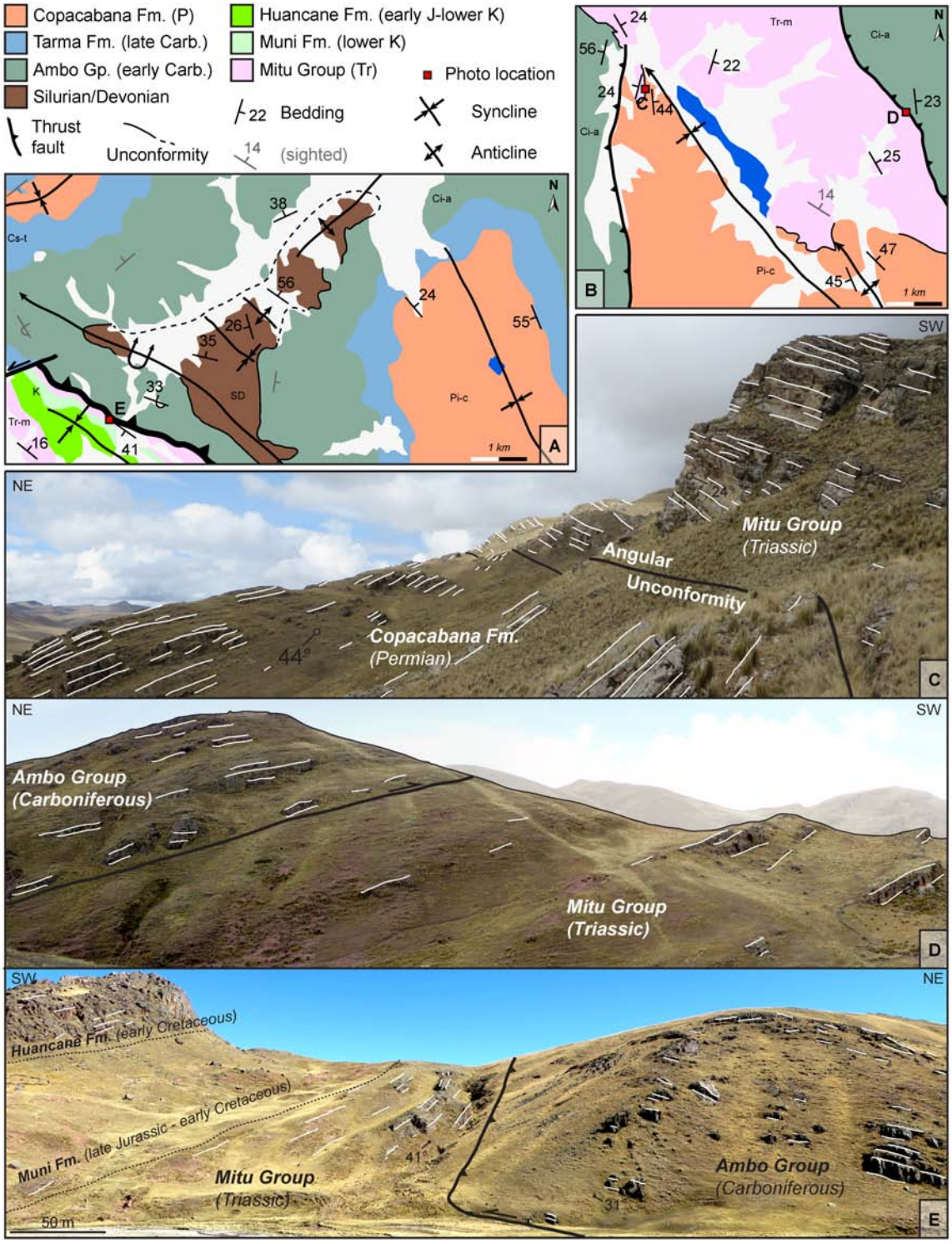
Copacabana Fm. (P)
Tarma Fm. (late Carb.)
Ambo Gp. (early Carb.)
Silurian/Devonian
Thrust fault
Unconformity
Huancane Fm. (early J-lower K)
Muni Fm. (lower K)
Mitu Group (Tr)
22 Bedding
14 (sighted)
Photo location
Syncline
Anticline
N
Cs-t
Ci-a
Tr-m
K
Pi-c
SD
E
A
1 km
B
C
D
SW
NE
Mitu Group
(Triassic)
Angular
Unconformity
Copacabana Fm.
(Permian)
44°
Ambo Group
(Carboniferous)
Mitu Group
(Triassic)
Huancane Fm. (early Cretaceous)
Muni Fm. (late Jurassic - early Cretaceous)
Mitu Group
(Triassic)
Ambo Group
(Carboniferous)
50 m
E

Figure 3.8. Structural relationships documenting pre-Andean deformation preserved in the Macusani Structural Zone. Map and photo locations from Figure 1.

Previous interpretations of these folds have been unclear, but suggest re-folding as a mode of curved fold creation (Laubacher, 1978). However, other curved folds from the Andes have been interpreted as the result of complex basement interaction (Jimenez et al., 2012) although the short strike length of these folds are difficult to reconcile with deep basement deformation. Another potential explanation of these folds may be deformation over an extremely weak detachment, likely Devonian shales.

A N-S thrust fault juxtaposes west dipping hangingwall flat Carboniferous quartzites and shales on east dipping footwall ramp Permian carbonates (Figure 8b). Mitu Group rocks are deposited in angular unconformity above the broad, variably oriented folds (Figure 8a, c) and N-S trending thrust fault. NNW trending fold axes and the N trending thrust fault are attributed to Juruá deformation observed below the Mitu Group, which dips ~20° E (Figure 8b). We interpret this observation as evidence that deposition of the Mitu Group occurred after folding and thrust fault deformation, sealing Juruá deformation. Our new geochronologic constraints from Mitu Group samples (Figure 3) paired with Late Permian biostratigraphic constraints on Copacabana Formation deposition (Grader et al., 2008) brackets the Juruá deformation between ~275-233 Ma.

Within the Macusani Structural Zone, Andean age deformation is accommodated differently than in other regions of the Eastern Cordillera. A NNW trending, ENE dipping thrust fault juxtaposes east dipping hangingwall flat Carboniferous rocks on generally east dipping footwall flat Mitu Group rocks (Figure 8b, d). This thrust fault cuts the Mitu Group and demonstrates that post-Triassic (potentially Andean) shortening reactivated structures parallel to earlier Juruá grain. The timing of this thrust fault remains poorly constrained. A NW trending, southwest verging thrust fault is parallel to Andean trends (Figure 8a). The hangingwall is defined by an overturned anticline with NE dipping axial plane developed in Carboniferous strata. This fault folds a NE trending

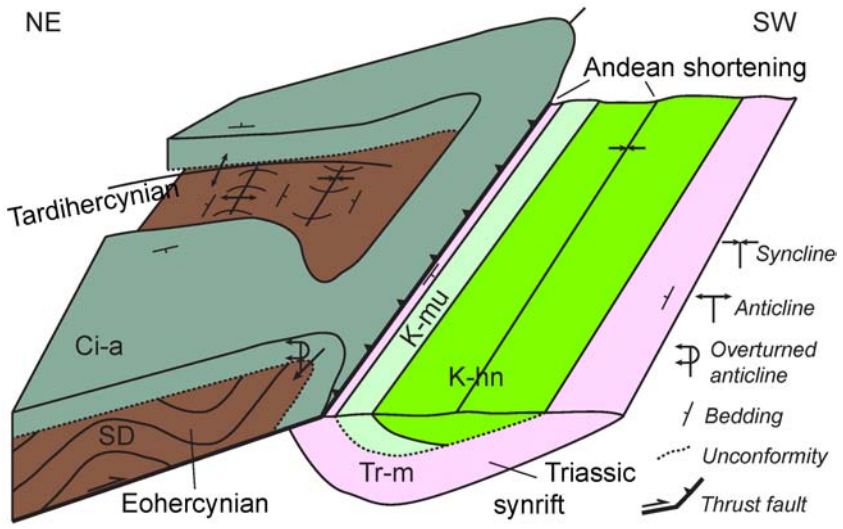

Figure 3.9. Schematic block diagram from Figure 8A. Note three phases of deformation. Eohercynian: small amplitude folds of Silurian/Devonian rocks (SD). Tardihercynian: Angular unconformity separating SD from overlying Carboniferous Ambo Group (Ci-a). The Ambo Group is folded by larger wavelength folds at angles oblique to typical Andean trends. Andean: Triassic Mitu Group rocks are separated unconformably from overlying Cretaceous Muni and Huancane formation rocks (K-mu, K-hn). The Triassic and Cretaceous rocks are folded into a syncline and in the footwall of an Andean thrust fault that juxtaposes Paleozoic rocks against Mesozoic rocks.

Juruá anticline. In the footwall, Mitu Group and Cretaceous rocks are folded into an upright NW trending syncline (Figure 8a, e) suggesting Andean deformation.

The complete record of Eohercynian and Juruá shortening, Triassic Mitu rifting and Andean shortening is present only to the NE of the San Anton boundary (Figure 9). This major pre-Andean normal fault played a key role in preserving pre-Andean deformation and compartmentalized styles of Andean deformation.

6. DISCUSSION

6.1. Selective reactivation of pre-Andean normal faults

Stratigraphic, structural, and subcrop relationships across the Eastern Cordillera identify pre-Andean normal faults. In this study we present examples of normal faults that are not reactivated, normal faults that are inverted as thrust faults, and normal faults that are interpreted to facilitate nucleation of new thrust faults dipping in opposite directions. The outcrop scale minor normal fault in the Eastern Cordillera (Figure 4) is an example of a preserved, non-reactivated normal fault. However, it is in the footwall of a larger Andean thrust that cross-cuts a probable major Triassic normal fault (Figure 5). The Andean thrust fault defines the structural boundary between the Cordillera de Carabaya and the NE margin of the Macusani Structural Zone, and is a major structure in the Eastern Cordillera fold-thrust belt.

A key map boundary between the CABB and the SW margin of the Macusani Structural Zone is likely the result of thrust reactivation of a conjugate normal fault. We interpret broad folds, non-coaxial structural patterns, and deeper structural levels in the Macusani Structural Zone as evidence for thick-skinned thrusts deforming a large

basement block. We interpret this block as elevated above the CABB by thrust reactivation of a major Triassic normal fault (Figure 10). A key observation identifying this structure are subcrop relationships (Figure 6) and map relationships, specifically the ~30 km long depositional contact between Cretaceous Muni Formation in the CABB and Triassic Mitu Group in the Macusani Structural Zone. In the Macusani Structural Zone, a >2 km thick Mitu Group package is deposited on ~4 km thick Carboniferous to Permian succession. Across the map contact in the CABB, <300 m thin Mitu Group rocks are deposited on Silurian/Devonian rocks, and the upper Paleozoic sequence is not preserved. In our proposed kinematic reconstruction (Figure 10), thick-skinned reactivation of the normal fault transfers slip upsection to a shallow basal Cretaceous detachment and guides thin-skinned deformation in the CABB. We suggest that the vergence direction of the CABB in southern Peru may result from inversion of this major pre-Andean normal fault.

The Ayaviri backthrust is proposed to be a thin-skinned thrust fault that nucleated from an inherited pre-Andean normal fault. The structure represents a long-lived and potentially crustal scale boundary (Carlier et al., 2005) that is present for >300 km along strike (Perez and Horton, 2014). As such, this structure represents a major Central Andean feature key to Altiplano evolution. Oligocene thrust reactivation of the Ayaviri fault accommodated deformation propagation from the CABB towards the Altiplano. Crustal loading from cover and basement thrust deformation induced rapid subsidence in the Ayaviri basin, controlled sediment provenance and was key to partitioning the Andean foreland basin into the modern hinterland setting (Perez and Horton, 2014; Horton et al., 2014). Structural inheritance and inversion has implications for both deformation style and flexural basin evolution during Andean orogenesis.

6.2. Mitu Group basin

Spatial and temporal constraints on Mitu Group provenance from southern Peru suggest accumulation in individual basins with localized provenance signals that evolved through time. Although the exact boundaries of these basins remain poorly constrained, study localities have unique detrital zircon provenance signatures that result from isolated, non-integrated rift basins separated by topographic barriers. The easternmost locality shows an upsection disappearance of a characteristic zircon age population sourced from cratonic blocks to the east. The upsection disappearance is interpreted as disruption of a west directed sediment transport network that eventually blocked sediment derived from the craton. The westernmost locality preserves characteristic Carboniferous zircon ages transported axially SW from the Cusco region. Other localities lack this signature, suggesting that axial sediment transport was also limited by rift basin geometries. We interpret this regional provenance variability as evidence for multiple rift basins with localized sources that resulted in regionally variable provenance signatures. Rapid changes in lithology and thickness of the Mitu Group support the idea for multiple basin centers.

The age of the Mitu Group was often thought to be late Permian to Triassic in age. New zircon U-Pb geochronologic constraints demonstrate Mitu Group deposition in the Triassic, from ~242 to 233 Ma. Recent studies have concluded a similar Triassic age for the Mitu Group ~700 km along strike (Reitsma, 2012). This age suggests initiation of the Triassic was synchronous along strike. In contrast, Sempere et al., (2002) interpreted the progressive southward decrease in pluton age as evidence for a southward propagating rift. Reconciling along strike patterns in synrift plutonism and the surface expression of rifting (basin formation, upper crustal fault motion) requires further investigation.

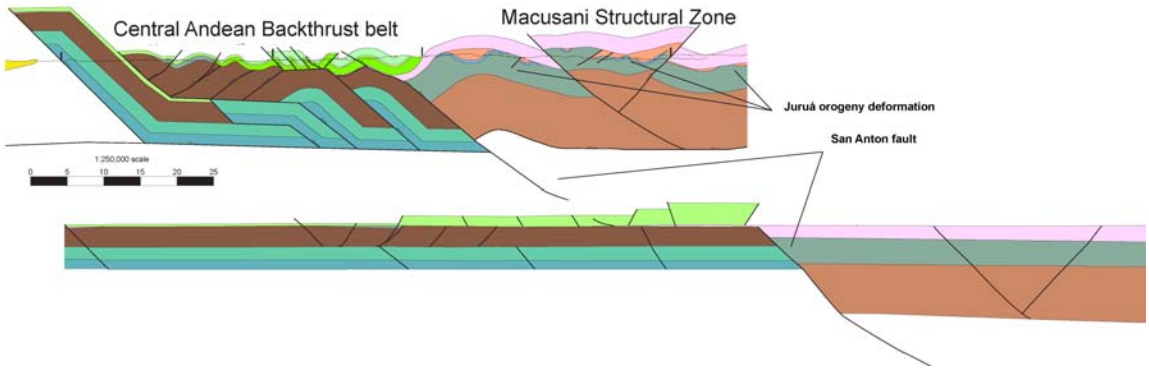

Figure 3.10. Part of a line balanced cross section spanning the Eastern Cordillera illustrating a kinematic model for thrust inversion of the Triassic San Anton normal fault.

6.3. The role of inherited structures on structural compartmentalization and Andean deformation

The complete record of Eohercynian and Juruá deformation is preserved only beneath Mitu Group deposits in the Macusani Structural Zone. In addition to the subcrop and thickness variations identified across this boundary, changes in structural style are also noted. These changes in style are evident from relatively few thrust faults that cut Mitu Group rocks and the orientation of bedding in this block. Many large panels of Mitu Group rocks dip uniformly, potentially suggesting post-depositional block tilting. Deformation of the Mitu Group is accommodated by faults and folds oriented obliquely to surrounding Andean trends. Throughout the rest of the Altiplano, Eastern Cordillera and Subandes, Paleozoic to Cenozoic rocks are deformed along dominantly NW-SE trending faults and folds (Figure 11) as evidenced by a well defined girdle to poles of bedding orientation measurements. In contrast, fault and fold orientations from the Macusani Structural Zone reflect non-coaxially deformation, and potentially large block tilting. We suggest that non-coaxial deformation was restricted to the Macusani Structural Zone block during Andean times because it is bounded by major Triassic normal faults, and preserves pre-Andean structural grains from Juruá and Eohercynian deformational events.

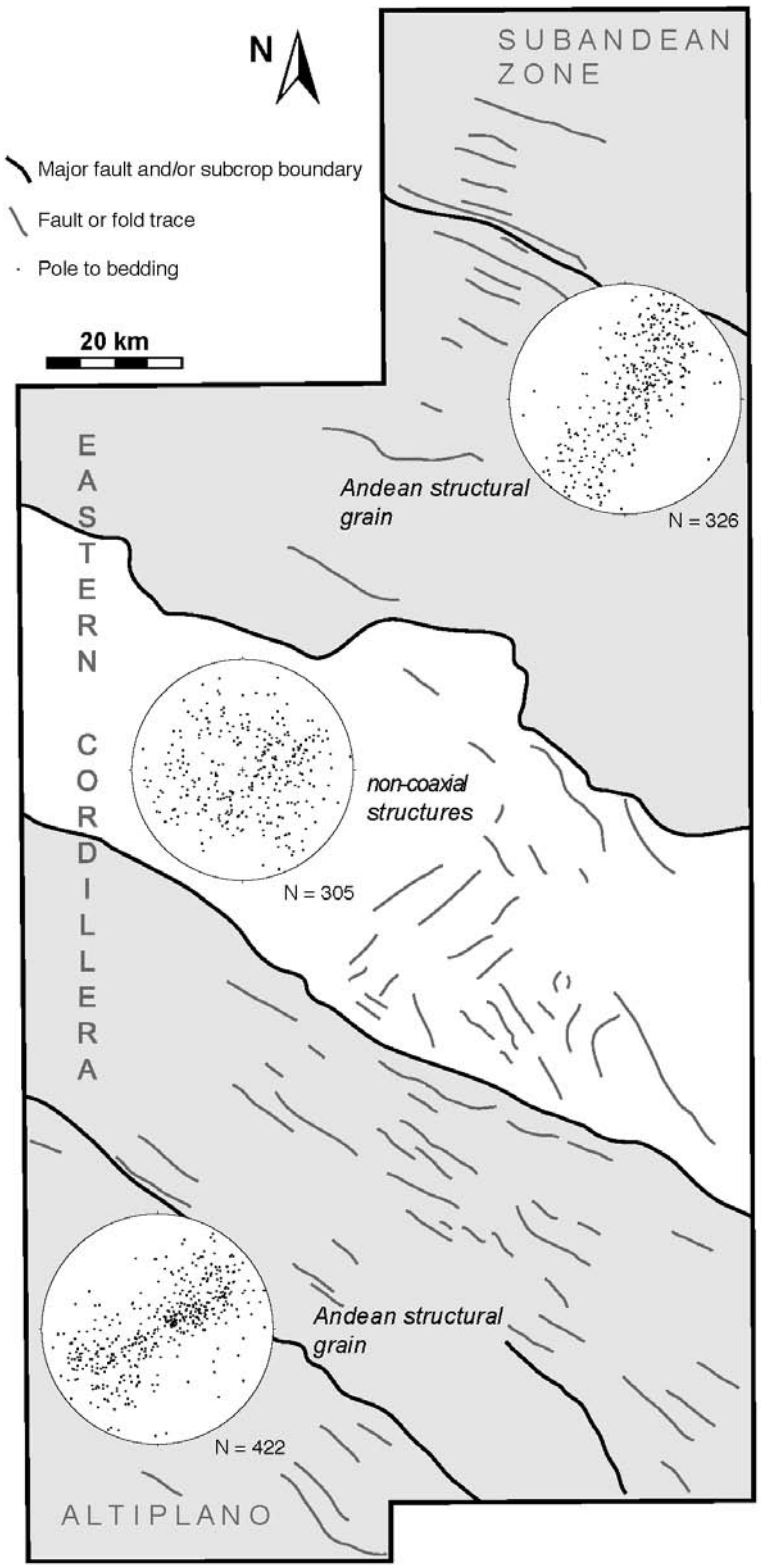
N
SUBANDEAN ZONE
Major fault and/or subcrop boundary
Fault or fold trace
Pole to bedding
20 km
Andean structural grain
N = 326
EASTERN CORDILLERA
non-coaxial structures
N = 305
Andean structural grain
N = 422
ALTIPLANO

Figure 3.11. Map of dominant structural trends highlight structural blocks within the Eastern Cordillera. Same map area and major fault/subcrop boundaries as Figure 1.

7. CONCLUSIONS

1) Detrital zircon U-Pb geochronologic results from the Mitu Group in the Eastern Cordillera of southern Peru reveals non-integrated compartmentalized rift basins with unique provenance characteristics. The stratigraphically lowest sample from the easternmost exposure preserves a significant Rondonia/San Ignacio cratonic source that disappears upsection. This disappearance is attributed to the development of an eastward rift shoulder that effectively blocked cratonic sediment contribution. The westernmost sample has the highest proportion of Carboniferous zircons that were sourced from the Cusco region, suggesting axial south-directed transport. The Triassic rift is interpreted as a mosaic of individual rift basins with unique provenance, as opposed to a single large rift basin with homogenous provenance.

2) Zircon U-Pb geochronologic data constrain the timing of Mitu Group deposition between ~242 and 233 Ma. The timing of deposition is consistent with other constraints from up to ~700 km NW along strike, suggesting nearly synchronous initiation of Mitu Group deposition in the Triassic. This finding refines previous chronostratigraphy, which assumed a late Permian to Triassic age of the Mitu Group. The synchronous initiation of Mitu rift deposition along strike is in contrast to the decreasing age of Eastern Cordillera plutons to the SW, originally interpreted as evidence for a SW propagating rift.

3) The locations of pre-Andean normal faults active during Mitu Group rifting and deposition are identified based on outcrop, regional subcrop relationships and thickness variations. Results show a mix of low and high stratigraphic throw associated

with identified normal faults. The identified normal faults trend parallel to modern Andean structural grain, although fault dip may vary between ~40° and 60°.

4) Reactivation and interaction with pre-Andean normal faults exerted considerable influence on Andean deformation. The Macusani Structural Zone represents a Triassic graben bounded by two major pre-Andean normal faults. The SW normal fault was inverted and guided deformation in the Central Andean Backthrust belt. The NE fault nucleated a thrust fault of opposite dip that established the boundary between the Cordillera de Carabaya and the Macusani Structural Zone.

5) Pre-Andean normal faults compartmentalized the style of deformation across the Eastern Cordillera. Multiple phases of non-coaxial deformation are preserved in the Macusani Structural Zone. In other parts of the Eastern Cordillera, fold-thrust deformation is parallel to Andean trends.

6) Mixed thin- and thick-skinned deformation during Cenozoic Andean deformation has implications for flexural loading of foreland basins and crustal thickening. Thick-skinned thrust faults may induce large-magnitude subsidence events, which have been identified in other Altiplano/Puna plateau basins. Thick-skinned segments of fold-thrust belts commonly do not accommodate similar high magnitudes of shortening compared to thin-skinned counterparts. Estimates of total shortening and accompanying crustal thickening need to account for varied structural styles in the northern Altiplano region.

Chapter 4: Magnitude of shortening and along-strike variations in exhumational cooling associated with thin- and thick-skinned deformation in southern Peru

ABSTRACT

A new balanced cross section spanning the Eastern Cordillera and Subandes of southern Peru constrains Andean shortening magnitudes, proposes selective inversion of inherited pre-Andean normal faults, and creates a structural framework to interpret new apatite and zircon (U-Th)/He thermochronologic data. Approximately 130 km of shortening (38%) is accommodated by thick- and thin-skinned fold-thrust belt development. Zircon (U-Th)/He results demonstrate Oligocene to Miocene (~26-18 Ma) cooling along the Eastern Cordillera. New apatite (U-Th)/He results from the Coasa pluton (Eastern Cordillera) reveal cooling at ~15 Ma, approximately 10 Myr older than plutons in similar structural positions 40 km NW along strike. Decreasing fluvial knickpoint elevations towards the NW mimic the observed decrease in apatite (U-Th)/He ages and highlight along strike variations in exhumation.

U-Pb detrital zircon geochronology results from the Cretaceous to Cenozoic rocks preserved in the Altiplano/Eastern Cordillera and the Subandean Zone reveal long-lived provenance differences between the two depocenters. Altiplano and Eastern Cordillera rocks lack diagnostic cratonic U-Pb zircon ages and record Eastern and Western Cordillera sediment contribution throughout Cretaceous to Cenozoic deposition. In contrast, Subandean rocks preserve strong cratonic provenance, lack Western Cordillera detrital zircon age signatures, and preserve minor Eastern Cordillera signals only in Cenozoic rocks.

We suggest that initial deformation and exhumation in the Eastern Cordillera may be linked to inversion of basement-involved structures. Subsequent deformation occurred in-sequence and was accommodated by a mix of thick- and thin-skinned deformation. Provenance variations from the hinterland and foreland depocenters may be attributed to a long-lived Eastern Cordillera structural high that prevented provenance mixing, or may represent distal regions of a large continuous foreland basin receiving sediment from its flanks. Similar Oligocene-Miocene ZHe cooling ages along strike suggest synchronous exhumation. In contrast, a NW decrease of AHe ages and fluvial knickpoint elevations suggest a change to diachronous exhumation along strike later in orogenic development. The NW trend towards younger exhumation ages may reflect complex structural geometries, a northward propagating wave of Altiplano uplift, interactions with mantle dynamics, or focused climatically driven incision.

2. INTRODUCTION

Testing models for the Cenozoic construction of the central Andes requires comparisons between geologic constraints (e.g., shortening magnitude, structural geometries, foreland basin histories, exhumation patterns), geophysical records of crust and lithosphere architecture, and emerging paleoaltimetry records. Presently, such datasets are more abundant in the Central Andean Plateau (CAP) of Bolivia and Argentina (Roeder, 1988; Allmendinger et al., 1990; Sheffels, 1990; Grier et al., 1991; Baby et al., 1992; Schmitz, 1994; Dunn et al., 1995; Kley, 1996; Zapata and Allmendinger, 1996; Baby et al., 1997; Lamb and Hoke, 1997; McQuarrie, 2002; Muller et al., 2002; Elger et al., 2005; Oncken et al., 2006; Barnes et al., 2006; Gillis et al., 2006;

McQuarrie et al., 2008) than in the northward Altiplano termination of southern Peru (Gil Rodriguez, 2001; Gil et al., 2001; Gotberg et al., 2010; Espurt et al., 2011). Throughout the CAP, debate persists regarding the timing of surface uplift, the role of crustal thickening on plateau development, and how lithospheric processes may alter the topographic response to shortening (Garzione et al., 2006; Ghosh et al., 2006; Leier et al., 2013). Protracted shortening in the Central Andes may (McQuarrie et al., 2005) or may not (Baby et al., 1997) explain observed modern crustal thickness magnitudes. Three-dimensional reconstructions of the CAP of Bolivia have demonstrated that along strike motion of crustal material is a key component to explaining modern crustal volumes (Hindle et al., 2005; Eichelberger and McQuarrie, 2015). Advancing similar reconstructions to the entire CAP, and eventually along the entire orogen, requires further studies of the magnitude, kinematics, style, and timing of deformation.

Along strike variations in structural style have been attributed to changes in pre-orogenic stratigraphic wedge architecture (Allmendinger et al., 1983; Allmendinger and Gubbels, 1996), changes in geometries of the subducting Nazca Plate (Barazangi and Isacks, 1976; Cahill and Isacks, 1992;) and inherited structural framework from pre-Andean deformation (Ramos et al., 1996; Kley et al., 1999). In the Bolivian CAP, most cross section reconstructions emphasize thin-skinned deformation, with minimal reactivation of pre-existing structures. In contrast, segments of the Argentinian (Giambiagi et al., 2011), northern Peruvian (Hermoza et al., 2005; Eude et al., 2015), and Colombian Andes (Mora et al., 2006; Bayona et al., 2008) demonstrate significant reactivation of pre-Andean structures that guided Cenozoic deformation. Recent syntheses document numerous pre-Andean structures along much of the orogen (McGroder et al., 2013), except in southern Peru despite the presence of a proposed Permo-Triassic rift (Sempere et al., 2002). Identifying the location and potential selective

reactivation of inherited structures is key to defining lateral variations in structural style, magnitude of deformation, and the kinematic links between well-documented segments of the Andean chain (Kay et al., 1989; Kley et al., 1999).

The proliferation of thermochronologic datasets has afforded the opportunity to test kinematic models of fold-thrust evolution and along strike changes in plateau-margin fluvial incision timing. Varying interpretations support either in-sequence thrust activation (McQuarrie et al., 2005) or synchronous deformation across broad zones of the CAP (Oncken et al., 2006), often summarized as a debate between simple and pure shear deformation, respectively (Allmendinger and Gubbels, 1996). Despite these debates, other patterns are evident. Existing exhumational records suggest Eocene and younger development of the Eastern Cordillera in southern Peru and Bolivia (Benjamin et al., 1987; Farrar et al., 1988; Gillis et al., 2006) interpreted as reactivation of inherited weaknesses from pre-Andean deformational events (McQuarrie et al., 2005). Many workers agree that deformation propagated to the Subandean Zone after ~25-20 Ma (Horton, 2005; Barnes et al., 2006; Barnes et al., 2008; Espurt et al., 2011; Eude et al., 2015). Existing thermochronologic studies from the western CAP margin show ~13-7 Ma canyon incision (Schildgen et al., 2007; Schildgen et al., 2009; Gunnell et al., 2010). Along the eastern CAP margin, Pliocene canyon incision determined from thermochronology has been linked to enhanced climate driven erosion (Lease and Ehlers, 2013), but existing studies have investigated just one of the many deep canyons along the Eastern Cordillera flank in southern Peru. In Bolivia, geomorphologic investigation of the Eastern Cordillera suggests mid-Miocene and younger erosion and exhumation was driven by tectonic, rather than climatic, processes (Whipple and Gasparini, 2014). Linking fluvial geomorphologic and thermochronologic datasets will afford along strike comparisons in the timing and style of exhumational cooling.

The Andes preserve a remarkable series of both hinterland basins in the orogen interior and well-developed foreland basins situated between the Andes and the continental craton (Horton, 2012). Ongoing debate centers on whether the two modern depocenters reflect a long-lived two basin system or whether the basins were once contiguous, and partitioned with uplift of the Eastern Cordillera. In central and northern Peru, the existence of a long-lived structural high (Marañon Geanticline, separating the East and West Peruvian Trough) has been proposed to explain observed stratigraphic relationships (Benavides-Caceres, 1956; Wilson, 1963; Dalmayrac et al., 1980; Mégard, 1984; Benavides-Caceres, 1999; Jaillard et al., 2005). The southward continuation of this feature is less well constrained (e.g. Scherrenberg et al., 2012). Eocene exhumation in the Eastern Cordillera has been interpreted as the initial partitioning of a once continuous foreland basin system (DeCelles and Horton, 2003; McQuarrie et al., 2005). Resolution of this issue has implications for paleogeographic reconstructions, and testing the genetic links between flexural foreland/hinterland basin evolution and fold-thrust belts.

This study from 13°-15° S in southern Peru presents estimates of total shortening across the Eastern Cordillera and Subandean zone constrained by a new balanced cross section, the timing of exhumational cooling from the Subandean Zone and parts of the Eastern Cordillera from apatite and zircon (U-Th)/He thermochronology, and initial constraints on the spatial distribution of rock uplift from patterns of fluvial geomorphology. We also identify major pre-Andean normal faults that have been selectively reactivated during Cenozoic orogenesis. Using U-Pb detrital zircon geochronology, we establish the Cretaceous through Cenozoic provenance record of both the Altiplano and Subandean basins. These data provide insights into the geometry, timing, and kinematics of deformation in southern Peru, the role of inherited structural and stratigraphic architectures on strain localization, the long term evolution of major

Andean depocenters, and the modern topographic expression of along strike changes in exhumation.

3. BACKGROUND

3.1. Tectonic Framework

The Andes occupy the western flank of South America and trend longitudinally. In southern Peru, the Andes define the northern limb of the Bolivian Orocline, where the dominant northwest-southeast structural grain is a departure from the N-S strike that characterizes much of the Andes. The Altiplano is a high-elevation, low relief plateau situated between the Western Cordillera (modern magmatic arc, today mostly Neogene volcanic exposures) and Eastern Cordillera (exhumed fold-thrust belt in Paleozoic-Mesozoic sandstones, shales, limestones, slates, schists) (Figure 1a). To the northeast is the Subandean Zone, which is the modern deformation front and foreland basin. The structural boundary between the Altiplano and the Eastern Cordillera is the northeast dipping Ayaviri fault, part of a larger fault system that spans ~400 km from Cuzco to northern Bolivia (Sempere et al., 1990). Locally, the Ayaviri fault is a thrust that juxtaposes Ordovician strata on Oligocene rocks preserved in the Ayaviri basin (Perez and Horton, 2014). The structural boundary separating the Eastern Cordillera and Subandean Zone is the Main Andean Thrust, which juxtaposes Ordovician rocks on Cretaceous and Cenozoic rocks.

The Eastern Cordillera is a doubly vergent thrust wedge that is composed of three structural domains, each ~50-60 km wide, and defined by abrupt changes in

Figure 4.1. Large foldout, see envelope with extra materials. A) DEM topography of Central Anges (after Garzione et al., 2014) showing general study area (red dashed rectangle). B) Compiled 1:100000 geology map quadrangles at 1:250000 scale. All bedding orientation, fault, fold data new. Note locations of new and previous thermochronology samples. C) Line length balanced cross section from transects across study area.

structural/stratigraphic depth exposed at the surface (Figure 1b). The Central Andean Backthrust Belt (CABB; McQuarrie and DeCelles, 2001) is a system of faults and folds that verges towards the southwest in southern Peru, and is continuous into Bolivia. The northern segment of the CABB in Bolivia is also known as the Huarina fold-thrust belt (Sempere et al., 1990). In southern Peru, most exposures in the CABB consist of Cretaceous sandstones, siltstones, and limestones, whereas in Bolivia lower Paleozoic structural levels are exposed. The Macusani Structural Zone, previously referred to as the Precordillera de Carabaya (Kontak et al., 1990; Sandeman et al., 1997) or "the domain of Tardihercynian folds" (English translation from French, Laubacher, 1978) is defined as region between the NE map boundary of the Cretaceous rocks of the CABB and the SW map boundary of the Cordillera de Carabaya. The Macusani Structural Zone is noteworthy because of the abrupt increase in exposed structural depth compared to the CABB, and because the orientations of faults and folds in Carboniferous to Permian strata are not parallel to typical Andean trends. This has been attributed to late Paleozoic deformation ("Tardihercynian"; Mégard et al., 1971; Laubacher, 1978; Dalmayrac et al., 1980; Clark et al., 1990). The Cordillera de Carabaya, also known as the Inner Arc (McBride et al., 1983; Clark et al., 1990; Sandeman et al., 1995), is defined by a series of Permo-Triassic plutons (Kontak et al., 1990; Mišković et al., 2009) that support the highest elevations in the study area. Northeast of the Cordillera de Carabaya is another discrete increase in exposed structural depth (Ordovician to Devonian rocks) that marks the SW boundary of the frontal Eastern Cordillera zone.

Much of the Phanerozoic stratigraphic record is preserved in the Eastern Cordillera of southern Peru. The sedimentary cover deformed by Andean deformation is up to ~16 km thick. The succession is defined by a continuous succession of marine Ordovician to Devonian siliciclastic deposits (~7 km thick). A discontinuous

Carboniferous to Permian succession is characterized by marine siliciclastic and carbonate rocks (~4 km thick). A Triassic succession, the Mitu Group, preserves non-marine conglomerate, volcanic and siliciclastic rocks interpreted as synrift deposits (>2 km thick) (Reitsma, 2012). Jurassic rocks are not preserved in the study area. A Cretaceous section preserves marine siliciclastic and carbonate rocks as well as non-marine siliciclastic deposits (~3 km thick). The thickest and most complete Paleozoic succession is preserved in the Macusani Structural Zone where thick Triassic and Carboniferous to Permian rocks are preserved. In other segments of the Eastern Cordillera, Triassic rocks are very thin or absent, and Carboniferous to Permian rocks are absent. In contrast to the Bolivian segment (McQuarrie et al., 2008), the southern Peru segment preserves unconformities, often angular, between the Devonian to Carboniferous, Permian to Triassic, and Triassic to Cretaceous that are attributed to pre-Andean deformational events (Newell, 1949; Mégard et al., 1971; Laubacher and Mégard, 1985; Sempere et al., 2002). Synorogenic (Cenozoic) deposits may approach thicknesses of 7 km and are preserved dominantly in the Altiplano and Subandean zone, with thin, areally restricted deposits preserved in the Eastern Cordillera.

The axis of a late Paleozoic to early Mesozoic rift is proposed to coincide with the modern Eastern Cordillera (Sempere et al., 2002). Rapid lateral changes in facies and thickness of the Mitu Group throughout the Eastern Cordillera of Peru have been interpreted as non-marine synrift fill. The Mitu Group is deposited on folded Paleozoic rocks. Existing chronostratigraphic constraints broadly define a Permo-Triassic depositional age, although recent geochronologic investigations suggest Triassic deposition (Reitsma, 2012; Perez and Horton, Chapter 3). Despite widespread preservation of the Mitu Group in the Eastern Cordillera, very few normal faults that controlled rift development have been identified. Exceptions include industry reflection

seismic datasets from central and northern Peru, which identify subsurface pre-Andean normal faults (PARSEP, 2000; Hermoza et al., 2005; Eude et al., 2015).

3.2. Existing thermochronology

Existing exhumational records from southern Peru are limited to the Western Cordillera flank (Schildgen et al., 2007, 2009), and the Eastern Cordillera. Here, we focus on the Eastern Cordillera records. Farrar et al., (1988) identified a narrow zone of young (~40-25 Ma) reset K/Ar and $^{40}Ar/^{39}Ar$ ages in the Eastern Cordillera. They defined the Zongo-San Gabán Zone, part of the Eastern Cordillera and Cordillera de Carabaya, and suggested that the zone records brief (<5 Myr) heating to 350° C and cooling by ~38 Ma. Similar cooling histories determined from apatite and zircon fission track studies of plutons in equivalent structural positions in Bolivia record initial cooling at ~40-45 Ma (Benjamin et al., 1987). Together, these data have been interpreted as the signal of initial shortening and exhumation associated with a rapid Eocene inboard advance of deformation.

Recent thermochronology results along the Rio San Gabán have identified a mid-Miocene phase of thrust related cooling, and a Pliocene pulse of rapid canyon incision (Lease and Ehlers, 2013). Zircon (U-Th)/He thermochronology samples collected across a SW verging thrust fault in the Eastern Cordillera record disparate Cretaceous and Miocene cooling histories for the footwall and hangingwall blocks, respectively. Those workers interpreted rapid Miocene cooling of the hangingwall as evidence for erosional exhumation due to thrust fault motion. Apatite (U-Th)/He analysis of the same sample suite reveal uniform ~4 Ma cooling across the fault. These data were interpreted as

exhumation driven by rapid canyon incision, potentially linked to Pliocene climate change.

3.3. Existing U-Pb zircon geochronology

U-Pb detrital zircon geochronology is a widely applied technique to determine zircon age populations in sedimentary rocks. The age spectra from individual samples can be used to constrain the maximum depositional age, possible sediment provenance, paleogeographic reconstructions and characteristics of the source terrane (Gehrels, 2011). In this study, we aim to constrain the provenance for Cretaceous to Cenozoic successions preserved in separate depocenters, the Altiplano/CABB and Subandean Zone. Previous workers have established the U-Pb detrital zircon geochronology populations of Proterozoic, Paleozoic and Mesozoic rocks exposed throughout the Western and Eastern Cordillera (Loewy et al., 2004; Chew et al., 2007; Chew et al., 2008; Mišković et al., 2009; Mišković and Schaltegger, 2009; Reimann et al., 2010; Bahlburg et al., 2011; Boekhout et al., 2013; Decou et al., 2013; Perez and Horton, 2014). Here we summarize key U-Pb zircon age populations observed in the Western and Eastern Cordillera that may have been sediment sources for Cretaceous and Cenozoic rocks deposited in the Altiplano and Subandean basins. These are compared to likely zircon ages from detritus shed from the South American craton, and the Cretaceous to recent magmatic arc.

Basement exposures such as the Arequipa/Antofalla terrane are characterized by zircon ages of 476-440 Ma, ~1.20-0.94 Ga, and ~2.02-1.79 Ga (Loewy et al., 2004; Decou et al., 2013). Neoproterozoic to lower Paleozoic rocks of the Eastern Cordillera of Peru are dominated by U-Pb zircon ages between ~450-700 Ma and 900 to 1300 Ma,

with minor populations of ~1.5-2.1 Ga zircons (Chew et al., 2008). Ordovician through Devonian rocks of the Eastern and Western Cordillera preserve dominant 400-800 Ma, 900-1200 Ma, and 1600-2200 Ma peaks, with minor occurrences of other populations (Reimann et al., 2010; Bahlburg et al., 2011; Decou et al., 2013; Perez and Horton, 2014). Plutonic rocks intruded throughout the Eastern Cordillera show a strong Gondwanide Orogeny signal (~350-160 Ma) (Mišković and Schaltegger, 2009). This age population is distinctive of the Eastern Cordillera. Mesozoic rocks of the Eastern and Western Cordillera are characterized by recycled populations observed in Paleozoic-Proterozoic rocks with populations ~350-160 Ma, 400-800 Ma, 900-1200 Ma, and 1400-2200 Ma. The Western Cordillera is distinguished as the main source of Cretaceous to Cenozoic zircons resulting from long-lived arc activity along the western South America margin. Cratonic blocks of eastern South America preserve characteristic age populations: 1.2-0.9 Ga, 1.55-1.2 Ga, 1.8-1.55 Ga, 2.0-1.8 Ga, 2.2-1.9 Ga, and >2.3 Ga (Restrepo-Pace et al., 1997; Ramos, 2000; Tassinari et al., 2000; Cordani et al., 2000; Bahlburg et al., 2006; Bahlburg et al., 2011).

The variety of detrital ages observed in the pre-Cretaceous rocks of the Western and Eastern Cordillera demonstrates that certain zircon populations have been reworked repeatedly. The Gondwanide population appears to be distinctive to the Eastern Cordillera, Cretaceous to Cenozoic ages are characteristic of the Western Cordillera, and Proterozoic ages define cratonic blocks in South America. With the establishment of distinctive populations from the Western and Eastern Cordilleras, and the South American cratonic blocks, we argue we can link key detrital zircon provenance signatures in the Cretaceous to Cenozoic detrital record from the Altiplano/CABB and Subandean Zone with their respective sources.

4. METHODS

4.1. Mapping

New mapping and structural transects were compiled from and conducted using existing 1:100000 geologic map quadrangles (INGEMMET, 1999). Few roads traverse the study area, although the Interoceanic Highway provides key access across the Altiplano, Eastern Cordillera and Subandean Zone. Fault, fold, stratigraphic and/or bedding data was collected at more than 1200 stations along a series of transects. These data govern our interpretations and balanced cross section construction. Original and updated maps were produced at 1:100000 scale and compiled onto 1:250000 scale maps overlain on SRTM 90 m digital elevation model topography (Jarvis et al., 2008). Transect orientations are perpendicular to structural grain, and change across strike as fault and fold orientations change. Breaks in section were chosen along significant structures that can be mapped along strike. Transects also follow zones of dense station coverage where exposures were optimized and road access was most efficient.

4.2. Thermochronology

We present new apatite and zircon (U-Th)/He data from multiple samples collected from the Triassic Coasa pluton within the Cordillera de Carabaya, a sample from Carboniferous quartzite that hosts the Coasa pluton, and Cretaceous sedimentary rocks from the Subandean Zone. The Coasa pluton samples are located ~40-50 km SE of the Rio San Gabán transect (Lease and Ehlers, 2013) and provide along strike constraints

on the exhumation history of rocks along the steep eastern front of the Peruvian Eastern Cordillera.

Apatite and zircon (U-Th)/He thermochronology methods constrain the timing of cooling to depths of ~2 and ~6 km, respectively, making them ideal tools to define rock cooling histories to shallow crustal levels (Ehlers and Farley, 2003). Radioactive decay of U, Th, and Sm nuclides to Pb by alpha-particle emission within the mineral grain result in ^{4}He creation. He is diffused out of the grain at higher temperatures, and retained at lower temperatures. Between temperatures defining an "open" (He diffusion) or "closed" (no He diffusion) system, the mineral transitions through the partial retention zone (PRZ). The PRZ is unique for each mineral and depends on cooling rate and grain sizes. For typical settings, apatite and zircon retain helium below effective closure temperatures of ~60° C and ~180° C, respectively. A sample is considered reset (buried above PRZ temperatures, then exhumed) if individual grain aliquot ages cluster together and are younger than the depositional or intrusive age of the rock. A sample is considered unreset if individual grain aliquot ages are older than the rock age. A sample is considered partially reset (buried to PRZ temperatures, then exhumed) when a spread of individual grain ages are both younger and older than the rock age.

Cooling ages from samples collected from a range of elevations can provide constraints on the rates and magnitudes of exhumation. For our study of the Coasa pluton in the Cordillera de Carabaya, we collected samples along Rio Achasiri and Rio Tambillo gorges. Most samples were collected from medium grained granodiorite and monzodiorite of the Coasa pluton. One sample was collected ~300 m from the SW pluton margin in Carboniferous Ambo Formation quartzite. Elevations span 3710 m to 4764 m a.s.l. Three samples were collected from medium to coarse-grained sandstones of the Cretaceous Vivian and Oriente Formations in the Subandean Zone. Samples were

prepared using standard mechanical, density and magnetic separation techniques. The most clear and euhedral apatite grains without inclusions or any other impurities or cracks were selected using a binocular microscope. Euhedral zircon grains were selected, but some had visible inclusions. The grain dimensions were measured for the calculation of the alpha-correction factor after Farley et al. (1996). Single grains were packed in Nb-tubes for U-Th/He analysis. In general we analyzed 3-5 aliquots per sample. Helium was measured in the Patterson Helium-extraction line at the University of Tübingen, which is equipped with a 960 nm diode laser. Apatite grains were heated for 5 min at 11 A and zircon grains for 10 min at 20 A. Each grain was re-heated and analyzed to make sure that the grain was degassed entirely in the first step. The re-extracts generally showed <1% of the first signal.

Concentrations of U, Th and Sm were determined by isotope dilution using the Thermo Fisher iCAP ICP-MS at University Tübingen equipped with an all-PFA sample introduction system. Apatite samples together with the Nb-tubes were spiked with a calibrated mixed spike of 233U + 230Th + 149Sm and dissolved overnight in 2 ml 5% HNO3 + 0.1% HF at 65 °C. The grain mass of each sample was estimated from measured 43Ca concentrations assuming 39.4 wt-% Ca in apatite.

The analytical error of the mass spectrometer measurements are generally very low and do not exceed 2%. In contrast, the reproducibility of the sample age constitutes a much larger error. We therefore report the mean U-Th/He age and the standard deviation of the measured aliquots as the sample error. For single grain ages we apply a 5% 2-sigma error based on the reproducibility of standard measurements in the lab.

4.3. Balanced Cross Section

Balanced cross sections provide testable hypotheses of possible subsurface structural geometries, estimates of shortening across strike of faulted and folded terranes, and potential kinematic solutions to development of structures. The technique is most useful where out-of-plane motion can be ruled out and in nonmetamorphic parts of orogens (Bally et al., 1966; Dahlstrom, 1969). The technique has been applied throughout the Andes and other orogens to constrain estimates of bulk shortening and crustal thickening, and to test kinematic solutions to fold-thrust belt evolution and rift inversion (Beach, 1981; Price, 1981; Boyer and Elliot, 1982; Roeder, 1988; Baby et al., 1992; Kley, 1996; Baby et al., 1997; Kley et al., 1999; McQuarrie, 2002; Teixell et al., 2003; Elger et al., 2005; Mora et al., 2006; McQuarrie et al., 2008; Gotberg et al., 2010; Giambiagi et al., 2011; Eichelberger et al., 2013; Eude et al., 2015).

These examples rely mostly on the sinuous bed method and line length balancing, which assumes no out-of-plane material motion and volume conservation throughout the history of deformation (Dahlstrom, 1969). An admissible cross section must reflect geologic data (exposures, topography, bedding orientation, structure style and locations). The cross section is viable if the deformed section can be restored to an undeformed section. The result is an admissible and viable cross section where the restored and deformed cross sections preserve bed lengths and cutoff angles between fault segments (Dahlstrom, 1969; Elliott, 1983; Woodward et al., 1989).

Despite their utility, some limitations of line length balanced cross sections include poorly defined uncertainty estimates, uncertainties regarding how subsurface space is filled, and the length of eroded hangingwall cutoffs projected above the surface. Judge and Allmendinger (2011) show that in addition to these issues, the original

stratigraphic thickness is the largest source of error. They propose the area balancing method as an alternative technique because it provides improved ability to analyze uncertainties. However, by only determining an area balanced solution, the proposed errors can not be assessed to ensure viability (Eichelberger et al., 2013). Thus, we evaluate the uncertainty of our cross section using the area balance technique (Judge and Allmendinger, 2011), but rely on shortening estimates from our line length balanced section because area balanced sections do not necessarily provide geometrically and kinematically viable cross section solutions. Combining both techniques provides an approach that creates admissible, viable cross sections and more accurate uncertainty analysis.

The new cross section was constructed from the compiled 1:250000 geologic map and honors map patterns, faults, folds, changes in structural level and bedding orientation. Variable exposure and road access do not permit a single cross section line across the Altiplano, Eastern Cordillera, and Subandean zone. To accurately capture data, we chose to create multiple section lines. The orientation of structures gradually rotates from ~310° strike in the Altiplano to ~290° in the Subandean zone. Section lines trend perpendicular to the dominant structural grain, assuming minimal out-of-plane motion. In the Macusani Structural Zone, Carboniferous-Permian strata are deformed along two main orientations, ~340° and 40° strike. We propose that Andean structures in this region are identified as structures that fault or fold the Triassic Mitu Group and Cretaceous units. The majority of Andean structures identified in this zone trend NW oblique to surrounding Andean trends. Section lines are perpendicular to the local structural grain within the Macusani Structural zone.

4.4. U-Pb detrital zircon geochronology

The application of U-Pb detrital zircon geochronology to foreland basin deposits has provided insights into the tectonic evolution of orogens, sediment routing pathways across continents, and the depositional age of formations (Dickinson and Gehrels, 2003; Horton et al., 2010; Lawton and Bradford, 2011; Gehrels, 2011). Here we investigate the provenance of the Cretaceous to Cenozoic stratigraphic sections preserved in the CABB/Altiplano and Subandean Zone. The two regions are separated by >100 km across the Eastern Cordillera where exposures of proposed Cenozoic and Cretaceous deposits are thin and restricted to small mapped exposures. The frontal Eastern Cordillera zone, where only Ordovician to Devonian rocks and Triassic plutons are exposed, is more than 50 km wide. By defining the Cretaceous to Cenozoic detrital zircon provenance signatures from both regions, we begin to address whether the depocenters represent two long lived, separate basins, or a once continuous depocenters that was partitioned during uplift of the Eastern Cordillera.

In the CABB we collected 5 total samples from the Cretaceous Muni, Huancane, Vilquechico, Auzangate Formations, and the Viluyo Formation of the Moho Group. In the Altiplano, we include a subset of 6 previously reported (Perez and Horton, 2014; Horton et al., 2015) samples collected throughout the Ayaviri basin from the Puno Group, San Jeronimo Group, and Tinajani Formations. In the Subandean zone, we collected three samples from the Cretaceous Vivian and Oriente Formations, and 6 samples from Cenozoic Pozo and Chambira Formations. Nearly all samples were collected from medium grained sandstones, or alternatively from fine grained sandstones when coarser deposits were not available.

Zircon crystals are extracted from samples by traditional methods of crushing and grinding, followed by separation with a Wilfley table, heavy liquids, and a Frantz magnetic separator. Samples are processed such that all zircons are retained in the final heavy mineral fraction. A large split of these grains (generally thousands of grains) is incorporated into a 1" epoxy mount together with fragments of our Sri Lanka standard zircon. The mounts are sanded down to a depth of ~20 microns, polished, imaged, and cleaned prior to isotopic analysis.

U-Pb geochronology of zircons is conducted by laser ablation multicollector inductively coupled plasma mass spectrometry (LA-MC-ICPMS) at the Arizona LaserChron Center (Gehrels et al., 2006, 2008). The analyses involve ablation of zircon with a Photon Machines Analyte G2 excimer laser using a spot diameter of 30 microns. The ablated material is carried in helium into the plasma source of a Nu HR ICPMS, which is equipped with a flight tube of sufficient width that U, Th, and Pb isotopes are measured simultaneously. All measurements are made in static mode, using Faraday detectors with $3x10^{11}$ ohm resistors for ^{238}U, ^{232}Th, ^{208}Pb-^{206}Pb, and discrete dynode ion counters for ^{204}Pb and ^{202}Hg. Ion yields are ~0.8 mv per ppm. Each analysis consists of one 15-second integration on peaks with the laser off (for backgrounds), 15 one-second integrations with the laser firing, and a 30 second delay to purge the previous sample and prepare for the next analysis. The ablation pit is ~15 microns in depth.

For each analysis, the errors in determining $^{206}Pb/^{238}U$ and $^{206}Pb/^{204}Pb$ result in a measurement error of ~1-2% (at 2-sigma level) in the $^{206}Pb/^{238}U$ age. The errors in measurement of $^{206}Pb/^{207}Pb$ and $^{206}Pb/^{204}Pb$ also result in ~1-2% (at 2-sigma level) uncertainty in age for grains that are >1.0 Ga, but are substantially larger for younger grains due to low intensity of the ^{207}Pb signal. For most analyses, the cross-over in precision of $^{206}Pb/^{238}U$ and $^{206}Pb/^{207}Pb$ ages occurs at ~1.0 Ga.

^{204}Hg interference with ^{204}Pb is accounted for measurement of ^{202}Hg during laser ablation and subtraction of ^{204}Hg according to the natural ^{202}Hg/^{204}Hg of 4.35. This Hg is correction is not significant for most analyses because our Hg backgrounds are low (generally ~150 cps at mass 204).

Common Pb correction is accomplished by using the Hg-corrected ^{204}Pb and assuming an initial Pb composition from Stacey and Kramers (1975). Uncertainties of 1.5 for ^{206}Pb/^{204}Pb and 0.3 for ^{207}Pb/^{204}Pb are applied to these compositional values based on the variation in Pb isotopic composition in modern crystal rocks.

Inter-element fractionation of Pb/U is generally ~5%, whereas apparent fractionation of Pb isotopes is generally <0.2%. In-run analysis of fragments of a large zircon crystal (generally every fifth measurement) with known age of 563.5 ± 3.2 Ma (2-sigma error) is used to correct for this fractionation. The uncertainty resulting from the calibration correction is generally 1-2% (2-sigma) for both ^{206}Pb/^{207}Pb and ^{206}Pb/^{238}U ages.

Concentrations of U and Th are calibrated relative to our Sri Lanka zircon, which contains ~518 ppm of U and 68 ppm Th. The analytical data are reported in Table 2 (supplementary materials). Uncertainties shown in these tables are at the 1-sigma level, and include only measurement errors. Analyses that are >20% discordant (by comparison of ^{206}Pb/^{238}U and ^{206}Pb/^{207}Pb ages) or >5% reverse discordant are not considered further.

The resulting interpreted ages are shown on relative age-probability diagrams using the routines in Isoplot (Ludwig, 2008). The age-probability diagrams show each age and its uncertainty (for measurement error only) as a normal distribution, and sum all ages from a sample into a single curve. Composite age probability plots are made from an in-house Excel program that normalizes each curve according to the number of

constituent analyses, such that each curve contains the same area, and then stacks the probability curves.

4.5. Fluvial geomorphology

The geomorphologic expression of the fluvial network draining and incising orogen margins is linked to tectonic, lithologic and climatic processes (Kirby et al., 2003; Wobus et al., 2006; Kirby and Whipple, 2012; Whittaker, 2012). As such, the main tool to investigate tectonic geomorphology is fluvial bedrock channel profile analysis. Fluvial channels in equilibrium with uplift and incision typically display smooth, concave up profiles. When equilibrium is altered by a change in rock uplift rate or base level fall, a wave of transient incision and erosion migrates upstream. In profile view, the wave of incision can be identified by knickpoints that separate upper reaches, which have lower indices of steepness and concavity that preserve previous equilibrium characteristics, from lower reaches, which have higher indices of steepness and concavity driven by a higher erosion rate. Although a number of metrics have been established, including the plan-view and along-profile distribution of concavity, steepness, and knickpoints, and the basin volume-to-area ratio (Frankel and Pazzaglia, 2006), in this study we focus only on identifying knickpoints in major fluvial channels incising the northeastern flank of the Eastern Cordillera of southern Peru. We suggest that the along strike distribution of channels with and without knickpoints may be linked to along strike changes in exhumational timing.

A mosaic of SRTM 90m digital elevation tiles was created for the study area. We extracted stream traces using ArcGIS and merged individual stream traces into

continuous fluvial systems that traversed from the headwaters in the Eastern Cordillera into the Subandean Zone. No channel smoothing was applied because we were interested in the presence or absence of knickpoints. Knickpoints were identified by visual inspection of channel profiles.

5. RESULTS

5.1. Geologic Mapping

5.1.1. Foreland

Previous workers have defined the thickness of the Paleozoic to Cenozoic succession in the Madre de Dios foreland basin using reflection seismic and borehole datasets and show that thick (>4 km) Cenozoic and thin (<2 km) Cretaceous sequences are deposited unconformably on a lower Paleozoic succession (Mathalone and Montoya, 1995). Surface exposures are dominated by cover and Neogene siliciclastic deposits. The basement-cover contact dips ~2° SW. Fluvial traces are often parallel to exposed frontal structures in the Subandean zone, suggesting broad, low relief folds are accommodating modern deformation and guiding fluvial channels.

5.1.2. Subandes

The Subandean zone in southern Peru is characterized by a narrow (~12-13 km) zone of Cretaceous marine siliciclastic rocks deformed mostly by folds and two major mapped thrust faults (Ingeomin, 1975; Mathalone and Montoya, 1995; Kley et al., 1999).

Small, local intraformational duplexes and tight folds are rarely observed at some outcrops (Figure 2a, b), but are below mapping and cross section resolution. These features are considered minor relative to thrust faults that offset the Cretaceous and Cenozoic, but suggest that a small magnitude of additional shortening is not represented by geologic mapping or cross section construction. Major map view folds are spaced ~5-6 km apart, with bedding dips between ~20° to 60°. A well-defined structural grain reveals northwest trending, non-plunging folds. The deepest structural level exposed in the Subandean zone is the Lower Cretaceous Oriente Group (Mathalone and Montoya, 1995), suggesting a detachment at the base of the Cretaceous above the Paleozoic. Both mapped thrust faults juxtapose Cretaceous marine siliciclastic rocks on fluvial Paleogene siltstones and sandstones.

5.1.3. Eastern Cordillera

The eastern flank of the Eastern Cordillera exhibits three zones that reflect discrete steps in structural depth that decrease from NE to SW as elevation increases. Map patterns define major folds of ~30 km wavelength. Slates, phyllites, quartzites and schists of the Ordovician to Devonian intruded by Triassic plutons dominate exposures in the frontal Eastern Cordillera. Data for this section of the transect were collected along the Interoceanic Highway along the Rio San Gabán canyon. The NE boundary of the Eastern Cordillera is defined by a SW dipping thrust fault that juxtaposes middle Ordovician rocks on Cretaceous rocks in the Subandean zone. The boundary represents a major increase in exposed structural depth relative to Cretaceous rocks of the Subandean zone. The deepest structural level exposed is the middle Ordovician San Jose Formation, suggesting a major regional décollement above the basement contact. Map contacts are

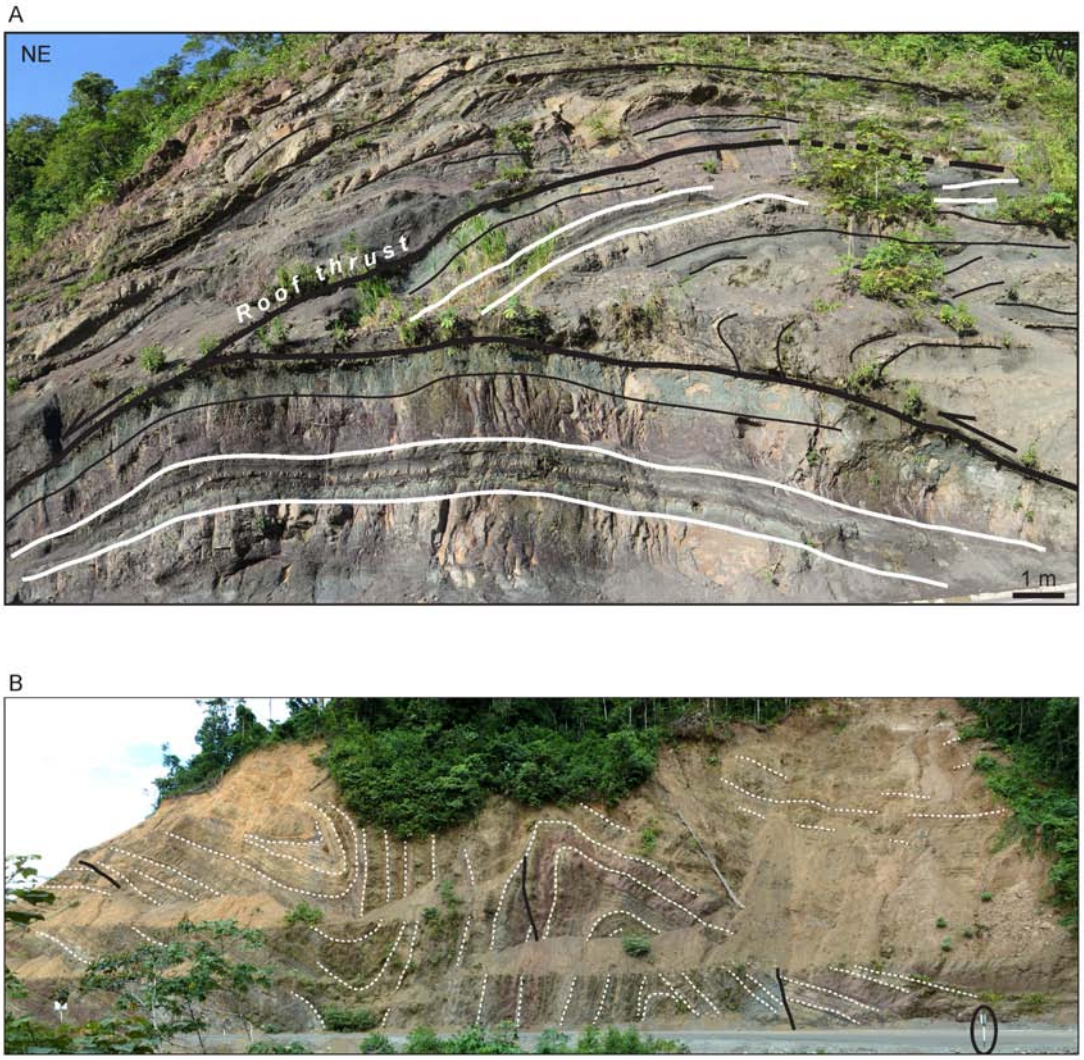

Figure 4.2. Examples of minor folding below resolution of mapping and cross section. A) Outcrop scale duplex of Cretaceous rocks from the Subandean Zone. B) Roadcut of folded Cretaceous rocks from the Subandean Zone. Note highway sign circled.

parallel to local Andean NW-SE trends. At outcrop scale, rocks exhibit a variety of tight folds over short distances, kilometer wide panels of similar dips, and bedding orientations that may be parallel to Andean NW-SE trends (~290-300° or 110-120°) or orientations oblique to Andean trends near N-S (~350°-170°). Similar patterns have been observed in other segments of the Eastern Cordillera (Eichelberger et al., 2013).

The NE zone of the Eastern Cordillera is ~60 km wide and characterized by a broad syncline/anticline pair that deforms middle Ordovician to Silurian/Devonian meta-sedimentary rocks and Triassic plutons. The NE syncline fold axis is defined by exposures of Silurian/Devonian. The NE syncline limb demonstrates a thin panel of middle Ordovician San Jose Formation and upper Ordovician Sandia Formation. The SW syncline limb has thicker panels of both units, suggesting original stratigraphic thicknesses tapered towards the craton. The boundary with the next zone to the SW is defined by a NE dipping, SW verging thrust fault that juxtaposes middle Ordovician San Jose Formation on upper Ordovician Sandia Formation. This second zone is characterized by a broad map syncline, with smaller scale internal folds concentrated towards the SW boundary, and a consistent structural depth throughout. Ordovician rocks are metamorphosed near a large Triassic pluton, but the age of metamorphism remains unknown. We suggest these rocks were metamorphosed during intrusion. This second zone is thrust over a narrow map exposure of NE dipping Silurian/Devonian rocks, suggesting a detachment below the upper Ordovician. The Silurian/Devonian rocks define a narrow third, structurally highest zone within the frontal Eastern Cordillera that is thrust over Jurassic pluton and Triassic Mitu Group deposits by a NE dipping reverse fault. This relationship suggests a third detachment at the base of the Silurian/Devonian.

5.1.4. Cordillera de Carabaya/Macusani Structural Zone

The Cordillera de Carabaya is defined by multiple Permo-Triassic plutons (McBride et al., 1983; Clark et al., 1990; Kontak et al., 1990; Sandeman et al., 1995; Mišković et al., 2009) and smaller, more rare Jurassic plutons that are aligned with NW-SE Andean structural grain. Permo-Triassic plutons are intruded into Ordovician-Carboniferous strata, but are in fault contact with Triassic Mitu Group deposits. Jurassic plutons intrude Triassic Mitu Group deposits. A NE dipping thrust fault juxtaposes Paleozoic rocks and Permo-Triassic plutons (hangingwall) against upper Paleozoic and Triassic rocks in the Macusani Structural Zone (footwall).

The Macusani Structural Zone is defined as the region situated between the SW thrust contact with the Cordillera de Carabaya plutons and lower Paleozoic rocks of the Eastern Cordillera, and the NE contact with Cretaceous rocks of the CABB. The Zone maintains a consistent structural elevation ~50 km across strike. Faults that deform Silurian to Permian strata often have short map traces (~10 km), and fold axial traces are ~6-7 km long. Fold orientations are conspicuously oblique or nearly perpendicular to regional Andean trends. The non-coaxially deformed upper Paleozoic strata (~4 km thick) are preserved only in the Macusani Structural Zone, and absent from the CABB, Eastern Cordillera, and Subandean Zone. These folds are sealed beneath Triassic Mitu Group rocks, suggesting late Paleozoic (pre-Mitu Group deposition) shortening. The sigmoidal fold patterns observed here have been interpreted as refolded en echelon NW trending folds that were proposed to have formed in the late Paleozoic due to left lateral shear (Laubacher, 1978). In other locations, similar sigmoidal structures have been interpreted as fold interference patterns related to basement-involved thrusts (Carrera et al., 2006). The broad, short map traces (~6-7 km), ~6-7 km fold wavelength, thick (>4 km) and lack of exposed basement rocks suggests a detachment above the basement-

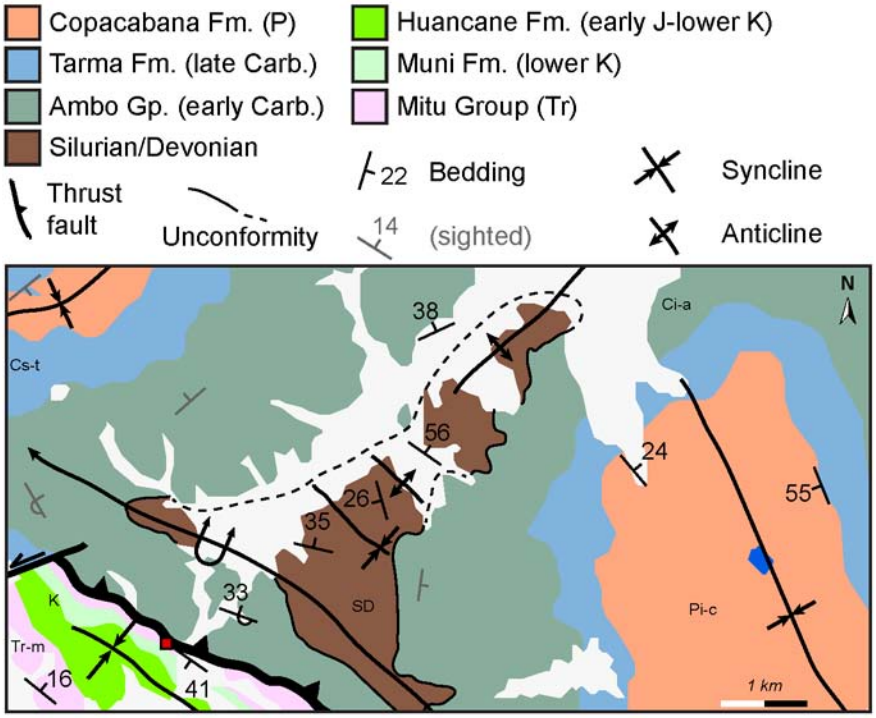

Figure 4.3. Map from Macusani Structural Zone (see Figure 1B for location) highlighting multiple pre-Andean deformation phases preserved in the area. Note folds in Silurian/Devonian beneath angular unconformity with overlying Carboniferous; multiple fold orientations in Carboniferous-Permian rocks; Silurian-Permian succession thrust over Triassic Mitu Group and Cretaceous Rocks.

cover interface. There are no paleomagnetic constraints to test potential vertical axis rotations expected for refolded folds.

We identify three main phases of deformation preserved in the region, which have been proposed by previous authors (Mégard et al., 1971; Laubacher, 1978; Mégard, 1978; Dalmayrac et al., 1980; Laubacher and Mégard, 1985; Jimenez et al., 2009). The first phase deforms Silurian/Devonian rocks about NW trending shallowing plunging synclines and anticlines (Figure 3). This first phase has been referred to as Eohercynian deformation (Dalmayrac, 1980; Laubacher, 1985) and occurred during late Devonian or early Carboniferous times. These folds are truncated by an erosional unconformity and covered by a ~4 km thick succession of Carboniferous to Permian shales, quartzites and carbonates. These upper Paleozoic units dominate exposures in the Macusani Structural Zone beneath Mitu Group deposits. The Carboniferous to Permian rocks preserve the faults and folds attributed to late Permian deformation ("Tardihercynian"; either refolded en echelon folds, or interference folds). Triassic Mitu Group deposits exhibit rapid lateral thickness (<~300 m to >2500 m) and facies variations. Despite proposed deposition in a Triassic rift environment (Newell, 1949; Sempere et al., 2002; Reitsma, 2012), only one normal fault example associated with Mitu Group deposition has been identified in outcrop (Figure 4). The Mitu Group is cut by NNW-trending thrust faults which also fold Cretaceous strata and are parallel to late Permian deformation orientations. We interpret these as late Permian structures reactivated during Andean deformation. Broadly, we interpret the Macusani Structural Zone as an inverted graben that preserved the Upper Paleozoic sequence, and accumulation of >2 km of Triassic Mitu Group rocks. The SE and NW margins of the zone are considered rift flanks that have been translated to the NE by motion along Andean basement thrusts.

Figure 4.4. Outcrop example of Triassic normal fault accommodating synrift accumulation of Mitu Group rocks. Note folded Permian carbonates unconformable below Mitu Group rocks, attributed to late Permian shortening.

5.1.5. Central Andean backthrust belt

The Central Andean backthrust belt is A ~50 km wide zone defined by NW-SE trending map contacts and exposures dominated by Cretaceous rocks. The NE margin is defined by late Jurassic (?) to early Cretaceous Muni Formation rocks in depositional contact above Triassic Mitu Group and upper Paleozoic rocks in the Macusani Structural Zone. The SW CABB margin is defined by the Ayaviri fault, which demarcates the Eastern Cordillera-Altiplano boundary. Faults and folds in the CABB are developed mostly in Cretaceous strata and verge towards the southwest. Faults are spaced ~1-3 km apart, and field relationships suggest an imbricate fold-thrust belt, as no evidence of a roof thrust is preserved. Isolated erosional windows in anticline cores expose Lower Cretaceous Muni Formation rocks deposited on thin (<300 m) accumulations of Triassic Mitu Group rocks that are deposited on Silurian/Devonian strata. In the CABB, Triassic Mitu Group rocks preserve evidence for pre-Cretaceous folding and penetrative fabric formation (Figure 5). The nature and distribution of such deformation remains unclear.

Thrust fault hangingwalls juxtapose Lower Cretaceous Muni Formation or Huancane Formation rocks on younger Cretaceous strata, suggesting the main shallow décollement is the base of the Cretaceous. Local exposures of uppermost Silurian/Devonian shales in anticline cores suggest this décollement may occasionally utilize a slightly deeper décollement below the base of the Cretaceous. Narrow fault spacing and fold width also support shallow décollement depth. Most hangingwall cutoffs are eroded. Fold limbs may be moderate (20°-30°) to steeply dipping (70°-80°). Map and field relationships suggest rounded, concentric folds rather than fault-bend folds. Tight, disharmonic folds are observed in some exposures of lower Cretaceous Ayavacas Formation carbonates (Figure 6). Other outcrop and map scale examples of complex fold patterns have been interpreted as features of slump and mass-wasting deposits (Callot et

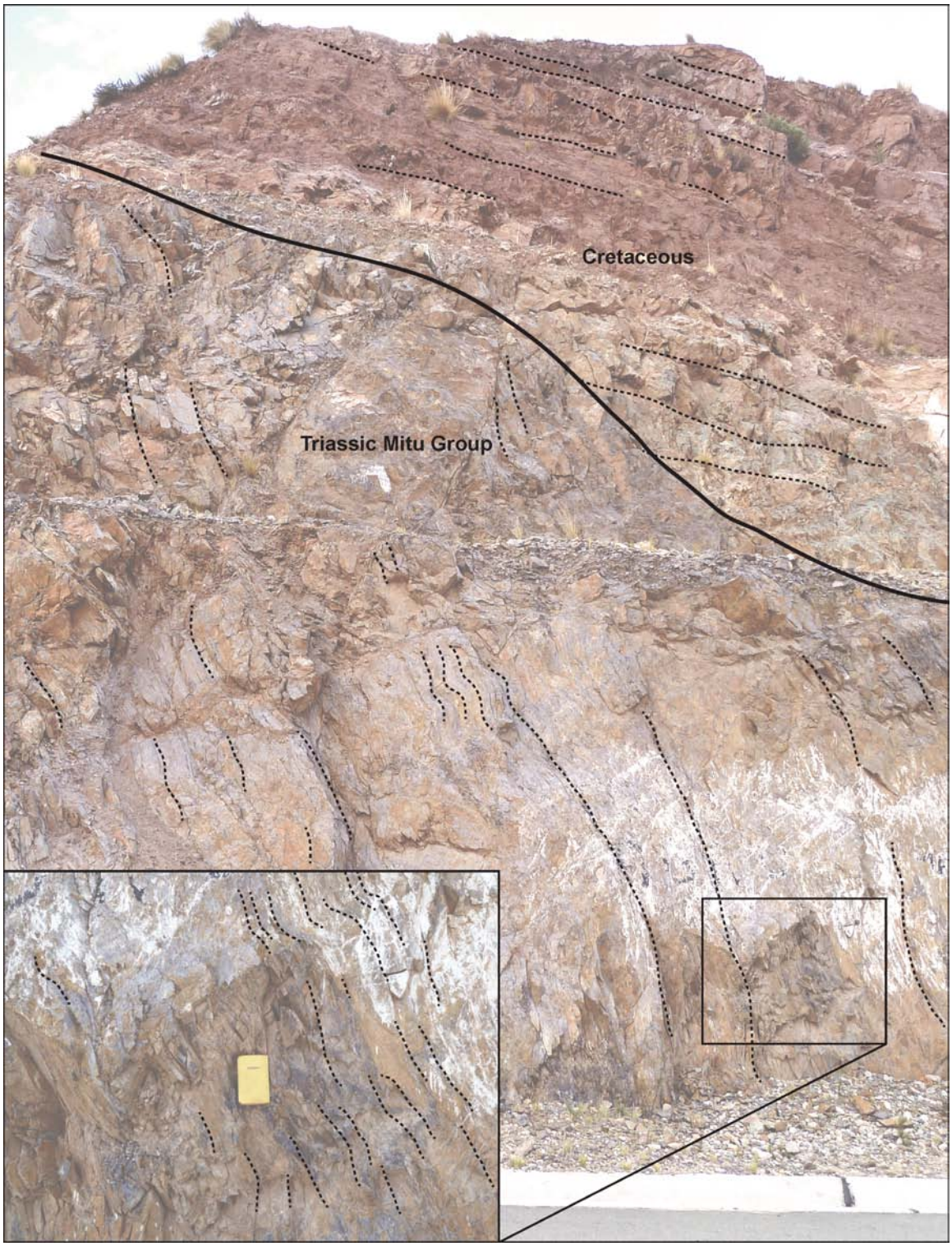
Cretaceous
Triassic Mitu Group

Figure 4.5. Roadcut example of penetrative foliation development and minor folds in Triassic Mitu Group rocks beneath angular unconformity overlain by Cretaceous rocks.

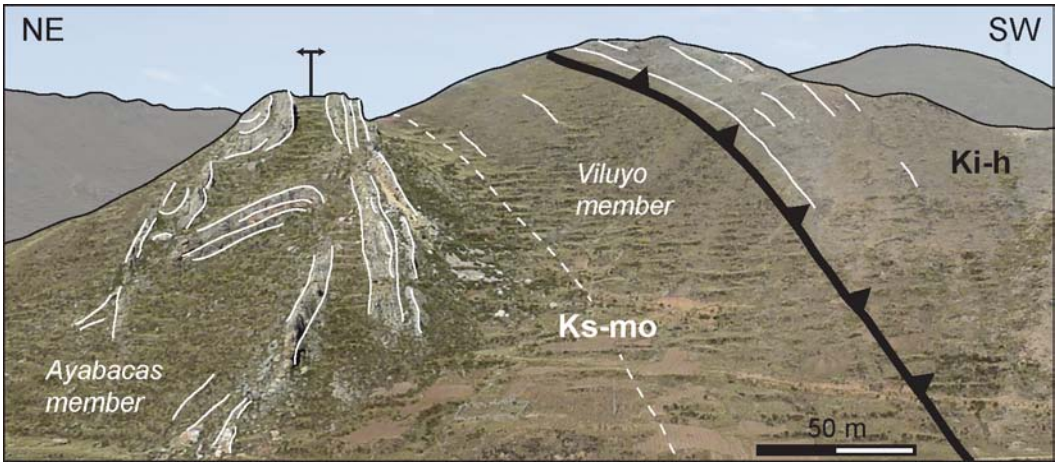

Figure 4.6. Outcrop example of non-harmonic folds typical of Cretaceous Ayavacas Formation exposures in the Central Andean Backthrust Belt. These rocks are in the footwall of a thrust, and local exposures of gypsum suggest folding is tectonically driven.

al., 2008a, b). We suggest some folding may be explained by CABB fold-thrust deformation, and the presence of gypsum intervals in Cretaceous Ayavacas Formation carbonates that allowed for disharmonic fold development.

The SW zone of the CABB exposes deeper structural levels throughout a ~15 km bivergent belt of lower Paleozoic rocks. A forethrust defining the NE margin of this narrow zone thrusts Carboniferous quartzites of the Ambo Formation on Cretaceous rocks. Within this narrow zone, localized exposures of Carboniferous and Silurian/Devonian rocks are thrust over thin accumulations Lower Cretaceous rocks. The SW CABB boundary is the Ayaviri fault, part of a larger fault system spanning southern Peru to Bolivia that defines the structural boundary between the Eastern Cordillera and Altiplano (Sempere et al, 1990; Carlotto, 2013). In the study area, the NE dipping, SW verging Ayaviri backthrust juxtaposes middle Ordovician Calapuja Formation rocks against Paleogene Puno Group rocks. Growth strata preserved in the Ayaviri fault footwall demonstrate ~28-26 Ma fault motion (Perez and Horton, 2014). In this ~15 km wide zone, Cretaceous rocks are deposited over Triassic or Silurian/Devonian rocks, resulting in a locally variable subcrop relationship.

5.1.6. Altiplano

Up to 3 km of Oligocene Puno Group and Miocene Tinajani Formation rocks are preserved in the Ayaviri basin (Rodriguez et al., 1999; Ibarra et al., 2004; Rousse et al., 2005; Carlotto, 2013; Perez and Horton, 2014). The basin is bounded to the NE and SW by the Ayaviri backthrust and the Pasani thrust, respectively. These fluvial and alluvial fan deposits are folded into a broad, NW trending asymmetric syncline, with NE limb dips generally 10°-15° SW and SW limb dips ~50°-70° NE. Along the NE Altiplano

boundary, Puno Group rocks preserve Oligocene growth strata in the footwall of the Ayaviri fault. Along the SW margin, coarse alluvial fan conglomerates of the Tinajani Formation preserve middle Miocene growth strata deposits in the footwall of the NE verging Pasani fault.

5.2. Cross Section

From field data and map relationships, we have identified main structures associated with Andean deformation. We have also identified five changes in structural elevation that are accommodated variably by duplexes in Paleozoic stratigraphy, basement thrust ramps, and inverted Triassic normal faults.

5.2.1. Subandean Zone

Field data, reflection seismic profiles and well logs were used to constrain the structural geometries observed in the Subandean Zone. Cretaceous rocks are mostly folded and rarely faulted. Narrow structure spacing and the lack of pre-Cretaceous rocks exposed in the Subandean Zone suggest a detachment at the base of the Cretaceous. Structural elevation of the Cretaceous rocks exposed at the surface in the Subandean above 4-5 km thick Cenozoic foreland basin deposits is best achieved by duplexing ~4 km thick Devonian to Ordovician succession. No Paleozoic rocks are exposed in the southern Peru Subandean Zone. Multiple major structures in the Eastern Cordillera have hangingwall flats in the Ordovician, suggesting the horizon is an important regional detachment. We use this detachment to create the three horses in the hinterland dipping duplex, and structurally elevate the Cretaceous. The space occupied by this duplex could

have also been filled with a basement thrust sheet, but this configuration would not have allowed sufficient space to shorten the Paleozoic the same amount as the Cretaceous. The frontal thrust has ~13 km of slip. This slip is necessary to balanced shortening in the Paleozoic duplex at depth. Some of the folds observed in the Subandean Zone are achieved by ramp-flat deformation along the Cretaceous detachment, whereas other folds are achieved by the subsurface duplex.

5.2.2. Eastern Cordillera

The Eastern Cordillera represents the second major increase of structural depth and is characterized by a >50 km wide structural high that we suggest was elevated by a basement thrust sheet. Exposed rocks include Ordovician through Devonian strata that were intruded by Triassic plutons. We suggest the map exposures of these plutons have been translated towards the NE due to motion of basement thrust B1 (Figure 1c). After restoration of the cross section, we projected schematic pluton roots at depth. We propose the root of these plutons is presently situated beneath the Macusani Structural Zone. The NE boundary of the Eastern Cordillera is defined by the SW dipping Main Andean Thrust that juxtaposes a syncline developed in Ordovician through Devonian strata on Cretaceous rocks. Map relationships show that the NE syncline limb is thinner than the SW limb. The SW increase in Paleozoic map thickness is achieved by increasing basement dip to 4°, and a second flat near the top of the middle Ordovician San Jose Formation. This hangingwall cutoff restores to the footwall cutoff of the westernmost horse in the Subandean duplex. Structural elevation of Ordovician rocks above Cretaceous rocks is achieved by motion of a 10 km thick basement thrust sheet over a basement ramp. Slip on this frontal basement thrust is accommodated by shortening of

the duplex and Cretaceous thrust faults in the Subandean zone and slip on the Main Andean Fault. The frontal section of the Eastern Cordillera is comprised of a single, ~30 km wide thrust sheet elevated above the basement thrust. Some deformation of this upper thrust sheet is achieved by folding over the underlying footwall cutoff, and folding of the westernmost Subandean horse into a syncline with the western limb tilted by the basement thrust sheet.

Within the Eastern Cordillera structural high, three smaller steps in structural elevation are observed. These step up to shallower exposure levels towards the hinterland in conjunction with increasing surface elevation. We modeled this pattern as a décollement horizon that steps up from the base of the middle Ordovician, to base of the upper Ordovician, and to the base of the Silurian/Devonian. A small duplex with backthrust sense elevates the upper Ordovician, and repeated Silurian/Devonian rocks achieve the third, structurally shallowest zone of the Eastern Cordillera. Although this zone of the cross section now appears as a large passive roof duplex over the underlying basement thrust sheet B1, we note that slip on B1 is fed to frontal Main Andean Thrust, and the Subandean Zone, not the Eastern Cordillera. Rather, we suggest that slip into zone of backthrusts in the Eastern Cordillera is restored to a basement thrust sheet B2 that was thrust on the frontal basement sheet B1.

5.2.3. Macusani Structural Zone

The boundary between the Eastern Cordillera and Macusani Structural Zone is defined by the Cordillera de Carabaya. These plutons were intruded into lower Paleozoic rocks and carried in the hangingwall of SW verging thrust faults over Triassic and upper Paleozoic rocks of the Macusani Structural Zone. The Macusani Structural Zone exhibits

shallower structural elevation than the Eastern Cordillera. Whereas Eastern Cordillera exposure levels are deeper because they have traveled over a basement thrust sheet, Macusani Structural Zone exposure levels are shallower because they have not been elevated to the top of the basement sheet. In our cross section, we achieve this on the SW side of the frontal basement ramp and on the back limb of the frontal basement thrust sheet B1. As noted above, evidence for multiple pre-Andean deformation phases are preserved in the Macusani Structural Zone. From field data and map relationships we show faults and folds in Permian through Carboniferous rocks preserved beneath Triassic Mitu Group deposits in the deformed section. In the restored section, we do not attempt to restore pre-Triassic deformation in the Carboniferous to Permian rocks to their pre-Andean state. Ordovician rocks are not observed in the Macusani Structural Zone, and Silurian/Devonian rocks are rarely observed. We do not attempt to model geometries associated with pre-Carboniferous deformation. Instead the Ordovician-Devonian rocks are depicted as continuous parallel units, but we note that they preserve pre-Andean deformation fabrics and were probably the main décollement levels for late Permian deformation.

We use field and map data demonstrating deformation of Cretaceous and Triassic Mitu Group rocks to define the location of key Andean thrust faults. These thrust faults are often aligned with late Permian compressional structures, but have longer map traces suggesting they have reactivated and propagated existing structural features. Thrust spacing is ~15-16 km. Slip along individual faults is generally < 5 km. Broadly folded Triassic Mitu Group deposits and wide fault spacing suggest these reverse faults root at least to the base of the Phanerozoic succession, which is at least ~13 km thick in the Macusani Structural Zone. In contrast, folded Carboniferous to Permian rocks have a ~2 km wavelength, suggesting a shallower detachment accommodated that phase of

deformation. The broad folds, wide thrust fault spacing, and thick sedimentary cover deformed in the Macusani Structural Zone represents a zone of basement-involved thick skinned shortening within the Eastern Cordillera.

The Macusani Structural Zone is interpreted as an inverted graben that subsided during Triassic rifting and Mitu Group deposition. A ~3-4 km thick Carboniferous to Permian sequence in the Macusani Structural Zone is attributed to preservation in the subsiding graben. Equivalent deposits were likely eroded from the horst flanks. Indeed, some exposures of Mitu Group conglomerate deposits are composed of Permian limestone clasts, suggesting erosion of Permian Copacabana Formation from the uplifted footwall was a primary sediment source. We identify two main normal faults that are reactivated as thrust faults. We model these faults as basement involved faults. Motion along the SW dipping, NE fault (B2) feeds slip into the backthrusts of the Eastern Cordillera. Motion along the NE dipping fault (B3) transfers slip into the CABB. Basement involved B3 thrust motion elevates the Macusani Structural Zone above the CABB. We suggest that inversion of the inherited thick-skinned B3 fault geometry played a key role in establishing the southern Peruvian segment of the SW verging thin-skinned CABB.

5.2.4. Central Andean Backthrust Belt

Field and map data demonstrate close fault spacing (1-3 km), the presence of Lower Cretaceous rocks in thrust fault hangingwalls, and tight folds that likely reflect a shallow detachment at the base, or near the base, of the Lower Cretaceous. The thin-skinned structural style of the CABB contrasts the thick-skinned style of the Macusani Structural Zone. The décollement probably occupies the Lower Cretaceous Muni

Formation, which is a fine-grained marine siltstone. A secondary detachment at the base of the Ayavacas Formation (lower Moho Group) may locally utilize evaporite deposits and create tight, disharmonic folds in the footwalls of some thrust faults (Figure 6). The Cretaceous section thins from ~2 km to <1 km towards the SW. The NE margin of the CABB is more highly deformed with tighter folds and multiple thrust faults, whereas the SW margin is deformed by open folds and fewer thrust faults. This suggests that deformation propagated from the NE to SW, creating an in-sequence imbricate fold-thrust belt. The CABB transferred displacement from the Eastern Cordillera to the Altiplano.

Cretaceous rocks in the CABB are deposited with angular unconformity on thin (<300 m) Triassic Mitu Group deposits, which are disconformable with underlying Silurian/Devonian strata. Only two thin isolated exposures of Carboniferous Ambo Formation strata are preserved near the SW margin of the CABB. In general, we suggest that the CABB was mostly a high standing, eroding block during Triassic rifting. Nearly all Carboniferous to Permian rocks that may have been present were eroded, and only thin accumulations of synrift Mitu Group deposits were preserved in the hangingwalls of minor normal faults.

Shortening of the Cretaceous rocks is achieved by duplexing and equivalent shortening of the Ordovician to Devonian strata. Here, we model two detachments to accommodate Paleozoic shortening. At the NE CABB margin, beneath the more tightly deformed Cretaceous rocks, one detachment at the base of the Ordovician creates a SW verging duplex. The décollement ramps up to the base of the Silurian/Devonian beneath the zone of the more broadly folded Cretaceous rocks. In one horse of this Silurian/Devonian duplex, a thin carapace of Carboniferous Ambo group rocks is preserved beneath thin Cretaceous deposits. This is the only region that preserves

Carboniferous deposits outside of the Macusani Structural zone. The frontal thrust of the CABB is the Ayaviri fault, which utilizes the main décollement at the base of the Ordovician. Growth strata geometries preserved in the footwall suggest hybrid trishear and fault-propagation fold kinematics during thrust motion.

5.2.5. Shortening magnitudes

Our new line length balanced cross section has a deformed length of 210 km measured between the surface traces of the Ayaviri fault and the regional pin line in the foreland. The restored section has a length of 340 km. Total Andean shortening across this transect is 130 km, or 38% shortening. The foreland regional pin line is less than 5 km from the thrust front, which will maximize agreement between true magnitude and percent shortening (Judge and Allmendinger, 2011). The shortening magnitude in the Subandean zone is 31 km. Within the Eastern Cordillera, total shortening magnitude is 24 km. The Macusani Structural Zone was shortened 30 km, whereas the CABB was shortened 45 km. Despite comparable ~50-60 km map widths of the Eastern Cordillera, Macusani Structural Zone, and the CABB, each zone accommodated different magnitudes of shortening. Despite being narrow, the Subandean zone accommodated a large magnitude of shortening, whereas the Eastern Cordillera accommodated the least shortening.

The new shortening estimates presented here are similar to the preferred shortening estimate of 123 km (40%) reported by Gotberg et al., (2010) along a section ~100-150 km NW along strike near Cusco, Peru. Approximately 400 km along strike to the SE, McQuarrie et al., (2008) document 276 km (40%) shortening. A ~47% reduction in shortening magnitude occurs between the study area of McQuarrie et al., (2008) and

our new cross section presented here. This reduction in shortening is consistent with previous workers who note a strong along strike gradient in total shortening from Bolivia to Peru (Gotberg et al., 2010).

5.2.6. Uncertainty estimates

Allmendinger and Judge (2011) discuss the lack or imprecision of uncertainty estimates in typical line length balanced cross sections, and propose area balanced cross sections as an alternative method to quantify uncertainty in shortening estimates. However, area balanced sections restore to a simple sedimentary wedge geometry with defined sedimentary thicknesses at the edges, a uniform décollement angle, and a horizontal upper surface. The area balance does not prescribe any kinematically viable solutions for acceptable errors presented for the Ocross section. Here we combine methods from Judge and Allmendinger (2011) and Eichelberger et al., (2013) to estimate uncertainties of our cross section.

A lower limit of uncertainty may be estimated from lengths of hangingwall cutoffs projected above the erosion surface. In our cross section, 71 km of hangingwall are projected above the surface, suggesting a minimum shortening magnitude of 59 km (130 ± 71 km, 54%) assuming Gaussian distribution (Judge and Allmendinger, 2011; Eichelberger et al., 2013). Shortening and uncertainty estimates using area-balanced techniques reveal different results. We calculated 319.8 ± 40.8 km shortening for post-basement rocks using the *AreaErrorProp* program (Judge and Allmendinger, 2011). This shortening magnitude is significantly higher than our line length estimate, and indeed approaches values cited for sections through the Bolivian Andes, where total shortening magnitudes are the greatest for the entire Andean margin (Sheffels, 1990; Lamb and

Hoke, 1997; McQuarrie, 2002). This discrepancy highlights the shortcomings of area balanced sections. The left and right margins of our restored section match thicknesses for the area balanced initial wedge. However, our line-balanced section has a thickened internal region corresponding to the Triassic Mitu Graben, and relies on changes in basement dip to accommodate observed increases in stratigraphic thickness. The increased thickness in the Mitu Graben accommodates area that is redistributed by the area balanced method. By redistributing this inherited change in stratal thickness, the area balanced method over estimates total shortening. As such, we prefer our shortening magnitudes estimated from line length methods.

5.3. Thermochronology

5.3.1. Overview

We report new apatite and zircon (U-Th)/He cooling ages to define the timing of exhumational cooling in the Subandean Zone, Cordillera de Carabaya and Ayaviri fault. Five zircon (U-Th)/He (ZHe) samples from the Coasa pluton have Oligocene to mid-Miocene mean sample ages. Eight apatite (U-Th)/He samples from the Coasa pluton preserve an exhumed PRZ at high elevations, and lower elevation samples suggest mid-Miocene cooling. Three AHe samples from the SAZ have ages that decrease towards the foreland, suggesting onset of cooling by the mid-Miocene, and in-sequence propagation of cooling and deformation.

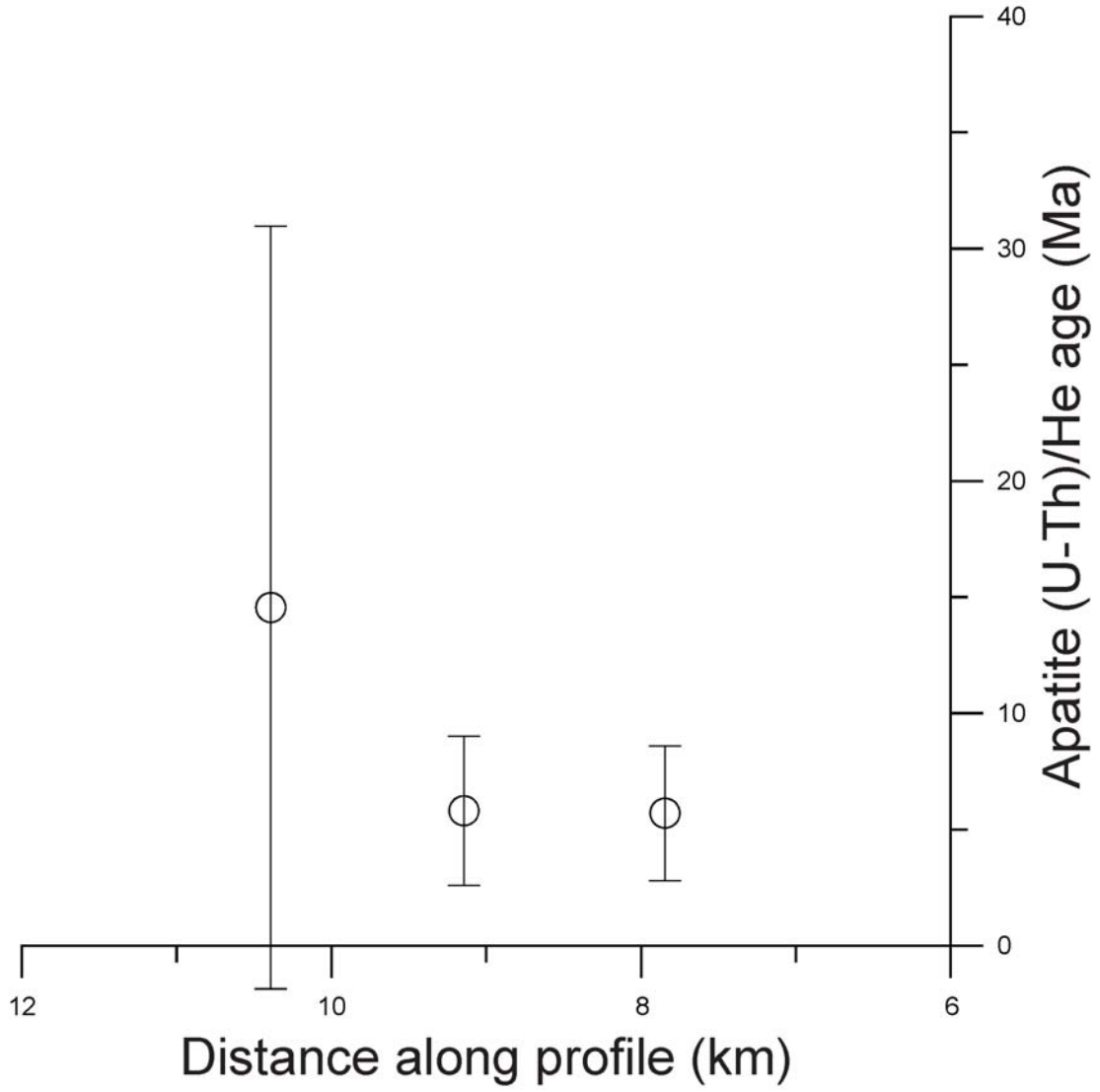

Figure 4.7. Age distance relationship for apatite (U-Th)/He samples from Cretaceous rocks of the Subandean Zone.

5.3.2. Subandean zone

The cooling histories of three samples from Cretaceous sandstones exposed in the Subandean zone were determined using apatite (U-Th)/He thermochronology. Four to five grains were analyzed per sample. The structurally shallowest sample situated most towards the hinterland exhibits high uncertainty (14.55 ± 16.42 Ma) due to individual grain ages of 3.0 Ma, 3.8 Ma, 13.1 Ma, and 38.2 Ma. The large spread in grain ages may suggest the sample is partially reset. Two additional samples situated towards the foreland have improved precision, with ages of 5.8 ± 3.2 Ma and 5.7 ± 2.9 Ma, respectively (Figure 7) that we interpret as fully reset ages. In general, mid- to late Miocene AHe cooling ages from Cretaceous rocks in the Subandean zone suggest onset of initial deformation by the mid-Miocene.

5.3.3. Coasa pluton

Seven samples were collected along a ~20 km long transect in NE trending incised canyons in the Coasa pluton. An additional sample was collected from Carboniferous Ambo Formation quartzite host rock ~300 m from the pluton contact. All 8 samples were analyzed for AHe, and 5 were analyzed for ZHe. Samples analyzed for ZHe cooling ages span elevations between 4576 and 3710 m a.s.l. Sample elevation generally increases towards the SW. Mean sample ages range from 18.6 ± 1.0 Ma to 25.7 ± 1.8 Ma. We interpret all samples as reset. No PRZ is preserved in high elevation samples, suggesting exhumation from depths greater than ~6 km. We interpret these data as rapid exhumational cooling during late Oligocene to early Miocene deformation in the Eastern Cordillera (Figure 8).

Eight AHe samples span elevations from 4764 to 3710 m a.s.l. The highest elevation sample exhibits the greatest spread among individual grain ages from 16.9 to

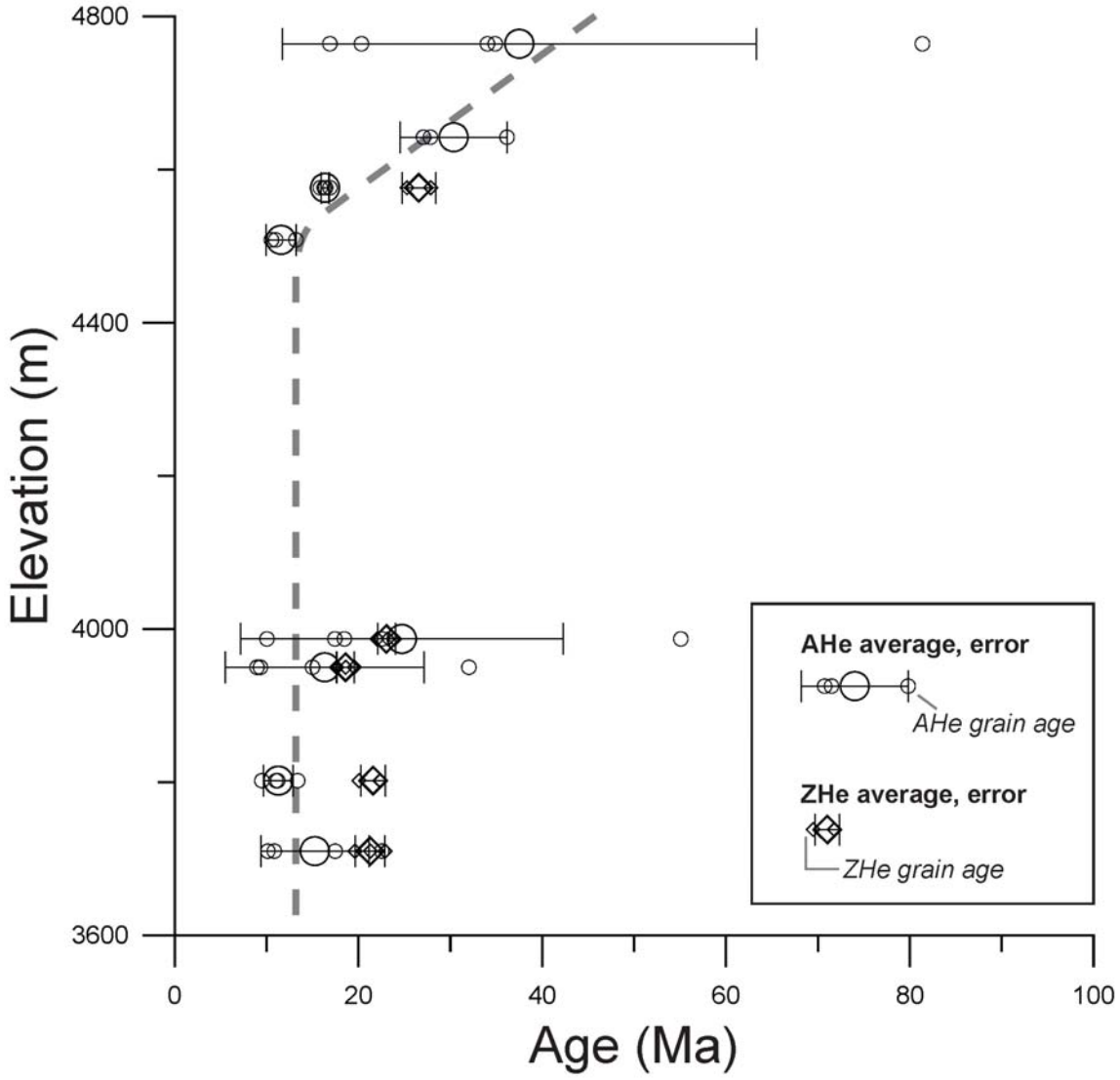

Figure 4.8. Age elevation relationships for apatite and zircon (U-Th)/He samples from the Coasa pluton, Cordillera de Carabaya, Eastern Cordillera.

81.4 Ma. We interpret this as a partially reset sample that was exhumed from the AHe PRZ. Samples at lower elevations have mean ages between 11.3 ± 1.6 Ma and 30.4 ± 5.8 Ma. The four lowest elevation samples define a steep age versus elevation relationship. The age versus elevation relationship for the four highest elevation samples lies along a different, less steep curve. Based on the age of this inflection point between high and low elevation samples, we suggest the AHe system experience rapid cooling beginning at ~15 Ma.

Five samples were analyzed with both AHe and ZHe methods. In these samples, ZHe ages are <10 Myr older than AHe ages. Some samples have ages that are identical within uncertainty. This relationship is expected, and suggests that both thermochronology systems record a protracted ~25-15 Ma cooling history associated with exhumation in the Eastern Cordillera and Cordillera de Carabaya.

5.4. U-Pb detrital zircon geochronology

5.4.1. Overview

We present results from 20 U-Pb detrital zircon geochronology samples (n=1997 grains) that characterize the provenance characteristics of the Cretaceous through Cenozoic deposits preserved in the Altiplano/CABB and Subandean Zone (Figure 9). We note distinct differences in zircon provenance between the two regions since at least the early Cretaceous. The Cretaceous to Cenozoic record in the Altiplano/CABB is characterized by detrital zircon age populations that reflect distinctive Eastern and Western Cordillera sources. Detrital zircon ages from Cretaceous rocks from the Altiplano/CABB are characteristic of dominantly Eastern Cordillera provenance, whereas

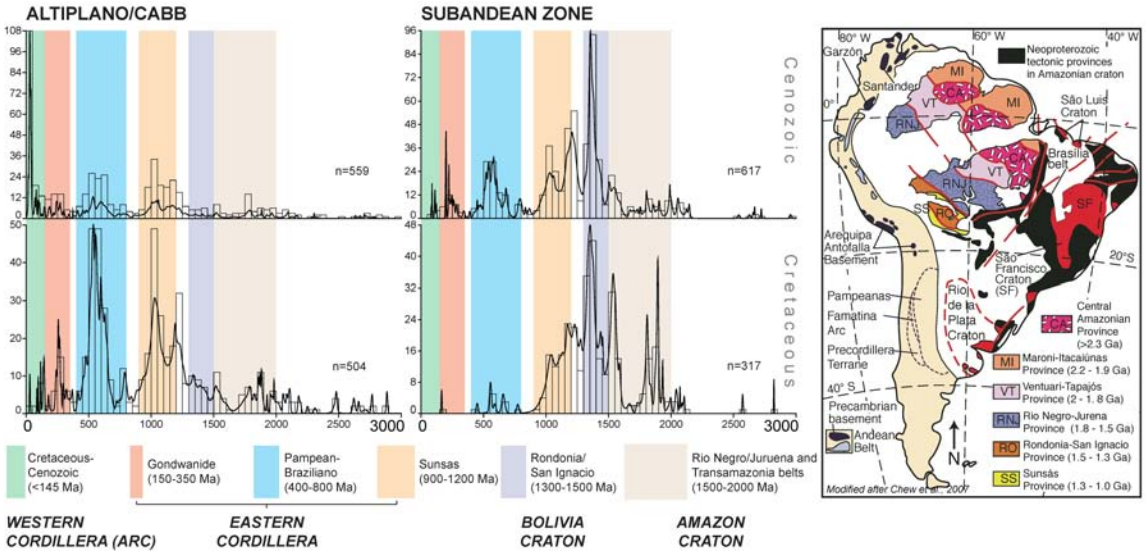

Figure 4.9. Comparison of U-Pb detrital zircon geochronologic analyses of Cretaceous through Cenozoic rocks from the Subandean Zone and Altiplano/CABB. Subandean Zone rocks have strong cratonic signatures and lack Western Cordillera zircons (see map) whereas Altiplano/CABB rocks have strong Eastern and Western Cordillera provenance, but lack characteristic cratonic populations.

Cenozoic rocks from the Altiplano/CABB reflect dominant sediment contribution from the Western Cordillera. In contrast, the Cretaceous to Cenozoic record preserved in the Subandean Zone is characterized by detrital zircon age populations similar to ages in South American craton, suggesting and important long-lived component of sediment sourced not from Andean Cordilleras, but rather from cratonic sources.

5.4.2. Altiplano and CABB

Five samples were collected from Cretaceous marine sandstones exposed in the CABB (n=504 grains). All five samples exhibit detrital zircon age populations that are found in Paleozoic rocks of the Eastern Cordillera (~400-800 Ma, ~900-1200 Ma, >1300 Ma). However, we consider the presence of Gondwanide zircons (~350-160 Ma) (Mišković and Schaltegger, 2009), which are characteristic of plutons exposed in the Eastern Cordillera, as diagnostic of a strong Eastern Cordillera provenance during Cretaceous deposition. Few (n<10) Cretaceous age zircons have been analyzed from the 5 samples. Six Cenozoic samples from the northern Altiplano reveal a transition to a dominantly Western Cordillera provenance. Cenozoic detrital zircon grains dominate the 6 samples (n>100), and 30 Cretaceous grains were analyzed from the Cenozoic rocks. The high proportion of Cretaceous and Cenozoic grains in Cenozoic rocks suggests sediment was sourced from the Western Cordillera and transported towards the east. Some Cenozoic samples from the Altiplano also contain zircon populations that are characteristic of Eastern Cordillera provenance, but these signals are not present in all samples.

Three Cretaceous samples from the Subandean Zone (n=317 grains) lack Cretaceous and Gondwanide zircons characteristic of the Western and Eastern

Cordilleras, respectively. The 400-800 Ma population is a minor component of the Cretaceous Subandean Zone population. Unlike Cretaceous rocks from the CABB, the Cretaceous rocks from the Subandean zone are dominated by a broad distribution of 900-1600 Ma zircons, with a main peak between 1300-1400 Ma. A second zircon population between ~1700-2100 Ma is also prominent. Most of these Proterozoic age zircons are represented in as recycled detrital zircon grains in Paleozoic rocks exposed throughout the Eastern Cordillera. The key population is the 1300-1400 Ma peak. This zircon age population is very minor throughout Western and Eastern Cordillera rocks. This age is characteristic of the Rondonia/San Ignacio cratonic block of Bolivia. We suggest that the Cretaceous rocks from the Subandean zone have a major component of detritus shed from the craton and transported from the east to the west, and lack significant contribution from Andean sediment sources.

Six Cenozoic samples from the Subandean zone and foreland basin were analyzed (n=617). A broad population of 900-1600 Ma zircons is present, characterized by a dominant peak between 1300 and 1400 Ma. The population of zircons > 1700 Ma is not a dominant peak in Cenozoic Subandean Zone samples. The abundance of 500-700 Ma zircons is higher relative to Cretaceous Subandean samples. The appearance of Gondwanide zircons, and n=5 Cretaceous zircons suggests that the Subandean zone received a minor contribution from Andean sources during Cenozoic deposition. No Cenozoic detrital zircons have been analyzed from Cenozoic samples in the Subandean Zone or Foreland basin. The persistent ~1300-1400 Ma detrital zircon population suggests continued sediment derived from cratonic sources. However, the minor appearance of Andean zircons (Gondwanide and Cretaceous populations) in Cenozoic sediments may provide constraints on in initial timing of significant Eastern Cordillera uplift.

We identify two main patterns in these data. First, the detrital zircon provenance of Cretaceous to Cenozoic stratigraphy in the CABB/Altiplano zones is characterized by a transition from Eastern to Western Cordillera sediment sources. We interpret the presence of Proterozoic zircons as material recycled from Paleozoic rocks of exposed in the Andes, rather than sediment sourced directly from Proterozoic cratonic blocks. Second, the Cretaceous to Cenozoic stratigraphy of the Subandean Zone is characterized a dominant cratonic signal, but Andean provenance is minor and restricted to the appearance of Eastern Cordillera derived zircon populations during the Cenozoic. Despite the appearance of Eastern Cordillera detrital zircons, the Subandean Zone lacks a significant Western Cordillera volcanic arc signature (Cretaceous to Cenozoic age zircons).

5.5. Geomorphology

5.5.1. Overview

We investigated 18 incised fluvial bedrock channels that traverse the Eastern Cordillera and flow into the foreland. Most channels flow N or NE, but two flow NW (Figure 10a). The channels span a ~400 km distance along strike of the Eastern Cordillera. We extracted each elevation profile along the sinuous channel length, and inspected elevation versus along-profile distance relationships to identify knickpoints. We identified three elevation ranges that exhibit knickpoints certain fluvial profiles: ~3900-4500 m, 3300-3700m, and ~1800-2800 (Figure 10b). The three channels situated farthest SE do not appear to have knickpoints. Additionally, two channels with low elevation headwaters do not have knickpoints. All other channels have at least one

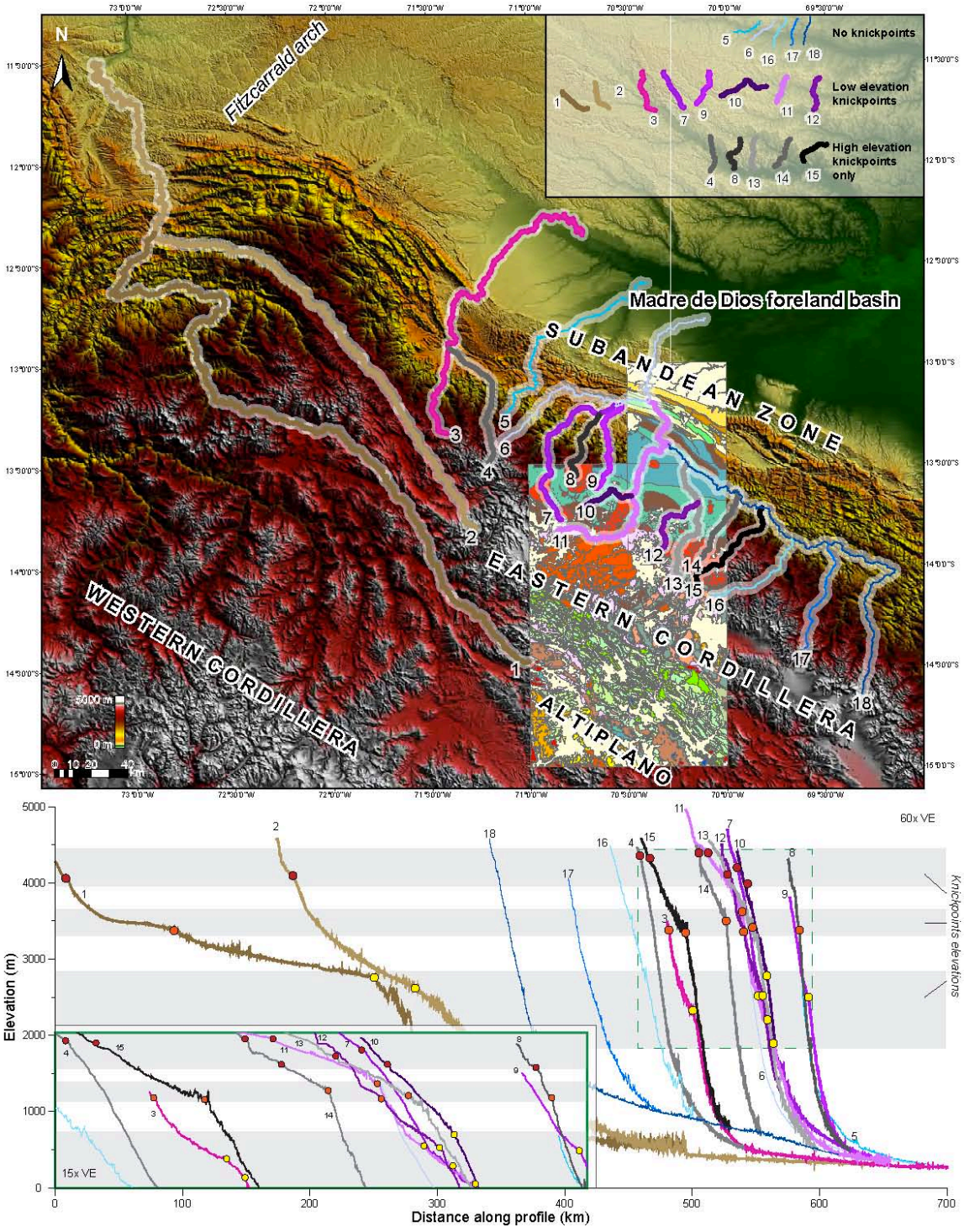
N
Fitzcarrald arch
No knickpoints
Low elevation knickpoints
High elevation knickpoints only
Madre de Dios foreland basin
SUBANDEAN ZONE
EASTERN CORDILLERA
WESTERN CORDILLERA
ALTIPLANO
60x VE
15x VE
Elevation (m)
Distance along profile (km)
Knickpoints elevations

Figure 4.10. A) DEM topography, geologic map, and traces of fluvial profiles shown in B). Note elevations of different knickpoint populations.

knickpoint. Based on the spatial distribution of the two highest elevation knickpoints populations, we suggest much of the region shared two events that created these knickpoints. The third, lowest elevation population of knickpoints is restricted to fluvial channels NW of the Coasa pluton, suggesting a separate event was restricted to this region and did not affect drainages SE of the Coasa pluton. The spatial distribution of knickpoint elevations may reflect multiple potential drivers including changes in structural kinematics, changes in the location and pace of rock uplift, basement fault geometries, climate driven erosion, or other lithospheric scale processes related to surface uplift. Further work should test these hypotheses using additional geomorphologic criteria including steepness and concavity indices (Kirby and Whipple, 2012; Whittaker, 2012), investigations of fluvial hanging valleys (Whipple and Gasparini, 2014), and comparisons of basin volume to area ratios (Frankel and Pazzaglia, 2006).

5.5.2. Channels without knickpoints

Channels 5, 6, 16, 17, and 18 exhibit smooth, concave up profiles. Channels 5 and 6 have headwaters that are at lower elevations than all other channels, and are situated in the frontal Eastern Cordillera. We suggest the lack of knickpoints in these two channel profiles, despite the presence of knickpoints in all surrounding fluvial channels, is because these channels are restricted to lower elevations. They may be situated forelandward of active zones of rock uplift, or any knickpoint that once existed has propagated through the fluvial channel. Channels 16, 17, and 18 traverse from above ~4000 m elevation and are situated to the SE along strike from the Coasa pluton. The absence of knickpoints in these three channels suggests the region SE of the Coasa pluton

has not experienced recent changes to rock uplift, and fluvial channels have established equilibrium relationships between incision and uplift.

5.5.3. Knickpoints above 3300 m

Channel profiles 1 through 4 and 7 through 15 have at least one knickpoint above ~3300 m elevation. The region defined by these profiles spans ~300 km from the Coasa pluton towards the NW. We find that knickpoints cluster at two elevation intervals, ~3900-4500 m, and ~3300-3700 m. We are unable to identify the driver of these knickpoints. However, incision and exhumation in the Peruvian and Bolivian Eastern Cordillera has been attributed both to climatic (Lease and Ehlers, 2013) and tectonic (Whipple and Gasparini, 2014) events. In general, we suggest that the entire region experienced two events that created two populations of knickpoints that have migrated upstream at similar rates along strike. These early phases of rock uplift rate increase suggest the region responded uniformly, and that the driver affected large spatial scales.

5.5.4. Knickpoints below 2800 m

Channel profiles 1-3, 7, and 9-12 preserve knickpoints across an elevation range spanning ~2800-1800 m and span an along strike distance of ~260 km NW of the Coasa pluton. Because these knickpoints are at lower elevations, and knickpoints migrate upstream, we suggest that the cause of these knickpoints affected the region NW of the Coasa pluton after the events that created knickpoints observed at higher elevations over larger spatial regions. The restriction of low elevation knickpoints to a smaller region potentially suggests a change in the driver of knickpoint creation. Alternatively, the driver could remain the same but the scope over which it acts was modified.

6. DISCUSSION

Integration of field, map, cross section, thermochronologic, geochronologic, and geomorphologic datasets can provide insights into the role of inherited structural framework on subsequent orogenesis, along strike variations in exhumation and crustal thickening, basin dynamics, and the surface expression of tectonism. We suggest that inversion of pre-Andean normal faults guided Andean shortening, exhumation patterns, and coeval foreland/hinterland basin evolution.

6.1. Inversion of pre-Andean normal faults

Previous workers have shown that some segments of the Andes are dominated by thin-skinned deformation (Roeder, 1988; Kley et al., 1996; Baby et al., 1997; McQuarrie, 2002), thick-skinned deformation (Grier et al., 1991; Kley et al.,, 1999; Giambiagi et al., 2011), and zones of interaction between thin- and thick-skinned deformation (Jordan and Allmendinger, 1986; Dengo and Covey, 1993; Cooper et al., 1995; Roeder and Chamberlain, 1995; Kley et al., 1997; Mora et al., 2006). Field and map relationships informed construction of a balanced cross section and demonstrated the location of pre-Andean normal faults. These normal faults control some of the major changes in structural elevation.

We identify 4 pre-Andean normal faults that have been selectively reactivated as thrust faults during Andean shortening (Figure 14). All examples preserve pre- or synrift rocks in normal fault hangingwalls. We suggest that corresponding units were eroded or

not preserved in the footwall. Subcrop relationships and rapid sediment thickness changes across each fault are most easily recreated with pre-Andean normal faults. SW dipping basement thrust B2 (Figure 1c) is interpreted as the basement root of a pre-Andean normal fault. NE dipping basement thrust B3 is considered an inverted conjugate normal fault of B2, together defining a Triassic graben. The Triassic graben preserves >6 km of Upper Paleozoic to Triassic synrift Mitu Group deposits and suggests these two faults may have been major normal faults controlling rift evolution. Two Andean thrust faults from the CABB are interpreted as inverted pre-Andean normal faults, but thin accumulations of pre- or synrift rocks suggest these are likely minor normal faults within the Triassic rift. Isolated exposures of lower Carboniferous Ambo Group rocks from the Pz1 thrust fault hangingwall (Figure 1c) are not observed across the fault in the corresponding footwall. The Ayaviri fault (AF, Figure 1c) is also interpreted as an inverted pre-Andean normal fault because exposures of Triassic synrift Mitu Group deposits are common along strike in the Ayaviri fault hangingwall, but are not observed in the footwall beneath Cretaceous rocks.

Selective reactivation of these faults played key roles in the kinematic development of the Eastern Cordillera. Thrust reactivation of the B2 fault fed displacement into backthrusts of the Eastern Cordillera. We suggest that initial Eocene Eastern Cordillera deformation inferred from K/Ar and $^{40}Ar/^{39}Ar$ cooling ages (Farrar et al., 1988) was linked to reactivation of the preexisting weakness related to the Triassic B2 normal fault (McQuarrie et al., 2005). Inversion of the basement involved B3 normal fault fed displacement upsection into the Lower Paleozoic and Cretaceous rocks of the CABB. The inherited orientation of the B3 fault was key in defining the location and vergence direction of the CABB. The Ayaviri fault represents the modern structural boundary between the Altiplano and CABB (Eastern Cordillera). We interpret this

structure as an inverted Triassic normal fault. The Ayaviri fault system persists for ~400 km along strike (Sempere et al., 1990). If the entire length of the structure represents an inherited feature, the development of the Altiplano may be linked to reactivation of pre-Andean structures. In summary, many kinematic and temporal characteristics of Andean Eastern Cordillera shortening are a function of inherited structures from pre-Andean deformational events.

6.2. Timing of Deformation

Thermochronology datasets constrain the timing of cooling that may be driven by erosion, uplift by fault motion, or post intrusion thermal relaxation. In actively shortening orogens that lack volcanic activity, thrust fault motion is proposed as the main driver of exhumational cooling (Farrar et al., 1988; Ege et al., 2003; Barnes et al., 2006; Gillis et al., 2006; Ege et al., 2007; Barnes et al., 2008; Lease and Ehlers, 2013; Eichelberger et al., 2013). We document the timing of exhumational cooling in the Coasa pluton and the Subandean zone using AHe and ZHe thermochronometers. ZHe results from the Coasa pluton show rapid cooling between ~26 and 18 Ma. AHe results from the same samples in the Coasa pluton record rapid cooling initiating at ~15 Ma. In general, our results suggest an Oligocene to mid-Miocene phase of exhumational cooling.

Previous studies from the Coasa pluton and Cordillera de Carabaya identified a narrow zone (Zongo-San Gabán Zone) that yield discordant biotite and muscovite K-Ar ages and $^{40}Ar/^{39}Ar$ age spectra. These data were interpreted as evidence for an Eocene phase of rapid heating attributed to burial by thick, potentially basement involved, backthrust sheets (Martinez, 1980; Farrar et al., 1988). However, the structure that

achieved this burial has not been identified. We suggest that reactivation of the basement involved SW dipping normal fault ("B2" in Figure 1c) fed displacement forward to lower Paleozoic rocks in the Eastern Cordillera. Motion along the EC1 backthrust (7.8 km thick lower Paleozoic hangingwall) would have buried modern exposure levels of Cordillera de Carabaya plutons to minimum ~10-11 km depth. This depth does not incorporate an unknown thickness of post Devonian to Eocene rocks that may have been eroded from the Eastern Cordillera, which would increase burial depth. In other sections of the cross section, Devonian to Eocene rocks may be > 5 km thick. With a 30° - 35° C/km geothermal gradient, burial by the EC1 backthrust would heat the Cordillera de Carabaya and Coasa pluton to cause discordant K-Ar and $^{40}Ar/^{39}Ar$ biotite and muscovite ages. Oligocene to mid-Miocene cooling of the Coasa pluton revealed by our AHe and ZHe results could be achieved by duplexing of Ordovician rocks at depth driven by insertion of the B2 basement thrust sheet.

AHe results from Cretaceous rocks Subandean Zone require onset of deformation by 6 Ma, but permit deformation onset as early as 15 Ma. Slip on the B1 basement fault fed slip forward into the Subandean zone. Duplexing in the lower Paleozoic caused structural elevation and subsequent erosional exhumation of the Cretaceous (Figure 7). This is consistent with other workers who suggest Subandean zone deformation did not initiate until after ~25-20 Ma (Horton, 2005; Barnes et al., 2006; Barnes et al., 2008; Espurt et al., 2011; Eude et al., 2015). However, these results do not permit resolving the precise timing of Subandean shortening.

New ZHe results from the Coasa pluton and previous results from the Rio San Gabán transect (Lease and Ehlers, 2013) show ages between ~26 and 15 Ma. Despite the lateral distance between the two sampling transects, age distance relationships of these samples show a characteristic partial U-shaped pattern (Figure 11), suggesting cooling by

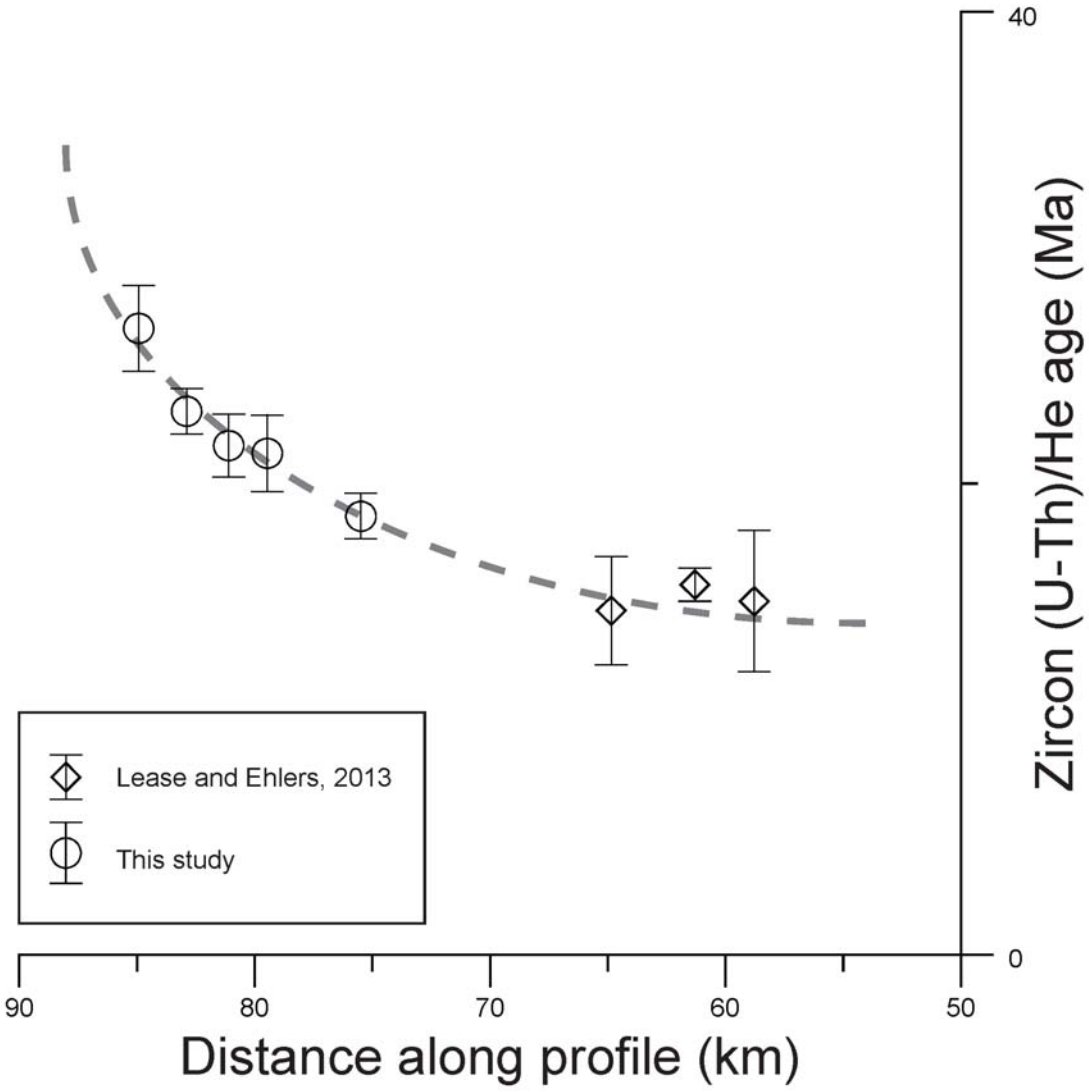

Figure 4.11. Age distance relationship combining ZHe results from this study and Lease and Ehlers (2013). Note one side of characteristic U-shaped pattern.

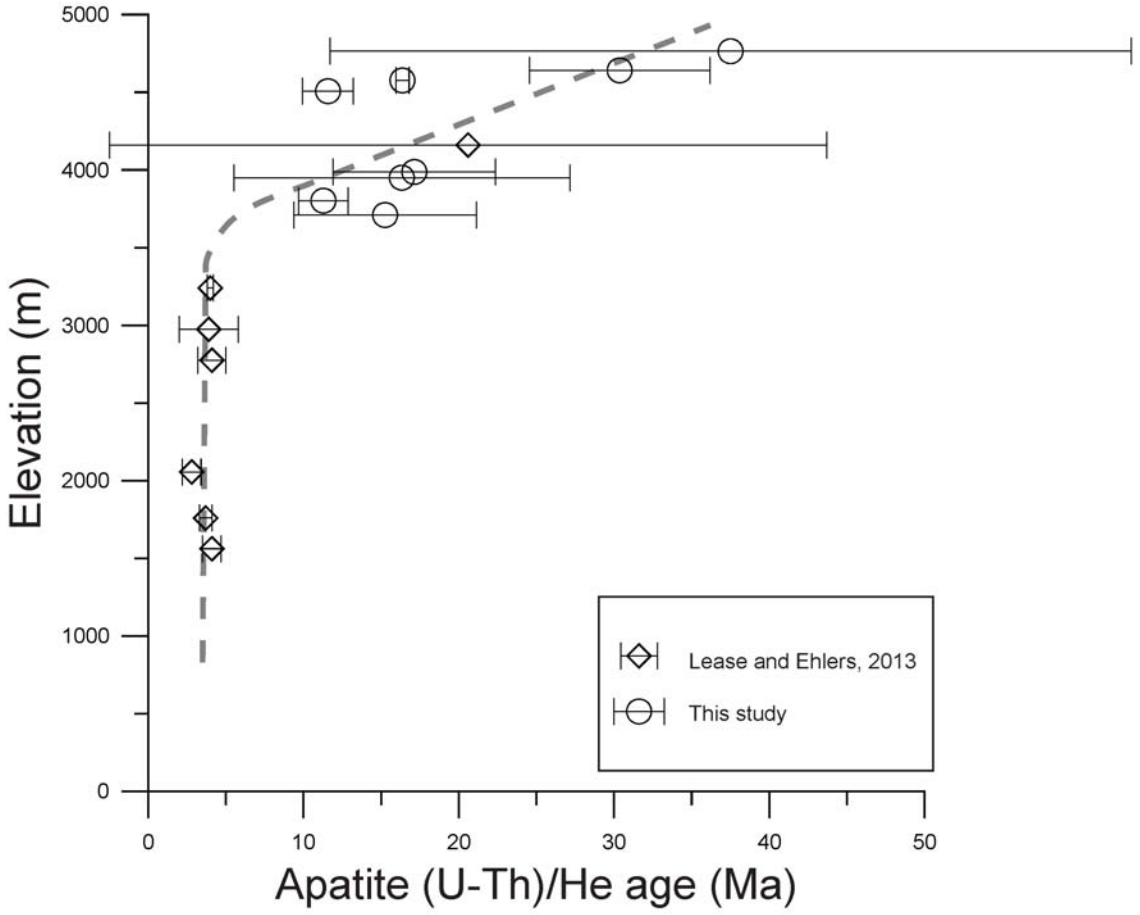

Figure 4.12. Age elevation relationship combing AHe results from this study and Lease and Ehlers (2013). Note age of inflection point, suggesting ~5 Ma rapid cooling.

motion over a thrust ramp at depth (Lock and Willett, 2008). We interpret the consistent trend between these samples as evidence for similar along strike structural controls acting on exhumation and ZHe cooling ages.

New AHe ages from the Coasa pluton demonstrate age elevation relationship with an inflection point at ~15 Ma, suggesting middle Miocene rapid cooling (Figure 8). Age elevation relationships combining our new data with AHe results from Lease and Ehlers (2013) reveal an inflection point at ~5-10 Ma, providing a different interpretation of the onset of cooling (Figure 12). The variation of inflection point ages highlights challenges with interpreting age elevation data from samples not collected along true vertical transects, separated by distances along strike, and that have experienced components of vertical and horizontal motion during exhumation (McQuarrie and Ehlers, 2015). Thus we do not calculate regression line slopes to constrain exhumation rates.

As demonstrated by Lock and Willett (2008) and McQuarrie and Ehlers (2015), characteristic patterns of data are linked with exhumation by translation over footwall ramps. Age distance relationships from our Coasa pluton data and existing AHe data from Rio San Gabán transect define partial U-shaped profiles (Figure 13). However, the U-shaped pattern from the Coasa pluton data is shifted ~8-10 Myr older than the pattern from the Rio San Gabán transect. The presence of U-shaped patterns in both datasets supports exhumation by motion over thrust ramps at both transect locations. Older ages in the Coasa pluton area suggest this region cooled through the AHe PRZ by thrust motion before the Rio San Gabán region. Future 2D thermokinematic modeling combining balanced cross section geometries and thermochronologic datasets is necessary to rigorously test these hypotheses.

Results from fluvial geomorphology reveal a general pattern of channels without knickpoints or channels with knickpoints above ~3300 m elevation situated SE and

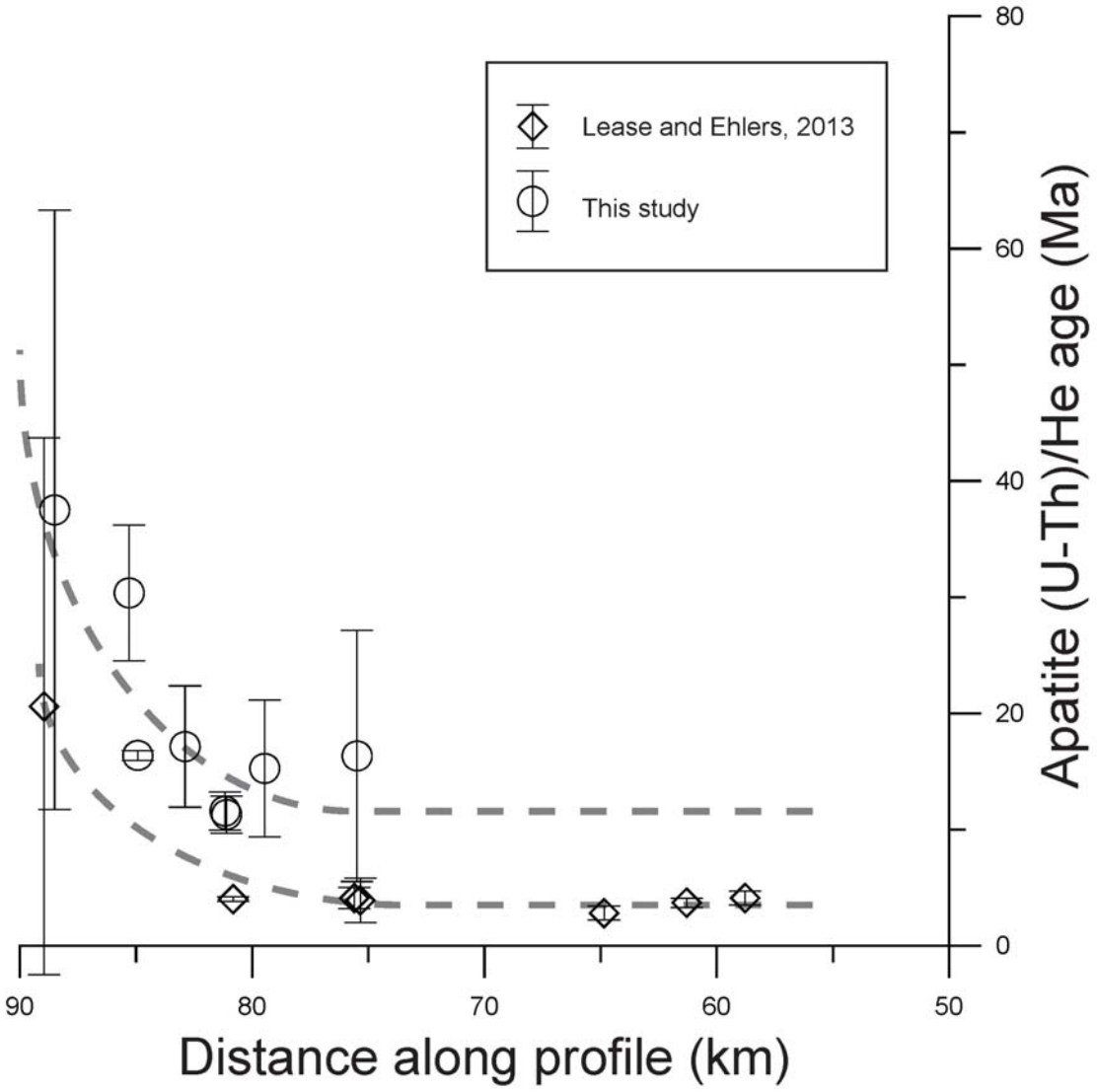

Figure 4.13. Age distance relationship for AHe results. Note half of characteristic U-shaped profiles from both datasets. Coasa pluton samples are ~8-10 Myr older than Rio San Gabán transect samples.

within the Coasa pluton, respectively. NW of the Coasa pluton, channels incising the Eastern Cordillera preserve knickpoints above ~3300 m, and also a population of knickpoints between ~2800-1800 m elevation. The SW-NE trend towards lower knickpoint elevations is qualitatively similar to AHe cooling ages that are younger NW of the Coasa pluton AHe ages. In the next section, we discuss potential reasons for along strike variation in thermochronologic and morphologic expression of exhumation timing.

6.3. Along strike variations in exhumation

Here we combine our new AHe and ZHe results from the Coasa pluton with those from Lease and Ehlers (2013) to define along strike patterns in exhumation. Then, we integrate the geomorphologic constraints on the location and relative timing of changes in rock uplift. We find that ZHe thermochronometers from the Coasa pluton and Rio San Gabán study areas record onset of cooling at ~25 Ma suggesting structurally controlled exhumation history of the Eastern Cordillera was uniform along strike. AHe results show rapid cooling in the Coasa pluton area are beginning at ~15 Ma. Lease and Ehlers (2013) demonstrate rapid AHe cooling in the Rio San Gabán area at ~4 Ma, ~11 Myr younger than in the Coasa pluton area. The similarity in ZHe histories but difference between AHe histories along strike is intriguing. The spatial distribution of knickpoints elevations reveals fluvial profiles SE of the Coasa pluton that do not have knickpoints, fluvial profiles cutting through the Coasa pluton have high elevation knickpoints, and most fluvial profiles NW of the Coasa pluton have an additional low elevation (more recent) knickpoint population. The general pattern from fluvial knickpoints suggests older, relict topography in the SE transitioning to youthful topography NW along strike and mimics

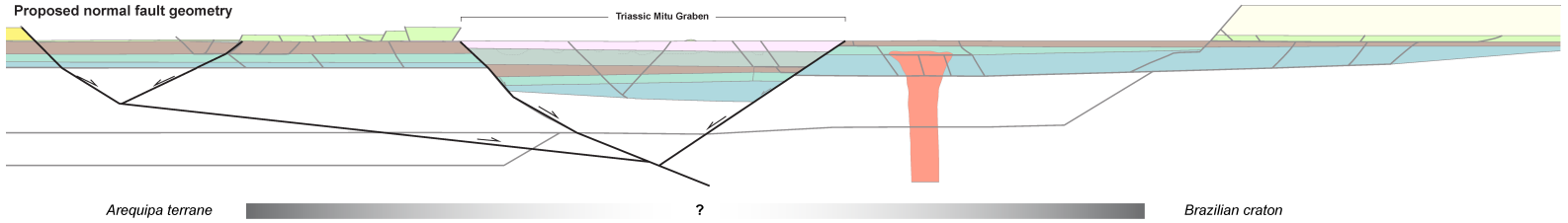
Proposed normal fault geometry
Triassic Mitu Graben
Arequipa terrane
?
Brazilian craton

Figure 4.14. Restored cross section overlain by proposed geometries for normal faults before Andean shortening

the pattern of decreased exhumation age towards the NW emerging from AHe datasets. We present four potential scenarios to explain along strike variations in AHe exhumation timing and fluvial profile patterns. In each scenario, we suggest that early ZHe exhumation was controlled structural cooling driven by exhumation over a thrust ramp. Future numerical modeling is needed to satisfactorily test these hypotheses.

6.3.1. Offset basement ramps

AHe cooling would be achieved as the system translated along a detachment towards the NE and approached two SW dipping ramps offset by a NE striking accommodation zone (Figure 15). The SW ramp corresponding to the Coasa pluton area is situated more hinterlandward. As the Coasa pluton is translated over the ramp, ~15 Ma AHe ages were established. The Rio San Gabán area continued translating along a flat until it reached a ramp situated farther towards the foreland. Because the Rio San Gabán area was thrust over a ramp later, it records ~4 Ma cooling. Fluvial profiles record a similar pattern; channels in the Coasa pluton record preserve high elevation knickpoints associated with older changes in rock uplift, whereas fluvial channels NE of the Coasa pluton preserve lower elevation (younger) knickpoints. We propose the subsurface location of the accommodation zone separating the two ramps is located immediately NW of the Coasa pluton along the NE striking contact with Triassic Mitu Group deposits. Map patterns suggest an apparent right lateral offset of ~ 9 km between the tip points of the two backthrusts. Map and satellite imagery do not reveal a continuation of the apparent strike slip offset beyond the tip points. In the field, we identified horizontal slickenlines only along this NE trending map contact, but sense of shear indicators were inconclusive. We find a striking similarity with analog models of offset ramps. These

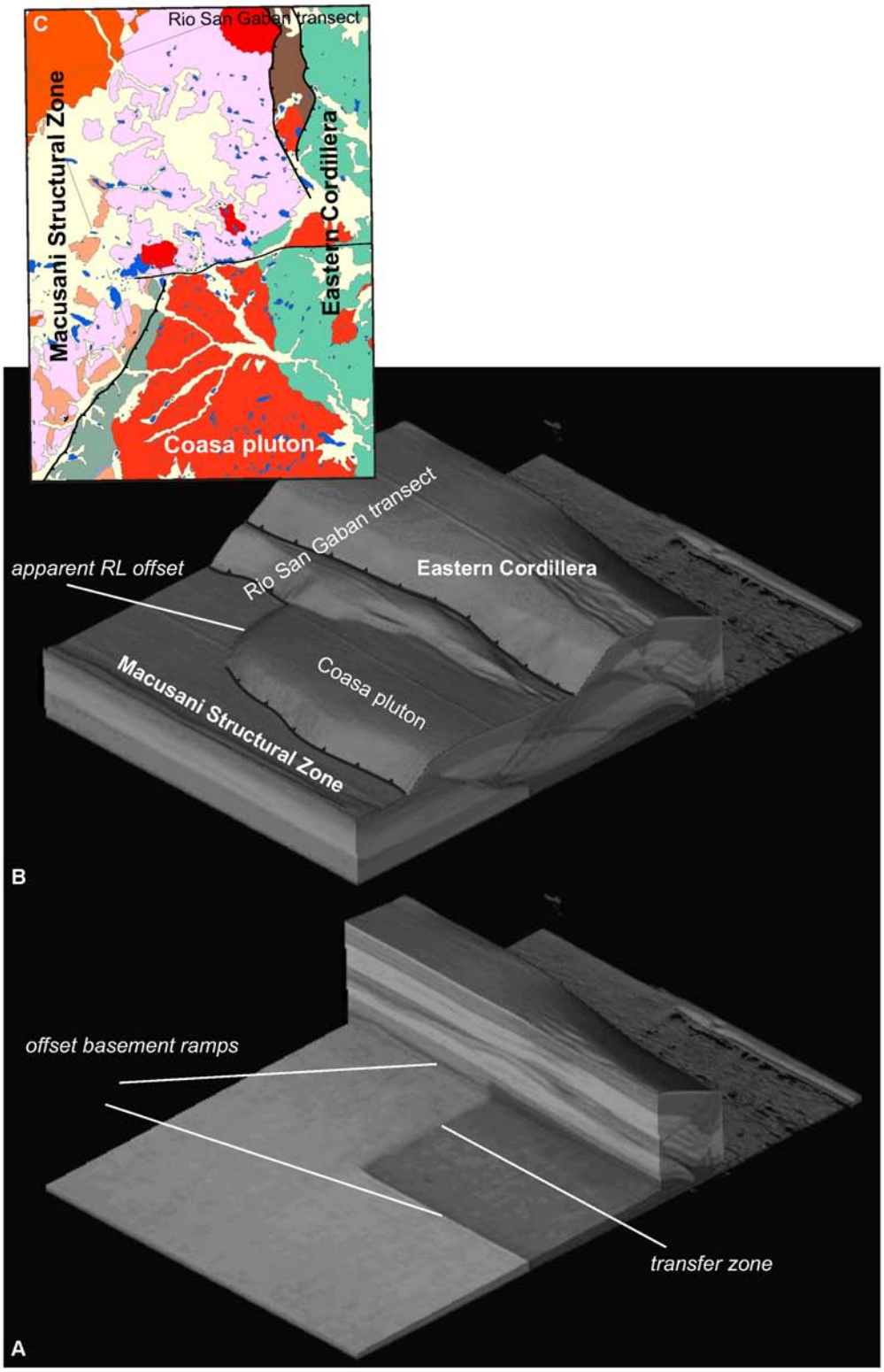
C
Rio San Gaban transect
Macusani Structural Zone
Eastern Cordillera
Coasa pluton
apparent RL offset
Rio San Gaban transect
Eastern Cordillera
Coasa pluton
Macusani Structural Zone
B
offset basement ramps
transfer zone
A

Figure 4.15. Sandbox model of thrust deformation over offset basement ramps. Patterns are similar to geologic map relationships.

models recreate similar map patterns of thrust fault traces as observed in the study area, suggesting motion over offset thrust ramps is a plausible option to explain map relationships. Thermokinematic modeling is needed to test whether exhumation over offset ramps can create similar patterns of AHe cooling ages. (Scheurs et al., 2001). This map pattern is similar to patterns associated with rift inversion, suggesting offset basement ramps that controlled Miocene exhumation may be inherited structural features (Grier et al., 1991).

6.3.2. NE propagating wave of uplift

In this scenario, we suggest that AHe cooling ages were driven by a NW propagating wave of uplift. Middle Miocene AHe cooling ages from the Coasa pluton (this study) are older than Pliocene AHe cooling ages from the Rio San Gabán transect (Lease and Ehlers, 2013) and consistent with a NW migrating wave of uplift. The lack of knickpoints in fluvial channels situated to the SE of the Coasa pluton can be explained as passage of sufficient time since knickpoint creation allowing migration through the top of the fluvial channel. The appearance of lower elevation knickpoints towards the NW is consistent with uplift propagating to the NW, occurring more recently and creating lower elevation knickpoints along strike.

A potential driver for a northward migrating wave of exhumation is consistent with topographic growth of the Altiplano from Bolivia northward into southern Peru (Garzione et al., 2014). We suggest that canyon incision may be the driver of cooling of low temperature AHe systems in the Coasa and Rio San Gabán transects, as this system is more sensitive to topographic variation (Mancktelow and Grasemann, 1997; Ehlers and Farley, 2003; Braun, 2005). Reduced relief in the Coasa pluton area is symptomatic of

earlier uplift, whereas higher relief in the Rio San Gabán transect is consistent with more recent uplift.

6.3.3. Climatically driven focused incision

Lease and Ehlers (2013) interpreted ~4 Ma AHe cooling ages along the Rio San Gabán as evidence for focused incision driven by Pliocene climate change. Our AHe data from the Coasa pluton ~40 km SE along strike reveal onset of rapid cooling at ~15 Ma. Although focused incision may be driven by climatic processes, we suggest that future sampling and modeling studies should investigate the potential length scales over which spatially variable incision can create ~10 Myr differences in canyon incision age. Previous work has demonstrated that creation of Andean topography has significant impact on precipitation, but that the magnitude of precipitation is not expected to vary over spatial scales of 10s km (Insel et al., 2010). Our AHe data from the Coasa pluton may lack evidence of Pliocene cooling because we do not have low elevation samples. Alternatively, Pliocene climate change may have affected both study areas equally, but lithologic variation may have allowed increased, focused exhumation in the Rio San Gabán transect compared to the Coasa pluton area, although geologic mapping shows similar lithologies along strike.

6.3.4. Localized uplift driven by mantle processes

Another potential driver of spatially variable uplift and exhumation is related to mantle circulation. Guillaume et al., (2010) showed that anomalous back arc volcanism and uplift in the Patagonian Andes could be linked to mantle flow and dynamic topography. In our study area, the Holocene Quimsachata volcano is evidence

for recent anomalous back arc volcanism. The NW decrease of AHe cooling ages may represent the exhumational response to dynamic topography linked to mantle upwelling driving back arc volcanism. The Quimsachata volcano is situated immediately SW of the modern flat slab segment (Eakin et al., 2015). We suggest future geophysical work could reveal potential links between the distribution anomalous mantle circulation patterns and slab geometry and provide an alternative explanation for recent back arc volcanism and focused young exhumational ages in southern Peru.

6.4. Pre-Andean structural control on Altiplano and Subandean basin provenance

U-Pb detrital zircon geochronologic results from the Cretaceous through Cenozoic stratigraphy preserved in the Altiplano/CABB and Subandean Zones show two key provenance differences. The Altiplano/CABB zone is characterized by strong Western and Eastern Cordillera provenance. In contrast, the Cretaceous rocks of the Subandean zone show strong cratonic (Rondonia/San Ignacio of Bolivia) affinities, and lack characteristic Western and Eastern Cordillera zircon populations. The Cenozoic rocks of the Subandean zone retain a strong cratonic detrital zircon signal, with minor Eastern Cordillera contributions. In contrast to Cenozoic rocks of the Altiplano, which are dominated by Western Cordillera zircons, only 5 Cretaceous zircons have been identified in Subandean samples, and no Cenozoic zircons have been identified.

The Cretaceous to Cenozoic rocks of the Subandean Zone have a strong sediment contribution from cratonic blocks, suggesting west-directed paleoflow. The distinctive cratonic detrital zircon population is not observed in Cretaceous and younger rocks of the Altiplano or CABB. Despite the clear evidence for Andean detrital zircon provenance in

Cretaceous through Cenozoic rocks of the Altiplano/CABB, suggesting protracted erosion and relief in the Western and Eastern Cordillera, the Andean detrital signal is remarkably minor in equivalent foreland basin deposits. We investigate two paleogeographic reconstructions and evaluate potential provenance records that could be expected from each scenario.

The first potential option mimics models that have been proposed for development of the Central Andes of Bolivia (DeCelles and Horton, 2003; Horton, 2012). This model suggests development of a volcanic arc and early fold-thrust belt created topography in the Western Cordillera during the Cretaceous (Chong, 1977; Vicente, 1989; Horton et al., 2002; Arriagada et al., 2006) flanked by a foreland basin system situated to the east that was partitioned by Eocene uplift of the Eastern Cordillera (Figure 16a) (Benjamin et al., 1987; Farrar et al., 1988; DeCelles and Horton, 2003; McQuarrie et al., 2005; Gillis et al., 2006). In this scenario, the Western Cordillera and South American craton would have been the main potential sources for detrital zircons during the Cretaceous, because the Eastern Cordillera did not begin to exhume until the Eocene. The presence of Cretaceous age zircons (sourced from the arc) and absence of Gondwanide (Eastern Cordillera) or cratonic zircons in Cretaceous sedimentary rocks would be diagnostic of Western Cordillera provenance during Cretaceous deposition and support this model. In distal eastern reaches of the foreland basin, proximity to cratonic blocks could add a distinctive Proterozoic detrital zircon population, and the Western Cordillera contribution might be diluted because of distance from the arc. After Eocene uplift of the Eastern Cordillera, subsequent Cenozoic Altiplano and foreland depocenters would record the appearance of distinctive Eastern Cordillera (Gondwanide age) provenance.

The second scenario is similar to proposed paleogeographic reconstructions of central and northern Peru, which emphasizes two separate depocenters (West and East

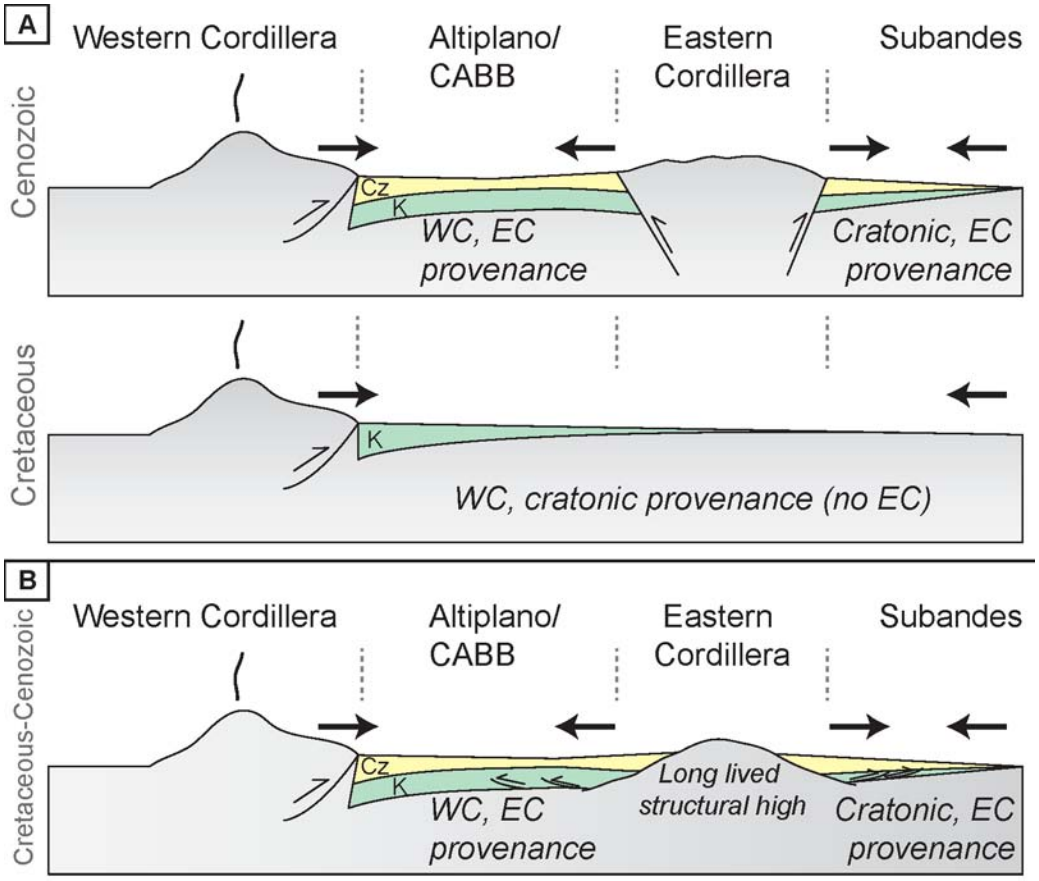

Figure 4.16. Two potential scenarios to explain provenance variation between the Altiplano/CABB and Subandean Zone. See text for explanation.

Peruvian troughs) separated by a structural high (Marañon geanticline) (Benavides-Caceres, 1956; Wilson, 1963; Dalmayrac et al., 1980 book; Mégard, 1984; Benavides-Caceres, 1999; Jaillard et al., 2005; Scherrenberg et al., 2012). The long-lived structural high could have acted as a barrier to sediment transport, and been a sediment source throughout Cretaceous and Cenozoic deposition. In this scenario, Cretaceous to Cenozoic deposition in the Altiplano would record mixed Western and Eastern Cordillera provenance, whereas Subandean Zone depocenters would preserve cratonic or Eastern Cordillera signatures (Figure 16b).

Based on the strong Eastern Cordillera detrital zircon provenance signature present in the Cretaceous rocks of the Altiplano, we suggest the Eastern Cordillera had a topographic expression in the Cretaceous. Furthermore, the lack of distinctive zircon populations sourced from the Rondonia/San Ignacio craton in the Altiplano depocenters suggests west-directed paleoflow was blocked by the Eastern Cordillera. Finally, the long-lived absence of Western Cordillera detrital zircons in the Subandean zone can also be explained by the presence of the Eastern Cordillera that could have blocked east-directed paleoflow. We suggest that scenario two supports our initial provenance records. This scenario may be at odds with the K-Ar and $^{40}Ar/^{39}Ar$ thermochronologic datasets from the Eastern Cordillera, which demonstrate Eocene exhumation from ~10 km depths. To satisfy both the provenance and thermochronologic datasets requires that the Eastern Cordillera plutons remained at ~10 km depths until the Eocene. This requires at least a similarly thick accumulation of Triassic Mitu Group deposits, and potentially Jurassic deposits as well. Inversion and erosion of this Jurassic depocenter may explain the anomalous absence of preserved Jurassic deposits in southern Peru, despite their presence throughout the rest of Peru (Rosas et al., 2007).

The Triassic rift that controlled Mitu Group deposition is located in the modern Eastern Cordillera in southern Peru. With our new balanced cross sections, we have demonstrated that some pre-Andean normal faults were inverted during Andean orogenesis. We suggest that a high standing rift shoulder may have created a topographic barrier that blocked sediment transport between the Altiplano and Subandean depocenters. Alternatively, minor Cretaceous inversion of Triassic normal faults could also have created a topographic barrier responsible for provenance variations between the two depocenters. Post-rift Jurassic Pucará Formation rocks are not preserved in the Eastern Cordillera of southern Peru, but are observed near other deposits of synrift Triassic Mitu Group throughout central and northern Peru. Penetrative foliation observed in Triassic Mitu Group deposits but not observed in overlying Cretaceous rocks of the CABB also suggest poorly constrained compression before the Cretaceous. The conspicuous absence of Jurassic Pucará Formation rocks in southern Peru, and the development of fabrics in Triassic rocks before Cretaceous deposition may be indicative of pre-Cretaceous shortening that established of a topographic barrier at the Eastern Cordillera, potentially guided by the location of Triassic normal faults.

7. CONCLUSIONS

1) Total shortening of 130 km (38%) was constrained from balanced cross section construction across the Eastern Cordillera and Subandean Zone from southern Peru. This estimate is consistent with total shortening estimates from transects near Cusco, and less than estimates in Bolivia, thus broadly consistent with proposed northward decrease in total shortening of the Central Andes. Because of abrupt lateral changes in stratigraphic

thickness inherited from pre-Andean rifting, area balanced techniques significantly over estimate total shortening.

2) Zircon (U-Th)/He thermochronologic results from the Coasa pluton in the Eastern Cordillera suggests a range of cooling ages between ~26 and 18 Ma. Ages are consistent with ZHe results from Lease and Ehlers (2013) collected ~40 km along strike, suggesting the older cooling history was similar across the region. The U-shaped pattern suggests cooling was driven by translation over a ramp.

3) Apatite (U-Th)/He thermochronologic results from the Coasa pluton suggests onset of rapid cooling at ~15 Ma. These ages are ~10-11 Myr older than AHe cooling ages reported by Lease and Ehlers (2013) obtained from similar structural positions 40 km along strike. The NW decrease in AHe ages reflects along strike changes in the timing of exhumation, a pattern that differs from ZHe results in the same samples.

4) Fluvial profiles along strike of the Eastern Cordillera demonstrate a SE to NW trend of decreasing knickpoint elevations consistent with recent increases in rock uplift rate focused NW of the Coasa pluton.

5) AHe and fluvial profiles both support a NW decrease in the timing of exhumation. Potential driving mechanisms include offset basement ramps, focused incision driven by Pliocene climate change, a NW migrating wave of uplift, or dynamic topography associated with subducting plate geometries and mantle circulation.

6) By identifying inverted pre-Andean normal faults, we propose a mechanism to explain thermochronologic records of Eocene burial by thrust sheets and exhumation in the Eastern Cordillera.

7) Apatite (U-Th)/He records demonstrate cooling in the Subandean had initiated by ~6 Ma and possibly as early as 15 Ma.

8) A comparison of U-Pb detrital zircon geochronologic records from the Cretaceous through Cenozoic sedimentary infill between the Altiplano/CABB and Subandean zone basins records long-lived provenance differences between the two basins. Altiplano/CABB basins preserved protracted Eastern and Western Cordillera provenance signatures, and lack characteristic cratonic provenance. In contrast, Subandean zone rocks preserve a strong cratonic signal, lack a Western Cordillera provenance, and record moderate sedimentary detritus from the Eastern Cordillera. This may reflect a long-lived structural high in the Eastern Cordillera that partitioned the two basins and blocked unique zircon populations from the Western Cordillera or craton, or may reflect variable provenance signatures from different segments of a large continuous foreland basin.

References

Ahlfeld, F., and Branisa, L., (1960). Geologa de Bolivia. Editorial Don Bosco. La Paz, 245 pp.

Allègre, C. J., et al. (1984), Structure and evolution of the Himalaya-Tibet orogenic belt, *Nature*, *307*(5946), 17-22.

Allmendinger, R. W. (1986), Tectonic development, southeastern border of the Puna plateau, northwestern Argentine Andes, *Geological Society of America Bulletin*, *97*(9), 1070-1082.

Allmendinger, R. W., V. A. Ramos, T. E. Jordan, M. Palma, and B. L. Isacks (1983), Paleogeography and Andean structural geometry, northwest-Argentina, *Tectonics*, *2*(1), 1-16.

Allmendinger, R. W., D. Figueroa, D. Snyder, J. Beer, C. Mpodozis, and B. L. Isacks (1990), Foreland shortening and crustal balancing in the Andes at 30-degrees-S latitude, *Tectonics*, *9*(4), 789-809.

Allmendinger, R. W., T. E. Jordan, S. M. Kay, and B. L. Isacks (1997), The evolution of the Altiplano-Puna plateau of the central Andes, *Annu. Rev. Earth Planet. Sci., 25,* 139 – 174.

Allmendinger, R. W., and T. Gubbels (1996), Pure and simple shear plateau uplift, Altiplano-Puna, Argentina and Bolivia, *Tectonophysics*, *259*(1-3), 1-13.

Anadòn, P., L. Cabrera, F. Colombo, M. Marzo and O. Riba (1986), Syntectonic intraformational unconformities in alluvial fan deposits, Eastern Ebro Basin margins (NE Spain), *Spec. Publs int. Ass. Sediment., 8,* 259-271.

Argand, E., (1916). Sur l'arc des Alpes occidentales. Eclogae Geologicae Helvetiae 14, 145-191.

Arriagada, C., P. R. Cobbold, and P. Roperch (2006), Salar de Atacama basin: A record of compressional tectonics in the central Andes since the mid-Cretaceous, *Tectonics*, *25*(1).

Aschoff, J. L., and J. G. Schmitt (2008), Distinguishing syntectonic unconformity types to enhance analysis of growth strata: An example from the cretaceous, southeastern Nevada, USA, *Journal of Sedimentary Research*, *78*(9-10), 608-623.

Audebaud, E., et al. (1973), Main geological features of central Andes (Peru, Bolivia), *Revue De Geographie Physique Et De Geologie Dynamique*, *15*(1-2), 73-+.

Audebaud, E., G. and Laubacher, (1969), Sur une discordance tardi-hercynienne dans la Cordillere orientale du Sud du Perou. C. R. Acad. Sc. Paris, t. 269. 2163-2166.

Baby, P., Sempere, T., Oller, T., Barrios, L., Herail, G., and R. Marocco (1990), Un basin en compression d'âge oligo-miocène dans le sud de l;Altiplano bolivien, *C. R. Acad. Sci., 311 (II)*, 341-347.

Baby, P., T. Sempere, J. Oller, and G. Herail (1992), Evidence for major shortening on the eastern edge of the Bolivian Altiplano - the Calazaya Nappe, *Tectonophysics*, *205*(1-3), 155-169.

Baby, P., P. Rochat, G. Mascle, and G. Herail (1997), Neogene shortening contribution to crustal thickening in the back arc of the Central Andes, *Geology*, *25*(10), 883-886.

Bahlburg, H., V. Carlotto, and J. Cardenas (2006), Evidence of Early to Middle Ordovician arc volcanism in the Cordillera Oriental and Altiplano of southern Peru, Ollantaytambo Formation and Umachiri beds, *Journal of South American Earth Sciences*, *22*(1-2), 52-65.

Bahlburg, H., J. D. Vervoort, S. A. DuFrane, V. Carlotto, C. Reimann, and J. Cardenas (2011), The U-Pb and Hf isotope evidence of detrital zircons of the Ordovician Ollantaytambo Formation, southern Peru, and the Ordovician provenance and paleogeography of southern Peru and northern Bolivia, *Journal of South American Earth Sciences*, *32*(3), 196-209.

Ballato, P., N. R. Nowaczyk, A. Landgraf, M. R. Strecker, A. Friedrich, and S. H. Tabatabaei (2008), Tectonic control on sedimentary facies pattern and sediment accumulation rates in the Miocene foreland basin of the southern Alborz mountains, northern Iran, *Tectonics, 27,* TC6001, doi:10.1029/2008TC002278.

Bally, A. W., Gordy, P. L., and Stewart, G. A. (1966). Structure, seismic data, and orogenic evolution of southern Canadian rocky mountains. Bull. Can. Petrol. Geol., 14, pp. 337-381.

Barazangi, M., and B. L. Isacks (1976), Spatial-distribution of earthquakes and subduction of Nazca plate beneath South America, *Geology*, *4*(11), 686-692.

Barke, R. and S. Lamb (2006), Late Cenozoic uplift of the Eastern Cordillera, Bolivian Andes, *Earth and Planetary Science Letters, 249,* 350-367, doi:10.1016/j.epsl.2006.07.012.

Barnes, J. B., T. A. Ehlers, N. McQuarrie, P. B. O'Sullivan, and J. D. Pelletier (2006), Eocene to recent variations in erosion across the central Andean fold-thrust belt, northern Bolivia: Implications for plateau evolution, *Earth and Planetary Science Letters*, *248*(1-2), 118-133.

Barnes, J. B., T. A. Ehlers, N. McQuarrie, P. B. O'Sullivan, and S. Tawackoli (2008), Thermochronometer record of central Andean plateau growth, Bolivia (19.5 degrees S), *Tectonics*, *27*(3).

Barragan, R., P. Baby, and R. Duncan (2005), Cretaceous alkaline intra-plate magmatism in the Ecuadorian Oriente Basin: Geochemical, geochronological and tectonic evidence, *Earth and Planetary Science Letters*, *236*(3-4), 670-690.

Barros, M.C., and Carneiro, E. de P., (1991). The Triassic Jurua orogeny and the tectonosedimentary evolution of Peruvian Oriente basin, exploration implications. IV Simposio Bolivariano, Bogota, Colombia, 44 pp.

Barth, A. P., J. L. Wooden, C. E. Jacobson, and K. Probst (2004), U-Pb geochronology and geochemistry of the McCoy Mountains Formation, southeastern California: A

Cretaceous retroarc foreland basin, *Geological Society of America Bulletin*, *116*(1-2), 142-153.

Batt, G. E., M. T. Brandon, K. A. Farley, and M. Roden-Tice (2001), Tectonic synthesis of the Olympic Mountains segment of the Cascadia wedge, using two-dimensional thermal and kinematic modeling of thermochronological ages, *Journal of Geophysical Research-Solid Earth*, *106*(B11), 26731-26746.

Bayona, G., M. Cortes, C. Jaramillo, G. Ojeda, J. J. Aristizabal, and A. Reyes-Harker (2008), An integrated analysis of an orogen-sedimentary basin pair: Latest Cretaceous-Cenozoic evolution of the linked Eastern Cordillera orogen and the Llanos foreland basin of Colombia, *Geological Society of America Bulletin*, *120*(9-10), 1171-1197.

Beach, A., (1981), Some observations on the development of thrust faults in the Ultradauphinois Zone, French Alps, *in* McClay, K., and Price, N. J., eds., Thrust and Nappe Tectonics, Geological Society of London Special Publication (9), p. 329-334.

Beck, R. A., et al. (1995), Stratigraphic Evidence for an Early Collision Between Northwest India and Asia, *Nature*, *373*(6509), 55-58.

Beck, S. L., and G. Zandt (2002), The nature of orogenic crust in the central Andes, *J. Geophys. Res., 107 (B10),* 2230, doi:10.1029/2000JB000124, 2002

Benavides-Caceres, V., (1956), Cretaceous system in northern Peru: *Bulletin of the American Museum of Natural History*, v. 108, p. 353-494.

Benavides-Caceres, V., (1999), Orogenic evolution of the Peruvian Andes: The Andean Cycle, *in* Skinner, B.J., ed., Geology and Ore Deposits of the Central Andes, Society of Economic Geologists, Inc., Special Publication 7, p. 61-107.

Benjamin, M. T., N. M. Johnson, and C. W. Naeser (1987), Recent rapid uplift in the Bolivian Andes - evidence from fission-track dating, *Geology*, *15*(7), 680-683.

Bettencourt, J. S., W. B. Leite, A. S. Ruiz, R. Matos, B. L. Payolla, and R. M. Tosdal (2010), The Rondonian-San Ignacio Province in the SW Amazonian Craton: An overview, *Journal of South American Earth Sciences*, *29*(1), 28-46.

Blair, T. C., and J. G. McPherson (1994), Alluvial fans and their natural distinction from rivers based on morphology, hydraulic processes, sedimentary processes, and facies assemblages, *J. Sediment. Res., A64,* 450–489.

Boekhout, F., T. Sempere, R. Spikings, and U. Schaltegger (2013), Late Paleozoic to Jurassic chronostratigraphy of coastal southern Peru: Temporal evolution of sedimentation along an active margin, *Journal of South American Earth Sciences*, *47*, 179-200.

Bonhomme, M.G., E. Audebaud, and G. Vivier (1985), Edades K-Ar de rocas hercinicas y neogenas de un perful E-W en el Peru meridional: Santiago, Chile, Departamiento Geologia, Universidad de Chile, *Comunicaciones, 35*, 27-30.

Boyer, S. E., and D. Elliott (1982), Thrust systems, *AAPG Bull.,* 66, 1196–1230.

Braun, J., (2005) Quantitative Constraints on the Rate of Landform Evolution Derived from Low-Temperature Thermochronology, *in* Reviews in Mineralogy and Geochemistry, (58), p. 351-374.

Burbank, D.W., and J. Verges (1994), Reconstruction of topography and related depositional systems during active thrusting, *Journal of Geophysical Research, 99,* 20281-20297.

Butler, R. W. H., E. Tavarnelli, and M. Grasso (2006), Structural inheritance in mountain belts: An Alpine-Apennine perspective, *Journal of Structural Geology*, *28*(11), 1893-1908.

Cahill, T., and B. L. Isacks (1992), Seismicity and shape of the subducted Nazca plate, *Journal of Geophysical Research-Solid Earth*, *97*(B12), 17503-17529.

Callot, P., F. Odonne, and T. Sempere (2008a), Liquification and soft-sediment deformation in a limestone megabreccia: The Ayabacas giant collapse, Cretaceous, southern Peru, *Sedimentary Geology*, *212*(1-4), 49-69.

Callot, P., T. Sempere, F. Odonne, and E. Robert (2008b), Giant submarine collapse of a carbonate platform at the Turonian-Coniacian transition: The Ayabacas Formation, southern Peru, *Basin Research*, *20*(3), 333-357.

Cardozo, N. (2015), Flex2D: 2D flexural modeling

Carlier, G., J. P. Lorand, J. P. Liegeois, and M. Fornari (2005), Potassic-ultrapotassic mafic rocks delineate two-lithospheric mantle blocks beneath the southern Peruvian Altiplano, *Geology*, *33*(7), 601-604.

Carlotto, V. (2013), Paleogeographic and tectonic controls on the evolution of Cenozoic basins in the Altiplano and Western Cordillera of southern Peru, *Tectonophysics*, *589*, 195-219.

Carlotto, V., Cárdenas, J., Reitsma, M., and Rodriguez, R., (2010), Las edades de la formación Ene y del Grupo Mitu: Propuesta de cambios en la cartografía regional: Abancay-Cusco-Sicuani, XV Congreso Peruano de Geología: Cusco, Peru, p. 830-833.

Carrapa, B., D. Adelmann, G. E. Hilley, E. Mortimer, E. R. Sobel, and M. R. Strecker (2005), Oligocene range uplift and development of plateau morphology in the southern central Andes, *Tectonics*, *24*(4).

Carrera, N., J. A. Munoz, F. Sabat, R. Mon, and E. Roca (2006), The role of inversion tectonics in the structure of the Cordillera Oriental (NW Argentinean Andes), *Journal of Structural Geology*, *28*(11), 1921-1932.

Carroll, A. R., S.A. Graham and M.E. Smith (2010), Walled sedimentary basin of China, *Basin Research, 22,* 17-32, doi: 10.1111/j.1365-2117.2009.00458.x.

Casero P., J.F. Salel and A. Rossato, (1997), Multidisciplinary correlative evidence for polyphase geological evolution of the foot-hills of the Cordillera Oriental (Colombia). IV Simposio Bolivariano "Exploaración Petrolera en la Cuencas Subandinas", T 1, p. 119-128.

Castaños, A., and Rodrigo, L.A., (1978). Sinopsis estratigrafica de Bolivia. Primera parte: Paleozoico. *Academia Nacional de Ciencias de Bolivia*, 146 pp.

Chew, D. M., U. Schaltegger, J. Kosler, M. J. Whitehouse, M. Gutjahr, R. A. Spikings, and A. Miskovic (2007), U-Pb geochronologic evidence for the evolution of the Gondwanan margin of the north-central Andes, *Geological Society of America Bulletin*, *119*(5-6), 697-711.

Chew, D. M., T. Magna, C. L. Kirkland, A. Mišković, A. Cardona, R. Spikings, and U. Schaltegger (2008), Detrital zircon fingerprint of the Proto-Andes: Evidence for a Neoproterozoic active margin?, *Precambrian Research*, *167*(1-2), 186-200.

Chong, G., (1977), Contribution to the knowledge of the Domeyko Range in the Andes of northern Chile: *Geologische Rundschau*, v. 66, p. 374–404.

Clark, A.H., E. Farrar, D.J. Kontak, R.J. Langridge, M.J. Arenas F., L.J. France, S.L McBride, P.L. Woodman, H.A. Wasteneys, H.A. Sandeman and D.A. Archibald, (1990) Geologic and Geochronologic Constraints on the Metallogenic Evolution of the Andes of Southeastern Peru, *Economic Geology, 85,* 1520-1583.

Colletta, B., F. Hebrard, J. Letouzey, P. Werner, and J. L. Rudkiewicz (1990), Tectonic style and crustal structure of the Eastern Cordillera (Colombia) from a balanced cross-section, *Petroleum and Tectonics in Mobile Belts*, *47*, 81-100.

Comínguez, A. H., and V. A. Ramos, (1995), Geometry and seismic expression of the Cretaceous Salta rift system, northwestern Argentina, *in* A. J. Tankard, R. Suárez S., and H. J. Welsink, Petroleum basins of South America: AAPG Memoir 62, p. 325–340.

Coira, B., J. Davidson, C. Mpodozis, and V. A. Ramos (1982), Tectonic and magmatic evolution of the Andes of northern Argentina and Chile, *Earth Sci. Rev., 18,* 303–332, doi:10.1016/0012-8252(82)90042-3.

Cooper, M. A., et al. (1995), Basin development and tectonic history of the Llanos basin, Eastern Cordillera, and middle Magdalena Valley, Colombia, *AAPG Bulletin-American Association of Petroleum Geologists*, *79*(10), 1421-1443.

Cordani, U.G., Sato, K., Teixeira, W., Tassinari, C.C.G., and Basei, M.A.S., (2000), Crustal evolution of the South American platform, *in* Cordani, U.G., Milani, E.J., Thomaz-Filho, A., and Campos, D.A., eds., Tectonic evolution of South America: Rio de Janeiro, Brazil, 31st International Geological Congress, p. 19–40.

Cordani, U. G., and W. Teixeira (2007), Proterozoic accretionary belts in the Amazonian Craton, *4-D Framework of Continental Crust*, *200*, 297-320.

Dahlstrom, C.D.A (1969), Balanced cross sections, *Canadian Journal of Earth Sciences*, 6, p. 407-439.

Dalmayrac, B., 1978. Geologie de la Cordillere orientale de la region de Huanuco: sa place dans une transversale des Andes du Perou central (9°S a 10°30' S). Geologie des Andes peruviennes, Travaux et documents de L'O.R.S.T.O.M. 93, 161.

Dalmayrac, B., Laubacher, G., and Marocco, R. (1980), *Geologie des Andes Peruviennes,* Travaux et Documents de L'ORSTOM.

Dalziel, I. W. D. (1981), Back-arc extension in the southern Andes - a review and critical reappraisal, *Philosophical Transactions of the Royal Society of Mathematical Physical and Engineering Sciences*, *300* (1454), 319-335.

Davila, F. M., and C. Lithgow-Bertelloni (2013), Dynamic topography in South America, *Journal of South American Earth Sciences*, *43*, 127-144.

DeCelles, P. G., M. B. Gray, K. D. Ridgway, R. B. Cole, P. Srivastava, N. Pequera, and D. A. Pivnik (1991), Kinematic history of a foreland uplift from Paleocene synorogenic conglomerate, Beartooth Range, Wyoming and Montana, *Geol. Soc. Am. Bull., 103,* 1458–1475, doi:10.1130/0016-7606(1991)103<1458:KHOAFU>2.3.CO;2.

DeCelles, P. G., and B. K. Horton (2003), Early to middle Tertiary foreland basin development and the history of Andean crustal shortening in Bolivia, *Geological Society of America Bulletin*, *115*(1), 58-77.

DeCelles, P. G. (2004), Late Jurassic to Eocene evolution of the Cordilleran thrust belt and foreland basin system, western USA, *American Journal of Science*, *304*(2), 105-168.

DeCelles, P. G., B. Carrapa, and G. E. Gehrels (2007), Detrital zircon U-Pb ages provide provenance and chronostratigraphic information from Eocene synorogenic deposits in northwestern Argentina, *Geology*, *35*(4), 323-326.

DeCelles, P.G., M.N. Ducea, P. Kapp, and G. Zandt (2009), Cyclicity in Cordilleran orogenic systems, Nature Geoscience, doi: 10.1038/ngeo469

Decou, A., H. von Eynatten, I. Dunkl, D. Frei, and G. Worner (2013), Late Eocene to Early Miocene Andean uplift inferred from detrital zircon fission track and U-Pb dating of Cenozoic forearc sediments (15-18 degrees S), *Journal of South American Earth Sciences*, *45*, 6-23.

Dengo, C. A., and M. C. Covey (1993), Structure of the Eastern Cordillera of Colombia - implications for trap styles and regional tectonics, *AAPG Bulletin-American Association of Petroleum Geologists*, *77*(8).

Dewey, J. F. (1988), Extensional collapse of orogens, *Tectonics*, *7*(6), 1123-1139.

Di Domenica, A., L. Bonini, F. Calamita, G. Toscani, C. Galuppo, and S. Seno (2014), Analogue modeling of positive inversion tectonics along differently oriented pre-thrusting normal faults: An application to the Central-Northern Apennines of Italy, *Geological Society of America Bulletin*, *126*(7-8), 943-955.

Dickinson, W. R., and G. E. Gehrels (2003), U-Pb ages of detrital zircons from Permian and Jurassic eolian sandstones of the Colorado Plateau, USA: paleogeographic implications, *Sedimentary Geology*, *163*(1-2), 29-66.

Dickinson, W. R., and C. A. Suczek (1979), Plate tectonics and sandstone compositions, *Am. Assoc. Pet. Geol. Bull., 63*, 2164–2182.

Dunn, J.F., Hartshorn, K.G., and Hartshorn, P.W., (1995), Structural styles and hydrocarbon potential of the Subandean thrust belt of southern Bolivia, *in* Tankard, A.J., Suarez, R., and Welsink, H.J., eds., Petroleum basins of South America: American Association of Petroleum Geologists Memoir 62, p. 523–543.

Eakin, C. M., M. D. Long, L. S. Wagner, S. L. Beck, and H. Tavera (2015), Upper mantle anisotropy beneath Peru from SKS splitting: Constraints on flat slab dynamics and interaction with the Nazca Ridge, *Earth and Planetary Science Letters*, *412*, 152-162.

Ehlers, T. A., and K. A. Farley (2003), Apatite (U-Th)/He thermochronometry: methods and applications to problems in tectonic and surface processes, *Earth and Planetary Science Letters*, *206*(1-2), 1-14.

Echavarria, L., R. Hernández, R. Allmendinger, and J. Reynolds (2003), Subandean thrust and fold belt of northwestern Argentina: Geometry and timing of the Andean evolution, *Am. Assoc. Pet. Geol. Bull., 87,* 965–985.

Ege, H., E. R. Sobel, V. Jacobshagen, E. Scheuber, and D. Mertmann (2003), Exhumation history of the central Andes of southern Bolivia by apatite fission track dating, *Rev. Tec. Yacimientos Petrol. Fis. Bolivianos*, 21, 165 – 172.

Ege, H., E. R. Sobel, E. Scheuber, and V. Jacobshagen (2007), Exhumation history of the southern Altiplano plateau (southern Bolivia) constrained by apatite fission-track thermochronology, *Tectonics*, 26, TC1004, doi:10.1029/2005TC001869.

Eichelberger, N., and N. McQuarrie (2015), Kinematic reconstruction of the Bolivian orocline, *Geosphere*, *11*(2), 445-462.

Eichelberger, N., N. McQuarrie, T. A. Ehlers, E. Enkelmann, J. B. Barnes, and R. O. Lease (2013), New constraints on the chronology, magnitude, and distribution of deformation within the central Andean orocline, *Tectonics*, *32*(5), 1432-1453.

Elger, K., O. Oncken, and J. Glodny (2005), Plateau-style accumulation of deformation: Southern Altiplano, *Tectonics*, *24*(4).

Elger, K., O. Oncken, and J. Glodny (2005), Plateau-style accumulation of deformation: Southern Altiplano, *Tectonics, 24,* TC4020, doi:10.1029/2004TC001675.

Elliott, D. (1983), The construction of balanced cross-sections, *Journal of Structural Geology*, *5*(2), 101-101.

Ellison, R.A., B.A. Klinck, M.P. Hawkins (1989), Deformation events in the Andean orogenic cycle in the Altiplano and Western Cordillera, southern Peru, *Journal of South American Earth Sciences, 2 (3),* 263-276.

Erslev, E. A. (1991) Trishear fault-propagation folding, *Geology, 19,* 617-620.

Espurt, N., J. Barbarand, M. Roddaz, S. Brusset, P. Baby, M. Saillard, and W. Hermoza (2011), A scenario for late Neogene Andean shortening transfer in the Camisea Subandean zone (Peru, 12 degrees S): Implications for growth of the northern Andean Plateau, *Geological Society of America Bulletin*, *123*(9-10), 2050-2068.

Eude, A., M. Roddaz, S. Brichau, S. Brusset, Y. Calderon, P. Baby, and J. C. Soula (2015), Controls on timing of exhumation and deformation in the northern Peruvian eastern Andean wedge as inferred from low-temperature thermochronology and balanced cross section, *Tectonics*, *34*(4), 715-730.

Farley, K. A., R. A. Wolf, and L. T. Silver (1996), The effects of long alpha-stopping distances on (U-Th)/He ages, *Geochimica Et Cosmochimica Acta*, *60*(21), 4223-4229.

Farrar, E., A. H. Clark, D. J. Kontak, and D. A. Archibald (1988), Zongo-San Gaban zone - Eocene foreland boundary of the Central Andean orogen, northwest Bolivia and southeast Peru, *Geology*, *16*(1), 55-58.

Fildani, A., T. D. Cope, S. A. Graham, and J. L. Wooden (2003), Initiation of the Magallanes foreland basin: Timing of the southernmost Patagonian Andes orogeny revised by detrital zircon provenance analysis, *Geology*, *31*(12), 1081-1084.

Flament, N., M. Gurnis, and R. D. Muller (2013), A review of observations and models of dynamic topography, *Lithosphere*, *5*(2), 189-210.

Flores, T. and Rodriguez, R., 1999, Las cuencas neogenas del sur del Peru: la cuenca Tinajani. Evolucion sedimentologica, estratigrafia, paleogeografica y tectonica. (Ayaviri, Puno), Tesis de Ingeniero Geologo, UNSAAC.

Flemings, P. B., and T. E. Jordan (1989), A synthetic stratigraphic model of foreland basin development, *Journal of Geophysical Research-Solid Earth and Planets*, *94*(B4), 3851-3866.

Flowers, R. M., R. A. Ketcham, D. L. Shuster, and K. A. Farley (2009), Apatite (U-Th)/He thermochronometry using a radiation damage accumulation and annealing model, *Geochimica Et Cosmochimica Acta*, *73*(8), 2347-2365.

Ford, M., E.A. Williams, and A. Artoni (1996), Progressive evolution of a fault-related fold pair from growth strata geometries, Sant Llorenç de Morunys, SE Pyrenees, *Journal of Structural Geology, 19,* 413-441.

Fornari, M., M. Mamani, I. Ibarra, and G. Carlier (2002), Datacion del perıodo volcanico ‘‘Tacaza’’ en el Altiplano de Peru´ y Bolivia, paper presented at XI Congreso Peruano de Geologıa, Geol. Del Peru, Lima.

Frankel, K. L., and F. J. Pazzaglia (2006), Mountain fronts, base-level fall, and landscape evolution: Insights from the southern Rocky Mountains, *Tectonics, Climate, and Landscape Evolution*, *398*, 419-434.

Garzione, C. N., P. Molnar, J. C. Libarkin, and B. J. MacFadden (2006), Rapid late Miocene rise of the Bolivian Altiplano: Evidence for removal of mantle lithosphere, *Earth and Planetary Science Letters*, *241*(3-4), 543-556.

Garzione, C. N., D. J. Auerbach, J. J. S. Smith, J. J. Rosario, B. H. Passey, T. E. Jordan, and J. M. Eiler (2014), Clumped isotope evidence for diachronous surface cooling of the Altiplano and pulsed surface uplift of the Central Andes, *Earth and Planetary Science Letters*, *393*, 173-181.

Gazzi, P. (1966), I minerali pesanti nei flysch arenacei fra Monte Ramaceto e Monte Molinatico (Appennino settentrionale), Mineral. Petrogr. Acta, 11, 197–212.

Gehrels, G.E., (2000), Introduction to detrital zircon studies of Paleozoic and Triassic strata in western Nevada and northern California, *in* Soreghan, M.J., and Gehrels, G.E.,

eds., Paleozoic and Triassic Paleogeography and Tectonics of Western Nevada and Northern California: *Geological Society of America Special Paper* 347, p. 1–17.

Gehrels, G., Valencia, V., Pullen, A., (2006), Detrital Zircon Geochronology by Laser Ablation Multicollector ICPMS at the Arizona LaserChron Center, *in* Olszewski, T., ed., Geochronology: Emerging Opportunities: Paleontology Society Papers, Volume 12, p. 67-76.

Gehrels, G.E., Valencia, V., Ruiz, J., (2008), Enhanced precision, accuracy, efficiency, and spatial resolution of U-Pb ages by laser ablation-multicollector-inductively coupled plasma-mass spectrometry: Geochemistry, Geophysics, Geosystems, v. 9, Q03017, doi:10.1029/2007GC001805.

Gehrels, G. (2011) Detrital Zircon U-Pb Geochronology: Current Methods and New Opportunities, in Tectonics of Sedimentary Basins: Recent Advances, eds. C. Busby and A. Azor, John Wiley & Sons, Ltd, Chichester, UK. doi: 10.1002/9781444347166.ch2.

Ghosh, P., C. N. Garzione, and J. M. Eiler (2006), Rapid uplift of the Altiplano revealed through C-13-O-18 bonds in paleosol carbonates, *Science*, *311*(5760), 511-515.

Giambiagi, L., M. Ghiglione, E. Cristallini, and G. Bottesi (2009), Kinematic models of basement/cover interaction: Insights from the Malargüe fold and thrust belt, Mendoza, Argentina, *Journal of Structural Geology*, *31*(12), 1443-1457.

Giambiagi, L., J. Mescua, F. Bechis, A. Martinez, and A. Folguera (2011), Pre-Andean deformation of the Precordillera southern sector, southern Central Andes, *Geosphere*, *7*(1), 219-239.

Giambiagi, L., J. Mescua, F. Bechis, A. Tassara, and G. Hoke (2012), Thrust belts of the southern Central Andes: Along-strike variations in shortening, topography, crustal geometry, and denudation, *Geological Society of America Bulletin*, *124*(7-8), 1339-1351.

Gil Rodriguez, W. F., (2001), Evolucion lateral de la deformacion de un frente orogenico: Ejemplo de las cuencas subandinas entre 0° y 16° S, Doctoral thesis, Universidad Paul Sabatier.

Gil Rodriguez, W., Baby, P., and Ballard, J.-F., (2001) Structure et contrôle paléogéographique de la zone subandine péruvienne, *Comptes Rendus De L'Academie Des Sciences Serie Ii*, *333,* 741-748.

Gilder, S., S. Rousse, D. Farber, B. McNulty, T. Sempere, V. Torres, and O. Palacios (2003), Post-Middle Oligocene origin of paleomagnetic rotations in Upper Permian to Lower Jurassic rocks from northern and southern Peru, *Earth and Planetary Science Letters, 210, 233-248,* doi:10.1016/S0012-821X(03)00102-X

Gillcrist, R., M. Coward, and J. L. Mugnier (1987), Structural inversion and its controls - examples from the Alpine foreland and the French Alps, *Geodinamica Acta*, *1*(1), 5-34.

Gillis, R. J., B. K. Horton, and M. Grove (2006), Thermochronology, geochronology, and upper crustal structure of the Cordillera Real: Implications for Cenozoic exhumation of the central Andean plateau, *Tectonics*, *25*(6).

Göğüş, O. H., and R. N. Pysklywec (2008), Near-surface diagnostics of dripping or delaminating lithosphere, *Journal of Geophysical Research-Solid Earth*, *113*(B11).

Gurnis, M. (1992), Rapid continental subsidence following the initiation and evolution of subduction, *Science*, *255*(5051), 1556-1558.

Gotberg, N., N. McQuarrie, and V. C. Caillaux (2010), Comparison of crustal thickening budget and shortening estimates in southern Peru (12-14 degrees S): Implications for mass balance and rotations in the "Bolivian orocline", *Geological Society of America Bulletin*, *122*(5-6), 727-742.

Grader, G. W., P. E. Isaacson, E. Diaz-Martinez, and M. C. Pope (2008), Pennsylvanian and Permian sequences in Bolivia: Direct responses to Gondwana glaciation, *Resolving the Late Paleozoic Ice Age in Time and Space*, *441*, 143-159.

Grier, M. E., J. A. Salfity, and R. W. Allmendinger (1991), Andean reactivation of the Cretaceous Salta rift, northwestern Argentina, *Journal of South American Earth Sciences*, *4*(4), 351-372.

Guillaume, B., M. Moroni, F. Funiciello, J. Martinod, and C. Faccenna (2010), Mantle flow and dynamic topography associated with slab window opening: Insights from laboratory models, *Tectonophysics*, *496*(1-4), 83-98.

Gunnell, Y., J. C. Thouret, S. Brichau, A. Carter, and K. Gallagher (2010), Low-temperature thermochronology in the Peruvian Central Andes: implications for long-term continental denudation, timing of plateau uplift, canyon incision and lithosphere dynamics, *Journal of the Geological Society*, *167*(4), 803-815.

Hampton, B. A., and B. K. Horton (2007), Sheetflow fluvial processes in a rapidly subsiding basin, Altiplano plateau, Bolivia, *Sedimentology, 54,* 1121–1148, doi:10.1111/j.1365-3091.2007.00875.x.

Hartley, A.J., A.E. Mather, E. Jolley and P. Turner (2005) Climatic controls on alluvial-fan activity, Coastal Cordillera, northern Chile in *Alluvial Fans: Geomorphology, Sedimentology, Dynamics,* edited by Harvey, A.M., A.E. Mather and M. Stokes, The Geological Society, London, Special Publications, 251, 95-115. 0305-8719/05/$15

Heller, P. L., S. S. Bowdler, H. P. Chambers, J. C. Coogan, E. S. Hagen, M. W. Shuster, N. S. Winslow, and T. F. Lawton (1986), Time of initial thrusting in the Sevier orogenic belt, Idaho, Wyoming and Utah, *Geology*, *14*(5), 388-391.

Hermoza, W., S. Brusset, P. Baby, W. Gil, M. Roddaz, N. Guerrero, and M. Bolanos (2005), The Huallaga foreland basin evolution: Thrust propagation in a deltaic environment, northern Peruvian Andes, *Journal of South American Earth Sciences*, *19*(1), 21-34.

Hilley, G. E., and M. R. Strecker (2005), Processes of oscillatory basin filling and excavation in a tectonically active orogen: Quebrada del Toro Basin, NW Argentina, *Geological Society of America Bulletin*, *117*(7-8), 887-901.

Hindle, D., J. Kley, O. Oncken, and S. V. Sobolev (2005), Crustal balance and crustal flux from shortening estimates in the Central Andes, *Earth and Planetary Science Letters*, *230*(1-2), 113-124.

Homke, S., J. Verges, M. Garces, H. Emami, and R. Karpuz (2004), Magnetostratigraphy of Miocene-Pliocene Zagros foreland deposits in the front of the Push-e Kush Arc (Lurestan Province, Iran), *Earth and Planetary Science Letters*, *225*(3-4), 397-410.

Horton, B.K., Hampton, B.A., and Waanders, G.L. (2001), Paleogene synorogenic sedimentation in the Altiplano plateau and implications for initial mountain building in the central Andes, *Geological Society of America Bulletin, 113,* 1387–1400.

Horton, B. K., A. Yin, M. S. Spurlin, J. Y. Zhou, and J. H. Wang (2002), Paleocene-Eocene syncontractional sedimentation in narrow, lacustrine-dominated basins of east-central Tibet, *Geological Society of America Bulletin*, *114*(7), 771-786.

Horton, B.K., B.A. Hampton, B.N. LaReau and E. Baldellon (2002) Tertiary provenance history of the northern and central Altiplano (Central Andes, Bolivia): a detrital record of plateau-margin tectonics, *Journal of Sedimentary Research, 72, (5),* 711–726

Horton, B. K. (2005), Revised deformation history of the central Andes: Inferences from Cenozoic foredeep and intermontane basins of the Eastern Cordillera, Bolivia, *Tectonics*, *24*(3).

Horton, B. K., J. E. Saylor, J. S. Nie, A. Mora, M. Parra, A. Reyes-Harker, and D. F. Stockli (2010), Linking sedimentation in the northern Andes to basement configuration, Mesozoic extension, and Cenozoic shortening: Evidence from detrital zircon U-Pb ages, Eastern Cordillera, Colombia, *Geological Society of America Bulletin*, *122*(9-10), 1423-1442.

Horton, B.K., (2012), Cenozoic evolution of hinterland basins in the Andes and Tibet, in Busby, C., and Azor, A., eds., Tectonics of Sedimentary Basins: Recent Advances: Wiley-Blackwell, Oxford, UK, p. 427-444.

Horton, B. K., N. D. Perez, J. D. Fitch, and J. E. Saylor (2015), Punctuated shortening and subsidence in the Altiplano Plateau of southern Peru: Implications for early Andean mountain building, *Lithosphere*, *7*(2), 117-137.

Ibarra, I., Mamani, M., Rodriguez, R., Sempere, T., Carlotto, C., and G. Carlier (2004) Estratigrafia y tectonica de la parte sur de la cuenca de Ayaviri, in Nuevas contribuciones del IRD y sus contrapartes al conocimiento geologico del sur del Peru, 143-155. Publicacion Especial No. 5, Institut de recherché pour le developpement, Paris

INGEMMET (1999), Mapa Geologico del Peru, 1:1000000 scale

Ingeomin, (1975). Mapa geologico del Peru. Instituto de Geologia y Mineria, Lima.

Insel, N., C. J. Poulsen, and T. A. Ehlers (2010), Influence of the Andes Mountains on South American moisture transport, convection, and precipitation, *Climate Dynamics*, *35*(7-8), 1477-1492.

Isaacson, P.E., 1975. Evidence for a western extracontinental land source during the Devonian Period in the central Andes. *Geological Society of America Bulletin* 86, 39–46.

Isacks, B. L. (1988), Uplift of the central Andean Plateau and bending of the Bolivian Orocline, *J. Geophys. Res., 93,* 3211 – 3231.

Jackson, J. A. (1980), Reactivation of basement faults and crustal shortening in orogenic belts, *Nature*, *283*(5745), 343-346.

Jaillard, E., Hérail, G., Monfret, T., Díaz-Martínez, E., Baby, P., Lavenu, A., and Dumon, J.F., (2000), Tectonic evolution of the Andes of Ecuador, Peru, Bolivia, and northernmost Chile, *in* Cordani, U., Milani, E.J., Thomas Filho, A., and Campos, D.A., eds., Tectonic Evolution of South America: Rio de Janeiro, Brazil, 31st International Geological Congress, p. 481–559.

Jaillard, E., P. Bengtson, and A. V. Dhondt (2005), Late Cretaceous marine transgressions in Ecuador and northern Peru: A refined stratigraphic framework, *Journal of South American Earth Sciences*, *19*(3), 307-323.

James, D.E., and I. S. Sacks (1999), Cenozoic Formation of the Central Andes: A Geophysical Perspective, in B.J. Skinner (Ed.), *Geology and Ore Deposits of the Central Andes*, pp. 1-25, Society of Economic Geologists, Inc. Special Publication no. 7.

Jarvis, A., H.I. Reuter, A. Nelson, E. Guevara, (2008), Hole-filled SRTM for the globe Version 4, available from the CGIAR-CSI SRTM 90m Database

Jennings, G. R., T. E. Lawton, and C. A. Clinkscales (2013), Late Cretaceous U-Pb tuff ages from the, Skunk Ranch Formation and their implications for age of Laramide deformation, Little Hatchet Mountains, southwestern New Mexico, USA, *Cretaceous Research*, *43*, 18-25.

Jimenez, G., J. Rico, G. Bayona, C. Montes, A. Rosero, and D. Sierra (2012), Analysis of curved folds and fault/fold terminations in the southern Upper Magdalena Valley of Colombia, *Journal of South American Earth Sciences*, *39*, 184-201.

Jimenez, N., S. Lopez-Velasquez and R. Santivañez (2009) Evolución tectonomagmática de los Andes Bolivianos, *Revista de la Asociacion Geologica Argentina 65 (1),* 36-67.

Jordan, T. E. (1981), Thrust loads and foreland basin evolution, Cretaceous, Western United States, *AAPG Bulletin-American Association of Petroleum Geologists*, *65*(12), 2506-2520.

Jordan, T. E., and R. W. Allmendinger (1986), The Sierras Pampeanas of Argentina - a modern analog of Rocky Mountain foreland deformation, *American Journal of Science*, *286*(10), 737-764.

Jordan, T. E., and R. N. Alonso (1987), Cenozoic stratigraphy and basin tectonics of the Andes Mountains, 20°–28° south latitude, *Am. Assoc. Pet. Geol. Bull., 71,* 49–64.

Judge, P. A., and R. W. Allmendinger (2011), Assessing uncertainties in balanced cross sections, *Journal of Structural Geology*, *33*(4), 458-467.

Kay, S. M., V. A. Ramos, C. Mpodozis, and P. Sruoga (1989), Late Paleozoic to Jurassic silicic magmatism at the Gondwana margin - analogy to the middle Proterozoic in North America, *Geology*, *17*(4), 324-328.

Kay, R.W., and S.M. Kay (1993), Delamination and delamination magmatism, *Tectonophysics, 201,* 177–189.

Khadivi, S., F. Mouthereau, J. C. Larrasoana, J. Verges, O. Lacombe, E. Khademi, E. Beamud, M. Melinte-Dobrinescu, and J. P. Suc (2010), Magnetochronology of synorogenic Miocene foreland sediments in the Fars arc of the Zagros Folded Belt (SW Iran), *Basin Research*, *22*(6), 918-932.

Kirby, E., Whipple, K.X., Tang, W., and Chen, Z., (2003), Distribution of active rock uplift along the eastern margin of the Tibetan Plateau: Inferences from bedrock river profiles: *Journal of Geophysical Research*, v. 108, 2217, doi:10.1029/2001JB000861.

Kirby, E., and Whipple, K.X., (2012). Expression of active tectonics in erosional landscapes: *Journal of Structural Geology*, v. 44, p. 54–75, doi:10.1016/j.jsg.2012.07.009

Kleiman, L. E., and M. S. Japas (2009), The Choiyoi volcanic province at 34 degrees S-36 degrees S (San Rafael, Mendoza, Argentina): Implications for the Late Palaeozoic evolution of the southwestern margin of Gondwana, *Tectonophysics*, *473*(3-4), 283-299.

Kley, J. (1996), Transition from basement-involved to thin-skinned thrusting in the Cordillera Oriental of southern Bolivia, *Tectonics*, *15*(4), 763-775.

Kley, J., C. R. Monaldi, and J. A. Salfity (1999), Along-strike segmentation of the Andean foreland: causes and consequences, *Tectonophysics*, *301*(1-2), 75-94.

Kontak, D. J., E. Farrar, A. H. Clark, and D. A. Archibald (1990), Eocene tectonothermal rejuvenation of an Upper Paleozoic Lower Mesozoic terrane in the Cordillera de Carabaya, Puno, Southeastern Peru, revealed by K-Ar and Ar-40 Ar-39 dating, *Journal of South American Earth Sciences*, *3*(4), 231-246.

Lamb, S., and L. Hoke (1997), Origin of the high plateau in the Central Andes, Bolivia, South America, *Tectonics*, *16*(4), 623-649.

LaTorre, O.O., F. Y. Oros, T. Sempered, M. Fornari and V. Carlotto (2004), Estratigrafia y evolucion paleogena del area de Llalli - Macari (departamento de Puno) in Nuevas contribuciones del IRD y sus contrapartes al conocimiento geologico del sur del Peru (pp. 143-155). Publicacion Especial No. 5, Institut de recherché pour le developpement, Paris

Laubacher, G. (1978), Geologie des Andes Peruviennes, *Travaux et documents de l'ORSTOM no 95*, Paris.

Laubacher, G., and F. Mégard, (1985), The Hercynian basement: a review. In *Magmatism at A Plate Edge: The Peruvian Andes,* (pp. 29-37) edited by W.S. Pitcher et al., Halsted Press, New York.

Lawton, T. F., and B. A. Bradford (2011), Correlation and provenance of upper Cretaceous (Campanian) fluvial strata, Utah, USA, from zircon U-Pb geochronology and petrography, *Journal of Sedimentary Research*, *81*(7-8), 495-512.

Lease, R. O., and T. A. Ehlers (2013), Incision into the Eastern Andean Plateau During Pliocene Cooling, *Science*, *341*(6147), 774-776.

Leeder, M.R, (1975), Pedogenic carbonates and flood sediment accretion rates: a quantitative model for alluvial arid-zone lithofacies, *Geol. Mag. 112 (3),* 257-270.

Leier, A.L., N. McQuarrie, B.K. Horton, G.E. Gehrels (2010), Upper Oligocene conglomerates of the Altiplano, central Andes: the record of deposition and deformation along the margin of a hinterland basin, *Journal of Sedimentary Research 80,* 750-762, DOI: 10.2110/jsr.2010.064.

Levina, M., B. K. Horton, F. Fuentes, and D. F. Stockli (2014), Cenozoic sedimentation and exhumation of the foreland basin system preserved in the Precordillera thrust belt (31-32 degrees S), southern central Andes, Argentina, *Tectonics*, *33*(9), 1659-1680.

Lock, J., and S. Willett (2008), Low-temperature thermochronometric ages in fold-and-thrust belts, *Tectonophysics*, *456*(3-4), 147-162.

Loewy, S. L., J. N. Connelly, and I. W. D. Dalziel (2004), An orphaned basement block: The Arequipa-Antofalla basement of the central Andean margin of South America, *Geological Society of America Bulletin*, *116*(1-2), 171-187.

Ludwig, K.R., (2008), Isoplot 3.60. Berkeley Geochronology Center, Special Publication No. 4, 77 p.

Mamani, M., I. Ibarra, G. Carlier and M. Fornari (2004), Petrologıa y geoquımica del magmatismo alcalino de la zona noroeste del Altiplano peruano (departamento de Puno), in *Nuevas contribuciones del IRD y sus contrapartes al conocimiento geologico del sur del Peru*, *Publ. Espec. 5,* edited by J. Jacay and T. Sempere, pp. 157 – 174, Soc. Geol. del Peru, Lima.

Mamani, M., Worner, G., and Sempere, T. (2010). Geochemical variations in igneous rocks of the Central Andean orocline (13 S to 18 S): Tracing crustal thickening

and magma generation through time and space. *Geological Society of America Bulletin, 122(1-2)*, 162-182.

Manceda, R., and D. Figueroa, (1995), Inversion of the Mesozoic Neuquén rift in the *369* Malargüe fold and thrust belt, Mendoza, Argentina, *in* A. J. Tankard, R. Suárez S., and H. J. Welsink, Petroleum basins of South America: AAPG Memoir 62, p. 369–382.

Mancktelow, N. S., and B. Grasemann (1997), Time-dependent effects of heat advection and topography on cooling histories during erosion, *Tectonophysics*, *270*(3-4), 167-195.

Marocco, R., (1978), Un segment est-ouest de la chaine des Andes péruviennes: la deflexion d'Abancay. Trav. e t Doc. ORSTOM, ***94.*** *195* p.

Martinez, C., (1980), Structure et evolution de la chaîne hercynienne et de la chaîne andine dans le nord de la Cordillere des Andes de Bolivie. Géologie des Andes Boliviennes, Travaux et documents de L'O.R.S.T.O.M. 119, 352.

Mathalone, J. M. P., and Montoya R., M., (1995), Petroleum geology of the sub-Andean basins of Peru, *in* A. J. Tankard, R. Suárez S., and H. J. Welsink, Petroleum basins of South America: AAPG Memoir 62, p. 423–444.

McBride, S., Robertson, R., and Clark, A. (1983). Magmatic and metallogenetic episodes in the northern tin belt, Cordillera Real, Bolivia. *Geologische Rundschau, 72(2),* 685-713.

McGroder, M.F., Lease, R.O., and Pearson, D.M., (2015), Along-strike variation in structural styles and hydrocarbon occurrences, Subandean fold-and-thrust belt and inner foreland, Colombia to Argentina, *in* DeCelles, P.G., Ducea, M.N., Carrapa, B., and Kapp, P.A., eds., Geodynamics of a Cordilleran Orogenic System: The Central Andes of Argentina and Northern Chile: *Geological Society of America Memoir* 212, doi:10.1130/2015.1212(05).

McQuarrie, N. (2002), The kinematic history of the central Andean fold-thrust belt, Bolivia: Implications for building a high plateau, *Geological Society of America Bulletin*, *114*(8), 950-963.

McQuarrie, N., and P. DeCelles (2001), Geometry and structural evolution of the central Andean backthrust belt, Bolivia, *Tectonics*, *20*(5), 669-692.

McQuarrie, N., J. B. Barnes, and T. A. Ehlers (2008), Geometric, kinematic, and erosional history of the central Andean Plateau, Bolivia (15-17 degrees S), *Tectonics*, *27*(3).

McQuarrie, N., B. K. Horton, G. Zandt, S. Beck, and P. G. DeCelles (2005), Lithospheric evolution of the Andean fold-thrust belt, Bolivia, and the origin of the central Andean plateau, *Tectonophysics*, *399*(1-4), 15-37.

McQuarrie, N., and Ehlers, T., (2015), Influence of thrust belt geometry and shortening rate on thermochronometer cooling ages: Insights from thermokinematic and erosion modeling of the Bhutan Himalaya, *Tectonics*, in press.

Mégard, F., B. Dalmayrac, G. Laubacher, R. Marocco, C. Martinez, J. Paredes, and P. Tomasi (1971), La chaine Hercynienne au Perou et en Bolivie premiers resultats, *Cah. ORSTOM, ser. Geol. III, 1,* 5-44.

Mégard, F. (1978) Etude Geologique des Andes du Perou central, *Memoirs No. 86 ORSTOM,* Paris.

Mégard, F. (1984), The Andean orogenic period and its major structures in central and northern Peru, *Journal of the Geological Society*, *141*(SEP), 893-900.

Meigs, A.J., D.W. Burbank and R.A. Beck (1995), Middle-late Miocene (>10 Ma) formation of the Main Boundary thrust in the western Himalaya, *Geology, 23 (5),* 423-426.

Mescua, J. F., and L. B. Giambiagi (2012), Fault inversion vs. new thrust generation: A case study in the Malargüe fold-and-thrust belt, Andes of Argentina, *Journal of Structural Geology*, *35*, 51-63.

Miall, A. D. (1977), A review of the braided-river depositional environment, *Earth Sci. Rev., 13,* 1–62, doi:10.1016/0012-8252(77)90055-1.

Miall, A.D. (1978) Lithofacies types and vertical profile models in braided river deposits: a summary in *Fluvial Sedimentology*, Canadian Society of Petroleum Geologists, Memoir 5, McAra Printing, Calgary.

Min, K. W., P. R. Renne, and W. D. Huff (2001), Ar-40/Ar-39 dating of Ordovician K-bentonites in Laurentia and Baltoscandia, *Earth and Planetary Science Letters*, *185*(1-2), 121-134.

Mišković, A., and U. Schaltegger (2009), Crustal growth along a non-collisional cratonic margin: A Lu-Hf isotopic survey of the Eastern Cordilleran granitoids of Peru, *Earth and Planetary Science Letters*, *279*(3-4), 303-315.

Mišković, A., R. A. Spikings, D. M. Chew, J. Kosler, A. Ulianov, and U. Schaltegger (2009), Tectonomagmatic evolution of Western Amazonia: Geochemical characterization and zircon U-Pb geochronologic constraints from the Peruvian Eastern Cordilleran granitoids, *Geological Society of America Bulletin*, *121*(9-10), 1298-1324.

Monaldi, C. R., J. A. Salfity, and J. Kley (2008), Preserved extensional structures in an inverted Cretaceous rift basin, northwestern Argentina: Outcrop examples and implications for fault reactivation, *Tectonics*, *27*(1).

Mora, A., M. Parra, M. R. Strecker, A. Kammer, C. Dimate, and F. Rodriguez (2006), Cenozoic contractional reactivation of Mesozoic extensional structures in the Eastern Cordillera of Colombia, *Tectonics*, *25*(2).

Mora, A., R. A. Ketcham, I. C. Higuera-Diaz, B. Bookhagen, L. Jimenez, and J. Rubiano (2014), Formation of passive-roof duplexes in the Colombian Subandes and Peru, *Lithosphere*, *6*(6), 456-472.

Mosolf, J. G., B. K. Horton, M. T. Heizler, and R. Matos (2011), Unroofing the core of the central Andean fold-thrust belt during focused late Miocene exhumation: Evidence from the Tipuani-Mapiri wedge-top basin, Bolivia, *Basin Res., 23,* 346–360, doi:10.1111/j.1365-2117.2010.00491.x.

Mouthereau, F., A. B. Watts, and E. Burov (2013), Structure of orogenic belts controlled by lithosphere age, *Nature Geoscience*, *6*(9), 785-789.

Mpodozis, C., and S. M. Kay (1992), Late Paleozoic to Triassic evolution of the Gondwana margin - evidence from Chilean Frontal Cordilleran batholiths (28°S to 31°S), *Geological Society of America Bulletin*, *104*(8), 999-1014.

Muller, J. P., J. Kley, and V. Jacobshagen (2002), Structure and Cenozoic kinematics of the Eastern Cordillera, southern Bolivia (21 degrees S), *Tectonics*, *21*(5).

Murray, B. P., B. K. Horton, R. Matos, and M. T. Heizler (2010), Oligocene-Miocene basin evolution in the northern Altiplano, Bolivia: Implications for evolution of the central Andean backthrust belt and high plateau, *Geol. Soc. Am. Bull., 122,* 1443–1462, doi:10.1130/B30129.1.

Nadon, G.C. (1991) The genesis and recognition of anastomosed fluvial deposits: data from the St. Mary river formation, southwestern Alberta, Canada, *Journal of Sedimentary Research, B64 (4),* 451-463.

Nemec, W., and R. J. Steel (1984), Alluvial and coastal conglomerates:Their significant features and some comments on gravelly mass-flow deposits, in Sedimentology of Gravels and Conglomerates, edited by E. H. Koster and R. J. Steel, *Can. Soc. Pet. Geol., Mem., 10,* 1–31.

Newell, N. D. (1949), Geology of the lake Titicaca region, Peru and Bolivia, *Mem. Geol. Soc. Am., 36,* 111 pp.

Newell, N.D., Chronic, J., and Roberts, T.G., (1953). Upper Paleozoic of Peru. *Geological Society of America Memoir* 58, 272 pp.

Nijman, W. and C. Puigdefabregas (1978), Coarse-grained point bar structure in a molasse-type fluvial system, Eocene Castisent Sandstone Formation, south Pyrenean basin, in *Fluvial Sedimentology*, Canadian Society of Petroleum Geologists, Memoir 5, McAra Printing, Calgary.

Noble, D. C., M. L. Silberman, F. Mégard, and H. R. Bowman (1978), Comendite (Peralkaline-Rhyolite) and basalt in the Mitu Group, Peru - evidence for Permian-Triassic lithospheric extension in the Central Andes, *Journal of Research of the Us Geological Survey*, *6*(4), 453-457.

Oncken, O., Hindle, D., Kley, J., Elger, K., Victor, P., and Schemann, K. (2006), Deformation of the Central Andean Upper Plate System – Facts, Fiction, and Constraints for Plateau Models, *in* Oncken, O., Chong, G., Franz, G., Giese, P., Gotze, H.-J., Ramos, V. A., Strecker, M. R., Wigger, P., eds., The Andes: Active Subduction Orogeny, Springer-Verlag Berlin Heidelberg, p. 3-28.

Panca, F., C. Breitkreuz, S. Rosas, V. Carlotto, (2011), The Triassic-Jurassic rift system of the Mitu Group in Peru: Preliminary results on the volcanosedimentary facies evolution in the Urubamba Valley northeast of Cuzco. 22nd LAK, Heidelberg, abstract.

PARSEP, (2000), The Huallaga Basin and Adjacent Area: The Hydrocarbon Potential of NE Peru Huallaga, Santiago and Marañón Basins Study, Technical report.

Perez, N. D., and B. K. Horton (2014), Oligocene-Miocene deformational and depositional history of the Andean hinterland basin in the northern Altiplano plateau, southern Peru, *Tectonics*, *33*(9), 1819-1847.

Pichavant, M., D. J. Kontak, J. Valencia Herrera, and A. H. Clark (1988), The Miocene-Pliocene Macusani volcanics, SE Peru, *Contrib. Mineral. Petrol.,* 100, 325–338.

Platt, N.H. (1989), Lacustrine carbonates and pedogenesis: sedimentology and origin of palustrine deposits from the Early Cretaceous Rupelo Formation, W Cameros Basin, N Spain, *Sedimentology, 36,* 665-684.

Price, R. A., (1981), The Cordilleran foreland thrust and fold belt in the southern Candian Rocky Mountains, *in* McClay, K., and Price, N. J., eds., Thrust and Nappe Tectonics, Geological Society of London Special Publication (9), p. 427-448.

Puigdefabregas, C. and A. Van Vliet (1978), Meandering stream deposits from the tertiary of the southern pyrenees, in *Fluvial Sedimentology*, Canadian Society of Petroleum Geologists, Memoir 5, McAra Printing, Calgary.

Ramos, V. A., M. Cegarra, and E. Cristallini (1996), Cenozoic tectonics of the High Andes of west-central Argentina (30-36 degrees S latitude), *Tectonophysics*, *259*(1-3), 185-200.

Ramos, V.A., (2000). The southern central Andes, *in* Cordani, U.G., Milani, E.J., Thomaz Filha, A., Campos, D.A., (Eds.), Tectonic Evolution of South America, 31st International Geological Congress, Rio de Janeiro, pp. 561-604.

Ramos, V. A. (2008), The basement of the Central Andes: The Arequipa and related terranes, *Annual Review of Earth and Planetary Sciences*, *36*, 289-324.

Ramos, V.A., (2009), Anatomy and global context of the Andes: Main geologic features and the Andean orogenic cycle, *in* Kay, S.M., Ramos, V.A., and Dickinson, W.R., eds., Backbone of the Americas: Shallow Subduction, Plateau Uplift, and Ridge and Terrane Collision: Geological Society of America Memoir 204, p. 31–65, doi: 10.1130/2009.1204(02).

Reimann, C. R., H. Bahlburg, E. Kooijman, J. Berndt, A. Gerdes, V. Carlotto, and S. Lopez (2010), Geodynamic evolution of the early Paleozoic Western Gondwana margin 14 degrees-17 degrees S reflected by the detritus of the Devonian and Ordovician basins of southern Peru and northern Bolivia, *Gondwana Research*, *18*(2-3), 370-384.

Reiners, P.W., Ehlers, T.A., and Zeitler, P.K., 2005, Past, Present and Future of Thermochronology, *in* Reiners, P.W., and Ehlers, T.A., eds., Low-Temperature Thermochronology: Techniques, Interpretations, & Applications: Mineralogical Society of America, Reviews in Mineralogy and Geochemistry Volume 58, p. 1–18.

Reitsma, M. J., (2012), Reconstructing the Late Paleozoic: Early Mesozoic plutonic and sedimentary record of south-east Peru : Orphaned back-arcs along the western margin of Gondwana, Univ. Genve, no. Sc. 4459.

Reitsma, M., Schaltegger, U., Spikings, R., Winkler, W., and Carlotto, V., (2010), Constraining the age of the Mitu group, South-East Peru: U-Pb ages of detrital and igneous zircons, EGU General Assembly, Volume 12: Vienna, Geophysical Research Abstracts, p. 4299.

Renne P. R., Deino A. L., Walter R. C., Turrin B. D., Shisher C. C. III, Becker T. A., Curtis G. H., Sharp W. D., and Jaouni A. -R. (1994) Intercalibration of astronomical and radioisotopic time. *Geology*. 22, 783–786.

Restrepo-Pace, P. A., J. Ruiz, G. Gehrels, and M. Cosca (1997), Geochronology and Nd isotopic data of Grenville-age rocks in the Colombian Andes: new constraints for late Proterozoic Early Paleozoic paleocontinental reconstructions of the Americas, *Earth and Planetary Science Letters*, *150*(3-4), 427-441.

Riba, O. (1976), Syntectonic unconformities of the Alto Cardener, Spanish Pyrenees: a genetic interpretation, *Sedimentary Geology, 15,* 213-233.

Rivas, S., 1971. Ordovícico en el corazon de Bolivia. Boletin del Servicio Geologico de Bolivia 15, 5–12.

Rochat, P., P. Baby, G. Herail, G. Mascle, O. Aranibar, B. Colletta (1999), Genesis and kinematic of the northern Bolivian Altiplano, paper presented at 3rd International Symposium of Andean Geodynamics, Inst. de Rech. pour le Dev., Paris.

Rodrıguez, R., T. Flores, and R. Marocco (1999), Analisis sedimentologico y estratigrafico de la Formacion Tinajani (Cenozoico del Altiplano del Sur del Peru). Aportes a la reconstruccion de la evolucion tectono-sedimentaria del Sur del Peru entre el Oligoceno superior y el Mioceno superior, *Bol. Soc. Geol. Peru, 89,* 33 – 44.

Roeder, D. (1988), Andean-age structure of Eastern Cordillera (province of La Paz, Bolivia), *Tectonics*, *7*(1), 23-39.

Roeder, D., and R. L. Chamberlain, (1995), Structural geology of sub-Andean fold and thrust belt in northwestern Bolivia, *in* A. J. Tankard, R. Suárez S., and H. J. Welsink, Petroleum basins of South America: AAPG Memoir 62, p. 459–479.

Roperch, P., T. Sempere, O. Macedo, C. Arriagada, M. Fornari, C. Tapia, M. Garcia, and C. Laj (2006), Counterclockwise rotation of late Eocene–Oligocene fore-arc deposits in southern Peru and its significance for oroclinal bending in the central Andes, *Tectonics, 25,* TC3010, doi:10.1029/2005TC001882

Rosas, S., L. Fontbote, and A. Tankard (2007), Tectonic evolution and paleogeography of the Mesozoic Pucara Basin, central Peru, *Journal of South American Earth Sciences*, *24*(1), 1-24.

Rousse, S., S. Gilder, D. Farber, B. McNulty, P. Patriat, V. Torres, and T. Sempere (2003) Paleomagnetic tracking of mountain building in the Peruvian Andes since 10 Ma, *Tectonics, 22,* doi:10.1029/2003TC001508

Rousse, S., S. Gilder, M. Fornari, and T. Sempere (2005), Insight into the Neogene tectonic history of the northern Bolivian Orocline from new paleomagnetic and geochronologic data, *Tectonics, 24,* TC6007, doi:10.1029/2004TC001760.

Royden, L., and G. D. Karner (1984), Flexure of lithosphere beneath Apennine and Carpathian foredeep basins - evidence for an insufficient topographic load, *AAPG Bulletin-American Association of Petroleum Geologists*, *68*(6), 704-712.

Rust, B.R. (1978) Depositional models for braided alluvium, in *Fluvial Sedimentology*, Canadian Society of Petroleum Geologists, Memoir 5, McAra Printing, Calgary.

Sandeman, H.A., A.H. Clark and E. Farrar (1995), An Integrated Tectono-Magmatic Model for the Evolution of the Southern Peruvian Andes (13-20° S) since 55 Ma, *International Geology Reviews, 37,* 1039-1073.

Sandeman, H. A., A. H. Clark, E. Farrar, and G. A. Pauca (1997), Lithostratigraphy, petrology and Ar-40-Ar-39 geochronology of the Crucero Supergroup, Puno Department, SE Peru, *Journal of South American Earth Sciences*, *10*(3-4), 223-245.

Saylor, J.E. and B.K. Horton (2014), Nonuniform surface uplift of the Andean plateau revealed by deuterium isotopes in Miocene volcanic glass from southern Peru, *Earth and Planetary Science Letters, 387,* 120-131.

Scherrenberg, A. F., J. Jacay, R. J. Holcombe, and G. Rosenbaum (2012), Stratigraphic variations across the Maranon Fold-Thrust Belt, Peru: Implications for the basin architecture of the West Peruvian Trough, *Journal of South American Earth Sciences*, *38*, 147-158.

Schildgen, T. F., K. V. Hodges, K. X. Whipple, P. W. Reiners, and M. S. Pringle (2007), Uplift of the western margin of the Andean plateau revealed from canyon incision history, southern Peru, *Geology*, *35*(6), 523-526.

Schildgen, T.F., K.V. Hodges, K.X. Whipple, M.S. Pringle, M. van Soeste, and K. Cornell (2009a), Late Cenozoic structural and tectonic development of the western margin of the central Andean Plateau in southwest Peru, *Tectonics, 28, TC4007,* doi:10.1029/2008TC002403.

Schildgen, T. F., T. A. Ehlers, D. M. Whipp Jr., M. C. van Soest, K. X. Whipple, and K. V. Hodges (2009b), Quantifying canyon incision and Andean Plateau surface uplift, southwest Peru: A thermochronometer and numerical modeling approach, *J. Geophys. Res., 114,* F04014, doi:10.1029/2009JF001305.

Schmitz, M. (1994), A balanced model of the southern Central Andes, *Tectonics*, *13*(2), 484-492.

Schmitz, M. D., and S. A. Bowring (2001), U-Pb zircon and titanite systematics of the Fish Canyon Tuff: an assessment of high-precision U-Pb geochronology and its application to young volcanic rocks, *Geochimica Et Cosmochimica Acta*, *65*(15), 2571-2587.

Schoenbohm, L. M., and Carrapa, B., (2015) Miocene–Pliocene shortening, extension, and mafic magmatism support small-scale lithospheric foundering in the central Andes, NW Argentina *in* DeCelles, P.G., Ducea, M.N., Carrapa, B., and Kapp, P.A., eds., Geodynamics of a Cordilleran Orogenic System: The Central Andes of Argentina and Northern Chile: *Geological Society of America Memoir* 212, doi:10.1130/2015.1212(05).

Schreurs, G., Hänni, R., and Vock, P., (2001), Four-dimensional analysis of analog models: Experiments on transfer zones in fold and thrust belts, *in* Koyi, H.A., and Mancktelow, N.S., eds., Tectonic Modeling: A Volume in Honor of Hans Ramberg: Boulder, Colorado, Geological Society of America Memoir 193, p. 179–190.

Sébrier, M., Lavenu, A., Fornari, M., and Soulas, J.P., 1988, Tectonics and uplift in central Andes (Peru, Bolivia and northern Chile) from Eocene to present: Géodynamique, v. 3, p. 85-106.

Seeber, L., and C. C. Sorlien (2000), Listric thrusts in the western Transverse Ranges, California, *Geological Society of America Bulletin*, *112*(7), 1067-1079.

Sempere, T., G. Herail, J. Oller, and M. G. Bonhomme (1990), Late Oligocene early Miocene major tectonic crisis and related basins in Bolivia, *Geology*, *18*(10), 946-949.

Sempere, T., Carlier, G., Soler, P., Fornari, M., Carlotto, V., Jacay, J., Arispe, O., Neraudeau, Cardenas, J., Rosas, S., Jimenez, N., (2002). Late Permian – Middle Jurassic lithospheric thinning in Peru and Bolivia, and its bearing on Andean-age tectonics. *Tectonophysics* 345, 153–181.

Shaw, J. H., E. Novoa, and C. D. Connors, 2004, Structural controls on growth stratigraphy in contractional fault-related folds, in K. R. McClay, ed., Thrust tectonics and hydrocarbon systems: AAPG Memoir 82, p. 400 – 412.

Sheffels, B. M. (1990), Lower bound on the amount of crustal shortening in the central Bolivian Andes, *Geology*, *18*(9), 812-815.

Siks, B. C., and B. K. Horton (2011), Growth and fragmentation of the Andean foreland basin during eastward advance of fold-thrust deformation, Puna plateau and Eastern Cordillera, northern Argentina, *Tectonics, 30, TC6017,* doi:10.1029/2011TC002944.

Sibson, R. H. (1985), A Note On Fault Reactivation, *Journal of Structural Geology*, *7*(6), 751-754.

Sibson, R. H. (1990), Rupture nucleation on unfavorably oriented faults, *Bulletin of the Seismological Society of America*, *80*(6), 1580-1604.

Smith, N.D. (1974) Sedimentology and Bar Formation in the Upper Kicking Horse River, a Braided Outwash Stream, *Geology, 82, (2),* 205-223.

Soler, P., and M. G. Bonhomme (1987), K-Ar radiochronological data on the granitoids of the Eastern Cordillera of central Peruvian Andes - tectonic implications, *Comptes Rendus De L'Academie Des Sciences Serie Ii*, *304*(14), 841-845.

Stacey, J.S., and Kramers, J.D., (1975), Approximation of terrestrial lead isotope evolution by a two-stage model, *Earth and Planetary Science Letters*, v. 26, p. 207-221.

Steinmann, G., and Hoek, H., (1912). Das Silur und Cambrium des Hochlandes von Bolivien und ihre Fauna. Neues Jahrbuch fur Minereralogie, Geologie und Palaontologie Beilagen Band 24, 176–252.

Steinmann, G. (1929), Geologie von Peru, Heidelberg, Carl Winters Universistats Buchhandlung, 448 p.

Stockli, D. F., T. A. Dumitru, M. O. McWilliams, and K. A. Farley (2003), Cenozoic tectonic evolution of the White Mountains, California and Nevada, *Geological Society of America Bulletin*, *115*(7), 788-816.

Suarez Soruco, R., (1976). El sistema Ordovícico en Bolivia. Revista Tecnica de Yacimientos Petroliferos Fiscales de Bolivia V, 111–223.

Suarez Soruco, R., (1992). El Paleozoico Inferior de Bolivia y Peru . In: Gutierrez-Marco, J.C., Saavedra, J., Rabano (Eds.), Paleozoico de Ibero-America. Universidad de Extremadura, pp. 225–239.

Suarez Soruco, R., (2000). Compendio de Geologıa de Bolivia. Revista Tecnica de Yacimientos Petroliferos Fiscales de Bolivia 18, 1–144.

Suppe, J., G.T. Chou, and S.C. Hook (1992) Rates of folding and faulting determined from growth strata, in K. R. McClay, ed., *Thrust Tectonics*: Chapman & Hall, London, 105-121.

Tankard, A., (2001). Tectonic framework of basin evolution in Peru. Proprietary Report.

Tapponier, P., X. Zhiqin, F. Roger, B. Meyer, N. Arnaud, D. Wittlinger, and Y. Jingsui (2001) Oblique Stepwise Rise and Growth of the Tibet Plateau, *Science 294,* 1671-1677.

Tassara, A., C. Swain, R. Hackney, and J. Kirby (2007), Elastic thickness structure of South America estimated using wavelets and satellite-derived gravity data, *Earth and Planetary Science Letters*, *253*(1-2), 17-36.

Tassinari, C.C.G., Bettencourt, J.S., Geraldes, M.C., Macambira, M.J.B., Lafon, J.M., (2000), The Amazon Craton. In: Cordani, U.G., Milani, E.J., Thomaz Filho, A.M, Campos, D.A. (Eds.), Tectonic evolution of South America. 31st International Geological Congress, Rio de Janeiro, pp. 41-95.

Teixell, A., M. L. Arboleya, M. Julivert, and M. Charroud (2003), Tectonic shortening and topography in the central High Atlas (Morocco), *Tectonics*, *22*(5).

Teixeira, W., Tassinari, C.C.G., Cordani, U.G., and Kawashita, K., (1989). A review of the geochronology of the Amazonian Craton: tectonic implications. *Precambrian Research* 42, 213–227.

Vandervoort, D. S., T. E. Jordan, P. K. Zeitler, and R. N. Alonso (1995), Chronology of internal drainage development and uplift, southern Puna plateau, Argentine central Andes, Geology, 23, 145–148, doi:10.1130/00917613(1995)023<0145:COIDDA>2.3.CO;2.

Vermeesch, P. (2004), How many grains are needed for a provenance study?, *Earth and Planetary Science Letters 224*, 441-451, doi:10.1016/j.epsl.2004.05.037.

Vermeesch P. (2012), On the visualisation of detrital age distributions, *Chemical Geology, 312-313*, 190-194, doi:10.1016/j.chemgeo.2012.04.021.

Vicente, J.-C., (1989), Early Late Cretaceous overthrusting in the Western Cordillera Of Southern Peru *in* Ericksen, G. E., Canas Pinochet, M. T., and Reinemund, J. A., eds., Geology of the Andes and its relation to hydrocarbon and mineral resources: Houston, Texas, Circum-Pacific Council for Energy and Mineral Resources Earth Science Series, v. 11, p. 91-117.

Welbon, A.I., and Butler, R.W.H., 1992. Structural styles in thrust belts developed through rift basins: a view from the western Alps. *in* Larsen, R.M. (Ed.), Structural and Tectonic Modeling and its Application to Petroleum Geology. Norwegian Petroleum Society Special Publication 1, pp. 469-479.

Wells, N.A. (1984), Sheet debris flow and sheetflood conglomerates in Cretaceous cool-maritime alluvial fans, South Orkney Islands, Antarctica, in E.H. Koster and R.J. Steel (Eds.) *Sedimentology of Gravels and Conglomerates*, pp. 133-146, *Can. Soc. Pet. Geol., Mem., 10*.

Whipple, K. X., and N. M. Gasparini (2014), Tectonic control of topography, rainfall patterns, and erosion during rapid post-12 Ma uplift of the Bolivian Andes, *Lithosphere*, *6*(4), 251-268.

Whittaker, A.C., (2012), How do landscapes record tectonics and climate?, *Lithosphere*, v. 4, no. 2, p. 160–164, doi: 10.1130 /RF.L003.1.

Wilson, J.J., (1963), Cretaceous stratigraphy of Central Andes of Peru, *AAPG Bulletin*, 47 (1), p. 1-34.

Wobus, C.W., Whipple, K.X., Kirby, E., Snyder, N., Johnson, J., Spyropolou, K., Crosby, B., and Sheehan, D., (2006), Tectonics from topography; procedures, promise, and pitfalls, *in* Willett, S.D., Hovius, N., Brandon, M.T., and Fisher, D.M., eds., Tectonics, Climate and Landscape Evolution: Geological Society of America Special Paper 398, p. 55–74.

Woodward, N., S. E. Boyer, and J. Suppe (1989), Balanced Geological Cross-Sections: An Essential Technique in Geological Rsearch and Exploration, Short Course Geol., vol. 6, AGU, Washington, D.C.

Yin, A., and T. M. Harrison (2000), Geologic evolution of the Himalayan-Tibetan orogen, *Annual Review of Earth and Planetary Sciences*, *28*, 211-280.

Zapata, T. R., and R. W. Allmendinger (1996), Thrust-front zone of the Precordillera, Argentina: A thick-skinned triangle zone, *AAPG Bulletin*, *80*(3), 359-381.